

PROTEOMIC DISSECTION OF LPS-INDUCIBLE PHF8-DEPENDENT SECRETOME
REVEALS NOVEL ROLES OF PHF8 IN TLR4-INDUCED ACUTE INFLAMMATION AND
ACTIVATION OF ADAPTIVE IMMUNITY

Özgün Erdoğan

A dissertation submitted to the faculty at the University of North Carolina at Chapel Hill
in partial fulfillment for the degree of Doctor of Philosophy in the Department of
Biochemistry and Biophysics in the School of Medicine.

Chapel Hill
2016

Approved by:

Xian Chen

Beverly Errede

William F. Marzluff

Leslie Parise

Yisong Wan

© 2016
Özgün Erdoğan
ALL RIGHTS RESERVED

ABSTRACT

Özgün Erdoğan: PHF8 regulates the gene-specific, transcriptionally active chromatin state to promote TLR4-induced acute inflammation and adaptive immunity
(Under the direction of Xian Chen)

This dissertation examines the role of PHF8 in the regulation of LPS-induced inflammatory response in macrophages and activation of adaptive immunity. I extend prior work on PP2Ac-dependent activation of endotoxin tolerance to reveal that PHF8 is negatively regulated by chronic-active PP2Ac in endotoxin tolerance, leading to our observation that PHF8 broadly regulates LPS-induced acute inflammation response in macrophages. This research offers four conclusions: (1) PHF8 enzymatic activity is important for LPS-induced cytokine expression in macrophages, (2) PHF8 targets H3K9me1/2 for demethylation to promote LPS-induced gene-specific transcription, (3) PHF8 binds to, and regulates NFκB transcription factor activity, and (4) PHF8 broadly regulates the secretion of molecules involved in activation of adaptive immunity. In addition to the biological and biochemical experiments that provide evidence for PHF8-dependent H3K9me1/2 demethylation, cytokine expression, and NFκB activation, we conducted proteomic dissection of LPS-induced macrophage secretome revealing important roles of PHF8 in activation of adaptive immunity. Moreover, the secretome analysis illustrates that PHF8 is a major regulator of LPS-induced secretion of molecules involved in activation of adaptive immunity. Further, through T cell proliferation and activation assays, I provide evidence that the activation of T cells by macrophages

depends on the LPS-induced PHF8 activity. Our findings advance our understanding of regulation of LPS response by PHF8, and reveal that PHF8 bridges the innate immunity, and adaptive immunity responses. These results also offer insights to differential regulation of acute- vs chronic-inflammation by the antagonistic activities of chromatin writers and erasers, namely H3K9me1/2 methyltransferase G9a and H3K9me1/2 demethylase PHF8, respectively.

To the loving memory of my late grandmother Ayşe Arslan.

ACKNOWLEDGEMENTS

I would like to thank my thesis advisor Dr. Xian Chen for giving me the opportunity to work in his lab. I appreciate that he welcomed me to his lab during a desperate time when I needed the help and encouragement the most. I would like to thank Dr. Beverly Errede, Dr. William F. Marzluff, Dr. Leslie Parise, and Dr. Yisong Wan, for their time, insightful comments, informative discussions, and endless support over the years; I am grateful that their doors were always open to me, and they were extremely kind in providing me guidance. I would like to acknowledge the Bioinformatics and Computational Biology certificate program as they provided funding for the first year of my graduate studies.

I would like to thank the members of the Chen lab, past and present, especially Dr. Qing Kong, Dr. Cui Liu, Dr. Li Wang, Dr. Xin Wei, and Dr. Ling Xie, for their help, discussion, and guidance; their input has been invaluable for my research. I would also like to thank our collaborator Dr. Bing Wu for his help in T cell experiments.

There are many people I should acknowledge for their support in healing from trauma: Dr. Nikola Gray, Dr. Sevinç Ercan, Dr. Patrick Brandt, Cassidy Johnson, EW Quimbaya-Winship, and OCRCC.

One cannot survive PhD without emotional strength coming from amazing friends. I am grateful to Dr. Racha Moussa, Dr. Wafa Hassouneh, Dr. Mikaëla M. Adams, Jennifer Park, Ayşe Gündoğdu-Şentürk, Esra Erdoğan, Berke Soyuer, Barış Can, İrem - Onur Dağlıyan, Selcan - Mert Aydın, Amy Stencel, and Jacques P. Le Roux for their enormous love, support, patience, kindness, and encouragement. I am grateful to my Chapel Hill parents Narjes - Khalil Moussa, who made Chapel Hill home for me with their warmth and kindness.

My soul-sister Gülfem Türel has been a source of encouragement, support, love, and patience for every step of my life. I can't imagine having survived all these years without her support and cheers. Her positivity was the only thing I could count on when I was in need. Her cheerful attitude was my guide during the darkest times. I am also grateful to my pseudo-wife Dr. Tishan Williams for her amazing companionship! She has become the most stable part of my last eight years. There was no place else to go to than her desk, in times of desperation or joy. She has been an inspiration to level up, excel, and go beyond limits.

Last but not least, I would like to thank my parents Songül and Macit for their unconditional love, endless support, and persistent faith in me. I am grateful to them for providing me every opportunity to follow my dreams in being a scientist; I owe the strength, hardwork, and perseverance to them.

TABLE OF CONTENTS

LIST OF TABLES.....	xiv
LIST OF FIGURES	xv
CHAPTER 1: INTRODUCTION	32
OVERVIEW	32
INNATE IMMUNITY AND TOLL-LIKE RECEPTORS.....	32
MyD88-Dependent Signaling.....	34
NFκB IN INFLAMMATION RESPONSE	35
IκB Family Proteins Regulate p65 Activity.....	36
Regulation of Transcriptional Activity of p65 via Phosphorylation.....	37
ENDOTOXIN TOLERANCE.....	38
EPIGENETIC REGULATION OF INFLAMMATION RESPONSE	40
Epigenetic Regulation of Transcription Through Methylation PTM	41
Role of Lysine Methylation in Regulation of Inflammation Response.....	45
FIGURES	48

CHAPTER 2: CHRONICALLY ACTIVE PP2Ac DEPHOSPHORYLATES VARIOUS CHROMATIN MODIFIERS TO REGULATE ENDOTOXIN TOLERANCE	59
OVERVIEW	59
INTRODUCTION	60
Protein Phosphatases and PP2A	60
PP2A: A Major Regulator of NFκB Signaling.....	61
Phosphoprotein Sequencing Using Quantitative Proteomics	63
MATERIALS AND METHODS.....	68
Reagents	68
Cell Culture	68
Quantitative Phosphoproteomic Analysis using AACT	70
Detection of the changes in Histone PTMs via Western Blotting	73
RESULTS	74
Phosphoproteomic analysis reveals broad range of signaling pathways regulated by PP2Ac in ET-macrophages	74
PP2Ac dephosphorylates various chromatin modifiers to regulate gene transcription in ET macrophages	76
PP2Ac regulates the cross-talk between TLR4 and AKT pathways through modulating the phosphoproteome in ET macrophages	78
PP2Ac-mediated ET is regulated by altered H3K9me2, H3K27me2, and H3S10P in macrophages.....	80

PP2Ac inhibits the activity of PHF8 in ET to repress transcription.....	81
DISCUSSION	82
FUTURE WORK.....	84
FIGURES	86
CHAPTER 3: PHF8 IS ACTIVATED IN LPS-INDUCED MACROPHAGES TO POSITIVELY REGULATE CYTOKINE EXPRESSION AND NFκB ACTIVITY	106
OVERVIEW	106
INTRODUCTION	107
Histone Demethylase PHF8.....	107
MATERIALS AND METHODS.....	110
Reagents	110
Cell Culture	111
Immunoblotting of Histone PTMs	111
RNA Isolation and qPCR for PHF8 mRNA expression analysis.....	112
Nuclear-Cytoplasmic Fractionation for Immunoblotting	112
Co-immunoprecipitation of PHF8-p65 Complexes.....	113
NF-κB reporter assay	114
RNA Isolation and qPCR for Pro-inflammatory mRNA expression.....	115
RESULTS	116

PHF8 Knockdown leads to increased H3K9me1 and H3K9me2 in LPS-induced macrophages.....	116
PHF8 is involved in regulation of p65-dependent gene-specific transcription of pro-inflammatory cytokines in macrophages upon LPS stimulation	118
PHF8 regulates gene-specific pro-inflammatory mRNA expression via regulating NFκB in LPS-stimulated macrophages.....	121
DISCUSSION	122
FUTURE WORK.....	123
FIGURES	125
CHAPTER 4: PHF8 REGULATES THE SECRETION OF SPECIFIC ‘TOLERIZABLE’ GENES INCLUDING CYTOKINES AND CHEMOKINES IN LPS-INDUCED MACROPHAGES FOR SUCCESSFUL ACTIVATION OF ADAPTIVE IMMUNITY	133
OVERVIEW	133
INTRODUCTION	134
The Role of Macrophage Secretome in Inflammation Response	134
Secretome Analysis Methods.....	138
MATERIALS AND METHODS.....	140
Reagents	140
Cell Culture	140
PHF8-dependent Secretome Profiling.....	141
RNA Isolation and qPCR	145

P14 CD8+ T cell activation assay	146
P14 CD8+ T cell proliferation assay	147
RESULTS	147
PHF8 selectively promotes the secretion of a specific group of ‘tolerizable’ proteins including cytokines and chemokines	147
PHF8-dependent T-class secretome is involved in regulation of diverse extracellular processes and pathways upon LPS stimulation.....	150
PHF8 positively regulates the activation and proliferation of T cells via secretion of specific proteins involved in antigen presentation and activation of adaptive immunity	158
DISCUSSION	160
FUTURE WORK.....	163
FIGURES	164
CHAPTER 5: PHF8 AND G9A WORK ANTAGONISTICALLY TO REGULATE THE SECRETION OF ‘TOLERIZABLE’ PROTEINS IN A PHENOTYPE- DEPENDENT MANNER	180
OVERVIEW	180
INTRODUCTION	181
Regulation of K9me-mediated Macrophage Inflammation Response	181
G9a Histone Methyltransferase	182
G9a in regulation of immunity	184
MATERIALS AND METHODS.....	185

Bioinformatic Analysis	185
RESULTS	187
PHF8 and G9a regulate a subset of inflammatory protein secretion in LPS- induced macrophages in a phenotype-dependent manner	187
PHF8 is a G9a-antagonist that regulates the inflammatory phenotype in acute inflammation	188
PHF8 and G9a are antagonistic regulators of translation, immune response, and cell adhesion/communication	189
DISCUSSION	190
FUTURE WORK.....	192
FIGURES.....	193
APPENDIX 1: T-CLASS SECRETOME	204
APPENDIX 2 : NT-CLASS SECRETOME.....	206
APPENDIX 3: COMMON PROTEINS WITH SECRETOME FROM MEISSNER ET AL.	207
APPENDIX 4: COMMON PROTEINS WITH SECRETOME FROM LIU ET AL.	210
APPENDIX 5: COMMON PROTEINS WITH LPS-INDUCIBLE SECRETOME FROM LIU ET AL.....	216
APPENDIX 6: PHF8-G9a COMMON SECRETOME	217
REFERENCES.....	222

LIST OF TABLES

Table 1 TLR ligands and cellular localization (Kumar et al, 2011)	34
Table 2 Histone lysine methyltransferases	42
Table 3 Epigenetic regulators with phosphosites in the phosphoproteome dataset.....	76
Table 4 ET-specific PP2Ac-targeted phosphosites of chromatin regulators	79
Table 5 Primer Sequences for qPCR	116
Table 6 Secretory products of mononuclear phagocytes (Manes et al, 2011).	135
Table 7 Macrophage products with similar activities (Manes et al, 2011).....	137
Table 8 Enzymes secreted by macrophages (Takemura & Werb, 1984).....	137
Table 9 Primer Sequences used in the qPCR of T-cell regulatory genes.....	146
Table 10 List of cytokines and chemokines identified in the LPS-inducible secretome	150
Table 11 T-class GOBP enrichment.....	151
Table 12 DAVID analysis of functionally active PHF8 targets (Wang et al, 2014a).....	155

LIST OF FIGURES

Figure 1 TLR structure.....	48
Figure 2 Mammalian TLR signaling pathways	48
Figure 3 Domain structure of the NFκB signaling proteins	49
Figure 4 NFκB dimers	49
Figure 5 NFκB bound to IκB proteins	50
Figure 6 Phosphorylated residues of p65 (RelA).....	50
Figure 7 Model of regulation of NFκB transactivation through phosphorylation.....	51
Figure 8 Chromatin modifications and regulators	52
Figure 9 Dynamic epigenetic regulation.....	53
Figure 10 Modifications of the histone histone tails	54
Figure 11 Chemical mechanism for FAD-dependent demethylation	55
Figure 12 Schematic diagrams of LSD1 Domains	55
Figure 13 Chemical mechanism for demethylation by JmjC	56
Figure 14 Structure of JMJD2A bound to substrate.....	56
Figure 15 Proinflammatory gene silencing by G9a during endotoxin tolerance.....	57

Figure 16 G9a stabilizes c-Myc and promotes cell survival in ET.....	57
Figure 17 Regulatory function of SET7/9 on NFκB and inflammatory gene expression	58
Figure 18 Role of PP2A in various signaling pathways	86
Figure 19 Schematic representation of diversity of the PP2A holoenzymes.....	87
Figure 20 Chronic-active PP2Ac regulates chromatin modifications	88
Figure 21 Schematic representation of phosphoprotein analysis workflow.....	89
Figure 22 Proteomic analysis using two-dimensional gel electrophoresis.....	90
Figure 23 Quantitative phosphoproteomics workflow.....	91
Figure 24 Phosphoproteomic analysis shows 99% phospho-enrichment efficiency.	91
Figure 25 Identified phosphopeptides mostly cover single phosphorylation	92
Figure 26 Distribution of Phospho STY identifications.....	92
Figure 27 Identified mass error.....	93
Figure 28 The top signaling pathways targeted by PP2Ac in ET macrophages	93
Figure 29 Top signaling pathways that are targeted by PP2Ac.....	98
Figure 30 PP2Ac affects a borad range of signaling pathways in ET.....	98
Figure 31 PP2Ac negatively regulates ATM signaling.....	99

Figure 32 The MS spectra of KDMs that are dephosphorylated by PP2Ac in ET.	100
Figure 33 The MS spectra of KMTs that are targeted by PP2Ac in ET.	101
Figure 34 The MS spectra of PP2Ac-targeted deacetylases and acetyltransferases.	102
Figure 35 MS-MS Spectra of known PP2Ac targets.	103
Figure 36 Growth factors and insulin regulation of mTORC signaling via AKT.	104
Figure 37 Histone PTM changes regulated by PP2Ac activity in ET.	105
Figure 38 The MS/MS (Left) and MS (Right) spectra of PHF8 phosphopeptides.	105
Figure 39 Domain structure and repeats of PHF8.	125
Figure 40 Mouse and human PHF8 sequence alignment.	125
Figure 41 The JmjC domain contains residues required for Fe(II) and α KG binding.	126
Figure 42 Transcriptional transcriptional co-activation by KDM7-family proteins.	127
Figure 43 Knockdown of PHF8 on mouse macrophage RAW cell line.	127
Figure 44 PHF8 regulates LPS-induced demethylation of H3K9me1/me2.	128
Figure 45 PHF8 regulates nuclear translocation of p65 in LPS response.	129
Figure 46 PHF8 is co-immunoprecipitated with p65.	129

Figure 47 PHF8 forms an LPS-inducible complex with p65.....	130
Figure 48 Nucleus-specific CoIP of PHF8 and p65	130
Figure 49 PHF8 positively regulates the transcriptional activity of p65.....	131
Figure 50 PHF8 regulates the expression of select pro-inflammatory cytokines.	132
Figure 51 Schematic of ELISA procedure.	164
Figure 52 Scheme of the protein profiling process with antibody microarrays.....	165
Figure 53 Workflow of the LFQ secretome analysis	166
Figure 54 Immunoblot of cell lysates for phenotype detection.....	166
Figure 55 Scatter plots showing Pearson correlation of samples.	167
Figure 56 The LFQ secretome heatmap	168
Figure 57 Comparison of the secretome to previous studies	169
Figure 58 T-class GOBP (Erdoğan et al, 2016).	170
Figure 59 T-class PHF8-dependent KEGG pathways (Erdoğan et al, 2016).	171
Figure 60 Processes associated with activated PHF8.	171
Figure 61 T-class GOCC (Erdoğan et al, 2016).	172
Figure 62 Detailed map of the human MHC	173

Figure 63 T-class GOMF (Erdoğan et al, 2016).	174
Figure 64 The overall protein-protein interaction network of the T-class secretome	175
Figure 65 IPA network analysis of T-class secretome	176
Figure 66 PHF8 regulates the mRNA expression of T cell activating proteins	177
Figure 67 T cell activation markers	178
Figure 68 T cell proliferation assay.....	179
Figure 69 Histone H3K9 methyltransferases (HMTs) and demethylases (HDMs).....	193
Figure 70 G9a structure.	193
Figure 71 Transcriptional repression and activation by G9a.....	194
Figure 72 G9a regulates hypoxia response.....	195
Figure 73 GOBP enrichment of the common secretome.....	196
Figure 74 GOMF enrichment of the common secretome	197
Figure 75 GOCC enrichment of the common secretome	198
Figure 76 Protein-protein interaction network of the common secretome.....	199
Figure 77 Top 10 canonical pathways regulated antagonistically by G9a and PHF8.....	200
Figure 78 Canonical pathways in cross talk regulated by both G9a and PHF8.....	201

Figure 79 Upstream regulators and targeted canonical pathways	202
Figure 80 The mechanism of the G9a- vs PHF8- dependent chromatin plasticity	203

LIST OF ABBREVIATIONS AND SYMBOLS

2D	Two-dimensional
53BP1	p53-binding protein 1
5mC	methylation of the 5 position of the pyrimidine ring of cytosine
AACT	Amino-acid-coded mass tagging
ACN	Acetonitrile
ADAM17	metalloproteinase domain-containing protein 17
ADAM8	metalloproteinase domain-containing protein 8
AP1	Activating Protein 1
APL	Acute promyelocytic leukemia
APP	amyloid precursor protein
AR	androgen receptor
ASH1	Absent, small, or homeotic 1
ASH1L	Ash1 Like
ATRA	All-trans retinoic acid
B2m	beta-2-microglobulin
BCL-3	B-cell lymphoma-3
Bcl2	B-cell Lymphoma 2
BMDM	bone marrow-derived macrophages
BP	Biological Processes
Brd4	Bromodomain Containing protein 4
CASP3	Caspase 3

CBP	CREB-binding Protein
CDK	Cyclin-dependent kinase
CDK	Cyclin-dependent kinase
CDS	Cytosolic DNA sensors
CEBP	CCAAT-enhancer binding protein
Cfb	Complement Factor B
Cfh	Complement Factor H
CFSE	Carboxyfluorescein diacetate succinimidyl ester
ChEP	Chromatin enrichment for proteomics
ChIP	Chromatin immunoprecipitation
ChIP-seq	ChIP-sequencing
CID	Collision-induced dissociation
CKII	Casein kinase II
CKII	Casein kinase II
CL/P	cleft lip/palate
CLR	C-type lectin receptors
CoIP	co-immunoprecipitation
CoREST	Corepressor for element-1-silencing transcription factor
CREB	cAMP response element-binding protein
CSF	Macrophage colony stimulating factor
CtBP	C-terminal binding protein
Ctsb	cathepsin B
DD	Death Domain

DM	Demethylases
DMEM	Dulbecco's minimal essential media
DMP	Dimethyl Pimelimidate
DNMT	DNA Methyl-transferase
DNMT3A/B	DNA Methyl-transferase 3A/B
Dot1	Disruptor of telomeric silencing
dsDNA	Double stranded DNA
DTT	Dithiothreitol
DTX1	Deltex 1
ECL	enhanced chemiluminescence
EIF2	Eukaryotic initiation factor 2
ELISA	Enzyme-linked immunosorbent assay
ESCC	Esophageal squamous cell carcinoma
ET	Endotoxin tolerance
EV	empty vector
EZH2	Enhancer of zeste 2 polycomb repressive complex 2 subunit
FAD	flavin adenine dinucleotide
FBS	Fetal bovine serum
FBXL11	F-box LRR protein 11
FDR	false-discovery-rate
FOXP3	Forkhead box P3
GAPDH	Glyceraldehyde 3-phosphate dehydrogenase
GO	Gene Ontology

GOBP	GO Biological Processes
GOCC	GO Cellular Components
GOMF	GO Molecular Functions
GSK3 β	Glycogen synthase kinase-3 Beta
H3PO4	phosphoric acid
HAT	Histone acetyl-transferase
HDAC	Histone deacetylase
HES1	hairy and enhancer of split-1
HIF1- α	Hypoxia-inducible factor 1-alpha
HIPK2	Homeodomain Interacting Protein Kinase 2
HP1	Heterochromatin protein 1
IAA	iodoacetamide
Icam1	intercellular adhesion molecule 1
ID	Intermediate domain
Ifi30	IFN γ -Inducible Protein 30
IFN β	Interfeuron- β
IFN γ	Interfeuron- γ
IKK	I κ B kinase
IL-1	Interleukin-1
IL-1R	Interleukin-1 Receptor
IL10	Interleukin 10
IL27	Interleukin 27
IL6	Interleukin 6

IL7R	IL7 Receptor
IL8	Interleukin 8
ILF3	Interleukin Enhancer Binding Factor 3
IMAC	Immobilized Metal Affinity Chromatography
IPA	Ingenuity Pathway Analysis
IRAK	IL-1R-associated kinase
Itga4	Integrin alpha 4
Itgb2	Integrin beta 2
Itmb2	integral membrane protein 2B
IκB	Inhibitor of kappaB
JARID1A	Jumonji/ARID domain-containing protein 1A (KDM5a or RBP2)
JARID1B	Jumonji/ARID domain-containing protein 1B or KDM5B
JmjC	Jumonji C-terminal domain
Jmjd2	Jumonji domain-containing 2
JmjN	Jumonji N-terminal domain
KDM	Lysine demethylase
KDM1A	Lysine demethylase 1
KDM5A	Lysine-specific Demethylase 5A also known as JARID1A or RBP2
KDM5B	Lysine demethylase 5B or JARID1B
KEGG	Kyoto Encyclopedia of Genes and Genomes
Kme	Lysine methylation
KMT	Lysine methyltransferase
LC	Liquid chromatography

LC-MS/MS	Liquid chromatography-tandem mass spectrometry
LFQ	Label-free Quantification
Lgals3BP	Lectin-Galactoside-Binding Soluble 3-Binding Protein
LHSCC	Laryngeal and hypopharyngeal squamous cell carcinoma
Lif	Leukemia inhibitory factor
LPS	Lipopolysaccharide
LRR	Leucine-rich repeat
LSD1	lysine-specific demethylase 1
Ly86	lymphocyte antigen 86
m/z	Mass-to-charge ratio
MCES	mRNA cap guanine-N7 methyltransferase
MCM	minichromosome maintenance
MD2	Lymphocyte antigen 96
MeCP2	methyl CpG binding protein 2
MHC	Major histocompatibility complex
MLL	Mixed lineage leukemia
MS	Mass spectrometry
MS/MS	tandem mass spectrometry
MSK1	Mitogen- and stress-activated protein kinase 1
MT	Methyltransferases
mTOR	Mechanistic target of rapamycin
MyD88	Myeloid differentiation primary response gene 88
MyD88s	MyD88short

MYND	Myeloid, Nervy, and DEAF1
MyoD	Myoblast determination protein
NEMO	NFκB essential modulator
NFκB	Nuclear factor kappa B
NLR	NOD-like receptors
NLS	Nuclear localization signal
NOTCH3	Neurogenic locus notch homolog protein 3
NSCLC	Non-small cell lung cancer
NSD1	Nuclear receptor-binding SET domain-containing protein 1
NSD2	Nuclear SET domain-containing protein 2
NSD3	Nuclear SET domain-containing protein 3
NT	Non-tolerizable
OA	Okadaic acid
P-p65	Phosphorylation of p65 at Ser536
PAMP	Pathogen-associated molecular patterns
PcG	Polycomb-group
PCR	Polymerase chain reaction
PHD	Plant Homeodomain
PHF8	PHD finger 8
PHF8-KD	PHF8 Knock-down
PKAc	Cyclic AMP-dependent kinase
PKCζ	Protein kinase C-ζ
PLAUR	Urokinase plasminogen-activator surface receptor

PP1 γ	protein phosphatase 1 γ
PP2A	Protein phosphatase-2A
PP2AA	Protein phosphatase-2A scaffold subunit
PP2AB	Protein phosphatase-2A regulatory subunit
PP2Ac	Protein phosphatase 2A catalytic domain
PP2Ac-KD	PP2Ac Knock-down
PP4	protein phosphatase 4
PPI	Protein-protein interaction
PPM1D	Protein Phosphatase, Mg ²⁺ /Mn ²⁺ Dependent, 1D
PPPs	Phosphoprotein phosphatases
PRC	Polycomb repressive complex
PrCA	Prostate cancer
PRMT5	Protein arginine methyltransferase 5
PRR	Pattern recognition receptors
PSPs	protein serine/threonine phosphatases
PTM	Post-translational modification
PVDF	Polyvinylidene fluoride
Pvrl1	poliovirus receptor-related 1
PYPs	phosphotyrosine phosphatases
qPCR	Real-time Polymerase chain reaction
Rac1	Ras-related C3 botulinum toxin substrate 1
RBP2	Retinoblastoma-binding protein 2 (KDM5a or JARID1A)
rDNA	ribosomal DNA

RHD	Rel-homology domain
RhoA	Ras homolog gene family, member A
RLR	RIG-like receptors
RNA-Pol	RNA polymerase II
RP	Reverse phase
rRNA	ribosomal RNA
RSK1	Ribosome-associated kinase-1
RT	room temperature
SAM	S-adenosylmethionine
SATB2	Special At-rich sequence-binding protein 2
SCX	strong cation exchange chromatography
Sdc4	syndecan 4
SDS-PAGE	sodium dodecyl sulfate polyacrylamide gel electrophoresis
SDS3	Suppressor of defective silencing 3 protein homolog
SerB	phosphoserine phosphatase
SET	Su(var)3-9, Enhancer-of-zeste and Trithorax
Set7	SET domain protein 7
Set9	SET domain protein 9
shCON	Wild-type
shPHF8	PHF8 Knock-down
SIRT1	Sirtuin 1
Smyd2	SET and MYND domain containing 2
SMYD3	SET, and MYND domain-containing 3

SOCS1	suppressor of cytokine signaling 1
SRGN	serglycin
STAT6	Signal Transducers and Activators of Transcription 6
STRING	Search Tool for the Retrieval of Interacting Genes/Proteins
Suv39h1	Suppressor Of Variegation 3-9 Homolog 1
SWI/SNF	Switch/Sucrose Non-Fermentable
T-class	“tolerizeable”
TAD	Trans-activation domain
TAK1	TGF- β -associated kinase 1
TAP	Tandem affinity purification
TFA	Trifluoroacetic acid
TGF- β	Transforming growth factor- β
Th	T helper cell
TiO ₂	Titanium dioxide
TIR	Toll-IL-1R
TLR	Toll-like receptors
TLR4/MD2	TLR4/Lymphocyte antigen 96 complexes
TNF	Tumor necrosis factor
TNFR	Tumor necrosis factor receptor
Tnfsf9	TNF Superfamily Member 9
TNF α	Tumor necrosis factor α
TP53	Tumor protein p53
TRAF6	TNFR-associated factor 6

TREM2	Triggering receptor expressed on myeloid cells 2
TRIF	TIR-domain containing adapter-inducing interferon β
TRM6	tRNA (adenine-N(1)-)-methyltransferase non-catalytic subunit
URA	Upstream Regulator Analysis
WD	Tryptophan-Aspartic acid
WDR5	WD-repeat domain 5
WIP1	wild-type p53-induced phosphatase 1
WT	Wild-type
XIC	Extracted ion chromatograms
XLMR	X-linked mental retardation
α KG	2-oxoglutarate or α -keto-glutarate

CHAPTER 1: INTRODUCTION

OVERVIEW

The mammalian immune system is a complicated and tightly regulated system that can recognize self and non-self cells or molecules, providing protection from a wide variety of pathogens. Recognition of non-self molecules leads cells of immunity to activate various signaling pathways, which lead to activation or repression of specific genes to induce inflammation response. At the core of this gene-specific regulation of inflammation is the chromatin remodeling. As the need to understand the tight regulation of epigenetics in inflammation response increases, various chromatin modifiers functioning as pro- or anti-inflammatory factors have been studied extensively. Here I provide an overview of innate immunity, Toll-like receptors (TLR), and epigenetic regulation of both transcription and inflammation response through methylation.

INNATE IMMUNITY AND TOLL-LIKE RECEPTORS

Mammalian immunity is composed of two systematic layers: innate and adaptive immunity. They are responsible for recognition of pathogens and elimination of them, respectively. As the first line of host defense, pathogen recognition in innate immunity is achieved through activation of pattern recognition receptors (PRRs). PRRs are activated through recognition of the specific pathogen-associated molecular patterns (PAMPs) (Janeway & Medzhitov, 2002). Currently the main PRRs known in the innate

immune system are the TLR, the NOD-like receptors (NLR), the RIG-like receptors (RLR), cytosolic DNA sensors (CDS), and the C-type lectin receptors (CLR) (Kawai & Akira, 2011). The first PRR family to be identified and most widely studied was TLR that recognizes a wide range of PAMPs and activates downstream pathways.

As type I transmembrane proteins, TLRs are composed of an extracellular ectodomain containing Leucine-rich-repeat (LRR) motif and a cytoplasmic Toll-interleukin-1 Receptor (Toll-IL-1R or TIR) domain responsible for relaying the signal to the downstream adapters (Akira et al, 2006) (**Figure 1A**). LRR domain consists of 19-25 tandem copies of the leucine-rich motif of 24-29 amino acids such as *XLXXLXLXX* and *XΦXXΦXXXXFXXLX* where *X* represents any amino acid and *Φ* represents a hydrophobic amino acid (**Figure 1B**) (Akira & Takeda, 2004). These repeats are composed of a β -strand and an α -helix connected with loops creating a concave surface responsible for ligand recognition (**Figure 1C-D**). On the other hand, TIR domains have only 20-30% sequence homology with three conserved regions required for signaling.

TLRs are divided into subfamilies based on the ligand they recognize: TLR1, TLR2, and TLR6 recognize lipids, TLR7, TLR8, and TLR9 recognize nucleic acids, TLR3 recognizes double stranded DNA (dsDNA) from viruses, TLR4 recognizes lipopolysaccharide (LPS) from Gram-negative bacteria, and TLR5 recognizes flagellin from Flagellated bacteria (**Figure 2, Table 1**) (Akira et al, 2006).

Table 1 TLR ligands and cellular localization (Kumar et al, 2011)

TLR and (co-receptors)	Cellular localization	TLR ligands
TLR1/2	Cell surface	Triacyl lipopeptides
TLR2 (Dectin-1, C-type lectin)	Cell surface	Peptidoglycan, lipoarabinomannan, hemagglutinin, phospholipomannan, glycosylphosphatidyl inositol mucin, zymosan
TLR3	Endosome	ssRNA virus, dsRNA virus, respiratory syncytial virus, murine cytomegalovirus
TLR4 (MD2, CD14, LBP)	Cell surface	Lipopolysaccharide, mannan, glycoinositolphospholipids, envelope and fusion proteins from mammary tumor virus and respiratory syncytial virus, respectively, endogenous oxidized phospholipids produced after H5N1 avian influenza virus infection, pneumolysin from <i>streptococcus pneumonia</i> , paclitaxel.
TLR5	Cell surface	Flagellin from flagellated bacteria
TLR6/2 (CD36)	Cell surface	Diacyl lipopeptides from mycoplasma, lipoteichoic acid
TLR7	Endolysosome	ssRNA viruses, purine analog compounds (imidazoquinolines). RNA from bacteria from group B streptococcus
TLR8 (only in human)	Endolysosome	ssRNA from RNA virus, purine analog compounds (imidazoquinolines).
TLR9	Endolysosome	dsDNA viruses herpes simplex virus and murine cytomegalovirus, CpG motifs from bacteria and viruses, hemozoin malaria parasite
TLR11 (only in mouse)	Cell surface	Uropathogenic bacteria, profilin-like molecule from <i>Toxoplasma gondii</i>

Upon ligand recognition, TLRs induce host defense genes through activation of two major downstream pathways based on the adapter protein involved: Myeloid differentiation primary response gene 88 (MyD88)-dependent and MyD88-independent, also known as TIR-domain containing adapter-inducing interferon- β (TRIF)-dependent, pathways (Janeway & Medzhitov, 2002). All TLRs except TLR3 are MyD88-dependent pathways while TLR4 stimulation activates both MyD88-dependent and –independent pathways (**Figure 2**). Throughout this dissertation, I focused mainly on studying the events downstream MyD88-dependent TLR4 signaling.

MyD88-Dependent Signaling

Since MyD88 is involved in all TLR signaling pathways except TLR3, it is critical for innate immunity signaling responses (Akira & Takeda, 2004). The structure of

MyD88 is composed of a C-terminal TIR domain, an N-terminal Death Domain (DD), and a short intermediate domain (ID) (Lin et al, 2010). TIR domain is responsible for the recruitment of MyD88 as a scaffold to the activated TLR to relay the signal to downstream elements (Ohnishi et al, 2009). On the other hand, DD is responsible for homophilic interaction with the downstream elements such as IL-1R-associated kinases (IRAKs) IRAK-1 and IRAK-4 (Akira et al, 2006). Activated IRAKs associate with Tumor necrosis factor (TNF) receptor (TNFR)-associated factor 6 (TRAF6), inducing ubiquitination of the Inhibitor of kappaB (I κ B) kinase (IKK)/Nuclear factor kappaB (NF κ B) essential modulator (NEMO) complex and itself. In addition, another complex composed of Transforming growth factor- β (TGF- β)-activated kinase 1 (TAK1) and TAK1 binding proteins is recruited to TRAF6. TAK1 recruitment is crucial for phosphorylation and subsequent activation of IKK- β for the degradation of I κ B, which in return exposes the nuclear-localization signal, thus enables the early-phase activation of NF κ B transcription factor for the pro-inflammatory cytokine expression (**Figure 2**).

NF κ B IN INFLAMMATION RESPONSE

Downstream TLR pathways, transcription factor NF κ B regulates the transcription of many immune response-related genes such as cytokines, growth factors, effector enzymes in response to activation of immunity-related receptors (Hayden & Ghosh, 2004). Proteins in the NF κ B family are divided into two subfamilies called the 'NF κ B' and the 'Rel' proteins, all of which include an amino-terminal conserved DNA-binding/dimerization domain called the Rel-homology domain (RHD) (**Figure 3**) (Gilmore, 2006). The NF κ B subfamily proteins p100 and p105 are

comprised of an inhibitory C-terminus with multiple ankyrin repeat domains; they get activated through removal of these inhibitory domains by proteolysis leading to the exposure of the active forms p52 and p50, respectively (Hoffmann & Baltimore, 2006). These activated forms, as they don't have trans-activation domains (TADs), require heterodimerization with the Rel proteins to initiate transcription (Hayden & Ghosh, 2012). The Rel proteins p65/RelA, RelB, and RelC have a C-terminal TADs, which can activate transcription across many species although their sequences are not conserved the same way (Gilmore, 2006). All five members of NF κ B family can form homodimers or heterodimers in vivo, except RelB, which exists only in heterodimers in vivo (**Figure 4**). The variety of different homodimers and heterodimers create a multi-layered regulation system as different dimers have different DNA-binding site specificities and protein-protein interactions at the promoters.

In this thesis, I mainly focus on the transcriptional activity of the p65 subunit downstream MyD88-dependent TLR4 pathways, because its nuclear translocation and DNA-binding are indicators of transcriptional activation of NF κ B target genes.

I κ B Family Proteins Regulate p65 Activity

NF κ B activity is regulated by interaction with seven I κ B family proteins I κ B α , I κ B β , I κ B γ , I κ B ϵ , B-cell lymphoma-3 (BCL-3), I κ B ζ , and I κ B η as well as the precursor proteins p100 and p105 (Hayden & Ghosh, 2012). I κ B family proteins contain five to seven ankyrin repeats that modulate the interaction NF κ B proteins (Hayden & Ghosh, 2004). This interaction covers the Nuclear localization signal (NLS) of p65 to successfully keep it in the inhibited state in the cytosol (**Figure 5**) (Gilmore, 2006). Through this inhibitory mechanism, the degradation of I κ Bs or the increased expression

of I κ Bs by NF κ B transcriptional activity leads to the dynamic balance between nuclear and cytoplasmic localization of NF κ B, respectively (Sun & Andersson, 2002).

Regulation of Transcriptional Activity of p65 via Phosphorylation

NF κ B activity is also regulated by post-translational modifications (PTMs), such as phosphorylation, acetylation, and methylation. Currently, phosphorylation of **p65** is the most common and most widely studied NF κ B PTM because it is associated with rapid transactivation and transcriptional activity of p65 (**Figure 6, Figure 7**) (Vermeulen et al, 2006); thus, in this overview I will focus on the p65 regulation through phosphorylation.

Currently, five phosphorylation sites have been discovered to regulate p65 activity: S276, S311, S468, S529, and S536 (**Figure 6**). S276 resides in the RHD and gets phosphorylated by cyclic AMP-dependent kinase (PKAc) (Zhong et al, 1997) and by Mitogen- and stress-activated protein kinase 1 (MSK1) upon TNF treatment (Vermeulen et al, 2003). Phosphorylation of this site is essential for gene activation (Zhong et al, 1998). Another important phosphorylation is the phosphorylation of S311 by Protein kinase C- ζ (PKC ζ) that is responsible for recruitment of cAMP response element binding protein (CREB)-binding Protein (CBP) and RNA polymerase II (RNA-Pol II) to the IL-6 promoter (Duran et al, 2003). Moreover, S529 is phosphorylated by casein kinase II (CKII) (Wang & Baldwin, 1998) and IKK2 enhancing transactivity of p65 (Sakurai et al, 1999). In addition to S529, IKK2 also phosphorylates S536 for transactivation upon I κ B phosphorylation leading to enhanced binding to promoters with LPS stimulation. Ribosomal S6-kinase 1 (RSK1) also phosphorylates S536 through DNA damage response via p53 signaling (Bohuslav et al, 2004). In contrary to the other

p65 phosphorylation sites, S468 phosphorylation is known as a negative regulator of transcription factor activity of p65 upon TNF or IL-1 (Buss et al, 2004; Mattioli et al, 2004).

It is important to note that the dynamic regulation of p65 phosphorylation status is sustained by the interplay between kinases and phosphatases. Protein phosphatase-2A (PP2A), protein phosphatase 4 (PP4), protein phosphatase 1 γ (PP1 γ), wild-type p53-induced phosphatase 1 (WIP1), and phosphoserine phosphatase (SerB) are some of the known negative regulators of p65 keeping it in the inactive state (Peng et al, 2015; Takeuchi et al, 2013; Yang et al, 2001; Yeh et al, 2004).

ENDOTOXIN TOLERANCE

Inflammatory response, if persistent, may lead to severe reaction in the form of chronic inflammation since excessive cytokine production is harmful to the host (Beutler et al, 1985; Kanterman et al, 2012). Thus, the immune system is programmed to turn off inflammation to prevent tissue damage by immunosuppression. This phenomenon is called endotoxin tolerance (ET) (Dobrovolskaia & Vogel, 2002).

There are multiple inhibitory mechanisms that regulate endotoxin tolerance. *First*, the expression and availability of the surface receptors are affected by the second exposure to the endotoxin (Fujihara et al, 2003). In ET, RAW 264.7 cells show decreased mRNA expression of TLR4 (Poltorak et al, 1998) as well as decreased association of TLR4/Lymphocyte antigen 96 complexes (TLR4/MD2) (Akashi et al, 2000; Nomura et al, 2000). *Second*, the signaling pathway downstream the receptor gets interrupted. For example, ET leads to decreased IKK activation (Kohler & Joly, 1997),

I κ B degradation (Medvedev et al, 2000), NF κ B translocation (Fujihara et al, 2000; Kohler & Joly, 1997; Medvedev et al, 2000), IRAK-1 activation (Jacinto et al, 2002; Li et al, 2000), and ratio of p50/p65 heterodimers to p50/p50 homodimers (Adib-Conquy et al, 2000). In addition, increased negative regulators of TLR signaling, such as kinase IRAK-M (Kobayashi et al, 2002), suppressor of cytokine signaling 1 (SOCS1) (Kinjyo et al, 2002), and MyD88short (MyD88s) (Burns et al, 2003), a short alternative spliced form of MyD88 lacking the ID, contributes to the ET. *The last inhibitory mechanism* is the regulation of secreted proteins/mediators via prolonged LPS stimulation, downregulating of cytokine expression in ET (Fujihara et al, 2003). For example, prolonged LPS-induced Interleukin 10 (IL10) secretion in macrophages disrupts expression of other inflammatory molecules such as cytokine Interfeuron- γ (IFN γ) (Varma et al, 2001), Tumor necrosis factor α (TNF α), Interleukin 6 (IL6), and macrophage colony stimulating factor (CSF) in ET (Berlato et al, 2002). Similarly, increased Interfeuron- β (IFN β) leads to decreased TNF α and Interleukin 8 (IL8) expression in ET (Zaric et al, 2011).

ET, or also known as acquired immune tolerance, including that to endotoxin or LPS, if deregulated, is a major molecular feature of the pathogenesis of many chronic diseases including asthma, sepsis, and cancer (Biswas & Tergaonkar, 2007). Deciphering the mechanisms that regulate LPS-induced diverse inflammatory responses will be beneficial for diagnosis of, prevention of, and therapies for various inflammation-associated diseases.

EPIGENETIC REGULATION OF INFLAMMATION RESPONSE

Inflammation response is also regulated at the epigenetic level by the LPS-induced gene-specific chromatin modifications, whereby the promoters of a select class of pro-inflammatory or “tolerizeable” (T-class) genes have differentially programmed chromatin based on the “inflammatory-phenotype”, acutely versus chronically inflamed nature, of the stimulated cells (Foster et al, 2007).

As the core components of the chromatin, the properties of histones can be altered by different PTMs to their N- terminal “tails” that leads to a predetermined combination of histone marks known as the “histone code” (Strahl & Allis, 2000). These differentially modified histone marks determined whether the promoter they are in is in an open/active or closed/repressed chromatin state called euchromatin or heterochromatin, respectively (**Figure 8**); thus, gene-specific transcription is regulated through histone PTMs to achieve specific biological outcomes, such as inflammation response (Adcock et al, 2007). The histone PTMs are added or removed by different enzymes termed “writers” and “erasers”, respectively (**Figure 8, Figure 9**) (Falkenberg & Johnstone, 2014). Moreover, to signal for recruitment and activity of downstream effectors, histone “readers” are recruited to histone PTM sites (Yun et al, 2011).

Currently there are various PTMs known to modify histone N-tails: methylation, acetylation, phosphorylation, citrullination, ubiquitination, SUMOylation, ADP-ribosylation, and proline isomerization (**Figure 10**) (Bayarsaihan, 2011; Rothbart & Strahl, 2014). DNA is also modified by methylation of the 5 position of the pyrimidine ring of cytosine (5mC) in somatic cells accompanying the histone PTMs for certain biological outcomes (Klose & Bird, 2006). Histone PTMs are known as highly dynamic

and reversible modifications and are regulated by the enzymatic activity of histone modifying enzymes such as acetyltransferases, deacetylases, methyltransferases, demethylases, kinases, phosphatases, ubiquitilases, and proline isomerases (Kouzarides, 2007). Here, I will focus on histone methylation since the scope of this research is more relevant to this PTM and provide information on how this PTM is regulated.

Epigenetic Regulation of Transcription Through Methylation PTM

Histone lysine methylation (Kme) is the most widely studied chromatin PTM with six well characterized lysines including H3K4, -9, -27, -36, -79, and H4K20 (Shi & Whetstine, 2007). In eukaryotes, Kme patterns regulate the chromatin architecture by dictating activated or repressed conformation (Barski et al, 2007). Particularly on histone H3, the transcription-associated Kme occurs at multiple lysine residues: methylated H3K4, H3K36, and H3K79 are associated with transcriptional activation of specific genes while methylated H3K9 and H3K27 are associated mostly with gene repression (Martin & Zhang, 2005). Site-specific Kme levels are tightly regulated by the antagonistic activities of lysine methyltransferases (KMTs) and lysine demethylases (KDMs) to maintain cell homeostasis. Specific biological processes that promote gene activation, such as induced inflammatory response, require coordinated changes in the activity of LPS-induced KMTs and KDMs increasing the activating methylation marks while decreasing the repressive methylation marks, respectively, at the promoters of those specific genes.

Histone lysine methyltransferases catalyze the transfer of a methyl-group from S-adenosylmethionine (SAM) to a lysine's ϵ -amino group (Bannister & Kouzarides, 2011). All KMTs, except Disruptor of telomeric silencing (Dot1), are comprised of a

conserved globular catalytic domain, which is called Su(var)3-9, Enhancer-of-zeste and Trithorax (SET) domain. KMTs are relatively specific; they modify the target lysine to a specific degree (mono-, di-, or tri-methyl state); for instance SET domain proteins 7 and 9 (Set7/9) can only mono-methylate H3K4. Various targets of known KMTs are listed in **Table 2**.

Table 2 Histone lysine methyltransferases
Methyltransferases, their target site, and function (Bannister & Kouzarides, 2011)

K-methyltransferases (KMTs)		Site	Function
KMT1A	Suv39H1	H3K9	Heterochromatin formation/silencing
KMT1B	Suv39H2	H3K9	Heterochromatin formation/silencing
KMT1C	G9a	H3K9	Heterochromatin formation/silencing
KMT1D	Eu-HMTase/GLP	H3K9	Heterochromatin formation/silencing
KMT1E	ESET/SETDB1	H3K9	Transcriptional repression
KMT1F	CLL8		
KMT2A	MLL1	H3K4	Transcriptional activation
KMT2B	MLL2	H3K4	Transcriptional activation
KMT2C	MLL3	H3K4	Transcriptional activation
KMT2D	MLL4	H3K4	Transcriptional activation
KMT2E	MLL5	H3K4	Transcriptional activation
KMT2F	hSET1A	H3K4	
KMT2G	hSET1B	H3K4	
KMT2H	ASH1	H3K4	
KMT3A	SET2	H3K36	Transcriptional activation
KMT3B	NSD1	H3K36	
KMT3C	SYMD2	H3K36/p53	Transcriptional activation
KMT4	DOT1L	H3K79	Transcriptional activation
KMT5A	Pr-SET7/8	H4K20	Transcriptional repression
KMT5B	SUV4-20H1	H4K20	DNA damage response
KMT5C	SUV4-20H2		
KMT6	EZH2	H3K27	Polycomb silencing
KMT7	SET7/9	H3K4/p53/TAF10	
KMT8	RIZ1	H3K9	Transcriptional repression

KMTs that belong to mixed lineage leukemia (MLL) protein family including MLL1, MLL2, MLL3, MLL4, SET1A, SET1B, and Absent, small, or homeotic 1 (ASH1) methylate H3K4 (Wang & Zhu, 2008). This family of KMTs are involved in development, and genetics, while MLL1 gene mutations were found associated with leukemia. In

addition, H3K4 is methylated by SET, and Myeloid, Nervy, and Deformed epidermal Autoregulatory Factor 1 (MYND) domain-containing 3 (SMYD3) during gene activation (Gibbons, 2005).

H3K9 methylation is involved in many biological processes such as transcriptional regulation, X chromosome silencing, heterochromatin formation, and DNA methylation (Wang & Zhu, 2008). One of the most widely studied H3K9 KMT is G9a, which dimethylates H3K9 in euchromatic regions; this G9a-mediated H3K9 methylation is responsible for the silencing of individual genes (Martin & Zhang, 2005). In addition to G9a, KMT Suppressor Of Variegation 3-9 Homolog 1 (Suv39h1) methylates H3K9 (Wang & Zhu, 2008). Suv39h1 targets both euchromatin and heterochromatin and regulates heterochromatin formation as well as transcriptional inhibition by tri-methylating H3K9. Moreover, Suv39h1-dependent H3K9 methylation recruits the chromodomain of Heterochromatin protein 1 (HP1) during meiosis and cell cycle leading to DNA methylation for transcriptional repression (Biel et al, 2005; Martin & Zhang, 2005; Peters et al, 2001).

H3K27 methylation is catalyzed by Enhancer of zeste 2 polycomb repressive complex 2 subunit (EZH2), which forms the Polycomb repressive complex (PRC) with other Polycomb-group (PcG) proteins (Wang & Zhu, 2008). As an H3K27 methyltransferase, EZH2 has an inhibitory effect on transcription and is known to regulate cell differentiation, fetal development, cell proliferation, and X chromosome inactivation (Biel et al, 2005; Wang & Zhu, 2008).

Histone demethylation was considered irreversible for decades due to the stability of the C-N bond (Mosammaparast & Shi, 2010). The first experimental evidence for an enzyme that catalyzes demethylation was the functional characterization of lysine-specific demethylase 1 (LSD1, also known as KDM1A) as a member of the *amine oxidase superfamily* (Shi et al, 2004). Demethylation by the amine oxidases occurs through cleavage of the α -carbon bond of the substrate leading to an imine intermediate that further gets hydrolyzed to produce an aldehyde and amine (Shi & Whetstine, 2007). This is a flavin adenine dinucleotide (FAD)-dependent reaction that requires a protonated nitrogen making it recognize only mono- or di-methylated lysine substrates (**Figure 11**) (Bannister & Kouzarides, 2011; Shi & Whetstine, 2007). Thus, LSD1 is specific for demethylation of H3K4me1/me2 (Varier & Timmers, 2011). However, LSD1 specificity and activity is regulated by protein-protein interactions (Shi & Whetstine, 2007). Although *in vitro* purified LSD1 can demethylate H3K4me1/2, nucleosomal H3K4me1/2 demethylation by LSD1 requires an interaction with the corepressor complex Corepressor for element-1-silencing transcription factor (CoREST) through the tower domain leading to increased stability of LSD1 (**Figure 12**) (Shi & Whetstine, 2007). Another protein-protein interaction regulating the LSD1 substrate specificity is the androgen receptor (AR) complex formation, which switches LSD1 from transcriptional repressor to transcriptional activator by changing the substrate specificity from H3K4me1/2 to H3K9me1/2 (**Figure 12**).

The second super family of KDMs is the *dioxygenase family* that demethylates histones in a α -keto-glutarate (α KG, also known as 2-oxoglutarate) and Fe(II)-ion

dependent manner through their catalytic Jumonji C-terminal (JmjC) domain (Varier & Timmers, 2011). The oxidative decarboxylation of α KG is coupled to hydroxylation of the methyl group that creates an unstable hydroxymethyl ammonium intermediate releasing formaldehyde (**Figure 13**) (Mosammaparast & Shi, 2010). The first JmjC proteins that were identified as KDMs are the Jumonji domain-containing 2 (JMJD2) family proteins and the very first characterized high-resolution structure belonged to JMJD2A, an H3K9 and H3K36 KDM, in this family. JMJD2A structure revealed that it consists of a Jumonji N-terminal domain (JmjN), a JmjC domain, a C-terminal zinc-finger motif, and a β -hairpin (**Figure 14A**). The catalytic core consists of the JmjC domain in which two histidine and one glutamate residue are essential for catalytic activity as they chelate the catalytic iron atom as shown in **Figure 14B**.

Role of Lysine Methylation in Regulation of Inflammation Response

The first histone Kme discovered regulating the inflammatory response is the dynamically regulated H3K9 methylation (Saccani & Natoli, 2002). Gene-specific activation and post-induction repression of some of the inducible inflammatory genes happens through demethylation and remethylation of H3K9, respectively. Moreover, demethylation and remethylation of H3K9 is correlated with RNA-Pol II recruitment and release, respectively, to the promoters.

In line with this observation, later on, H3K9me2 was found as a major regulator of ET through the activity of HAT G9a in the promoters of “T-class” genes (El Gazzar et al, 2008). Moreover, by doing so, G9a recruits HP1 forming a repressive complex at promoters of RelB-dependent genes in ET, diminishing the NF κ B binding (Chan et al, 2005; Chen et al, 2009; El Gazzar et al, 2007). Subsequently, DNA Methyl-transferase

(DNMT) 3A/B (DNMT3A/B) gets recruited to the repressive complex for CpG methylation (**Figure 15**) (El Gazzar et al, 2008). G9a also recruits members of other repressive complexes such as CoREST, C-terminal binding protein (CtBP), and Switch/Sucrose Non-Fermentable (SWI/SNF), creating a strong transcriptionally repressive environment for immunosuppression at ET and leading to global changes in the histone PTM landscape, chromatin remodeling, and activities of select transcription factors (**Figure 16**) (Liu et al, 2014).

H3K27me₃, another repressive histone PTM, regulates expression of specific inflammatory genes (De Santa et al, 2007). Regulation of H3K27me₃ is achieved by the opposite activities of KDM Jumonji domain-containing 3 (JMJD3, also known as KDM6B) and KMT complex PcG in macrophage response (De Santa et al, 2007; Ishii et al, 2009; Köhler & Villar, 2008). JMJD3 is induced with inflammatory stimulation and gets recruited to PcG target genes, decreasing H3K27me₃ levels at Signal Transducers and Activators of Transcription 6 (STAT6) promoter and enhancing transcriptional activity. The subsequent activation of STAT6 enhances binding to JMJD3 promoter and positively regulates the expression of specific inflammatory genes. Interestingly, JMJD3 controls the transcription of the 70% of the LPS-inducible genes (De Santa et al, 2009), indicating the essential role of histone PTM changes in macrophage activation.

Lysine demethylase 5B (KDM5B, also known as Jumonji/ AT-rich interactive domain - or ARID- domain-containing protein 1B or JARID1B) is another histone demethylase that regulates inflammation response (Ptaschinski et al, 2015). KDM5B is a histone H3K4 demethylase that negatively regulates innate cytokine expression to alter the immune response, as in ET, contributing to the development of chronic lung

disease. Similarly, LSD represses inflammatory genes in preadipocytes through increased recruitment of CCAAT-enhancer binding protein (CEBP) and p65 to the IL6 promoter (Hanzu et al, 2013). With obesity, LSD1 gets decreased leading to expression of pro-inflammatory cytokines and obesity-associated inflammation. There have been other reports demonstrating evidence for the role LSD1 in cytokine repression of IL1 α , IL1 β , IL6, and IL8 (Janzer et al, 2012).

Histone KMTs, which target activating methyl-marks on H3, may act as co-activators of inducible inflammatory genes; one such example is the H3K4 KMT Set7/9 that regulates select inflammatory gene transcription through regulation of NF κ B recruitment to the cytokine-induced inflammatory promoters (**Figure 17**) (Fujimaki et al, 2015; Li et al, 2008). Similarly, a H3K4 KMT MLL1 regulates the TNF-induced activation of NF κ B target genes (Wang et al, 2014b). Activated NF κ B recruits MLL1, through binding, to the target genes.

On the other hand, there are repressive KMTs that suppress pro-inflammatory gene expression in immunosuppression or ET. For example, H3K4/H3K36 KMT ASH1 Like (ASH1L) suppresses NF κ B signaling and proinflammatory gene expression for successful immunosuppression (Xia et al, 2013). Similarly, SET and MYND domain containing 2 (Smyd2) is a negative regulator of macrophage activation (Xu et al, 2015). With macrophage activation Smyd2 expression gets dramatically decreased and in ET Smyd2 dimethylates H3K36 at TNF and IL6 promoters and inhibits NF κ B signaling in macrophages.

FIGURES

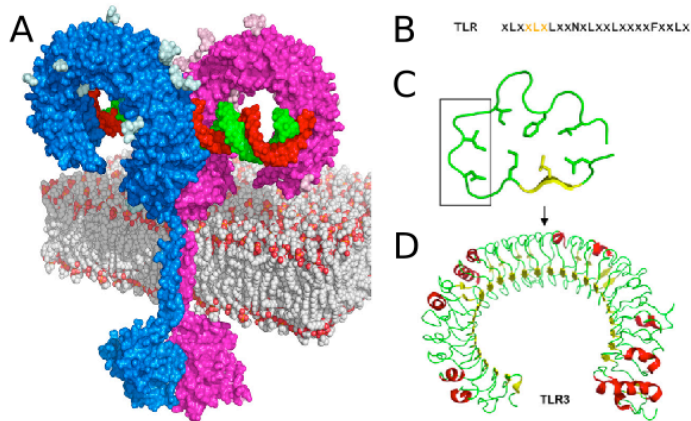


Figure 1 TLR structure

(A) Structural model of TLR3-dsRNA complex based on the mTLR3-dsRNA structure (3CIY) and TLR3 TIR domain homology model on the TLR10 TIR structure structure (2J67) (Botos et al, 2011). (B) LRR consensus sequence for TLR3 where orange highlighted residues represent the β -sheets (Botos et al, 2011). (C) A LRR loop from hTLR3 with the conserved residues forming the hydrophobic core where the box highlights the ligand binding residues. (D) Ribbon diagram of TLR3 ectodomain structure (2A0Z) (Bell et al, 2005).

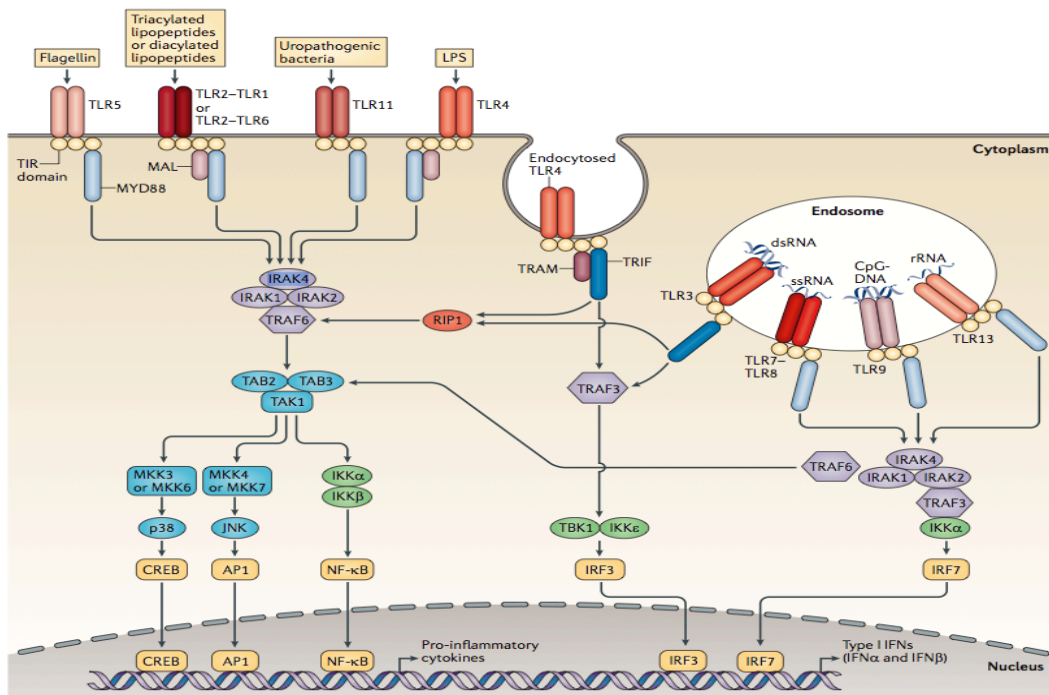


Figure 2 Mammalian TLR signaling pathways

TLR5, TLR11, and the heterodimers of TLR2-TLR1, or TLR2-TLR6 reside on the cell surface to bind to their respective ligands. TLR7-TLR8, TLR9, and TLR13 reside in the endosomes to recognize the microbial nucleic acids. TLR4 localizes to both cell surface and endosomes. Surface TLRs lead to activation of pro-inflammatory cytokines while the endosomal TLRs induce type I IFN (O'Neill et al, 2013).

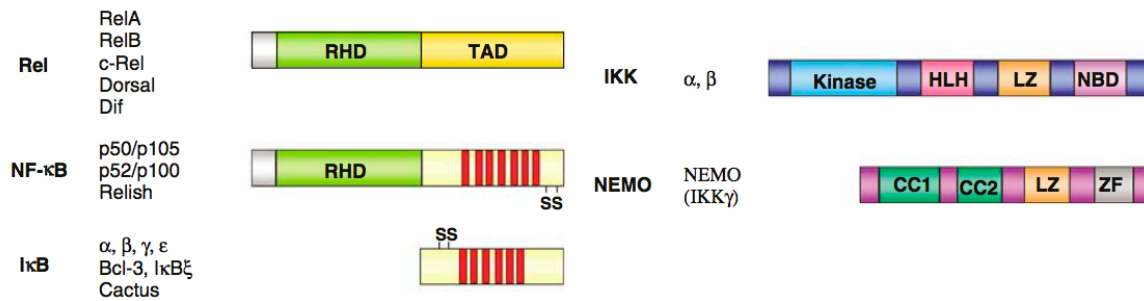


Figure 3 Domain structure of the NFκB signaling proteins

The general domain structure of Rel and NFκB subfamily transcription factors (left) consists of a conserved DNA-binding/dimerization domain called the Rel homology domain (RHD) with nuclear localization and IκB binding sequences. The C-terminal halves of the Rel proteins have transcriptional activation domains (TAD). The C-terminal halves of the NFκB subfamily proteins have ankyrin repeat-containing inhibitory domains (red bars), which can be removed by proteasome-mediated proteolysis. As with the C-terminal domains of the NF-κB proteins, the independent IκB proteins consist mainly of ankyrin repeats, and several (IκBα, IκBβ, IκBε, IκBγ) have two N-terminal serine residues (S) that serve as IKK phosphorylation sites, which signal the protein for ubiquitination and degradation. The generalized structures of IKKα and β (kinase domain; HLH, helix-loop-helix; LZ, leucine zipper; NBD, NEMO binding domain) and of NEMO (CC, coiled coil; LZ, leucine zipper; ZF, zinc finger) are also shown (right) (Gilmore, 2006).

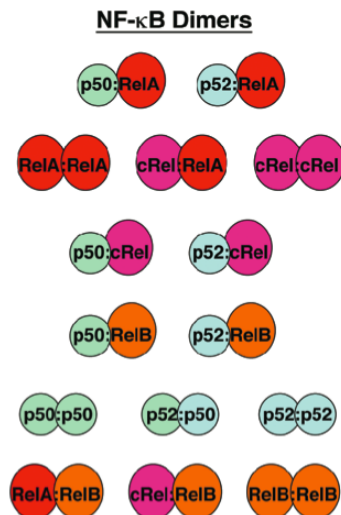


Figure 4 NFκB dimers

Five NFκB polypeptides can form 15 transcription factor homo- and hetero-dimers. The top four rows show nine dimers that can function as transcriptional activators, the fifth row indicates dimers lacking transcriptional activation domains, and the bottom row shows dimers that are not able to bind DNA (Hoffmann & Baltimore, 2006).

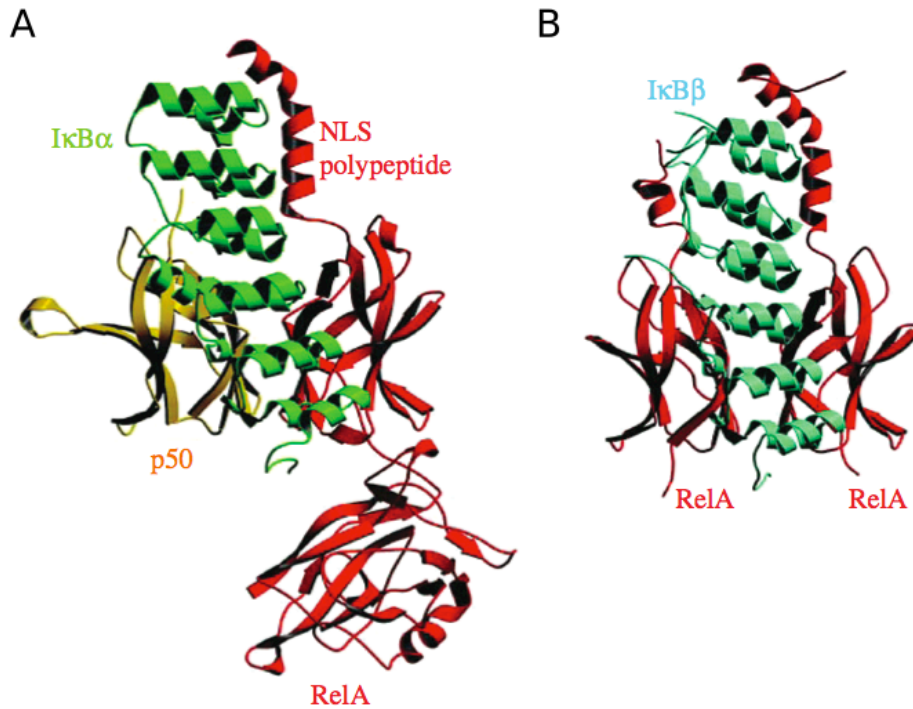


Figure 5 NFκB bound to IκB proteins

(A) The structure of IκBα to the p50:RelA heterodimer where the NLS of RelA, which is unstructured in the absence of IκB proteins, folds into a helical structure when bound to IκBα while the NLS of p50 doesn't interact with IκBα. (B) The structure of IκBβ bound to RelA homodimer. One NLS interacts with IκBβ as that in A while the other has weak contacts (Hoffmann & Baltimore, 2006).

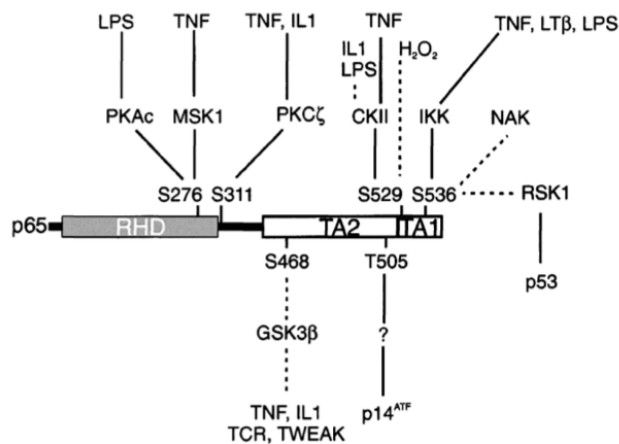


Figure 6 Phosphorylated residues of p65 (RelA)

The known phosphorylated residues are S276, S311, S468, S529, and S536 (Vermeulen et al, 2006).

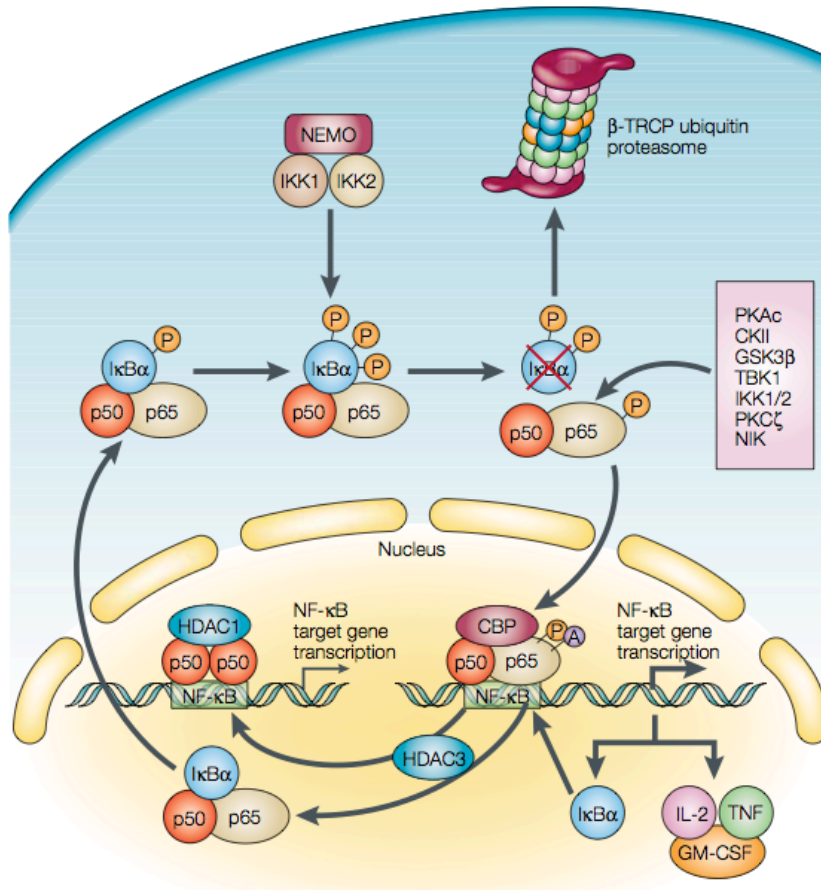


Figure 7 Model of regulation of NFκB transactivation through phosphorylation
Following stimulation, activated IKK complexes phosphorylate IκB, leading to its degradation. NFκB dimers enter the nucleus as p65 is phosphorylated and binds to CBP. The inactive p50-p50-HDAC1 complex gets replaced by the active p50-p65-CBP complexes activating the transcription of target genes. Furthermore, HDAC3 might help to switch off NFκB activity by deacetylating p65 and enhancing the binding affinity between p65-p50 and IκBα (Li & Verma, 2002).

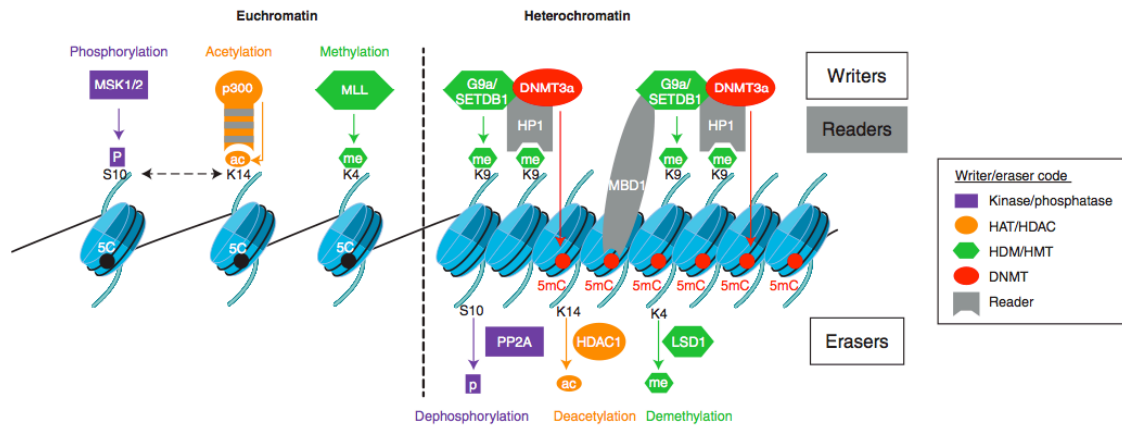


Figure 8 Chromatin modifications and regulators

Chromatin modifications open or close the chromatin structure, thereby activating or repressing gene expression. These modifications are catalyzed or reversed by different enzymes known as “writers” or “erasers,” respectively. An example of writer and eraser for each modification is shown in the color of the modification. Modified residues are recognized and interpreted by different protein modules, known as “readers.” Overall, the chromatin compaction, loss of histone activation marks, and removal of transcription factors accompany gene (Bierne et al, 2012).

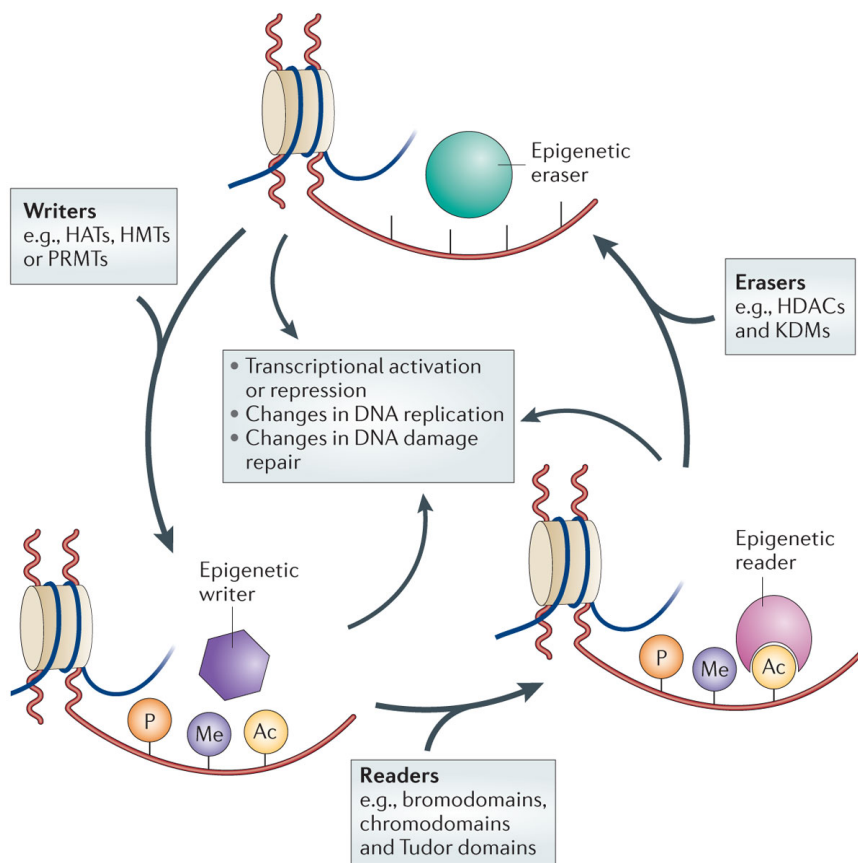


Figure 9 Dynamic epigenetic regulation

Epigenetic writers such as histone acetyltransferases (HATs), histone methyltransferases (HMTs), protein arginine methyltransferases (PRMTs) and kinases lay down epigenetic marks on amino acid residues on histone tails. Epigenetic readers such as proteins containing bromodomains, chromodomains and Tudor domains bind to these epigenetic marks. Epigenetic erasers such as histone deacetylases (HDACs), lysine demethylases (KDMs) and phosphatases catalyse the removal of epigenetic marks. Addition and removal of these post-translational modifications of histone tails leads to the addition and/or removal of other marks in a highly complicated histone code. Together, histone modifications regulate various DNA-dependent processes, including transcription, DNA replication and DNA repair (Falkenberg & Johnstone, 2014).

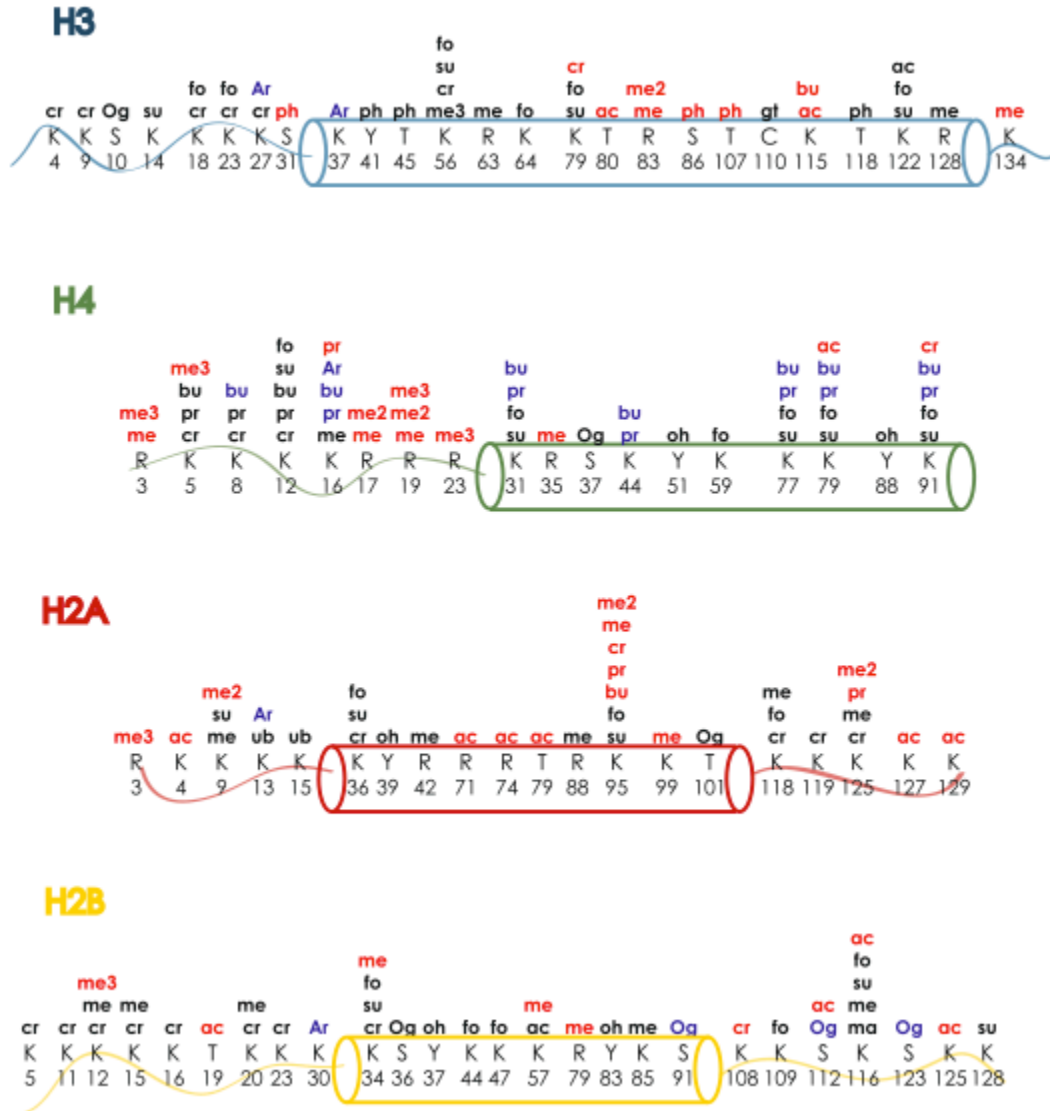


Figure 10 Modifications of the histone histone tails
The sites of the PTMs are indicated with corresponding cellular functions on the left (Arnaudo & Garcia, 2013).

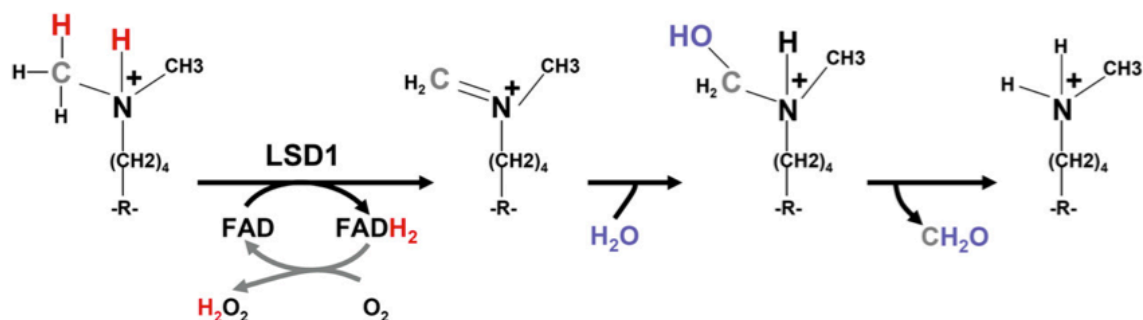


Figure 11 Chemical mechanism for FAD-dependent demethylation

The reaction schematic shows LSD1 removing a methyl group from a dimethylated lysine residue and the reaction can be repeated until lysine is unmethylated (Shi & Whetstine, 2007).

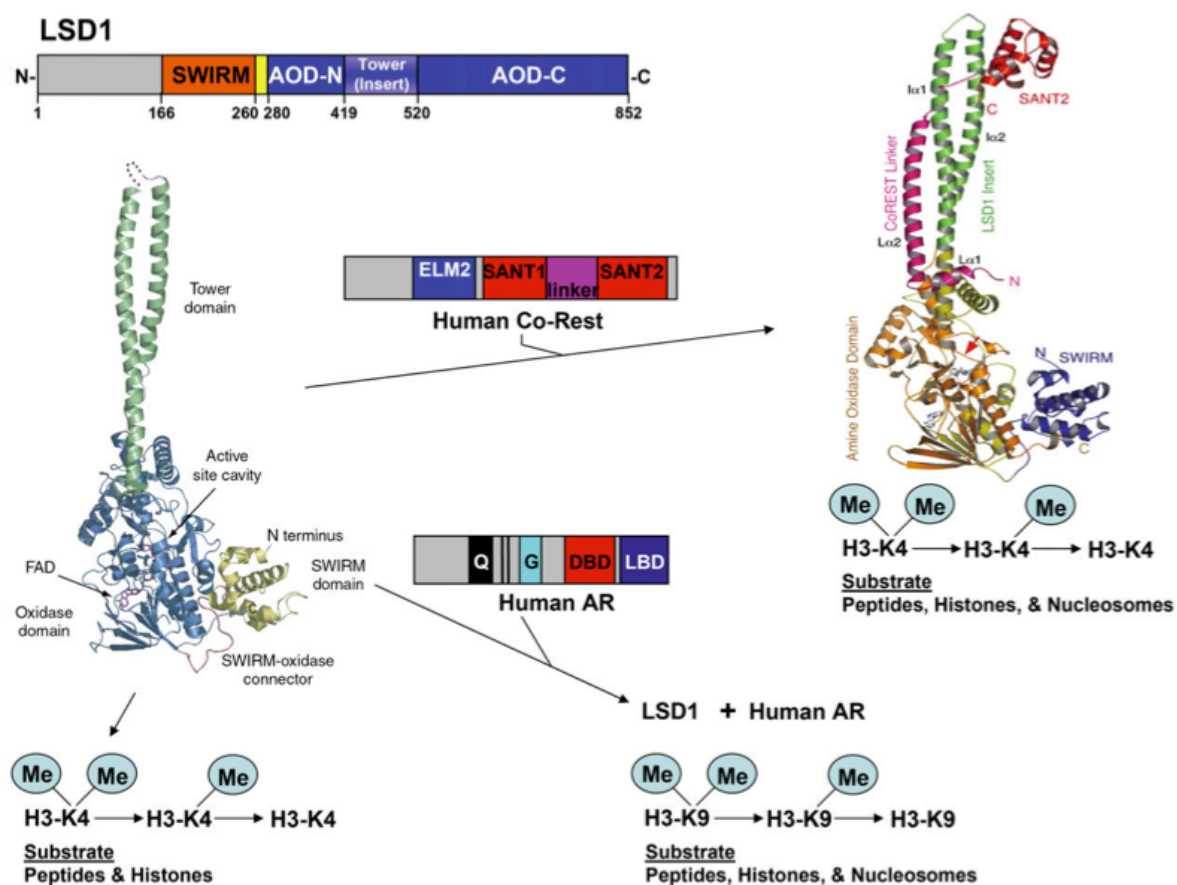


Figure 12 Schematic diagrams of LSD1 Domains

3D structures, and mechanism of action are shown. LSD1 domains are indicated by different colors (AOD: Amine oxidase domain). LSD1 alone demethylates H3K4me1/2. CoREST interacts with the tower region of LSD1 (upper interaction) leading to nucleosomal demethylation. The human androgen receptor has also been shown to interact with LSD1 to demethylate H3K9me1/2 (Shi & Whetstine, 2007).

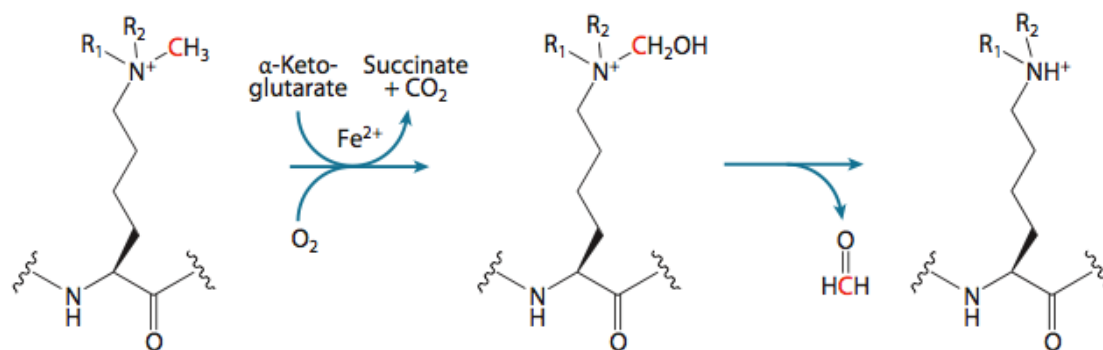


Figure 13 Chemical mechanism for demethylation by JmjC
The reaction schematic shows Fe(II) and the α -keto-glutarate-dependent dioxygenase-mediated demethylation. Red indicates carbons that are demethylated in each reaction (Mosammaparast & Shi, 2010).

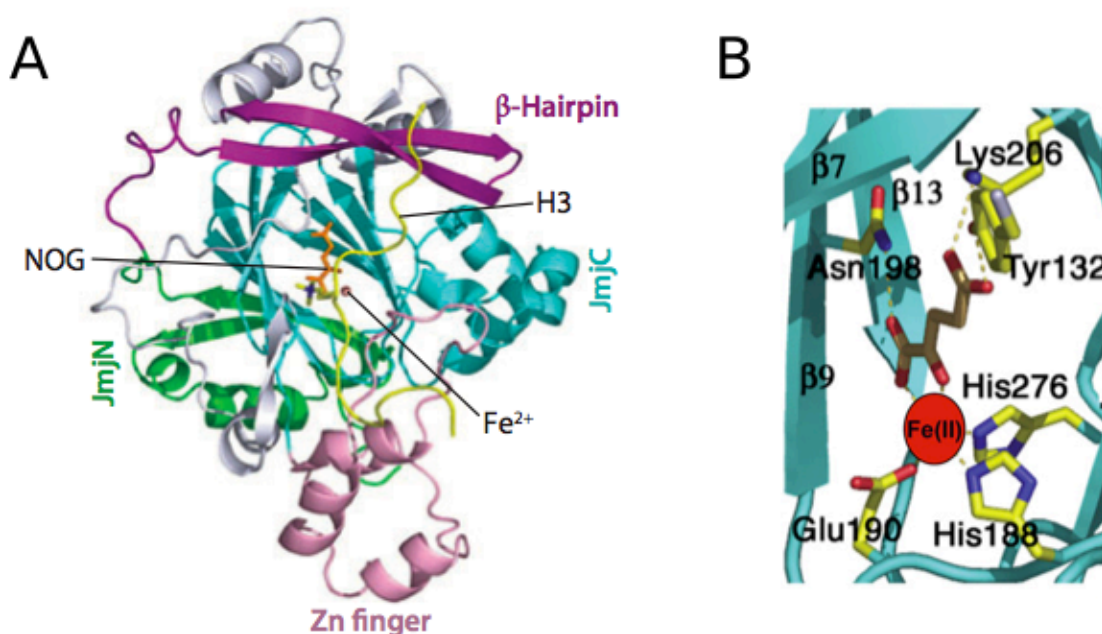


Figure 14 Structure of JMJD2A bound to substrate
(A) Overall structure showing the domains of JMJD2A bound to H3K36me3 and inhibitor N-oxalglycine (NOG) (Mosammaparast & Shi, 2010). (B) The catalytic core of JMJD2A consists of His and Glu aminoacids responsible for coordinating the Fe(II) (red circle) and α -ketoglutarate (Shi & Whetstine, 2007).

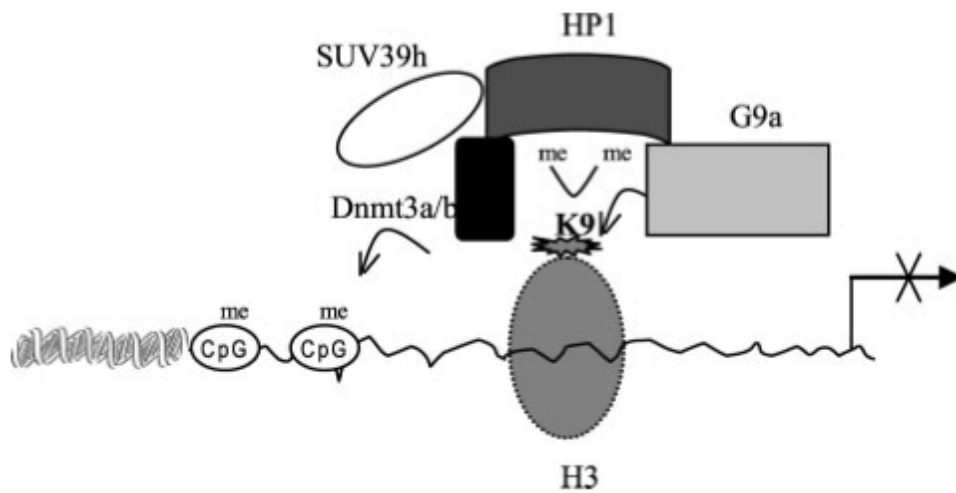


Figure 15 Proinflammatory gene silencing by G9a during endotoxin tolerance
G9a is responsible for the recruitment of DNA methyltransferases in addition to increased repressive histone H3K9 methylation (El Gazzar et al, 2008).

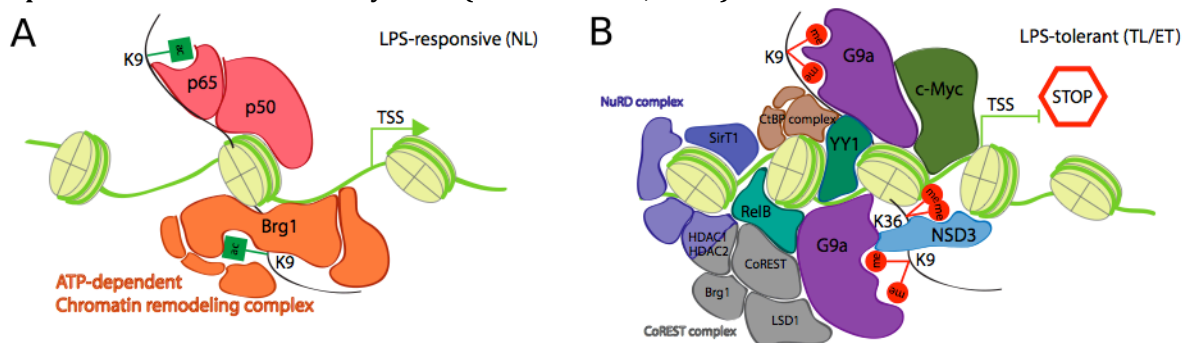


Figure 16 G9a stabilizes c-Myc and promotes cell survival in ET
(A) In LPS-responsive macrophages the chromatin remodeling complex favors the acetylated H3K9 for active transcription of pro-inflammatory genes. (B) In ET, G9a recruits the repressive chromatin remodeling complexes for silencing of proinflammatory genes while selectively promotes c-Myc transcription factor activity to repress select genes (Liu et al, 2014).

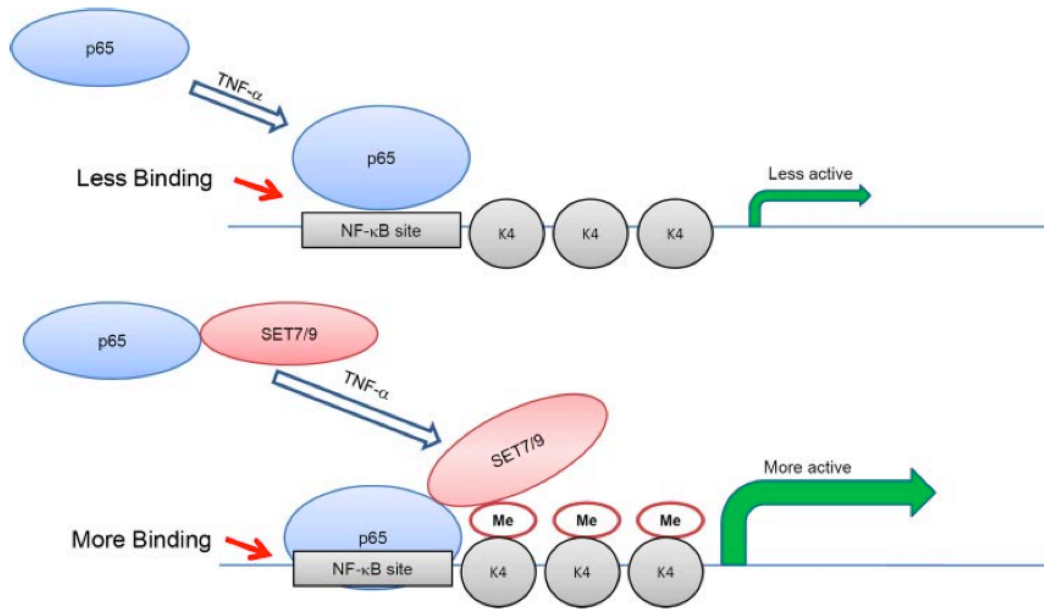


Figure 17 Regulatory function of SET7/9 on NFκB and inflammatory gene expression
 SET7/9 transforms the promoter from a “dormant” state to “active” state as it stabilizes and enhances p65 recruitment to select gene promoters where H3K4 methylation is increased simultaneously for augmented expression (Li et al, 2008).

CHAPTER 2: CHRONICALLY ACTIVE PP2Ac DEPHOSPHORYLATES VARIOUS CHROMATIN MODIFIERS TO REGULATE ENDOTOXIN TOLERANCE

OVERVIEW

Protein phosphatase PP2A is a major regulator of ET in macrophages (Xie et al, 2013). PP2Ac not only dephosphorylates NF κ B for successful suppression of target genes, but also affects the chromatin modeling in ET; however, it is still not clear how PP2Ac broadly affects the changes on the chromatin state. Here, we proposed to *screen ET-specific PP2Ac targets that get dephosphorylated in ET using Amino-acid-coded mass tagging (AACT)-based quantitative phosphoproteomics to clarify the exact pathways and biological processes modulated by chronically active PP2Ac activity*. Our phosphoproteomic analysis revealed that the over-represented biological processes extensively affected by chronically active PP2Ac were chromatin-associated. Identifying ET-specific PP2Ac-targeted chromatin regulators helped us identify both functionally characterized and novel phosphosites involved in phenotypic control of acute versus chronic inflammation, leading to discovery of additional roles of PP2Ac in ET-specific immunosuppression. Moreover, analysis of the PP2Ac-dependent changes in the histone PTMs revealed H3K9me2 and H3K27me2 as the mostly affected histone PTM sites; thus, we conclude that the chromatin regulators, including PHF8, targeting these sites are crucial in the regulation of inflammatory phenotype.

INTRODUCTION

Protein Phosphatases and PP2A

Protein phosphorylation regulates many cellular processes, including regulation of proteolysis, transcription, metabolism, cell-cycle progression, cell differentiation, cytoskeleton organization, cell movement, apoptosis, cell-cell communication, neuronal functions, and immune responses (Johnson, 2009). With such diverse functional roles in the cell, phosphorylation mainly targets hydroxyl-group containing amino acids serine, threonine, and tyrosine with 86.4%, 11.8% and 1.8% degree of phosphorylation, respectively (Seshacharyulu et al, 2013). The high diversity of proteins regulated by phosphorylation demands high diversity of these enzymes enabling the proper regulation of the phosphorylation-dependent events in the cell (Virshup, 2000).

Phosphoprotein phosphatases (PPPs), grouped into protein serine/threonine phosphatases (PSPs) and phosphotyrosine phosphatases (PYPs), are the enzymes that are responsible for the removal of the phosphate group in the presence of a water molecule. There are many subfamilies of PPPs: PP1, PP2A, PP2B, PP4, PP5, PP6, and PP7 (Seshacharyulu et al, 2013).

PP2A is one of the most highly expressed phosphatase subunit constituting up to 1% of the cellular protein (Virshup, 2000). It controls many cellular events, including metabolism, cell cycle, DNA replication, transcription, translation, signal transduction, cell proliferation, cytoskeleton dynamics, cell mobility, and apoptosis (**Figure 18**). PP2A holoenzymes exist in either dimeric or trimeric form; dimeric form is composed of a catalytic subunit (PP2Ac) and a scaffold subunit (PP2AA) while the trimeric form also

includes the regulatory subunit (PP2AB) (**Figure 19**) (Seshacharyulu et al, 2013). The C-terminal tail of PP2Ac is responsible for interaction with regulatory and scaffold subunits (Seshacharyulu et al, 2013). The scaffold subunit, PP2AA, has multiple regulatory roles. In the heterotrimeric holoenzyme, PP2AA creates a structural bridge to accommodate the interaction between the catalytic subunit, regulatory subunit, and the substrates. On the other hand, in the dimeric form, it regulates the catalytic specificity. However, the main regulator of the holoenzyme is the regulatory subunit, PP2AB; it modulates the temporal and spatial specificity.

PP2A: A Major Regulator of NF κ B Signaling

One of the most important regulators of inflammatory response is the phosphatase PP2A; inhibition of PP2A catalytic activity was previously reported to affect macrophage regulation, cytokine expression, superanion generations, and phagocytosis (Barber et al, 1995; Mayer et al, 1995; Sung & Walters, 1993; Zhang et al, 2000). Moreover, various effects of the PP2A activity on the regulation of NF κ B, such as inhibition of host response, have been characterized (Maslash-Hubbard, 2011). First, PP2A dephosphorylates and inhibits IKK α and IKK β to regulate NF κ B activity (Barisic et al, 2008; DiDonato et al, 1997); this effect is reversed with the PP2A inhibitor Okadaic acid (OA) treatment (Sun et al, 1995). PP2Ac also downregulates MAPK pathways broadly, affecting cytokine expression through Activating Protein 1 (AP1) transcription factor inhibition (Shanley et al, 2001). More importantly, PP2Ac directly dephosphorylates p65 to downregulate its transcriptional activity (Hsieh et al, 2011; Yang et al, 2001); thus, its activity is an important regulator of immune tolerance (Sun et al, 2015b).

PP2A activity is associated with chronic inflammation while its inhibition exacerbates the acute cigarette smoke-induced acute inflammation in lungs (Wallace et al, 2012). Recently, PP2Ac was functionally characterized as a major transcriptional regulator of ET in macrophages for successful immunosuppression of pro-inflammatory genes (Sun et al, 2015b; Xie et al, 2013). *Constitutively active PP2Ac inhibits TLR4-MyD88 complex, gets translocated into the nucleus with MyD88, and selectively silences pro-inflammatory genes by establishing an immunosuppressive pattern on the chromatin (Figure 20)* (Xie et al, 2013).

Although PP2A activity leads to ET-specific repressive chromatin state, the functional determinants of downstream modulators that are involved in the maintenance of the repressive chromatin are still missing. PP2Ac might directly target and remove the transcriptionally active mark phospho-H3S10 from nucleosomes in ET as it does in regulation of cell cycle and heat-shock response (Nowak et al, 2003; Simboeck et al, 2010). On the other hand, PP2Ac might regulate the activity of chromatin modifying enzymes through dephosphorylation to maintain ET-specific chromatin state. Although some Histone deacetylases (HDACs), including HDAC4, HDAC5, and HDAC7, and Histone acetyl-transferases (HATs), including p300 and PCAF, show PP2Ac-mediated dephosphorylation-dependent change in enzymatic activity, there is no evidence for a similar mechanism in PP2Ac-dependent ET control.

To provide evidence for PP2Ac-dependent activity in the regulation of chromatin modifying enzymes, various strategies, such as phosphoproteomic analysis, can be used. In this chapter, I aim to screen ET-specific PP2A targets to identify the phosphorylation sites on chromatin modifying enzymes that may be involved in the ET-specific

chromatin states. Here, we use a phosphoproteomic screening method first, to identify possible PP2Ac-targeted phosphorylation sites within the cell, followed by an immunoblotting-based screening methods, to identify which histone PTMs are affected as a result of ET-induced PP2Ac activity.

Phosphoprotein Sequencing Using Quantitative Proteomics

Protein phosphorylation is one of the most widely studied PTM controlling the protein function (Delom & Chevet, 2006). As a reversible and highly dynamic PTM, phosphorylation cannot be predicted by the genome and analytical measurements (Goshe, 2006). Various traditional biochemical methods have been developed to characterize phosphorylation site of a protein of interest, many of which involve ^{32}P -labeling of the proteins to analyze potential phospho-sites (Delom & Chevet, 2006; Goshe, 2006). These methods depend on immunoblot analysis with phospho-imaging to determine the level of ^{32}P -label incorporation and phospho-site specific antibodies for detection (Goshe, 2006). The technical limitations of these traditional methods include inconvenience of radioactivity, post-lysis labeling, time-consuming sample preparation, lack of adaptation to high throughput pipelines, difficulty in antibody generation/validation, and low antibody specificity (Delom & Chevet, 2006). Recently the development of mass spectrometric methods has overcome many of these technical limitations although there are still technical challenges for analysis of phosphoproteins due to five main reasons. First, phosphorylation stoichiometry is relatively low since a small fraction of cellular protein is phosphorylated at a given time. Second, any given phosphoprotein is heterogenous since there may be multiple phosphorylated sites and states and phosphorylation occurs at the solvent accessible space; thus, bottom-up

approach enables higher protein sequence coverage. Third, phosphorylated targets may have low abundance in cells, and thus need enrichment before analysis. Fourth, most analytical techniques may locate major phosphorylation sites but minor sites may be difficult to identify. Finally, during sample preparation cellular phosphatases may target those phosphorylation sites unless phosphatase inhibitors are used.

One of the most widely used techniques for separation of proteins is sodium dodecyl sulfate polyacrylamide gel electrophoresis (SDS-PAGE) which can be used with Liquid chromatography-tandem mass spectrometry (LC-MS/MS) in combination with immunoprecipitation to identify and characterize phosphoproteins (**Figure 21**) (Goshe, 2006). The major drawback of the gel-based LC-MS/MS analysis of phosphoproteins is that at least two unique peptides are required for confirmation of protein abundance in a gel slice. Moreover, even when sample amount is increased, sequence coverage can be low if the protein has low efficiency of peptide extraction from the gel. The peptide coverage can be increased with two-dimensional (2D) gel analysis in which proteins are separated by isoelectrophoresis in addition to the molecular weight (**Figure 22**). Although it enhances the peptide coverage, the efficiency of separation of highly acidic, highly basic, very small, or very large proteins with 2D-PAGE is low. Using protein mixture isolated from cells overcomes the issues related to gel analysis. This 'bottom-up' method involves proteolytic digestion of the cellular proteins to produce peptides that are resolved by liquid chromatography and analyzed by the mass spectrometer.

Here, we employed the 'bottom-up' method to quantitatively analyze the phosphoproteome to overcome potential issues that may arise from gel-based

proteomic approaches such as low protein abundance, low efficiency of peptide extraction or enrichment, and protein degradation.

Phosphoproteome Enrichment Methods

Since phosphorylated proteins constitute a small portion of the isolated proteins from cell lysates, their detection requires preferential enrichment of phospho-peptides by noncovalent binding and recognition of phosphate groups via specific chemical derivatization, immunoprecipitation, or Immobilized Metal Affinity Chromatography (IMAC) (Goshe, 2006).

Specific Chemical Derivatization: This approach takes advantage of the chemistry of phosphorylated amino acids by β -elimination or the addition of cystamine (Delom & Chevet, 2006). One of the main disadvantages of chemical derivatization is the requirement for high amount of protein for successful Mass spectrometry (MS) identification. Moreover, the selectivity of these methods still needs to be validated.

Immunoprecipitation: Phosphorylated proteins can be immunoprecipitated using phospho-specific antibodies with an efficiency correlated with the specificity of the antibody (Delom & Chevet, 2006). Currently antibodies specific to phospho-tyrosine residues are widely used to enrich even low-abundance tyrosine phosphorylated proteins although their selectivity is low. On the other hand there are no phospho-serine-specific and/or phospho-threonine-specific antibodies for enrichment of proteins that are phosphorylated on either serine or threonine residues; thus, it still is a challenge to enrich these proteins using immunoprecipitation.

IMAC: IMAC relies on the high affinity of phosphate groups to cations such as Zn^{2+} , Fe^{3+} , and Ga^{3+} bound to tethered chelating reagents present on solid phase columns (Goshe,

2006). In this method first proteins are digested into peptides; phosphopeptides are isolated by IMAC and analyzed off-line or on-line using LC-MS/MS (Delom & Chevet, 2006). It should be noted that aspartyl- and glutamyl-peptides have high affinity for the strong cations used in IMAC, causing non-specific binding. Moreover multiply phosphorylated residues have higher affinity to the metal and get more enriched. Non-specific binding can be decreased by using esterification of acidic residues, i.e. converting the carboxylic acid groups of peptides to their corresponding methyl esters, prior to IMAC procedure. In the recent years higher selectivity and sensitivity is achieved by using Titanium dioxide (TiO_2) as a potent chelator for phosphopeptides. Thus, in our approach, we employed TiO_2 -based phosphoenrichment of peptides for its advantages in terms of sensitivity, selectivity, and coverage.

MS Analysis

After the enrichment step, the phosphopeptides are sequenced in the mass spectrometer with precise identification (Delom & Chevet, 2006). The methods used for phospho-peptide sequencing are precursor ion and neutral loss scanning. Precursor scanning relies on collision-induced dissociation (CID) since phosphopeptides produce sequence-specific fragments as well as phosphate-specific fragments. Negative ion mode produces ions at mass-to-charge ratio (m/z) 79 and 63 corresponding to PO_3^- and PO_2^- groups, respectively. Moreover, in the positive ion mode, CID of phospho-serine- and phospho-threonine-containing peptides causes neutral loss of Phosphoric acid (H_3PO_4) via β -elimination corresponding to a loss of 98 Da and 49 Da from single charged and double charged precursors, respectively. While β -elimination does not happen for phospho-tyrosine residues, they produce a characteristic immonium ion at

m/z 216. Precursor ion scanning method screens only the peptides with a chosen marker ion (m/z is 79 for phosphorylation) eliminating all other species, but this method is not amenable for inline LC-coupling. However precursor ion scanning has high selectivity and specificity to phospho-residues while it enables detection of serine, threonine, and tyrosine phosphorylations. On the other hand neutral loss scanning uses the mass shift of gas-phase β -elimination reaction that causes a neutral loss of H_3PO_4 (H_3PO_4 -98 Da) or dephosphorylation (HPO_3 -80 Da). Due to the chemistry of the serine and threonine residues a shift of 69 Da and 83 Da indicates the location of phosphorylated serine and threonine residues, respectively. Phosphotyrosines are tolerant to this loss. One weakness of this method is the requirement of prior knowledge of the charged state of the phosphopeptide. In addition, false positive identification is a big disadvantage of this scanning method.

Data Analysis

After the identification of individual phosphopeptides, careful analysis of quantitative changes is required. Based on the quantitative changes observed, the biological interpretation and relevance of the results should be analyzed carefully based on the current knowledge of direct/indirect interaction between proteins, interaction of the biological pathways, phosphorylation-dependent changes in signaling pathways, experimentally observed biological functions of those proteins, known functional significance of the identified phosphorylation sites, and other known PTMs interacting with identified phosphorylation sites. Various data analysis databases and programs that can achieve such thorough analysis are widely used in interpretation of the results and identification of the novel PTM sites. Here, we used Ingenuity Pathway Analysis

(IPA) to do the network analysis, identification of targeted biological processes, and interconnected pathways.

MATERIALS AND METHODS

Reagents

LPS was purchased from Invitrogen. All protease inhibitor cocktails were purchased from Sigma-Aldrich (St. Louis, MO). All culture media and fetal bovine serum (FBS) were obtained from GIBCO and dialyzed FBS was purchased from Invitrogen. All stable isotope-enriched amino acids, including $^{12}\text{C}_6$ -arginine, $^{13}\text{C}_6$ -arginine, and $^{13}\text{C}_6^{15}\text{N}_4$ -arginine, $^{12}\text{C}_6$ -lysine, $^{13}\text{C}_6$ -lysine and $^{13}\text{C}_6^{15}\text{N}_2$ -lysine, were obtained from Cambridge Isotope and Sigma-Aldrich. Trypsin was purchased from Promega. All chemicals were sequence- or HPLC-grade unless specifically indicated. Antibodies for p-I κ Ba (S32), I κ Ba, p-p65 NF κ B (S536), and p65 were purchased from Cell Signaling. Antibody for PP2Ac (clone 1D6) was from Millipore. Antibodies for Lmn1 and p65 were from Santa Cruz Biotechnology while antibodies to γ -tubulin, histone H3, H3K9me2, H3K9me1, H3K27me2 were from Abcam. Bacterial clones for shRNA against PP2Ac or against PLKO.1 were purchased from Sigma-Aldrich.

Cell Culture

RAW 264.7 cells were maintained in 4.5 g/L glucose Dulbecco's minimal essential media (DMEM) with 10% FBS. For all LPS pre-treatment 0.1 $\mu\text{g/mL}$ LPS is used while high dose LPS treatment and second challenges were done with 1 $\mu\text{g/mL}$ LPS.

Transfection and Stable PP2Ac Knock-down (PP2Ac-KD) RAW Cell Line

The lentiviral plasmids pLKO.1 expressing shRNA-PP2Ac (targeting sequences CCAGATACAAATTACCTGTT and CGACGAGTGTTTAAGGAAATA) were purchased from Sigma. A pLKO.1 empty vector (EV) without a specific shRNA sequence was used as the wild-type (WT) control. To produce virus, pLKO.1-shRNA plasmids were co-transfected into 293T cells with ViraPowerMix (Invitrogen) by jetPRIME™ in vitro DNA and siRNA transfection reagent (Polyplus). Pseudo-virus in supernatants was collected 48 h after transfection and used to transduce RAW 264.7 cells by spinoculation. 48 h after transfection, 8 µg/ml puromycin was added to select puromycin-resistant clones. Stable clones were maintained in medium containing 4 µg/mL puromycin. The PP2Ac expression in PP2Ac-KD cell line was monitored with immunoblotting and Real-time Polymerase chain reaction (qPCR).

AACT-labeling

Mass tagging with both Arg and Lys was performed to increase the phosphoproteomic coverage. Stable isotope labeled media was prepared by using 4.5 g/L glucose DMEM without Lysine and Arginine and 10% dialyzed FBS. Cells were grown in the media supplemented with either $^{12}\text{C}_6$ - Arg/ $^{12}\text{C}_6$ -Lys (K0R0, “L”), or $^{13}\text{C}_6$ - Arg/ $^{13}\text{C}_6$ -Lys (K6R6, “M”), or $^{13}\text{C}_6$ $^{15}\text{N}_4$ -Arg/ $^{13}\text{C}_6$ $^{15}\text{N}_2$ -Lys (K8R10, “H”) until >95% incorporation of isotope labeling is achieved and the labeling efficiency was checked using MS.

The RAW 264.7 cells stably expressing shRNA for pLKO.1 empty vector were cultured in “L” medium and remained unstimulated (WT-N). This control cell line was also cultured in “M” medium, was stimulated with 0.1 µg/mL LPS for 24 h, and then

challenged with 1.0 µg/mL LPS for 15 min (WT-TL). RAW cells expressing shRNA for PP2Ac in double-tagged “H” medium were also stimulated with 0.1 mg/mL LPS for 24 h followed by a second challenge with 1.0 mg/mL LPS for 15 min (PP2AKD-TL) before samples were prepared for phosphoproteomic analysis (**Figure 23**).

Quantitative Phosphoproteomic Analysis using AACT

Sample Preparation

All cells were harvested and lysed in lysis buffer containing 8 M urea, 50 mM Tris pH 8.0, 75 mM NaCl, 1 mM MgCl₂, 500 units Benzonase, and protease-phosphatase inhibitor cocktail set I and II (Calbiochem). 5 mg of each lysate was mixed equally and reduced with Dithiothreitol (DTT) followed by alkylation with iodoacetamide (IAA). Proteins were digested first with endoproteinase Lys-C (Wako USA). The solution was then diluted 4-fold with 25 mM Tris pH 8.0, 1 mM CaCl₂ and further digested with trypsin (Promega). The digestion was stopped by 0.4 % Trifluoroacetic acid (TFA) (final concentration). Desalting was achieved on a Sep-Pak Light C18 cartridge (Waters) and peptides were freeze-dried. Dried peptides were resuspended in 30 % Acetonitrile (ACN), 0.1% TFA and loaded on a 1 mL Resource 15S (GE Healthcare) column for strong cation exchange chromatography (SCX). A linear gradient was performed from 5 mM to 100 mM KCl in 30% ACN, 5 mM KH₂PO₄, 0.1% TFA. Negatively charged peptides were eluted with high salt buffer (350 mM KCl in 30% ACN, 5 mM KH₂PO₄, 0.1% TFA). The phospho-peptides were enriched directly in SCX fractions (Xie et al, 2013). Briefly, 1-5 mg of 5 mm Titansphere beads (GL Sciences) suspended in 80% ACN/1% TFA was added to each fraction and incubated for 30 min at room temperature (RT). The beads

were collected by centrifugation and washed three times with 150 μ L 60% ACN/1% TFA, then transferred on to the top of a C8 disc (Empore) placed in a 200 μ L pipette-tip. Bound phosphopeptides were eluted with 15% NH_4OH /40% ACN. Elutes were dried and desalted on a StageTip containing a 4 x 1 mm C18 extraction disk (3M).

Mass Spectrometry

Samples were analyzed via reverse phase (RP) LC-MS/MS using a nano-LC ultra2D system coupled to a Velos Orbitrap mass spectrometer (Thermo Scientific, San Jose, CA). LC-MS experiments were performed in a data-dependent mode with Full-MS (externally calibrated to a mass accuracy of < 5 ppm, and a resolution of 60 000 at m/z 400) followed by CID-MS/MS of the top 10 most intense ions. Mass spectra were processed, and peptide identification was performed using the Andromeda search engine in MaxQuant (Max Planck Institute) against a mouse uniprot database. All searches were carried out using cysteine carbamidomethylation as a fixed modification while methionine oxidation and protein N-terminal acetylation, and phosphorylation at STY residues were selected as dynamic modifications. AACT/SILAC quantitation was performed in MaxQuant [ver. 1.2.2.5] with the Andromeda search engine.(Cox et al., 2011) The searches were carried out initially at 200 ppm. Precursor ion mass tolerance followed by a main search of the m/z , and retention time corrected features using a precursor ion mass tolerance of 5 ppm. Peptides were confidently identified using a target-decoy approach with a peptide false-discovery-rate (FDR) of 1% and a protein FDR of 5%. Phosphorylation sites were localized using PTM score with phosphorylation site localization FDR of 1%. Data processing and statistics were performed using Perseus [ver. 1.2.0.17] (Cox and Mann, 2011). Protein quantitation was performed on

biological replicate runs and a two sample t-test statistics was used with a p-value of 5% to report statistically significant fold changes. In this experiment, mass tagging with both Arg and Lys was performed to increase the phosphoproteomic coverage. The AACT ratios of the proteins were derived from the comparison of the extracted ion chromatogram peak areas of all matched light (L) peptides with those of the medium (M) or heavy (H) peptides. The ratios of M/L or H/L were also verified by visual inspection of the raw mass spectra. In MS spectra, for each arginine-containing peptide, a set of three isotope signals with the mass spacing of 6 Da and 10 Da was observed as L isotope peak was originally from the non-stimulated WT cells, and the 6 Da (M) or 10 Da heavier (H) isotope peaks came from either WT-TL or PP2Ac-KD-TL cells, respectively. In reference to the criteria previously established by our group (Xie et al., 2009) as well as others (Zhang et al., 2006), an approximate 30% increases in isotope intensity or a M/L or H/L value over 1.3 was determined as the quantitative threshold to distinguish the PP2Ac targeted phosphopeptides. M/L and H/L ratios for each protein were determined by averaging the ratio found for at least two unique AACT-containing peptides. Most proteins were identified in high confidence with more than one peptide. For those proteins that were identified by a single peptide, the MS/MS spectra were manually inspected to ensure correct identification. For most proteins, the relative standard deviation for quantification between peptides of the same protein was less than 20%.

Canonical Pathway Analysis

Biological processes and molecular functions of the proteins identified as potential PP2Ac targets were categorized by Ingenuity Pathway Analysis (IPA, QIAGEN

Redwood City, <http://www.qiagen.com/ingenuity>). Normalized M/L ratios were used to identify the change in phosphorylation of the peptides with ET in WT cells compared to unstimulated WT cells while H/L ratios revealed the phosphorylation change in PP2Ac-KD-TL peptides compared to unstimulated WT cells. To focus on the phosphopeptides that are regulated downstream PP2Ac, the dataset was trimmed to include only the peptides that showed an increase in phosphorylation in PP2Ac-KD-TL compared to WT-TL. The canonical pathways were similarly ordered according to the ratio of phosphopeptides that showed an increase in PP2Ac-KD-TL compared with WT-TL.

Detection of the changes in Histone PTMs via Western Blotting

Paired WT and PP2Ac-KD RAW cells were stimulated with 1.0 µg/mL LPS for 0, 5, 15, and 30 mins with (TL) or without (NL) a low dose (0.1 µg/mL) LPS pre-treatment. Cells were harvested and lysed with buffer containing 0.5% NP-40, 10 mM Tris pH 7.5, 150 mM NaCl, 0.4 mM EDTA, 2 mM Na₃PO₄, 1x phosphatase inhibitor cocktail (Pierce), 1x protease inhibitor cocktail (Sigma-Aldrich). The lysates were sonicated twice at level 3 for 5 sec for successful release of the chromatin, then were separated on an SDS-PAGE gel under reducing conditions and then transferred to a Polyvinylidene fluoride (PVDF) membrane. The membranes were blocked with milk for 1 h at RT on an orbital shaker. Following primary antibody incubation for 1 h at RT, we probed the membranes with a horseradish peroxidase conjugated secondary antibody and bands were detected using an enhanced chemiluminescence (ECL) Western Blotting Detection Kit (GE Life Sciences). Densitometry analysis was performed using ImageJ software and comparing

the amount of H3K9me2 and H3K27me2 to total H3. The densities were then normalized to the unstimulated sample.

RESULTS

Phosphoproteomic analysis reveals broad range of signaling pathways regulated by PP2Ac in ET-macrophages

The quantitative phosphoproteomics of PP2Ac-targeted proteins in ET macrophages revealed 1319 proteins in total, 18 of which (1%) were not phosphorylated while 1301 proteins included phospho-peptides (**Figure 24, left**). This indicates that our phospho-enrichment technique was highly efficient (99%). Moreover, out of the 18,492 peptides that were identified (**Figure 24, right**), 18,298 were phospho-peptides that had only one (61%) phosphorylation (**Figure 25, left**) while phosphopeptide enrichment successfully discovered peptides with up to 6 phosphorylations (**Figure 25, right**). In addition, we analyzed the distribution of various phospho-STY residues, and observed that 86% phosphosites were identified as phospho-S, 13% were identified as phospho-T, and 1% were identified as phospho-Y (**Figure 26**).

For accurate quantification we used the Mass Error data from MaxQuant database search to normalize the quantification of the peak intensities (**Figure 27**). Moreover, we used the ratios of intensities H/L, M/L, and H/M that refer to the relative ratio of abundance of each peptide in PP2Ac-KD-TL compared to WT-N, WT-TL compared to WT-N, and PP2Ac-KD-TL compared to WT-TL, respectively. Further, we trimmed the dataset to the peptides that show increased phosphorylation in PP2Ac-KD-

TL compared to WT-TL since we aim to identify the phosphopeptides that are directly or indirectly targeted by PP2Ac in ET.

Using IPA analysis, the top 10 signaling pathways to include the highest number of proteins targeted by PP2Ac specifically in ET macrophages (i.e. the phosphorylation of these proteins showed an increase in PP2Ac-KD cell line compared to WT in ET-macrophages) were identified as DNA Methylation and Transcriptional Repression, PI3/AKT Signaling, Prostate Cancer Signaling, Insulin Receptor Signaling, Superpathway of Inositol Phosphate Compounds, Rac Signaling, HGF Signaling, ERK/MAPK Signaling, Telomerase Signaling, and ATM Signaling (**Figure 28**). Moreover 8 of these pathways showed PP2Ac-dependent dephosphorylation of chromatin regulators in ET macrophages as shown in **Figure 29A-I**. In addition to these, many other various PP2Ac-targeted signaling pathways crosstalk, indicating PP2Ac-targeted proteins broadly affect the signaling pathways (**Figure 30**).

In our previous PP2Ac study, we demonstrated that chronic-active PP2Ac dephosphorylates caspases to inhibit apoptosis (Xie et al, 2013). PP2Ac is also known as a major regulator of cell survival through dephosphorylation of ATM, leading to decreased apoptosis (**Figure 31**) (Goodarzi et al, 2004). Here, identification of ATM signaling pathway as an ET-specific PP2Ac target demonstrates an alternative pathway for PP2Ac-induced cell survival in LPS-stimulated macrophages supporting our conclusion that chronic-active PP2Ac is important for regulation of cell survival.

PP2Ac dephosphorylates various chromatin modifiers to regulate gene transcription in ET macrophages

Since the over-represented pathways showed PP2Ac-dependent dephosphorylation of chromatin regulators in ET macrophages as shown in **Figure 30**, we manually trimmed the dataset to chromatin regulators to understand how PP2Ac may regulate ET-specific gene regulation in macrophages and observed various chromatin regulators with various phosphosites in the dataset (**Table 3**). Among these chromatin regulators, demethylases (DM) **KDM1A** (also known as **LSD1**), Lysine-specific Demethylase 5A (**KDM5A**, also known as Jumonji/ARID domain-containing protein 1A or **JARID1A**, and Retinoblastoma-binding protein 2 or **RBP2**), and Plant Homeodomain (PHD) Finger 8 (**PHF8**) (**Figure 32**), and methyltransferases (MT) methyl CpG binding protein 2 (**MeCP2**), mRNA cap guanine-N7 methyltransferase (**MCES**), tRNA (adenine-N(1)-)-methyltransferase non-catalytic subunit (**TRM6**), Nuclear SET domain-containing protein 2 (**NSD2**), **EZH2**, **MLL1**, Nuclear SET domain-containing protein 3 (**NSD3**), **DNMT3A**, **DNMT1**, and **MLL4** (**Figure 31**) showed ET-specific PP2Ac-dependent dephosphorylation. In addition, we found deacetylases **HDAC1**, **HDAC2**, and Suppressor of defective silencing 3 protein homolog (**SDS3**), and acetyltransferase **MYST1** with ET-specific PP2Ac-dependent dephosphorylation patterns (**Figure 33**).

Table 3 Epigenetic regulators with phosphosites in the phosphoproteome dataset

Demethylases
IHD2C, KDM1A, KDM2B, KDM5A, KDM5C, PHF8
Methyltransferases
ASH1L, COMT, DNMT3A, DNMT1, EZH2, MCES, MECP2, MLL1, MLL4, NSD2, NSD3, RG9D2, TRM6

Deacetylases HDAC1, HDAC2, SDS3, SAP30
Acetyltransferases MYST1, MYST2, NAA15, NAA30

Among the potential ET-specific PP2Ac-targeted phosphosites of chromatin modifiers, only a few were previously characterized functionally: **KDM1A** phosphorylations at P-S132 and P-S138 (**Figure 32, top-left**), **PHF8** phosphorylation at S843 (**Figure 30, bottom-right**), **MeCP2** phosphorylation at S80 (**Figure 33, top-left**), **HDAC1** phosphorylations at S421 and S423 (**Figure 34A, top-left**), and **HDAC2** phosphorylations at S422 and S424 (**Figure 34A, top-middle**). S132 and S138 of **KDM1A** are phosphorylated by Casein Kinase 2 (CK2) to positively regulate DNA damage response by recruiting p53-binding protein 1 (53BP1) to DNA damage sites (Mosammaparast & Shi, 2010; Peng et al, 2015), and are dephosphorylated by Protein Phosphatase, Mg²⁺/Mn²⁺ Dependent, 1D (PPM1D). Since these phosphorylations are involved in cell growth regulation (Fradet-Turcotte et al, 2013; Ward et al, 2003) and DNA damage response is activated in the LPS-induced TLR4 signaling (Harberts & Gaspari, 2013; Kutikhin et al, 2014), their dephosphorylation by PP2Ac in ET may be involved in the negative regulation of the TLR4-induced DNA damage response pathways in ET. On the other hand, S843 phosphorylation of **PHF8** by Cyclin E-CDK (Sun et al, 2015a) positively regulates its activity in the control of cell cycle progression. Therefore PP2Ac-dependent dephosphorylation in ET might contribute to the immunosuppression of inflammation-related genes through deactivation of PHF8. **MeCP2** S80 (**Figure 35A**) is a Homeodomain Interacting Protein Kinase 2 (HIPK2)

target in fibroblasts in regulation of apoptosis (Bracaglia et al, 2009) and is important for MeCP2-chromatin association (Tao et al, 2009). Since S80 phosphorylation of MeCP2 is correlated to the induction of apoptosis, its dephosphorylation by PP2Ac in ET might be one of the anti-apoptotic mechanisms that underlies PP2Ac-mediated immunosuppression. In addition, both phosphorylations of **HDAC1** and **HDAC2** (**Figure 35B-C**) are important for their catalytic activity and their ability to form active complexes (Adenuga & Rahman, 2010; Pflum et al, 2001). Since these deacetylases are responsible for gene-specific activation of transcription, PP2A-dependent dephosphorylation might be one of the mechanisms for PP2Ac to suppress inflammatory response in ET.

PP2Ac regulates the cross-talk between TLR4 and AKT pathways through modulating the phosphoproteome in ET macrophages

The phosphosite database analysis (Hornbeck et al, 2004) of the potential novel PP2Ac-targets revealed that these phosphorylations were identified in previous phospho-enrichment studies (**Table 4**) in LPS-induced TLR4 activation (Weintz et al, 2010; Wu et al, 2012), growth hormone-induced AKT signaling (Hsu et al, 2011), and insulin receptor-induced AKT signaling (Humphrey et al, 2013; Yu et al, 2011). Growth hormone- or insulin receptor-induced AKT signaling is a major regulator of survival, transcription, proliferation, and cell growth (**Figure 36**) (Tchevkina & Komelkov, 2012). Especially since PP2Ac is chronically active with prolonged LPS stimulation, the phosphosites shared by the phosphoproteome of LPS-induced TLR4 activation reveals the enzymes whose phosphorylation is involved in the phenotype-specific chromatin changes. Moreover the phosphosite database analysis of the potential novel PP2Ac

targets revealed that these phosphorylations were shared in phosphoproteomic studies of both growth hormone-induced and insulin-induced AKT signaling (**Figure 36**). As AKT signaling is identified in the IPA analysis among the most overrepresented pathways that get dephosphorylated by PP2Ac in ET (**Figure 26, Figure 27B**), we conclude that AKT signaling and downstream transcriptional machinery that of gets regulated by PP2Ac in LPS-tolerant macrophages.

Table 4 ET-specific PP2Ac-targeted phosphosites of chromatin regulators
These phosphosites are shared by other phosphoproteomic studies

LPS-induced TLR4 activation by Wu et al	
PHF8: S768 and S820	MCES: S11 and S15
DNMT3A: S102	MLL1: S3032
DNMT1: S138	NSD2: T110
EZH2: S362 and S366	TRM6: T284
LPS-induced TLR4 activation by Weintz et al	
DNMT1: S138	MYST1: S37 and T45
Growth hormone-induced AKT signaling (Hsu et al)	
PHF8: S768, S817, and S820	EZH2: S362 and S366
NSD3: S561	
Insulin-induced AKT signaling by Yu et al	
PHF8: S817	NSD2: T115
KDM5A: S1598 and S1603	EZH2: S362 and S366
MeCP2: S78 and S80	NSD3: S561
MCES: S11 and S15	MLL4: S1927 and S1932
MYST1: S37 and S42	SDS3: S45, T49, and S53
Insulin-induced AKT signaling by Humphrey et al	
KDM5A: S1598 and S1603	DNMT3A: S102
MCES: S11 and S15	NSD3: S561
NSD3: S561	MLL4: S1927 and S1932
MYST1: S37 and S42	SDS3: S45, T49, and S53

AKT is a known substrate of PP2Ac in regulation of pro- or anti-survival signaling (Kuo et al, 2008). More importantly, AKT activity induces survival, and is regulated by LPS-induced TLR4 activation (Bauerfeld et al, 2012) through MyD88 and IRAK1 (Li et al, 2003). Thus, the PP2Ac-targeted phosphosites we identified that also occur in the AKT-signaling datasets provide novel targets for AKT-targeted regulators

of survival in LPS response. Moreover these common phosphosites indicate the strength of our phosphoproteomic strategy in covering known interactions between TLR4 and other signaling pathways and discovering novel targets of major kinases/phosphatases in an unbiased screening. In addition, they indicate that these results are replicable and not artifacts.

PP2Ac-mediated ET is regulated by altered H3K9me2, H3K27me2, and H3S10P in macrophages

To understand the phenotypic outcome of the PP2Ac activity on the chromatin PTM and thereby to screen functionally responsible chromatin modifiers, we performed immunoblotting of the various histone PTMs in paired WT and PP2Ac-KD RAW macrophages that were either non-stimulated, or stimulated with a high dose LPS (1 µg/mL) for 5, 15, and 30 mins with (TL) or without (NL) a prior-stimulation of low dose LPS (0.1 µg/mL) for 24 h (**Figure 37, left**). We immunoblotted for PP2Ac and P-p65 (S536) to screen the knockdown efficiency and inflammation phenotype, respectively, and we used γTubulin immunoblot as a total protein control. Moreover, Since PP2Ac is known as a major regulator of chronic inflammation in macrophages (Xie et al, 2013), we confirmed that the PP2Ac-KD cells were hypersensitive to LPS stimulation, as determined by the increase in P-p65 (S536), in both acute (NL) and chronic (TL) LPS stimulation.

We compared histone PTM immunoblots in WT and PP2Ac-KD cell line and observed that

- Repressive ET-specific H3 PTMs H3K9me2 and H3K27me2 show a TL-specific decrease in PP2Ac-KD compared to WT RAW cells (**Figure 37, right panel**). This

indicates that PP2Ac activity in ET is significant for abundance of these repressive PTMs and lack thereof leads to increased demethylation.

- H3S10P is diminished in WT-TL cells while it is increased in PP2Ac-KD –TL cells compared to their non-stimulated pairs. H3S10 phosphorylation is one of the earliest PTMs characterized as active-promoter mark in LPS-induced response (Saccani et al, 2002). Previously, PP2Ac was reported as the major phosphatase removing this phosphorylation in ET-macrophages (Xie et al, 2013). Thus, we observed diminished H3S10 phosphorylation in ET in WT cells and a significant increase in phosphorylated H3S10 mark in all conditions of PP2Ac-KD cells. Since PP2Ac activity is significantly enhanced in ET, the increase in H3S10 phosphorylation in PP2Ac-KD cells compared to that of WT cells is augmented in TL condition. This indicates that the activation marker H3S10P is dephosphorylated by PP2Ac in ET macrophages.
- Not only H3K9me2 but also the combination of H3K4me2 and H3K9me2 (referred to as H3K4me2K9me2) shows significant TL condition-specific decrease in PP2Ac-KD cells compared to WT cells. This indicates that, not only the repressive PTMs, but also the activating PTMs, such as H3K4me2, get regulated by the chronic-active PP2Ac for activation of ET-specific genes.

PP2Ac inhibits the activity of PHF8 in ET to repress transcription

The repressive H3K9me2 and H3K27me2 methylations are associated with decreased response to LPS and decreased pro-inflammatory gene expression (El Gazzar et al, 2008; Wen et al, 2008). On the other hand, increased H3K9me2 and H3K27me2 abundance at the LPS-induced promoters is identified as an ET-specific gene regulation

mechanism in macrophages (El Gazzar et al, 2008; Liu et al, 2014; Turgeon et al, 2013). In TL condition, these repressive methylations are highly abundant and they show a significant decrease in specifically TL condition with PP2Ac-KD. This indicates the significance of PP2Ac in possibly *increasing the corresponding KMT activity, decreasing the corresponding KDM activity, or both* through dephosphorylation in prolonged LPS stimulation. Given the H3K27me3 blot shows the opposite trend, we conclude that PP2Ac targets ***H3K9me2- and H3K27me2/me3-specific KDMs*** to inhibit their demethylase activity for transcriptional repression in ET macrophages. As mentioned above, the only ET-specific PP2Ac-targeted KDMs in our dataset were KDM1A and KDM5A, which demethylate H3K4 (Christensen et al, 2007; Klose et al, 2007; Metzger et al, 2005), and PHF8, which demethylates H3K9me1/2 and H3K27me2 (Zhu et al, 2010). Thus, we derived the data-dependent hypothesis that PHF8 activates gene-specific transcription through demethylation of repressive histone PTMs H3K9me1/2 and H3K27me2 in LPS-induced inflammation and its enzymatic activity is negatively regulated by PP2Ac-dependent dephosphorylation in ET. In line with our hypothesis, we found that PHF8 is the only chromatin regulator that showed more than 2 phosphopeptides that are dephosphorylated by chronic active PP2Ac in ET (**Figure 38**).

DISCUSSION

Phosphorylation is one of the most abundant reversible PTM in the cell. It is involved in regulation of signaling pathways, degradation of proteins, cross-linking pathways, formation of protein complexes, and enzymatic activity of various significant enzymes. PP2Ac is a broad regulator of various signaling pathways as it targets a broad

range of proteins for dephosphorylation. Specifically in ET, PP2Ac negatively regulates the LPS-induced gene expression (Xie et al, 2013). The impact of PP2Ac on the transcriptional chromatin elements is not known.

Here we employed a powerful phosphoproteomic strategy to screen chronic active PP2Ac targets that play a role in the regulation of ET. Our quantitative analysis revealed transcriptional repression as the most extensively regulated signaling pathway by PP2Ac in ET. More importantly, validating the phenotypic response, we identified well-known phosphorylation sites of PP2Ac-targeted chromatin modifiers such as HDAC1 and MeCP2. Moreover, we discovered various novel phosphosites on chromatin regulators that may contribute to the transcriptional repression in ET via regulation by PP2Ac-dependent dephosphorylation; thus, these novel phosphosites may be major candidates for further studies investigating transcriptional regulation of LPS-induced TLR4 signaling and/or ET. In addition, we found that H3K9me2 and H3K27me2 are the most extensively affected histone H3 PTMs by the PP2Ac-KD in specifically ET phenotype, which suggests that PP2Ac mediates the *inactivation of the histone demethylases, the activation of histone methyltransferases, or both* targeting these repressive sites.

Through detailed analysis of PP2Ac-targeted phosphorylations we observed that, among the identified KDMs, PHF8 includes the highest number of phosphosites that are targeted by ET-specific PP2Ac activity. Interestingly, Ser843 (Ser880 in human) of PHF8 that we found targeted by chronically active PP2Ac was reported to be phosphorylated by CDK2/cyclin E kinase, enhancing the KDM activity of PHF8 toward H3K9me2 and promoting rDNA transcription and S-phase progression of 293T, HeLa, or U2OS cells

(Sun et al, 2015a). Because of the transcriptionally repressive nature of chronically active PP2Ac and PP2Ac-mediated dephosphorylation of catalytically important S843 of PHF8, we postulate that the KDM activity of PHF8 could be modulated in a phosphorylation-dependent way, independently from cyclin E/Cyclin-dependent kinase 2(CDK2).

Further biochemical and biophysical studies on the effect of PP2Ac-mediated dephosphorylation on the activity of various chromatin regulators will help us understand the mechanism on gene-specific transcriptional regulation downstream PP2Ac in ET and, similarly, discover how acute inflammation may be regulated in the transcriptional level through chromatin remodeling. Understanding the major regulators of LPS-induced gene-specific transcription would help us treat innate inflammation-related or -induced diseases, understand the mechanisms of dysregulated immunity, develop alternative methods and developments in immunotherapy, and prevent chronic inflammation-induced cancer progression.

FUTURE WORK

To understand the mechanism underlying the PP2Ac-mediated regulation of chromatin remodeling, more biochemical experiments exploring the changes in activity of the potential PP2Ac-targeted chromatin regulators that were found in the phosphoproteomic analysis mentioned above. For this particular experiment set, we will need to compare the specific histone demethylase and methyltransferase activities in paired WT and PP2Ac-KD cells. Currently, the commercially available histone demethylase or methyltransferase activity assay kits enable quantification of

modification-specific overall activity of various enzymes, rather than the enzyme-specific activity; thus, we will need to immunoprecipitate those chromatin modifiers to measure, and compare, their specific enzymatic activity. Understanding whether, and how enzymatic activity of each KDM or KMT gets altered by PP2Ac-KD in ET phenotype will help us pinpoint how PP2Ac might regulate ET-specific transcriptional repression. Once specific enzymes are discovered, we will perform mutation studies (Ser to Ala and Ser to Asp) to demonstrate whether these PP2Ac-targeted phosphosites are (1) significant for the KDM or KMT activity, (2) involved in the for phenotypic-transcriptional regulation of inflammatory genes, (3) actually dephosphorylated by PP2Ac, and (4) playing a role in the stability of these enzymes. The initial candidate for such extensive analysis is PHF8 as it is regulated by PP2Ac in ET according to our phosphoproteomic data.

Moreover, bottom-up and top-down quantitative proteomic screening of histone PTMs of paired WT and PP2Ac-KD cells in different inflammation phenotypes (N, NL, and TL) will also help us discover histone PTMs that are significant for phenotypic and transcriptional regulation of LPS-induced inflammation. Overexpression and knockdown studies of PHF8 would also be helpful to screen histone PTMs to demonstrate PHF8-dependent histone combinatorial code regulation with LPS stimulation in macrophages. In addition, mutational studies of PHF8 to screen demethylation of various PTMs would decipher specific PTMs of PHF8 that regulate its enzymatic activity.

FIGURES

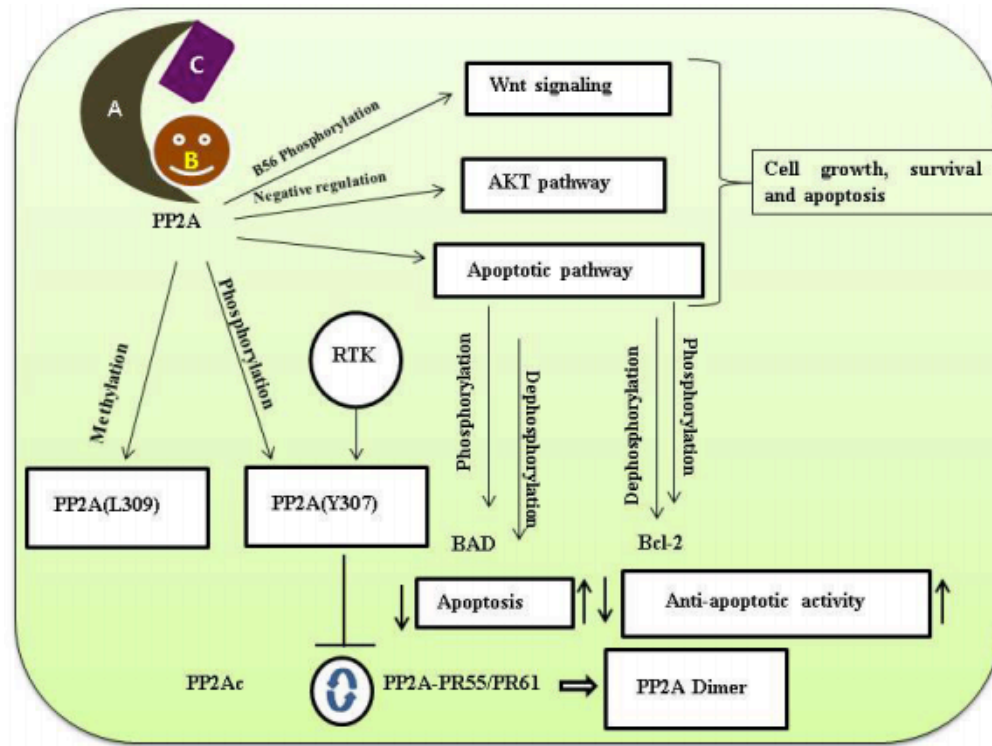


Figure 18 Role of PP2A in various signaling pathways

Methylation and phosphorylation PTMs regulate PP2A activity occurring in the conserved C-terminal sequence TPDYFL. PP2A activity is an important part in the majority of the cellular pathways, including AKT, Wnt, apoptosis, and cell growth survival

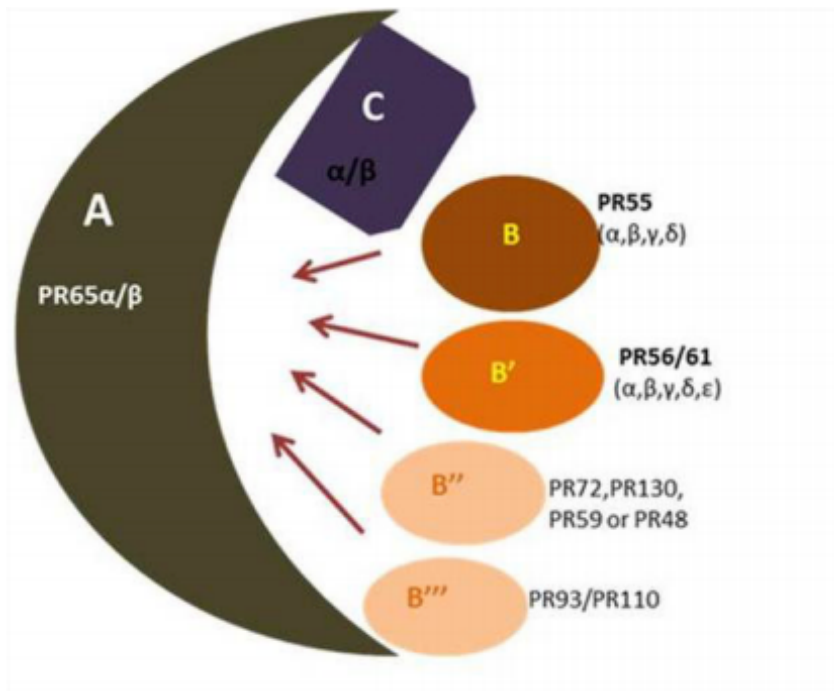


Figure 19 Schematic representation of diversity of the PP2A holoenzymes
 PP2A holoenzymes are heterotrimers consisting of a scaffold (A) and a catalytic (C) subunit that is associated with one of the regulatory subunits (B).

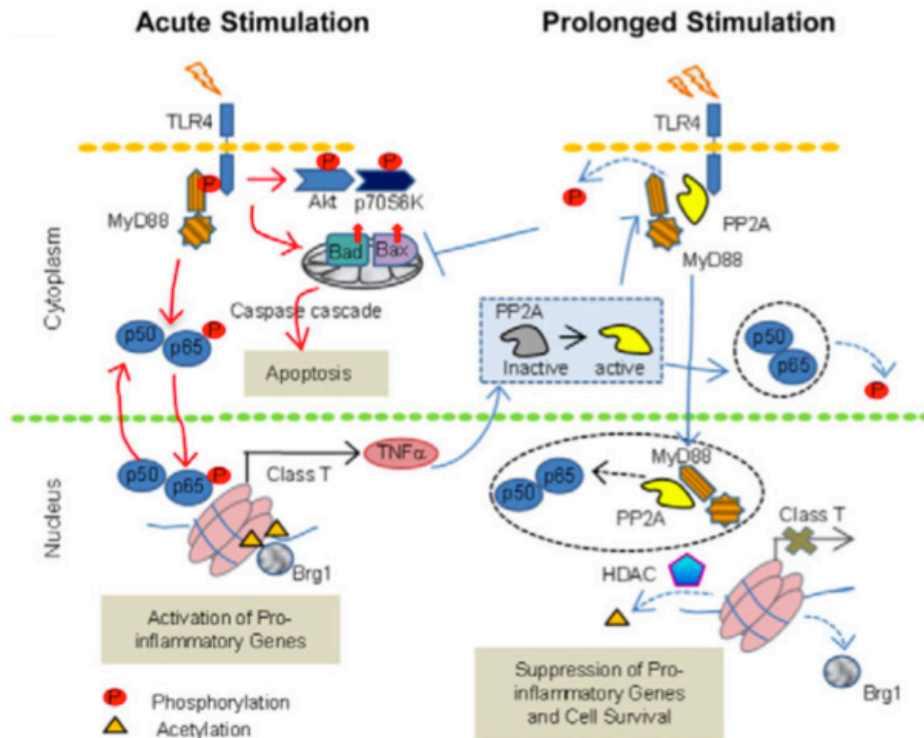


Figure 20 Chronic-active PP2Ac regulates chromatin modifications
The chronic-active PP2Ac-mediated control of the inflammation occurs via regulation of TLR-induced, MyD88-dependent, gene-specific chromatin modifications (Xie et al, 2013).

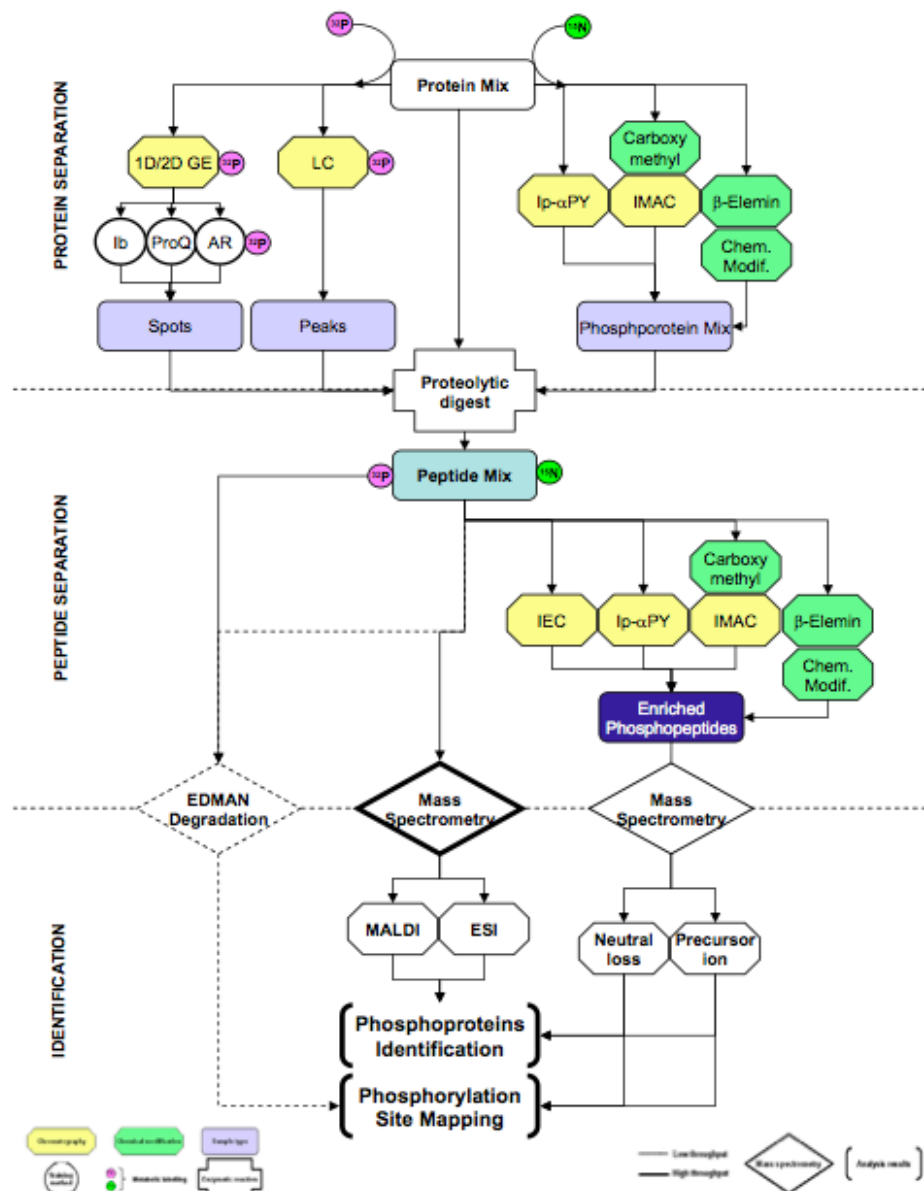


Figure 21 Schematic representation of phosphoprotein analysis workflow

The most commonly used methods to resolve, to purify or to enrich phosphoproteins are shown in the Protein separation section. Peptides resulting from trypsin digestion of phosphoproteins may be analyzed directly by MS or by Edman degradation. Other approaches may be used for the enrichment of phosphopeptides as shown in the Peptide separation section. MALDI and ESI are usually used for identification of phosphoproteins. The two predominant techniques for identification of the precise sites of phosphorylation are i) Edman degradation and ii) MS analysis (Neutral loss and Precursor ion) as shown in the Identification section. 1D/2D GE: On-dimensional/Two-dimensional gel electrophoresis. Chem. Modif.: Chemical Modification. ESI: Electrospray Ionisation. Ib: Immunoblot. IMAC: Immobilized Metal Affinity Chromatography. Ip-αPY: Immunopurification using a phospho-tyrosine antibody. LC: Liquid Chromatography. MALDI: Matrix-Assisted Laser Desorption Ionization. ProQ: Pro-Q DiamondTM. AR: Autoradiography. β-Elemin: β-elimination reaction (Delom & Chevet, 2006).

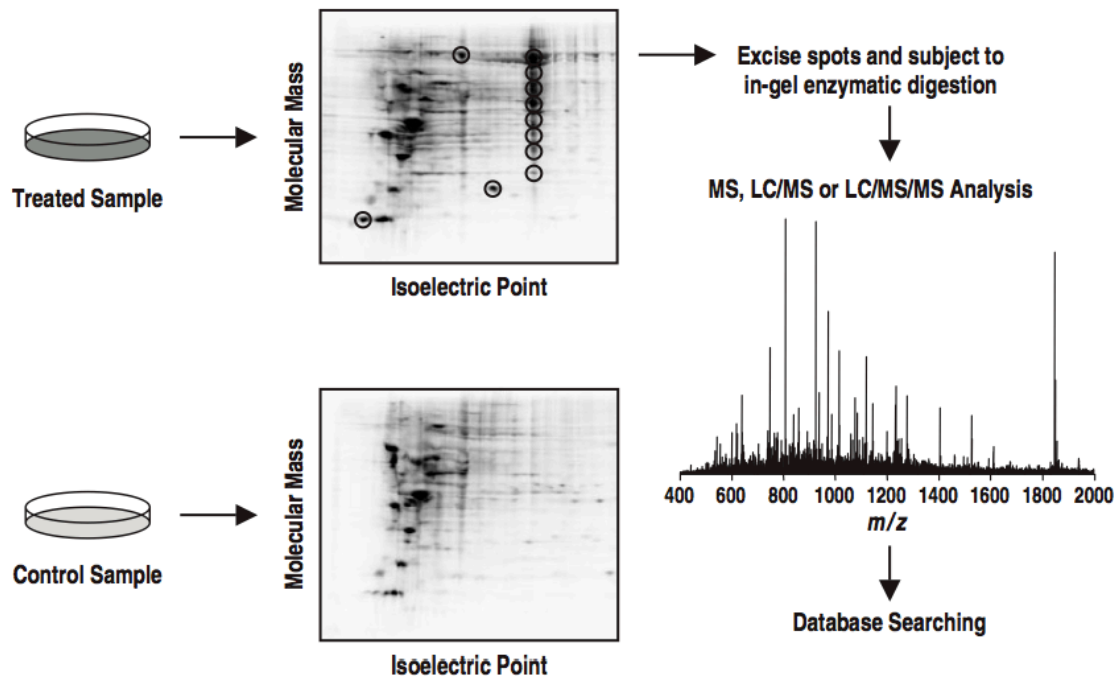


Figure 22 Proteomic analysis using two-dimensional gel electrophoresis

Proteins obtained from both control and treated samples are separated based on their isoelectric point in the first dimension (isoelectric focusing) and their molecular mass in the second dimension (SDS-PAGE). Spot intensity detected by differential phosphoprotein staining is used to quantify changes in phosphorylation. Spots of varying intensity, reflecting a measurable change in protein phosphorylation (a few are indicated with circles), are excised, and the proteins contained in each gel slice are subjected to in-gel proteolysis. The resulting peptides are extracted and analyzed by MS. Based on the mass spectral data acquired, a variety of database searching algorithms are used to identify the peptides and map sites of phosphorylation, which in turn, identify the phosphoproteins present in the sample (Goshe, 2006).

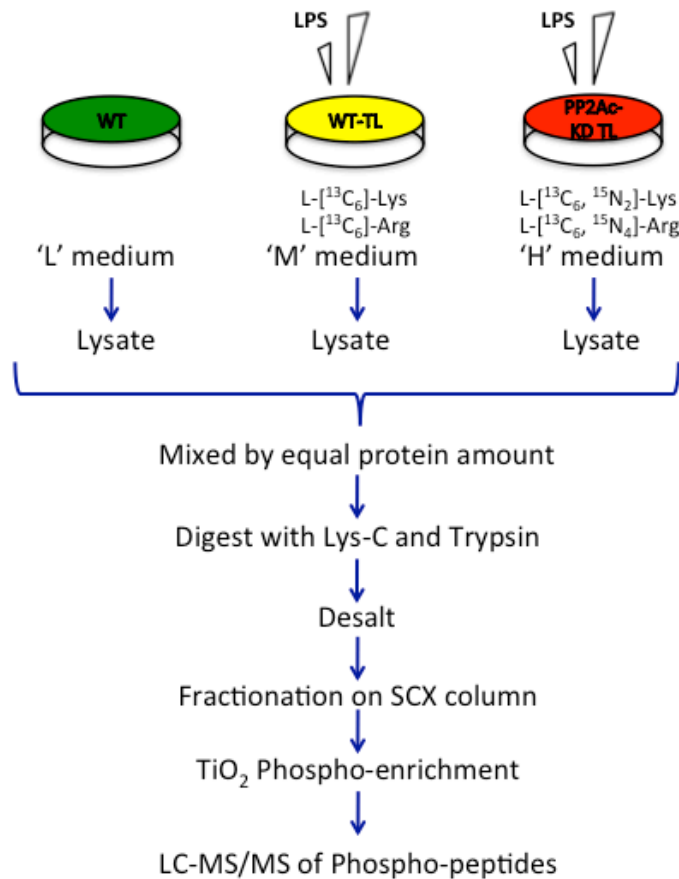


Figure 23 Quantitative phosphoproteomics workflow. Workflow of LPS stimulation and sample preparation involves amino acid-coded labeling, lysis, digestion, desalting SCX fractionation, followed by TiO₂ Phosphoenrichment (Erdoğan et al, 2016).

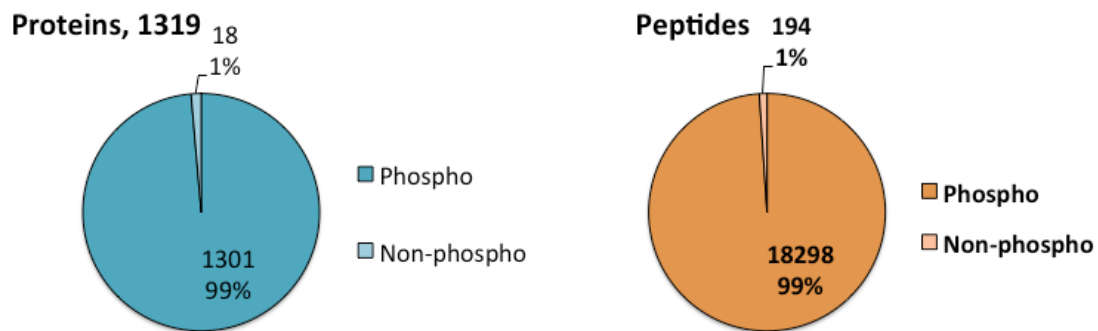


Figure 24 Phosphoproteomic analysis shows 99% phospho-enrichment efficiency. Proteins (left, blue) and peptides (right, orange) that were identified in the phosphoproteomic analysis revealed 99% phospho-enrichment efficiency. 1319 total proteins and 18,492 total peptides were identified. 1301 of the proteins were phosphorylated while 18,298 peptides were phosphopeptides.

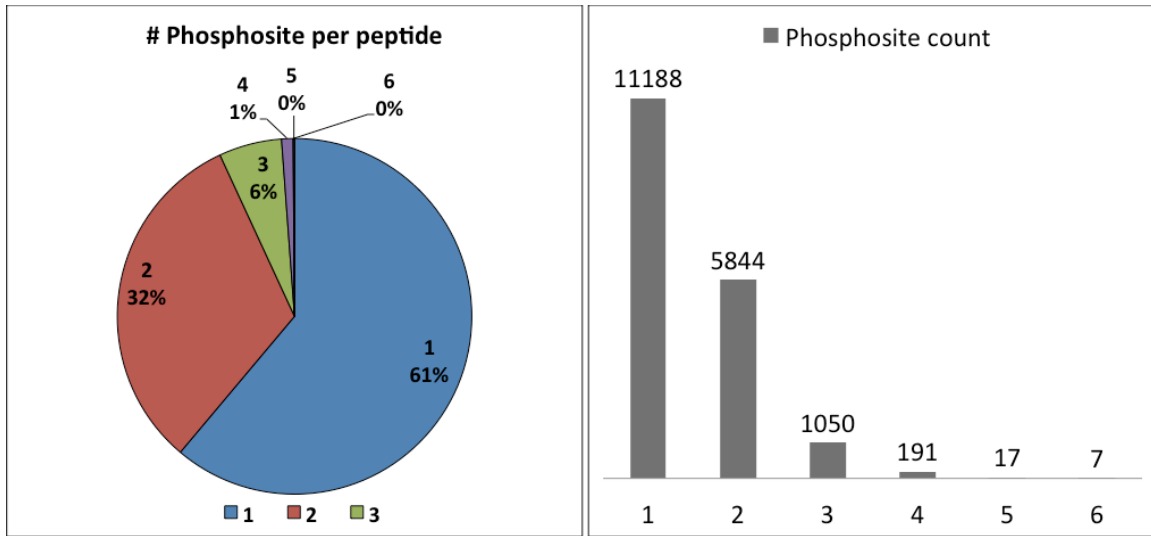


Figure 25 Identified phosphopeptides mostly cover single phosphorylation
The percentage of the number of phosphorylation per peptide is given on the left while the right graph depicts the histogram showing the number of peptides having a given number of phosphorylations

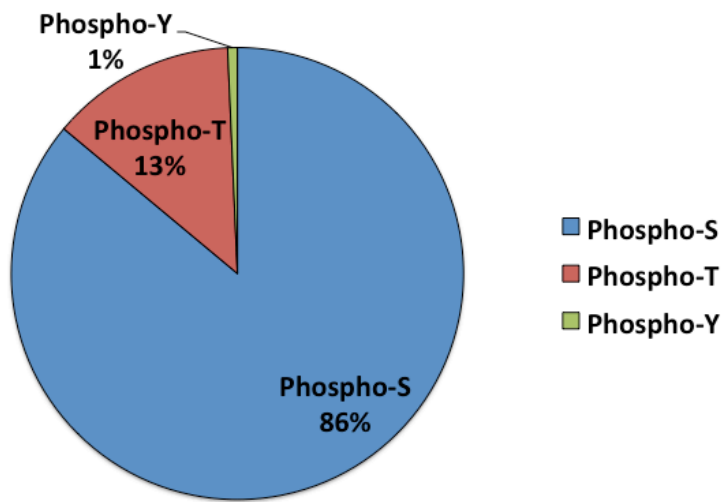


Figure 26 Distribution of Phospho STY identifications
86% of the phosphopeptides were Phospho-S, while 13% and 1% were Phospho-T and Phospho-Y, respectively.

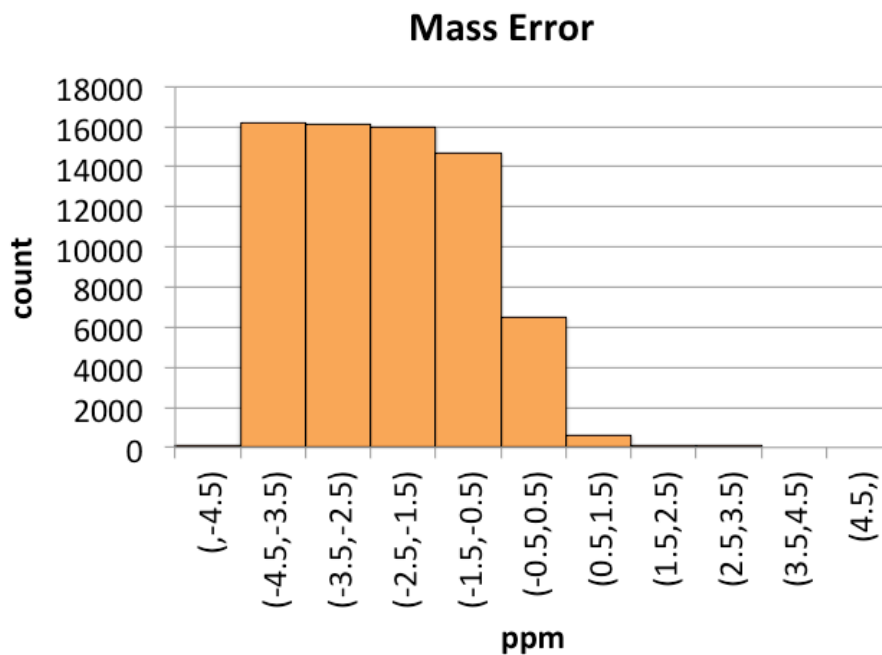


Figure 27 Identified mass error
The mass error was identified by MaxQuant for normalization of the quantitative proteomics

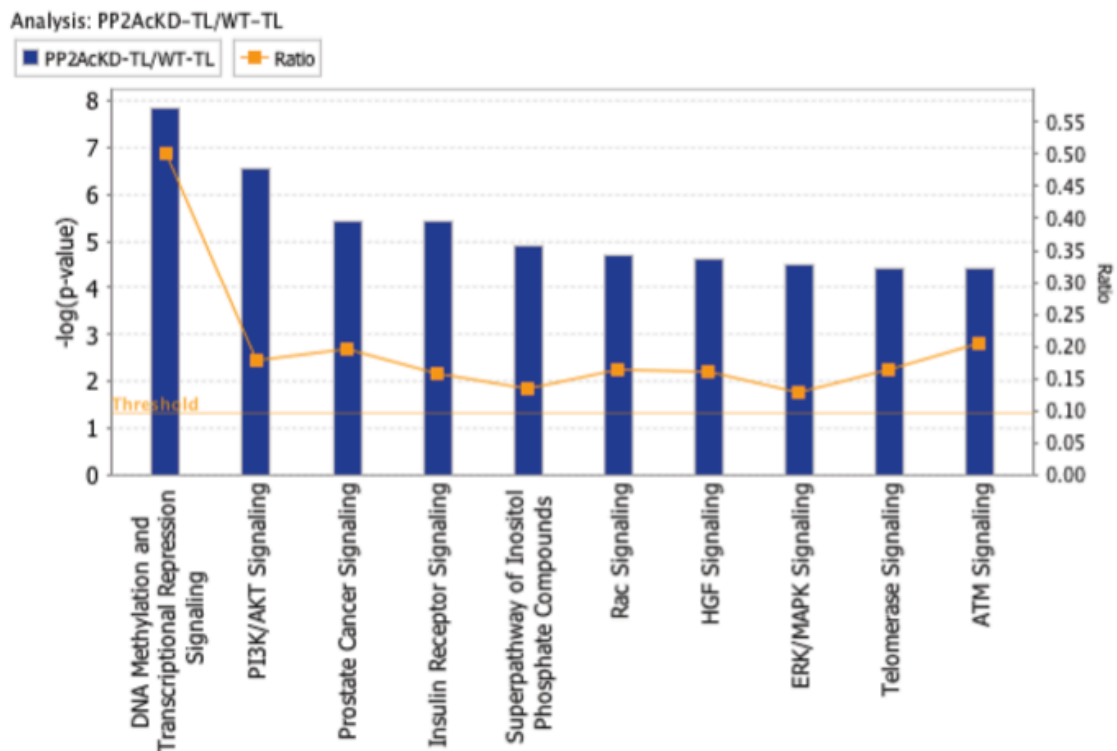
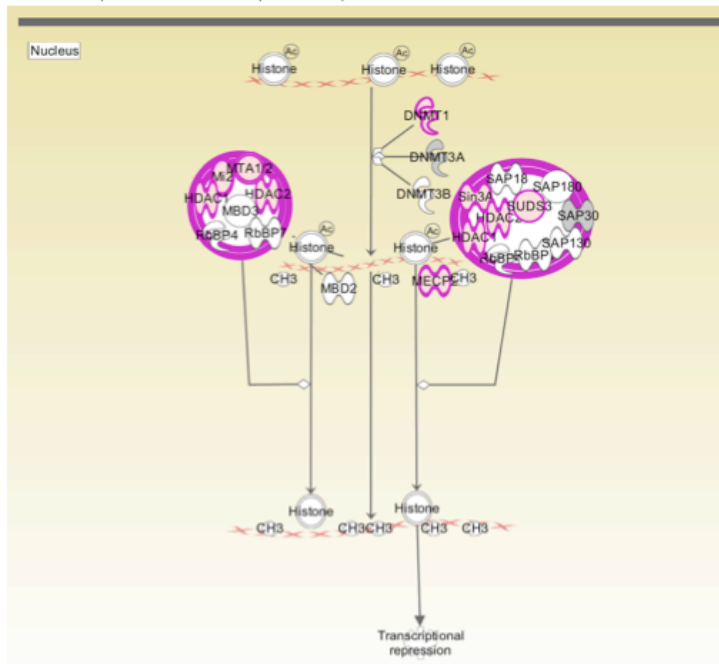
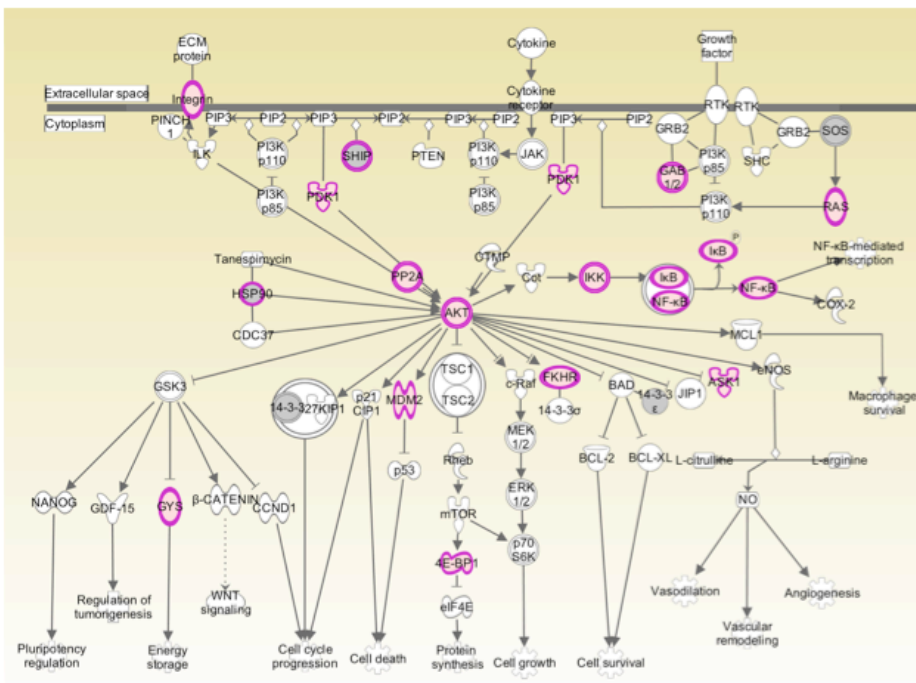


Figure 28 The top signaling pathways targeted by PP2Ac in ET macrophages
Only the top 10 over-represented signaling pathways are shown.
These signaling pathways include the highest number of proteins that show increased phosphorylation in PP2Ac-KD RAW cells compared to WT RAW cells in ET (Erdoğan et al, 2016).

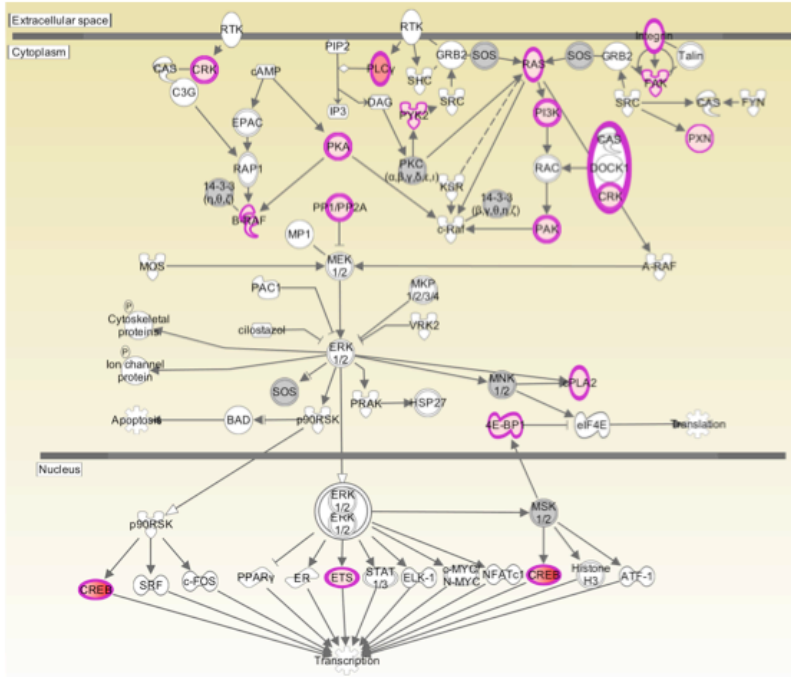
A DNA Methylation and Transcriptional Repression



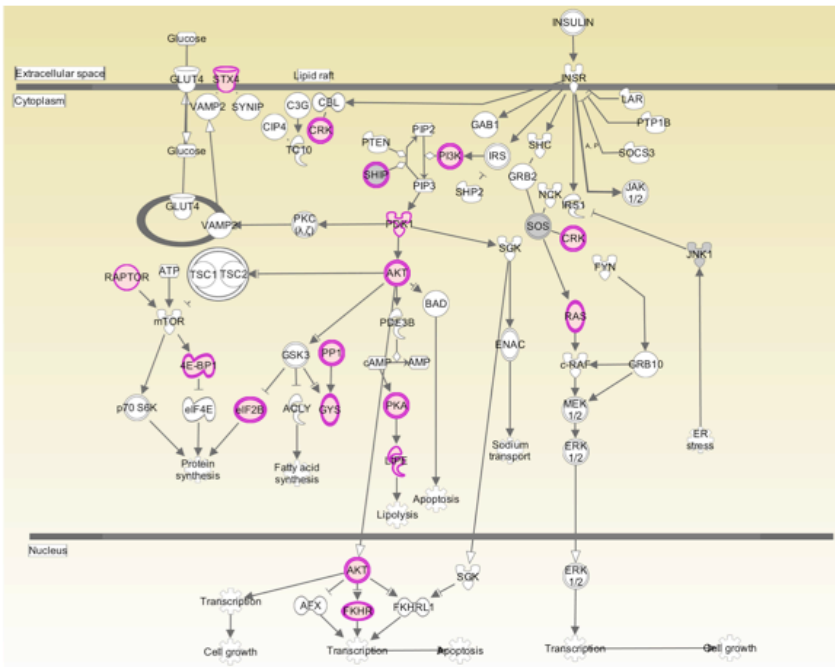
B PI3K/AKT signaling



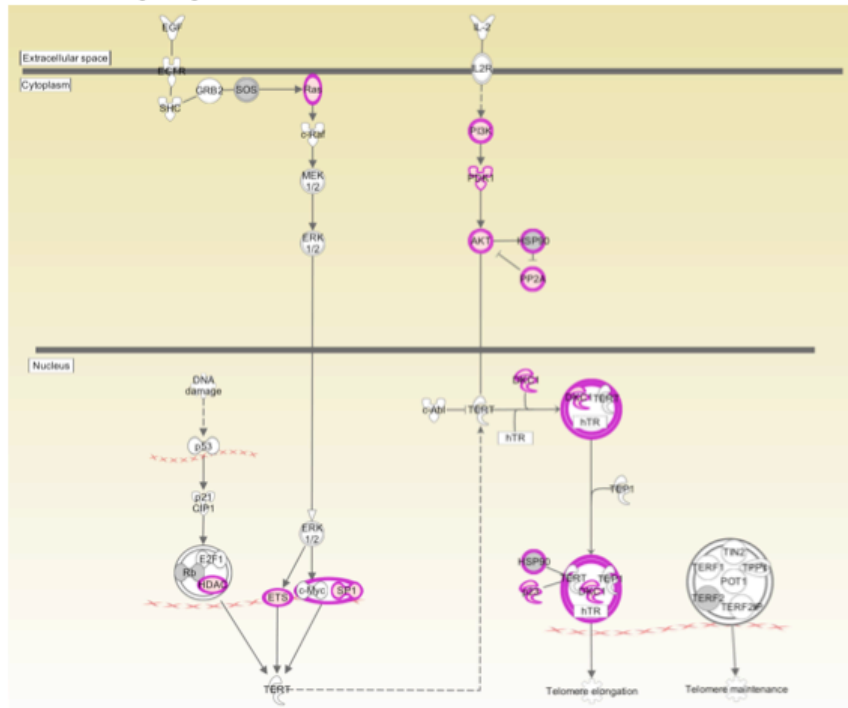
C



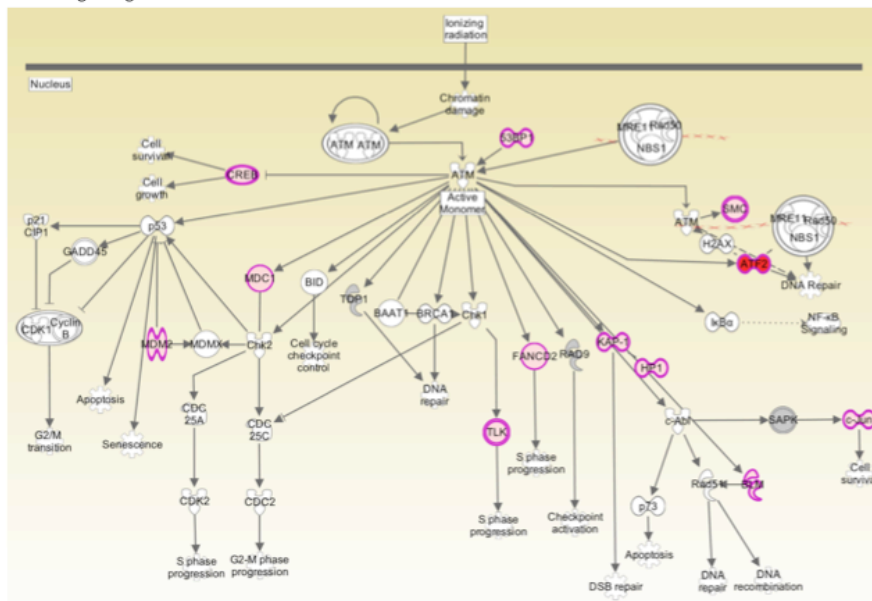
D



G



H



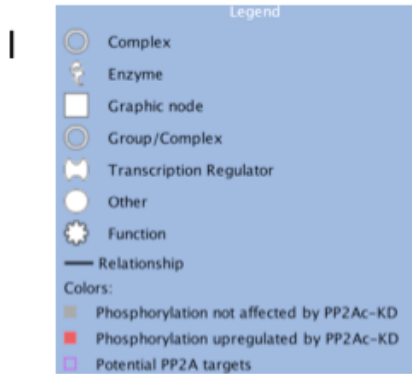


Figure 29 Top signaling pathways that are targeted by PP2Ac

PP2Ac broadly targets the signaling pathways through dephosphorylating chromatin regulators in ET. The top signaling pathways including proteins with increased phosphorylation in PP2AcKD-TL compared to WT-TL include many chromatin regulators (Erdoğan et al, 2016). The most extensive change in PP2Ac-dependent dephosphorylation occurs in the DNA Methylation and Transcriptional Pathway in line with transcriptionally-repressive role of PP2Ac. A. DNA Methylation and Transcriptional Pathway, B. PI3/AKT Signaling, C. Insulin Receptor Signaling, D. Rac Signaling, E. HGF Signaling, F. ERK/MAPK Signaling, G. Telomerase Signaling, H. ATM Signaling, and I. Legend for shape and shade colors.

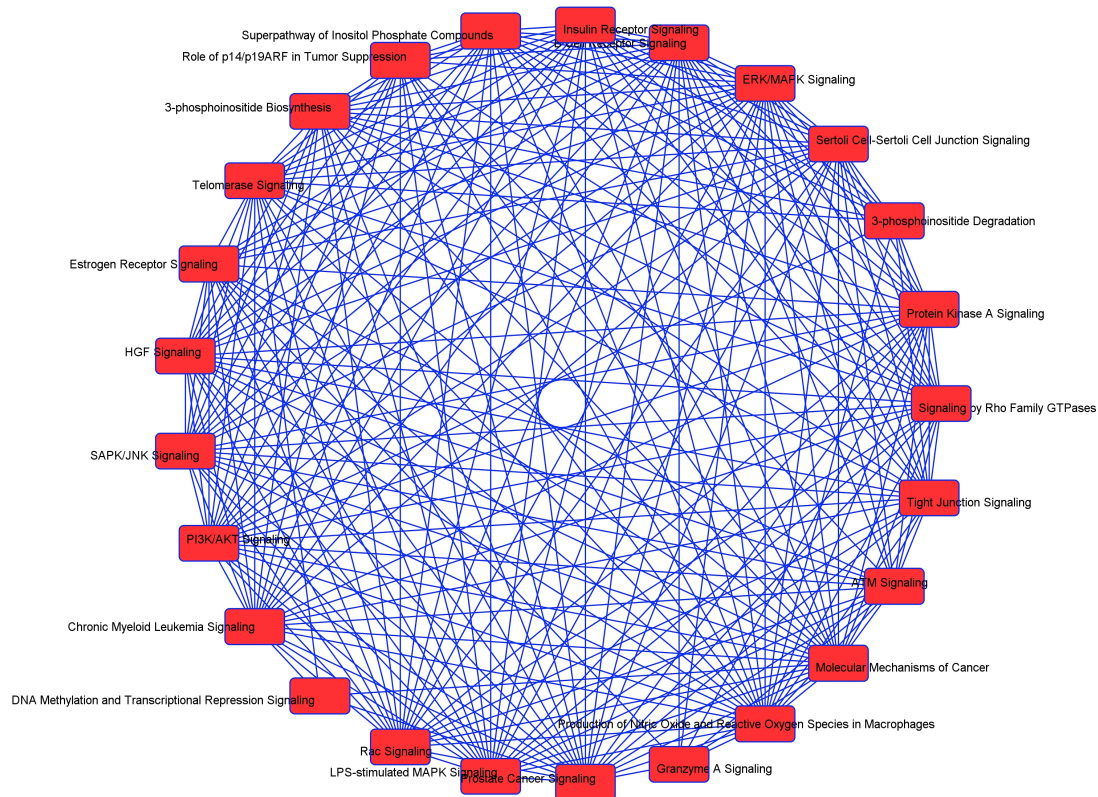


Figure 30 PP2Ac affects a broad range of signaling pathways in ET.

IPA Canonical Pathway Analysis reveals the signaling pathways whose proteins show increased phosphorylation with PP2Ac-KD compared to WT RAW cells in ET-tolerant macrophages.

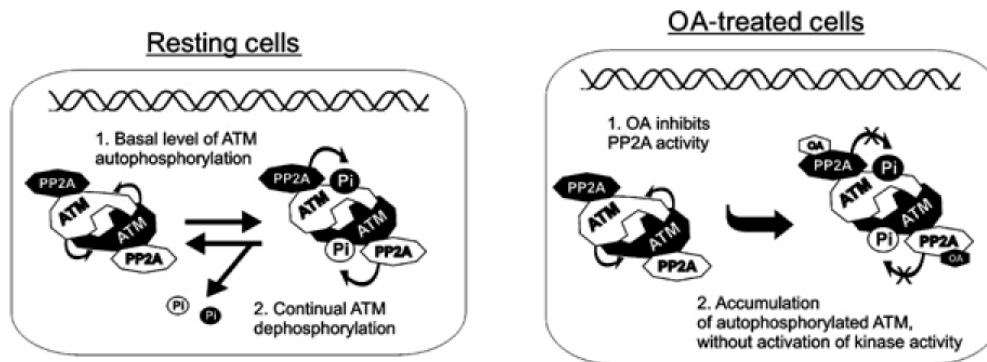
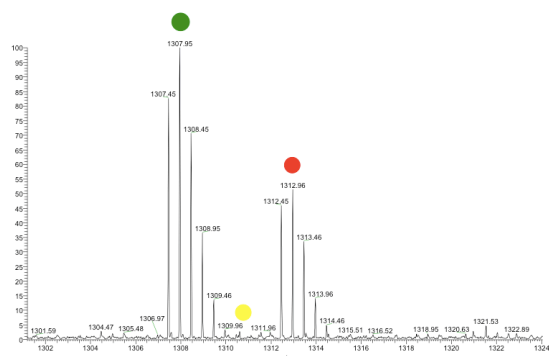
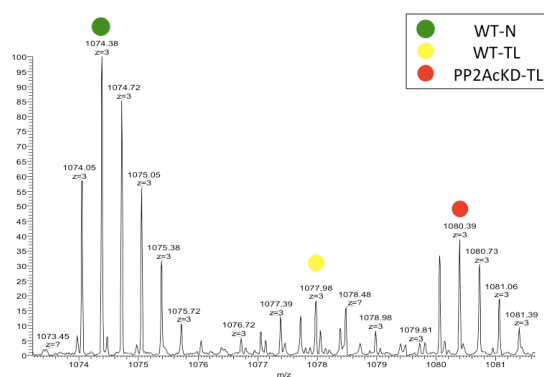


Figure 31 PP2Ac negatively regulates ATM signaling.
ATM activity is regulated by authophosphorylation which is negatively regulated by PP2Ac activity (Goodarzi et al, 2004).

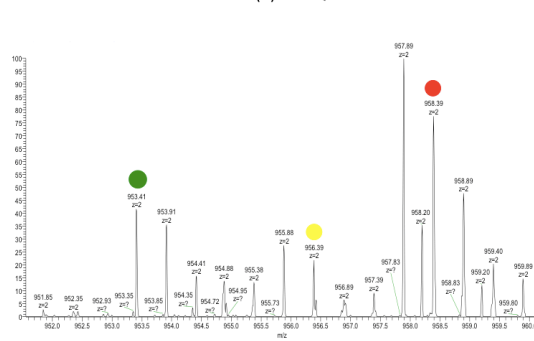
KDM1A P-S132 – P-S138: EMDESLANLS(p)EDEYYS(p)EEER



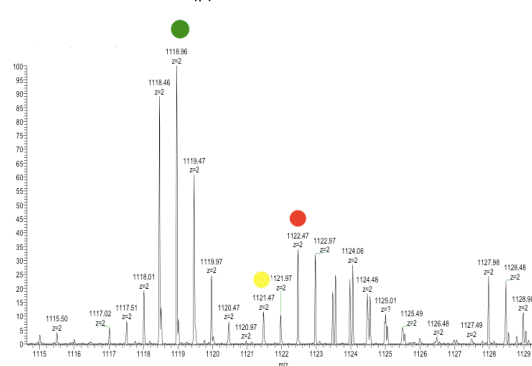
KDM5A P-S1598 – P-S1603: YDWS(P)GAEES(P)DDENAVCAAQNCQRPCK



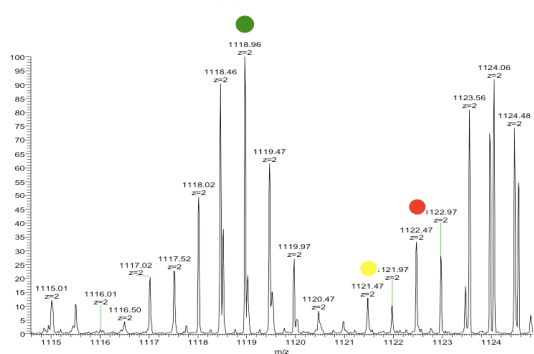
PHF8 P-S766: SSGSSSSGLGTVSS(p)SPASQR



PHF8 P-S817: DAEYIYPS(p)LESDDDDPALK



PHF8 P-S820: DAEYIYPSLES(p)DDDDPALK



PHF8 P-S843: NSDDAPWS(P)K

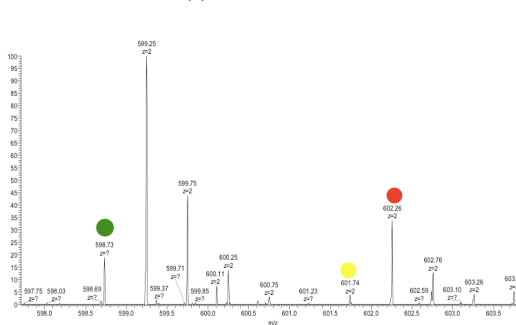


Figure 32 The MS spectra of KDMs that are dephosphorylated by PP2Ac in ET.
Top Row: KDM1A (P-S132 and P-S138) and KDM5A (P-S1598 and P-S1603), Middle and Bottom Rows: PHF8 (P-S766, P-S817, P-S820, and P-S843). Green circle: m/z of WT-N (Light), Yellow circle: m/z of WT-TL (Medium), and Red circle: m/z of PP2Ac-KD-TL (Heavy).

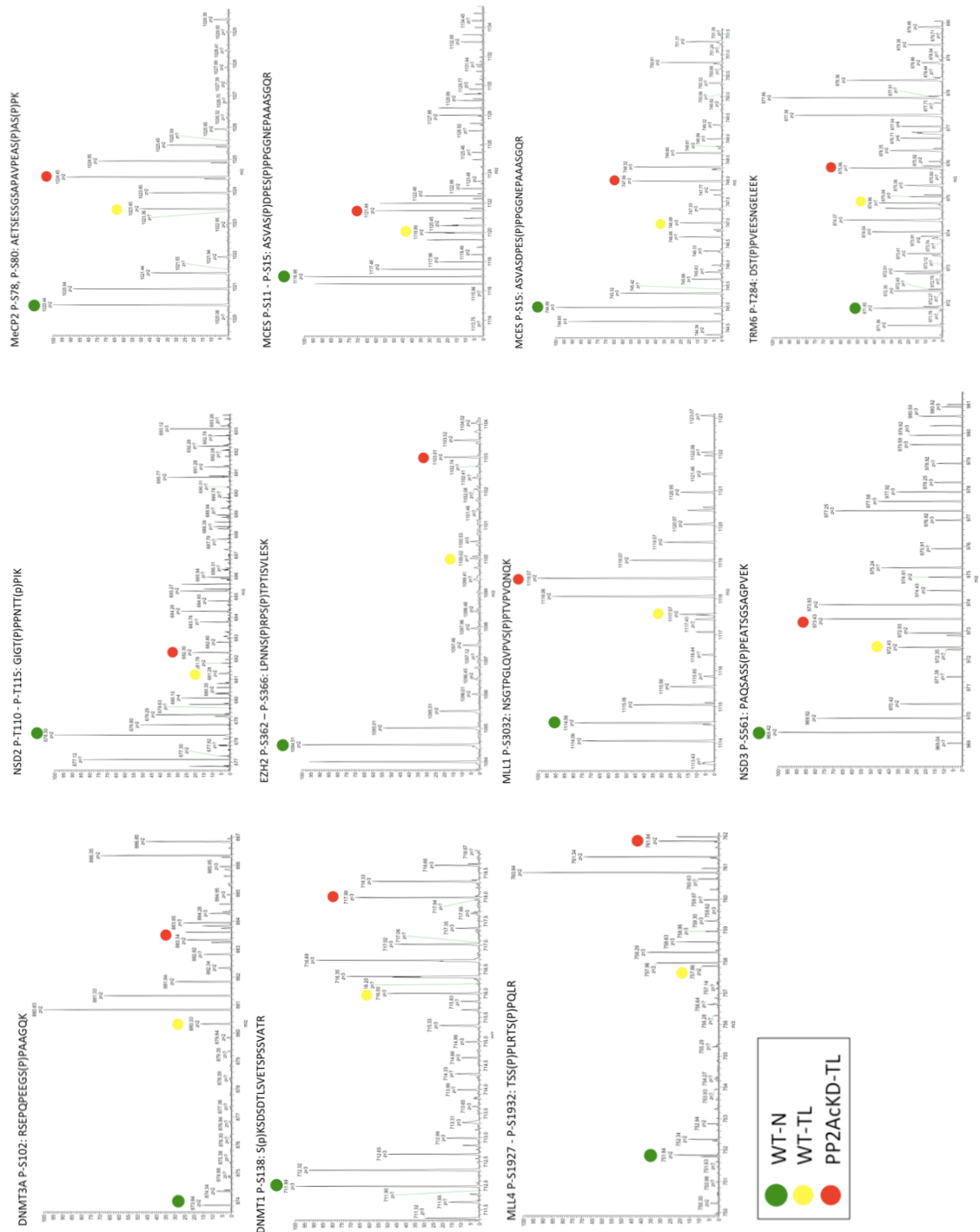
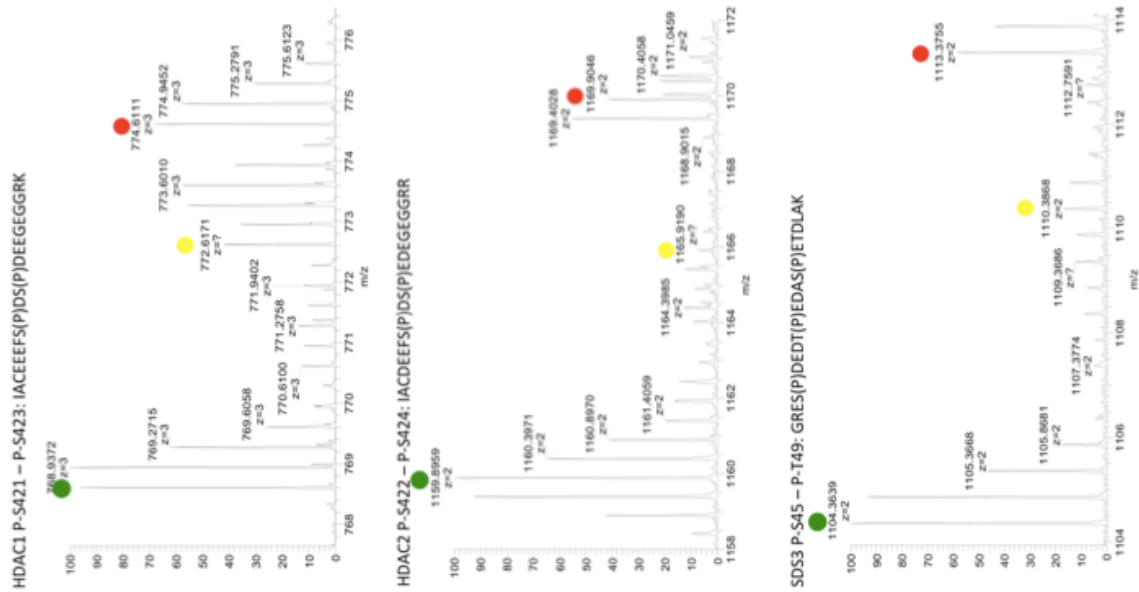


Figure 33 The MS spectra of KMTs that are targeted by PP2Ac in ET. Top Row: MeCP2 P-S78/P-S80, MCES P-S11/P-S15, MCES P-S152, and TRM6 P-T284. 2nd Row: NSD2 P-T110/P-T115, EZH2 P-S362/P-S366, MLL1 P-S3032, and NSD3 P-S561, and Bottom Row: DNMT3A P-S102, DNMT1 P-S138, and MLL4 P-S1927/P-S1932. Green circle: m/z of WT-N (Light), Yellow circle: m/z of WT-TL (Medium), and Red circle: m/z of PP2Ac-KD-TL (Heavy).

A



B

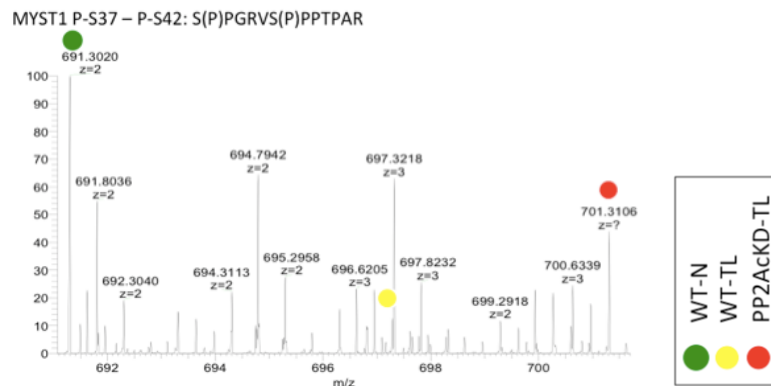


Figure 34 The MS spectra of PP2Ac-targeted deacetylases and acetyltransferases (A) deacetylases and (B) acetyltransferases (B) that are targeted by PP2Ac in ET. Green circle: m/z of WT-N (Light), Yellow circle: m/z of WT-TL (Medium), and Red circle: m/z of PP2Ac-KD-TL (Heavy).

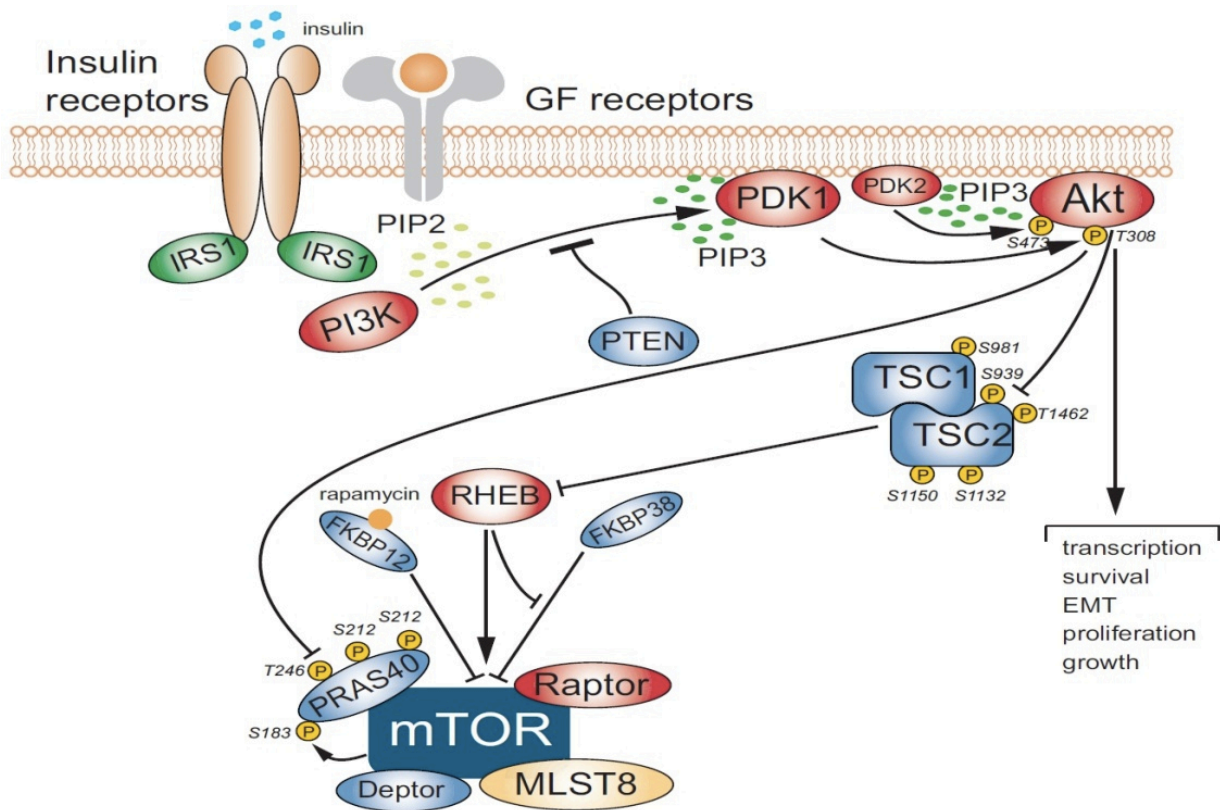


Figure 36 Growth factors and insulin regulation of mTORC signaling via AKT. mTORC1 activity is modulated by a number of positive (shown in red) and negative (shown in blue) regulators. Growth factors activate mTORC1 indirectly by suppressing the function of its negative regulator TSC1/TSC2 complex. PI3K-AKT dependent phosphorylation inhibits the TSC1/2 complex allowing activation of TORC1. AKT also activates mTORC1 through negative phosphorylation of mTORC1 suppressor, PRAS40. (REF: DOI: 10.5772/48274)

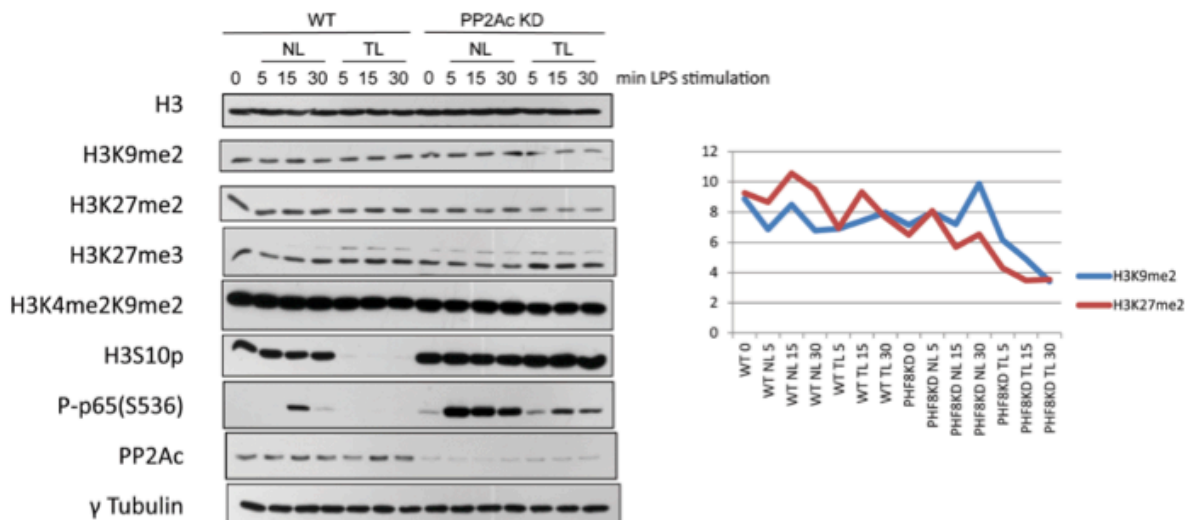


Figure 37 Histone PTM changes regulated by PP2Ac activity in ET
Left panel shows the immunoblotting of histone PTMs H3K9me2, H3K27me2, H3K27me3, H3K4meK9me2, and H3S10P using H3 immunoblot as a loading control for these. Inflammation phenotype was confirmed with the P-p65 (S536) immunoblot, PP2Ac immunoblot shows the PP2Ac knockdown efficiency, and γ tubulin is used as the cellular loading control. Right panel shows the quantification of the densitometer scanning of H3K9me2 (blue line) and H3K27me2 (red line) bands from the immunoblots (Erdoğan et al, 2016).

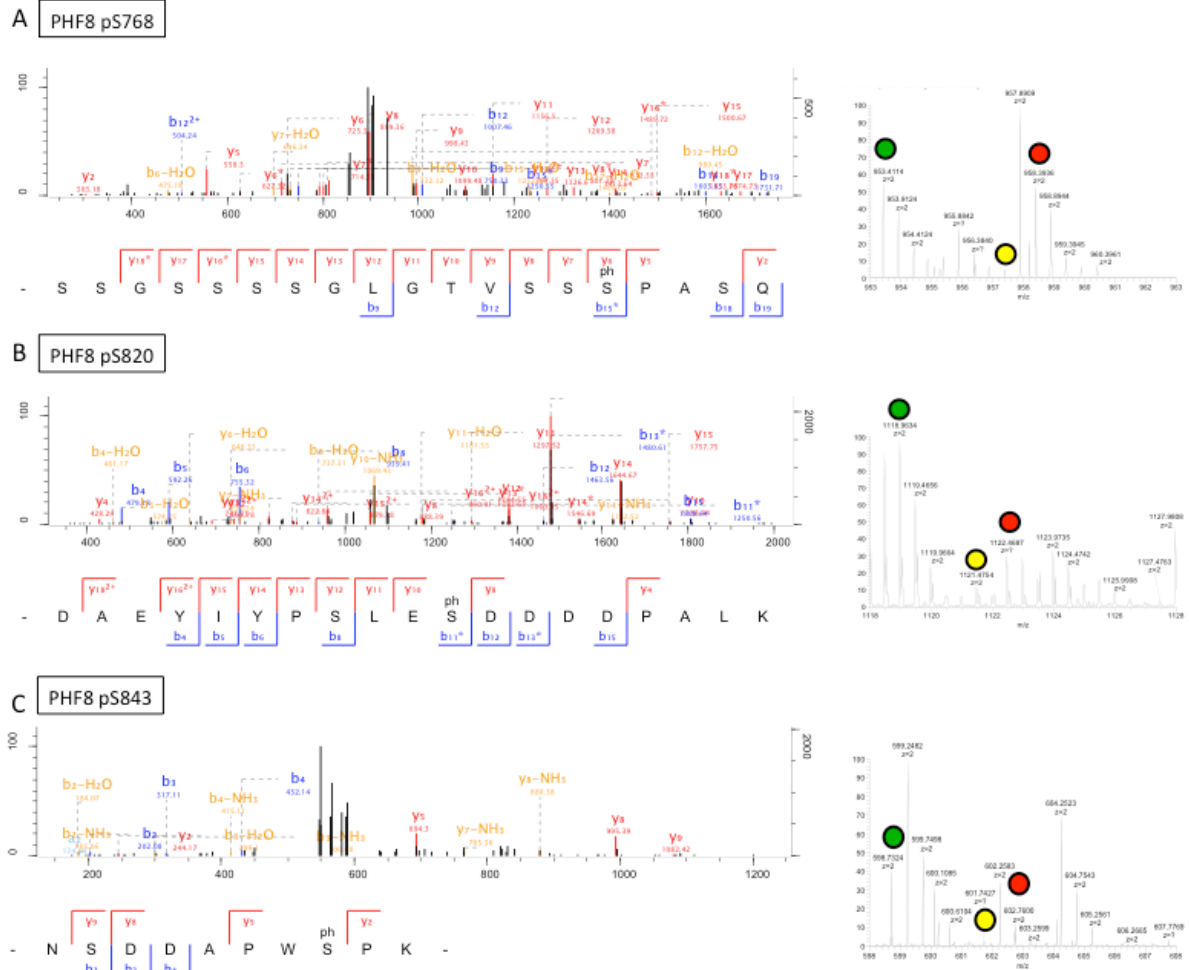


Figure 38 The MS/MS (Left) and MS (Right) spectra of PHF8 phosphopeptides.
These phosphopeptides are targeted by PP2Ac in ET (Erdoğan et al, 2016).

CHAPTER 3: PHF8 IS ACTIVATED IN LPS-INDUCED MACROPHAGES TO POSITIVELY REGULATE CYTOKINE EXPRESSION AND NFκB ACTIVITY

OVERVIEW

Epigenetic regulation of gene-specific transcription determines the phenotype-specific LPS-induced inflammation response in macrophages. Through the phosphoproteomic screening of PP2Ac-targeted chromatin modifiers in ET-macrophages, we identified PHF8 as a positive regulator of LPS-induced acute inflammation. To understand how PHF8 regulates the LPS-induced acute inflammation response, we performed immunoblotting to understand the histone PTMs that are altered by PHF8 in LPS response. Our analysis identified H3K9me1 and H3K9me2 as the major targets of PHF8 during LPS-induced inflammation response in macrophages. Then, by performing co-immunoprecipitation (CoIP), we demonstrated that PHF8 binds to p65 subunit of NFκB in acute inflammation, regulates the nuclear translocation of phosphorylated p65, and the complex formation is weakened with prolonged LPS stimulation. These results indicate that the PHF8-dependent NFκB regulation in LPS-stimulated macrophages is transient. Moreover, via dual luciferase-reporter assay, we demonstrated that, by binding to p65, PHF8 positively regulates NFκB transcriptional activity upon LPS stimulation. To further prove the gene-specific transcriptional regulation of inflammatory genes by PHF8 in LPS response, we performed qPCR experiments and demonstrated that PHF8 is involved in the gene-specific

transcriptional regulation of pro-inflammatory cytokines. Overall the transient activation of PHF8 supports our conclusions that *PHF8 is activated in LPS-induced acute inflammation, positively regulates NFκB transcriptional activity, modulates the gene-specific pro-inflammatory cytokine expression, and is negatively regulated by PP2Ac-dependent dephosphorylation in ET.*

INTRODUCTION

Histone Demethylase PHF8

PHF8 is a JmjC domain containing histone KDM that removes the repressive methyl marks from H3K9me1/2, H3K27me2, or H4K20me1, promoting the transcription of target genes (Fortschegger et al, 2010; Klose et al, 2006). The domain structure of PHF8 is composed of an amino-terminal PHD Finger domain responsible detection of Kme and a catalytic JmjC domain (**Figure 39**) (Klose et al, 2006). The Serine-rich region is towards the carboxy-terminus. The PP2Ac-targeted phospho-Serine residues identified in the phosphoproteomic study occur at or near the Ser-rich domain and they are conserved among human and mouse (**Figure 39, Figure 40**). Based on the crystal structure, JmjC domain has eight β-sheets that create an enzymatic core that binds to Fe(II) and αKG, hydroxylating the substrate and leading to removal of the methyl group in the form of formaldehyde (**Figure 41**) (Clifton et al, 2006; Yu et al, 2010; Yue et al, 2010). PHF8 activity regulates brain and craniofacial development in zebrafish and its truncated or missense mutations lead to X-linked mental retardation (XLMR) associated with cleft lip/palate (CL/P) (Kleine-Kohlbrecher et al, 2010; Laumonnier et al, 2005; Qi et al, 2010). More recent studies shed light on

the functional mechanism of neuronal development by PHF8 activity through regulation of cytoskeletal dynamics (Asensio-Juan et al, 2012). PHF8 regulates organization of actin cytoskeleton, cell adhesion, and neuronal growth through H4K20me1 demethylation at the promoters of Ras homolog gene family, member A (RhoA), Ras-related C3 botulinum toxin substrate 1 (Rac1), and Glycogen synthase kinase-3 Beta (GSK3 β).

PHF8 is a transcriptional coactivator that recognizes H3K4me3 mark at the promoters of the active or poised genes and gets recruited to those promoters for interaction with RNA-PII (Figure 42) (Fortschegger et al, 2010). PHF8 was also identified as a transcriptional regulator of ribosomal RNA (rRNA) through its H3K9me2 demethylase activity (Zhu et al, 2010). To positively regulate ribosomal DNA (rDNA) transcription, PHF8 interacts with RNA-PI and Tryptophan-Aspartic acid (WD)-repeat domain 5 (WDR5)-containing H3K4 KMT complexes (Feng et al, 2010). On the other hand, PHF8 is an essential regulator of cell cycle progression through its H4K20me1 demethylase activity (Liu et al, 2010). Following recruitment to the promoters of cell-cycle related genes, PHF8 demethylates repressive H4K20me1 marks to enable G1/S transition. Moreover, in prophase, *phosphorylation dependent dissociation of PHF8 from the promoters* lead to increased H4K20me1. H4K20me1 demethylation by PHF8 is also crucial for G2/M transition (Lim et al, 2013); it activates the G2/M gene expression for progression of mitosis and its loss leads to prolonged G2 phase or defective mitosis. More importantly, this regulation of cell-cycle by PHF8 is a phosphorylation-dependent process (Sun et al, 2015a). Cyclin E/CDK phosphorylates PHF8 at S844 activating H3K9me2 demethylation to induce PHF8-dependent rRNA transcription and cell cycle

progression. Phosphorylation-dependent regulation of PHF8 activity was also reported in the all-trans retinoic acid (ATRA) response in acute promyelocytic leukemia (APL)(Arteaga et al, 2013). Overall, these suggest that phosphorylation may be a broad mechanism for regulation of PHF8 activity.

In line with its role in cell-cycle progression, PHF8 regulates the migration and invasion of Prostate cancer (PrCa) (Björkman et al, 2012), (ESCC) (Sun et al, 2013), non-small cell lung cancer (NSCLC) (Shen et al, 2014), and laryngeal and hypopharyngeal squamous cell carcinoma (LHSCC) (Zhu et al, 2015); more importantly, in all of these cancers, high PHF8 expression leads to poor survival, indicating that PHF8 may be a potential diagnostic marker. The knockdown studies revealed that PHF8 knockdown leads to DNA damage and apoptosis (Shen et al, 2014), decreased cell motility (Björkman et al, 2012), reduction in the migratory and invasive cells (Sun et al, 2013), and increased expression of pro-apoptotic genes Tumor protein p53 (TP53), B-cell Lymphoma 2(Bcl2)-like protein 4 (BAX), and Caspase 3 (CASP3) (Muranko, 2014). These indicate that PHF8 is an important target in cancer progression as it positively regulates the cell migration and invasion.

Recent studies revealed that PHF8 has a role of inhibiting the Akt-Mechanistic target of rapamycin (mTOR) pathway both in vivo and in vitro (Liu et al, 2015). Moreover, PHF8 is a major regulator of bone repair and wound healing through regulation of special At-rich sequence-binding protein 2 (SATB2) expression (Han et al, 2015). These functional roles of PHF8 might be involved in LPS-induced cell response, as cytoskeleton changes, cell cycle, cell migration, and transcription are important

events in inflammation response. However, the role of PHF8 in the control of inflammation response hasn't been investigated.

Here, we are first to identify PHF8 as a major regulator of inflammatory gene expression. Our results show that it demethylates H3K9me1/me2, binds to p65, positively regulates the transcriptional activity of p65, and regulates the gene-specific transcription of pro-inflammatory cytokines upon LPS stimulation in macrophages.

MATERIALS AND METHODS

Reagents

LPS was purchased from Invitrogen. All protease inhibitor cocktails were purchased from Sigma-Aldrich (St. Louis, MO). All culture media and FBS were obtained from GIBCO. Trypsin was purchased from Promega. All chemicals were sequence- or HPLC-grade unless specifically indicated. Antibodies for p-I κ Ba (S32), I κ Ba, p-p65 NF κ B (S536), and p65 were purchased from Cell Signaling. Antibodies for Lmnb1 and p65 were from Santa Cruz Biotechnology while antibodies to γ -tubulin, histone H3, H3K9me2, H3K9me1, and H3K27me2 were from Abcam. Antibody for PHF8 was from Bethyl Labs. Bacterial clones for shRNA against PHF8 or against PLKO.1 were purchased from Sigma-Aldrich. 293-TLR4-MD2-CD14 cells were purchased from Invivogen. PureProteome Magnetic beads for CoIP experiments were purchased from Millipore.

Plasmids

pMSCV-hPHF8-FLAG-Neo and EcoPak viral packaging plasmids were kindly provided by Dr. Greg Wang. pBabe-puro (EV) was purchased from Sigma.

Cell Culture

RAW 264.7 cells were maintained in 4.5 g/L glucose DMEM with 10% FBS. For all LPS pre-treatment 0.1 µg/mL LPS is used while high dose LPS treatment and second challenges were done with 1 µg/mL LPS.

Transfection and Stable PHF8 Knock-down (PHF8-KD) RAW Cell Line

The lentiviral plasmids pLKO.1 expressing shRNA-PHF8 (targeting sequences CGACCCTGATAATAAGACCAA and GCAAGATGAAACTCGGTGATT in human and mouse, respectively) were purchased from Sigma. A pLKO.1 empty vector without a specific shRNA sequence was used as the wild-type control. To produce virus, pLKO.1-shRNA plasmids were co-transfected into 293T cells with ViraPowerMix (Invitrogen) by jetPRIME™ in vitro DNA and siRNA transfection reagent (Polyplus). Pseudo-virus in supernatants was collected 48 h after transfection and used to transduce RAW 264.7 cells by spinoculation. 48 h after transfection, 8 µg/ml puromycin was added to select puromycin-resistant clones. Stable clones were maintained in medium containing 4 µg/mL puromycin. The expression level of PHF8 in PHF8-KD cell line was monitored with immunoblotting and qPCR.

Immunoblotting of Histone PTMs

Paired WT and PHF8-KD RAW cells were stimulated with 1.0 µg/mL LPS for 0, ¼, 2, 8, and 24 h. Cells were harvested and lysed with buffer containing 0.5% NP-40, 10 mM Tris pH 7.5, 150 mM NaCl, 0.4 mM EDTA, 2 mM Na₃PO₄, 1x phosphatase inhibitor cocktail (Pierce), and 1x protease inhibitor cocktail (Sigma-Aldrich). The lysates were sonicated twice at level 3 for 5 sec for successful release of the chromatin, then were

separated on an SDS- PAGE gel under reducing conditions, and transferred to a PVDF membrane. The membranes were blocked with milk for 1 h at RT on an orbital shaker. Following primary antibody incubation for 1 h at RT, we probed the membranes with a horseradish peroxidase conjugated secondary antibody and bands were detected using an ECL Western Blotting Detection Kit (GE Life Sciences).

RNA Isolation and qPCR for PHF8 mRNA expression analysis

Stable cell lines were seeded into 12 well cell culture dishes and treated with LPS for indicated times. Total RNA was isolated using illustra RNAspin Mini Kit (GE Healthcare Life Sciences). First-strand cDNA was synthesized by M-MLV reverse transcriptase (Promega) and diluted 5-fold for qPCR. qPCR was performed using Maxima SYBRGreen/ROX (Thermo Scientific), and primer sequences “5-aacacaacaaatgctaactct-3”, and “5-agaagttccctccgaatgct-3”. All measurements were normalized against Glyceraldehyde 3-phosphate dehydrogenase (GAPDH) as the internal control using 2- $\Delta\Delta C_t$ method with primer sequences “5-aactttggcattgtggaagg-3”, and “5-acacattggggtaggaaca-3”.

Nuclear-Cytoplasmic Fractionation for Immunoblotting

RAW 264.7 cells under different inflammatory conditions were washed once with cold PBS, scraped, and collected by centrifugation. The nuclear and cytoplasmic proteins were fractionated with a CellLytic NuCLEAR Extraction Kit (Sigma) according to the manufacturer’s instructions. Briefly, the cell pellets were resuspended in hypotonic lysis buffer (10 mM Hepes pH 7.9, 1.5 mM MgCl₂, and 10 mM KCl, 10 mM DTT, protease inhibitors, and phosphatase inhibitors). Resuspended cells were incubated on

ice for 15 min for to swell the cells, which were then lysed gently using 10% IGEPAL CA-630 (NP40) solution at a final concentration of 0.6 %; the lysates were vortexed and centrifuged immediately for 30 sec at 10,000 x g. The supernatants containing the cytoplasmic fraction were removed to new tubes. After removal of cytoplasmic fraction, the nuclear fraction was lysed with buffer containing 50 mM TrisHCl, pH 7.5; 150 mM NaCl, 0.5% Triton-X 100, 1X phosphatase inhibitor cocktail (Pierce), 1 X protease inhibitor cocktail (Sigma-Aldrich) followed by a sonication for 10 sec at level 3 (5 sec on, 5 sec off; twice) for the removal of DNA from chromatin. The cytosol and nucleus protein mixtures were run on SDS-PAGE gels in reducing conditions and the proteins were transferred onto PVDF membranes. The membranes were blocked in milk at RT for 1 h. Primary antibody incubation was performed at RT on a rotator for 1 h while secondary antibody incubation was performed at 4 °C overnight.

Co-immunoprecipitation of PHF8-p65 Complexes

PureProteome magnetic beads (20 µL per CoIP sample) were washed with PBS three times, re-equilibrated with PBS-Tween 20 (0.1 % final). The antibody (IgG, p65 or PHF8) was added into the mixture (1 µg per CoIP sample) and incubated rotating at 4 °C. The next day the antibody-bound beads were washed with PBS and then crosslinked to reduce the antibody contamination in eluted protein solution by incubating in 5.2 mg/mL Dimethyl Pimelimidate (DMP) for 30 min at RT. The crosslinking was quenched with 100 mM ethanolamine in PBS rotating for 2 h at RT. The cross-linked antibodies were stored in PBS-Tween 20 (0.1 % final) with 0.1 % sodium azide at 4 °C for a day until the lysates were prepared. For whole cell lysate coIP, we lysed the non-stimulated and LPS-stimulated cells in nuclear lysis buffer and

sonicated for 10 sec (5 sec on, 5 sec off) at level 3. For the nuclear-lysate specific CoIP, after the LPS stimulation for 0, 15, 30, and 60 min, or 24 h, cytoplasmic and nuclear proteins were fractionated as mentioned above. 10% of the equal amounts of sonicated nuclear lysates for each condition were separated as the input control in immunoblotting. The remaining nuclear lysates were used for CoIP. The cross-linked antibody mixtures were washed and equilibrated with the nuclear lysis buffer. The samples were added to the antibody mixture and incubated on a rotator overnight at 4 °C. The unbound-proteins were washed with lysis buffer for three times and eluted in 60 µL 1 X SDS-loading buffer by boiling for 10 min. The protein fractions including cytosol, nuclear, and CoIP were separately ran on SDS-PAGE gels under reducing conditions and then transferred to PVDF membranes. The membranes were blocked with milk for 1 h at RT on an orbital shaker. Following primary antibody incubation for 1 h at RT, we probed the membranes with a horseradish peroxidase conjugated secondary antibody and bands were detected using an ECL Western Blotting Detection Kit (GE Life Sciences).

NF-κB reporter assay

293/TLR4-MD2-CD14 Cells were seeded on 24-well plates one day before transfection so that they will be 90 % confluent at the time of transfection. The next day, cells were transfected with 225 ng pGL2-ELAM promoter Firefly luciferase transgene plasmid and 450 ng plasmids indicated. The pRL- TK plasmid, which expresses Renilla luciferase, was transfected into cells at 75 ng as an internal control to normalize transfection efficiency and sample handling. The cells were stimulated with 1 µg/mL LPS for 6 hours before harvesting. The activities of the two kinds of luciferase were

measured with their respective substrates with a dual luciferase assay kit (Promega). The luminescence reading reflecting NF- κ B activity was obtained from the division of Firefly luciferase reading by Renilla luciferase reading. The data represented in the corresponding figures were the luminescence normalized to the control sample transfected with empty vector instead of functional plasmids. Y-axis indicates relative NF- κ B activity. The error bar represents standard deviation of triplicates. Similar results were obtained in three independent biological experiments.

RNA Isolation and qPCR for Pro-inflammatory mRNA expression

The same methods for PHF8 RNA isolation and qPCR for PHF8 mRNA expression was used. We prepared 2 sets of the same cells with the same stimulation conditions to simultaneously prepare samples for immunoblots in addition to RNA extraction. Stable cell lines were seeded into 12 well cell culture dishes and treated with LPS for indicated times. Total RNA was isolated using illustra RNAspin Mini Kit (GE Healthcare Life Sciences). First-strand cDNA was synthesized by M-MLV reverse transcriptase (Promega) and diluted 5-fold for qPCR. qPCR was performed using Maxima SYBR Green/ROX (Thermo Scientific). All measurements were normalized against GAPDH as the internal control using $2^{-\Delta\Delta C_t}$ method. The sequences of primers are included in **Table 5.**

	Gene	Primer Sequence	
		Left (5' to 3')	Right (5' to 3')
Mouse	IL1a	gcaacgggaagattctgaag	tgacaaacttctgcctgacg
	IL1b	gcccacctctgtgactcat	aggccacaggtatctgtcg
	IFN β	ccatccaagagatgtccag	gtggagagcagttgaggaca
	IL6	ccggagaggagacttcacag	cagaattgccattgcacaac
	IL10	ggttgccaagccttatcgga	acctgctccactgccttgct
	GAPDH	aactttggcattgtggaagg	acacattgggggtaggaaca
	TNF α	cccaaagggatgagaagtt	gtgggtgaggagcacgtagt
	PHF8	aacacaacaaatgctaattct	agaagttccctccgaatgct

Table 5 Primer Sequences for qPCR

RESULTS

PHF8 Knockdown leads to increased H3K9me1 and H3K9me2 in LPS-induced macrophages

As a KDM negatively regulated by PP2Ac-dependent dephosphorylation in ET, we wanted to explore the role of PHF8 in acute LPS response in macrophages. First we used a lentiviral shRNA-based strategy to knockdown PHF8 mRNA expression. Our immunoblotting and qPCR results show that we successfully knocked down PHF8 with 70% efficiency as shown in **Figure 43**.

After a few passages we validated the stable cell line and performed a time-course LPS-stimulation (0, ¼, 2, 8, and 24 h) on paired WT and PHF8-KD cells to immunoblot for various histone PTMs. In this *screening* method, we wanted to identify the histone PTMs showing an increase in the PHF8-KD cell line as they are potentially

or directly, targeted by PHF8. Initially, we confirmed the LPS-response phenotype by blotting NF κ B transactivation marker phospho-p65 (S536), which significantly increased within the first 15 min LPS stimulation and gradually decreased over time until 8 h, diminishing by 24 h (**Figure 44, top**). We used γ Tubulin as cellular loading control. On the other hand, we performed the histone PTM immunoblots using total H3 immunoblot as the loading control (**Figure 44, bottom**). In WT RAW cells, H3K9me1 and H3K9me2 marks showed a decrease with LPS stimulation while H3K9me2 was specifically increased with prolonged LPS stimulation. On the other hand, the initial decrease in these marks wasn't observed in the PHF8-KD cells indicating that PHF8 is involved in the H3K9me1/me2 demethylation in early LPS response. Moreover, as oppose to WT, in PHF8-KD cells H3K9me1 abundance increased significantly with prolonged LPS stimulation indicating that PHF8 doesn't demethylate H3K9me2 with prolonged LPS stimulation but it may still demethylate H3K9me1 in this phenotype. PHF8 is known to demethylate H3K27me2 *in vitro*; thus, we checked the H3K27me2 levels and observed that PHF8-KD caused an increase in H3K27me2 both with and without LPS stimulation. More importantly, the LPS-induced gene-specific activation mark H3S10 phosphorylation (Xie et al, 2013) abundance dramatically decreased in early activation and diminished with several hours earlier with LPS stimulation in PHF8-KD cells compared to that in WT cells. PHF8-dependency of the abundance of the activation marker H3S10P indicates that the gene-specific activation of LPS-induced transcription is dependent on the LPS-induced activity of PHF8.

PHF8 is involved in regulation of p65-dependent gene-specific transcription of pro-inflammatory cytokines in macrophages upon LPS stimulation

In our initial immunoblots (**Figure 43** and **Figure 44**), we observed that p65 phosphorylation showed a slight decrease in PHF8-KD compared to that one in WT cells in acute LPS response, indicating that PHF8 may be positively regulating the transactivation of p65. To understand how PHF8 may regulate p65 activity, we performed a series of experiments that compare WT and PHF8-KD cells such as immunoblots of nuclear-cytoplasmic fractionation to screen P-p65 abundance, CoIP of p65 and PHF8 to detect complex formation, and p65 Luciferase activity assay to detect changes in p65 activity.

PHF8 regulates LPS-induced nuclear translocation of p65

Our immunoblot screening of nuclear and cytoplasmic fractions of WT and PHF8-KD cells that were stimulated with LPS for 0, ¼, 1, and 24 h revealed that total abundance of p65 and P-p65 in cytoplasmic fraction is similar in both cell lines. However, we observed a dramatic decrease in the fraction of both p65 and P-p65 (S536) that are translocated to nucleus with PHF8-KD (**Figure 45**). Moreover, the abundance of PHF8 is decreased in both cytosol and nucleus with 24 h LPS stimulation. The abundance of IκBα and P-IκBα were used for inflammation phenotype confirmation while Lmn1 and γTubulin immunoblots were used as loading control for nuclear fraction and total protein, respectively.

PHF8 and p65 form a complex in an LPS-induced manner

To understand whether PHF8 binds to p65 to regulate its LPS-induced nuclear translocation, we performed a series of CoIP experiments. First, as an initial screen, we co-immunoprecipitated the p65-bound complexes from the whole cell lysates of paired WT and PHF8-KD cells that were either non-stimulated or stimulated with LPS for 15 mins (**Figure 46**). Within those complexes, we identified PHF8 co-immunoprecipitated with p65 pull-down in WT RAW cells while no such interaction was observed in the PHF8-KD cells. However, we observed that the percentage of the PHF8 that was pulled down with p65 was very low in comparison to the input (whole cell lysate). This may be explained by high abundance of PHF8 mostly in nuclear fraction while most of the p65 still exists in the cytoplasmic fraction, even with the LPS stimulation, as we showed in **Figure 45**. Thus, we decided to perform the following CoIP experiments only using the nuclear fractions. For the nuclear CoIP, we also decided to use an additional 24 h LPS stimulation as a negative control for p65 translocation. Our subcellular fractionation results, consistent with our previous nuclear-cytoplasmic fractionations, showed that both total and phosphorylated p65 abundance in nuclear fraction decreased with PHF8-KD (**Figure 47, Right**). In line with our previous observation of lower PHF8 expression with prolonged LPS stimulation in **Figure 45**, we detected less PHF8 in both cytoplasmic and nuclear fractions of WT cells with 24 h LPS stimulation while non-stimulated or acutely stimulated cells had similar PHF8 protein expression. This observation supports our initial hypothesis that PHF8 activity is negatively regulated by PP2Ac in ET and can be explained by decreased stability or solubility of PHF8 with dephosphorylation. Moreover, the nuclear CoIP revealed that PHF8 formed a nucleus-

specific complex with p65, the complex formation diminished with prolonged LPS stimulation as p65 abundance in nucleus decreased, and PHF8 binding was independent of phosphorylation of p65 (**Figure 47, Left**). Further, to understand whether there is a transient binding between p65 and PHF8, we performed another nuclear CoIP including more time points (1/2 and 1 h) of LPS stimulation as p65 abundance in nucleus gradually decreases between ¼ h and 1 h. In addition, we simultaneously performed CoIP of PHF8-bound complexes in WT cells to validate the transient p65-PHF8 complex formation (**Figure 48**). This experiment revealed that

- *PHF8 is bound to nuclear p65 in WT RAW cells only in the LPS-induced fraction since p65 abundance in nucleus is negligible without LPS stimulation.*
- *The complex formation didn't occur in PHF8-KD cells, indicating that the PHF8-p65 binding is not due to non-specific binding.*
- *More importantly, the amount of p65 and P-p65 detected in the nuclear p65 immunocomplexes dramatically increased in PHF8-KD cells compared to that in WT cells indicating that PHF8 regulates the nuclear p65 translocation.*
- *Nuclear p65 and P-p65 (S536) were in the immunocomplexes of PHF8 in WT RAW cells.*
- *PHF8-bound p65 and P-p65 amount increased with acute LPS stimulation while showing a decrease with prolonged LPS stimulation, indicating that the PHF8-dependent nuclear translocation of p65 is LPS-dependent and phenotype-specific.*

In summary, our CoIP experiments demonstrated that **PHF8 regulates p65 nuclear translocation in an LPS-dependent manner** in mouse macrophages.

PHF8 binds to p65 regulating its transcriptional activity in macrophages upon LPS stimulation

In addition to subcellular localization, we assayed the transcriptional activity of p65 using a dual-reporter luciferase assay to determine whether p65 transcriptional activity is controlled by PHF8 in LPS-induced TLR4 response. Our luciferase activity assay, as shown in **Figure 49**, demonstrated that the transcriptional activity of p65 was significantly reduced in PHF8-KD cells compared to WT cells. This observation indicates that *PHF8 positively regulates the transcriptional activity of p65*.

PHF8 regulates gene-specific pro-inflammatory mRNA expression via regulating NFκB in LPS-stimulated macrophages

Since we found PHF8 as a regulator of the p65 transcriptional activity, we wanted to validate the conclusion by performing qPCR for selected pro-inflammatory cytokines IL1α, IL10, IL6, TNFα, and IFNβ (**Figure 50**). To confirm the inflammatory phenotype of the cells we performed immunoblots (**Figure 50A**) showing the diminished PHF8 in PHF8-KD cells, and increased P-p65 (S536) coupled with decreased IκBα in acute LPS stimulation in both cell lines. The qPCR also confirmed the PHF8-KD (**Figure 50B**). We observed that cytokines **IL1α**, **IL10**, and **IL6** mRNA expression significantly reduced in PHF8-KD beyond 2h of LPS stimulation (**Figure 50B**). This indicates that *PHF8 promotes the mRNA transcription of IL1α, IL10, and IL6 through positively regulating NFκB transactivation*. On the other hand TNFα expression didn't show significant difference with PHF8-KD possibly due to other signaling events that aren't regulated by PHF8. Importantly, IFNβ, shows significantly higher LPS-induced mRNA expression in the PHF8-KD cells, can act as an inhibitor of inflammation (Billiau,

1995). Thus, in PHF8-KD cells, the increased mRNA expression of IFN β in combination with decreased mRNA expression of pro-inflammatory cytokines implies *that PHF8-dependent activation of cytokines is both gene-specific and pro-inflammatory phenotype-specific*. Because these cytokines are regulated by NF κ B, our data demonstrates that PHF8 positively regulates LPS-induced, NF κ B-dependent transcription of select pro-inflammatory genes.

DISCUSSION

LPS-induced inflammation response is tightly regulated in multiple layers of signaling events. As it is the closest layer to inflammatory gene expression, understanding the dynamic and transient transcriptional regulation by chromatin modifiers is essential to provide therapies or prevention methods against inflammatory disorders. Various chromatin modifiers have been identified in the regulation of transcription in inflammation response and TLR4 signaling and are not limited to G9a-HP1 complex (Chan et al, 2005; El Gazzar et al, 2008), DNMT3A/B (El Gazzar et al, 2008), JMJD3 (De Santa et al, 2007), KDM5B (Ptaschinski et al, 2015), KDM1A (Hanzu et al, 2013), and MLL1 (Wang et al, 2014b). Our study is the first to provide the proof for PHF8-dependent LPS response in macrophages. This functional characterization of PHF8 as one of the chromatin modifiers regulating the pro-inflammatory cytokine expression not only deciphers the H3K9-demethylase-dependent activation of LPS-induced inflammation response, but also connects the missing link between PP2Ac-activity and its role in chromatin regulation of ET.

The second layer of LPS response regulation is through the modulation of transcriptional activity of NF κ B via regulating complexes and PTMs on its subunits. The

most extensively studied and well known PTM on p65 subunit is the phosphorylation of p65 on S536 (Sakurai et al, 1999), which is essential for p65 translocation to the nucleus. Transcriptional activity of p65 is also regulated by other PTMs such as methylation and acetylation (Vermeulen et al, 2006); however, the involvement of a chromatin modifier in p65 nuclear translocation hasn't been identified, yet. Here we provide the *first evidence for the regulation of p65 transactivation by demethylase PHF8 upon LPS stimulation in macrophages*. Moreover, functional characterizations of various p65 PTMs, except Phospho-S536, in regulation of NFκB transcriptional activity still need validation. By providing evidence for PHF8-dependent nuclear translocation of p65 with LPS stimulation, *our study is the first to demonstrate the control mechanism for NFκB activity change downstream S536 phosphorylation by IKK2*.

The pro-inflammatory cytokine production is an essential step of macrophage biology in innate immunity of mammals. Even though post-transcriptional and post-translational regulation of cytokines affect the overall cytokine production or secretion, the initial step is regulation of NFκB signaling. Here, this study is the *first to functionally identify PHF8 demethylase as a regulator of gene-specific cytokine expression in TLR4-dependent macrophage response*. Our analysis revealed a very important piece in the epigenetic regulation of cytokines while showing evidence for PHF8 as a target to develop therapeutic strategies in inflammation-induced diseases.

FUTURE WORK

Here we identified PHF8 as a major regulator of innate immune response downstream TLR4 signaling pathway; this regulation occurs through LPS-induced activation of PHF8, complex formation between p65 and PHF8, increased nuclear

translocation of p65, increased transcriptional activity of p65, and decreased repressive H3K9me1/2 at p65 target genes. However the mechanism of p65-PHF8 binding in LPS-induced inflammation is still unclear. To understand the role of this complex on the activity and nuclear-translocation of p65, we will need information on whether PHF8 activity leads to any PTM changes on p65, affects nuclear translocation through making NLS exposed to the environment through conformational changes, regulates other activity-inducing complexes of p65, or modulates other enzymes targeting p65 PTMs downstream LPS. To understand whether PHF8 catalytic activity alters any p65 PTMs, we will perform proteomic screening on co-immunoprecipitated p65-PHF8 complexes. This will help us detect any PTMs that occur on p65 with (LPS-induced) and without (unstimulated) PHF8 activity in macrophages for further validation via mutational studies. In addition, CoIP of p65 NLS, using an antibody specifically binding to p65 NLS, in paired WT and PHF8-KD cells, with and without LPS stimulation, will reveal whether PHF8 leads to change in the release of NLS from I κ B complex. On the other hand, proteomic studies screening to compare co-immunoprecipitates of p65 with and without LPS stimulation in WT and PHF8-KD cells will help us understand how PHF8 alters the complexes that p65 forms with LPS stimulation. Moreover, immunoblotting of the various CoIP products of p65 from the same set of cells against I κ B and PP2Ac antibodies will be significant as these are the most widely-known p65 regulators inhibiting its transcriptional activity. We would expect to see increased I κ B or PP2Ac binding to p65 with LPS stimulation in PHF8-KD cells compared to that in WT cells. Structural and biochemical binding studies will also reveal mechanistic significance of PHF8 activity on the p65 regulation.

FIGURES

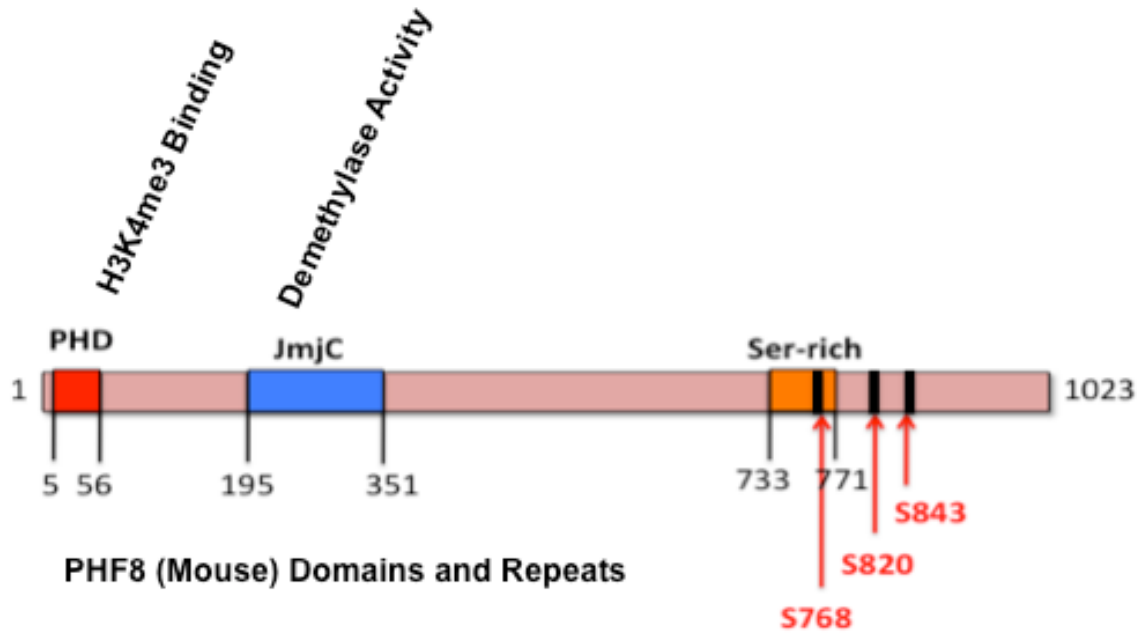


Figure 39 Domain structure and repeats of PHF8

PHF8 domain structure. PHD domain is shown in red, JmjC domain is shown in blue and Ser-rich repeat is shown in orange. Black bars represent the Ser residues that are dephosphorylated by PP2Ac in ET (Erdoğan et al, 2016).



Figure 40 Mouse and human PHF8 sequence alignment.

The alignment shows PP2Ac-targeted PHF8 residues. PHF8 sequence and the corresponding Ser residues are color coded in red (mouse) and blue (human) (Erdoğan et al, 2016).

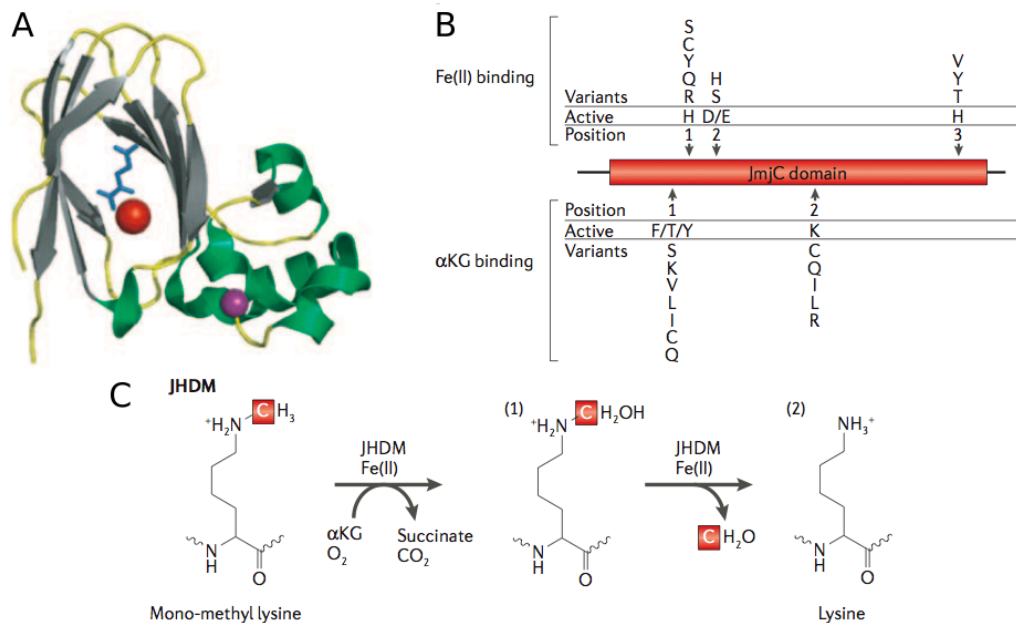


Figure 41 The JmjC domain contains residues required for Fe(II) and αKG binding
(A) A three-dimensional cartoon depicting the polypeptide backbone structure of the JmjC (Jumonji C) domain of JHMD3A/JMJD2A. The eight β-sheets of the cofactor-coordinating pocket are shown in grey, with the Fe(II) ion in red and αKG in blue. The α-helical region that associates with the zinc ion is shown in green and the zinc molecule in purple. **(B)** A schematic representation of the JmjC domain showing the position of the Fe(II)-binding (top) and αKG-binding (bottom) residues. The amino-acid identity of residues within active hydroxylases and demethylases and amino-acid substitutions found in other JmjC-domain proteins are shown above and below the indicated cofactor-binding residue position. **(C)** JHDM histone demethylases can demethylate mono-, di- and trimethylated lysine by an oxidative mechanism that requires Fe(II) and αKG as cofactors. Demethylation is thought to occur by direct hydroxylation of the methyl group (1), which results in an unstable hydroxymethyl product that is spontaneously released as formaldehyde (2) (Klose et al, 2006).

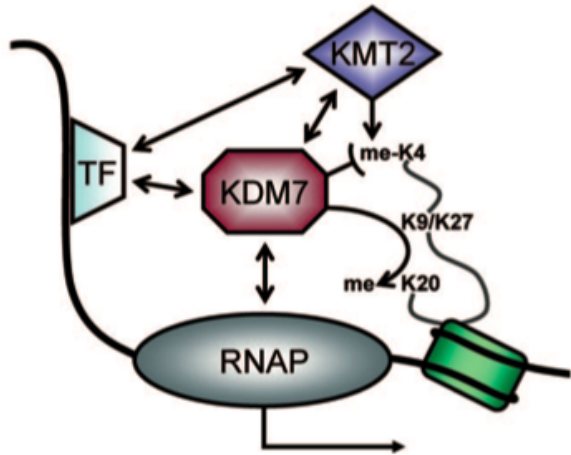
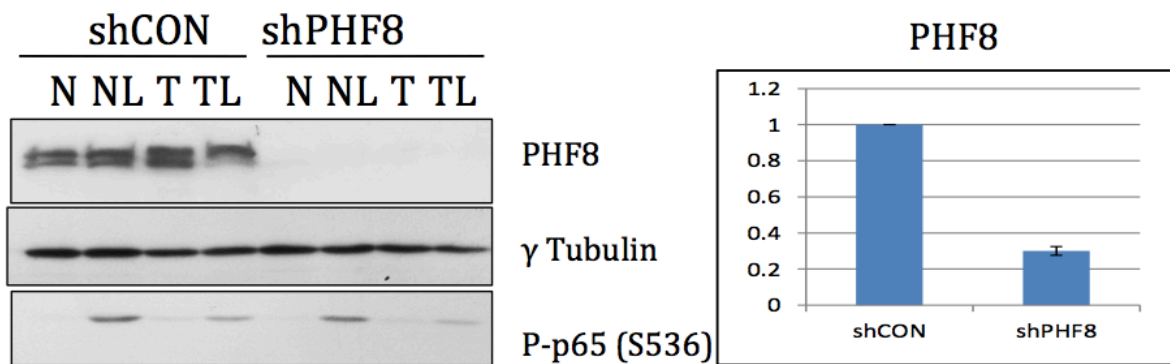


Figure 42 Transcriptional co-activation by KDM7-family proteins
 Upon gene induction, transcription factors (TF) bind to specific DNA-sequences and recruit co-activators such as H3K4-methyltransferases (KMT2). The latter introduce methyl-marks on histone H3 tails (me-K4) which protrude from nucleosomes. These activation chromatin marks are bound by proteins such as histone demethylases of the KDM7-family. This class of chromatin-modifying enzymes removes repressive methyl-marks from K9 or K27 on H3 or K20 on H4. Furthermore KDM7 can interact with RNA polymerases I or II (RNAP) and other chromatin-associated factors (such as E2F1 and ZNF711). Both mechanisms lead to the activation of transcription (Fortschegger et al, 2010).



NL: 1.0 µg/mL LPS, 15 min
 T: 0.1 µg/mL LPS, 24 hrs
 TL: 0.1 µg/mL LPS, 24 hrs + 1.0 µg/mL LPS, 15 min

Figure 43 Knockdown of PHF8 on mouse macrophage RAW cell line
 Using shRNA against GFP and PHF8 in RAW cells, we made stable WT (shCON) and PHF8-KD (shPHF8) cell lines, respectively. Different inflammation conditions are shown as N (non-stimulated), NL (acute LPS stimulation), T (prolonged LPS stimulation), and TL (prolonged LPS stimulation with a second LPS challenge). We measured mRNA expression of PHF8 to confirm the knock-down efficiency as 70% using qPCR (right) (Erdoğan et al, 2016).

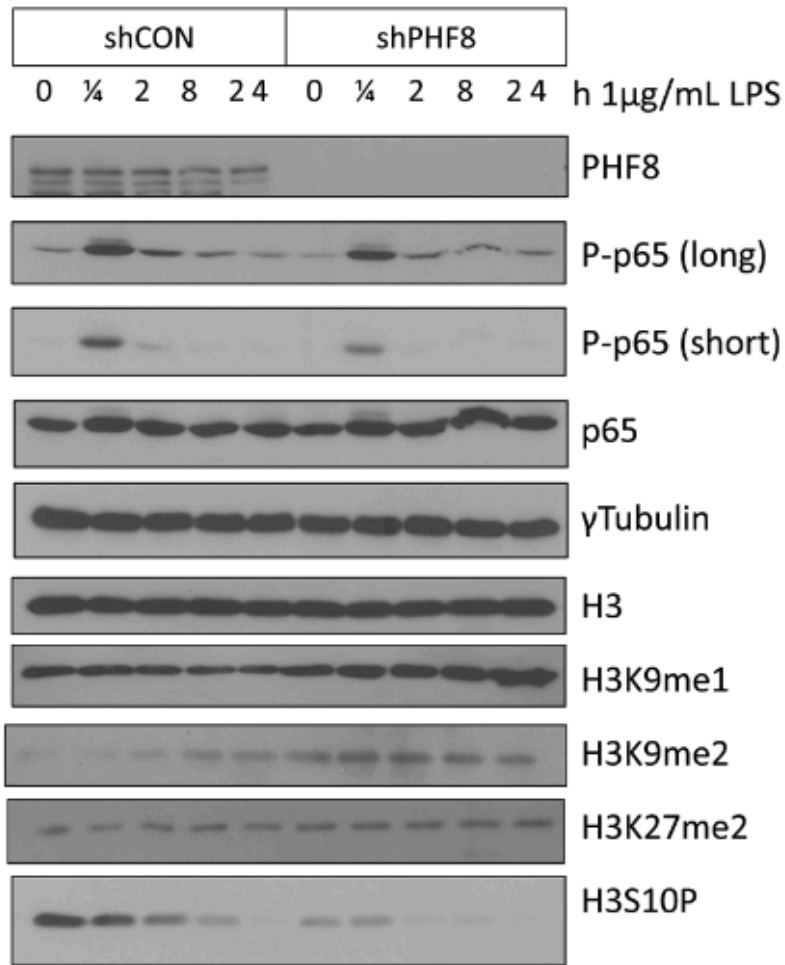


Figure 44 PHF8 regulates LPS-induced demethylation of H3K9me1/me2
 Site-specific lysine methylations on H3 were comparably analyzed in paired WT (shCON) versus PHF8-KD (shPHF8) RAW 264.7 cells using immunoblotting. The macrophages were collected at the indicated time points of LPS stimulation (1/4, 2, 8, and 24 h) (Erdoğan et al, 2016).

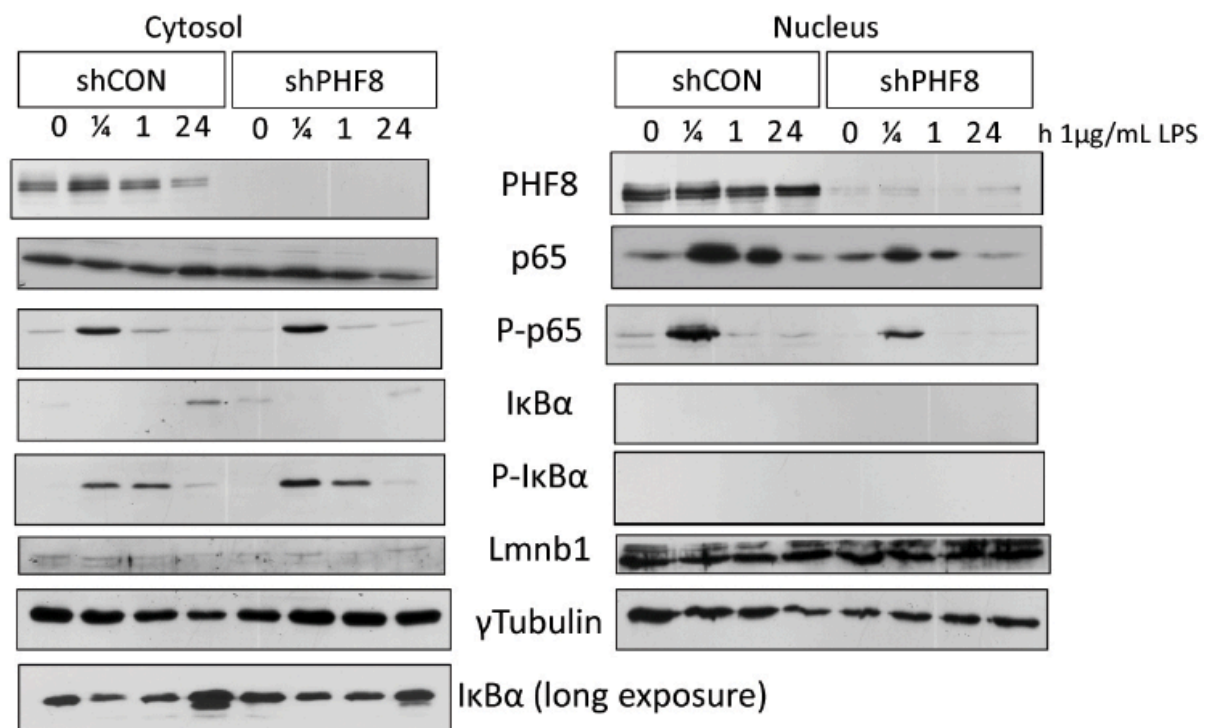


Figure 45 PHF8 regulates nuclear translocation of p53 in LPS response. Immunoblot analysis of the p53 and P-p53 abundance in the cytosol and nucleus of paired WT (shCON) and PHF8-KD (shPHF8) cells with LPS stimulation for indicated duration (0, 1/4, 1, and 24 h).

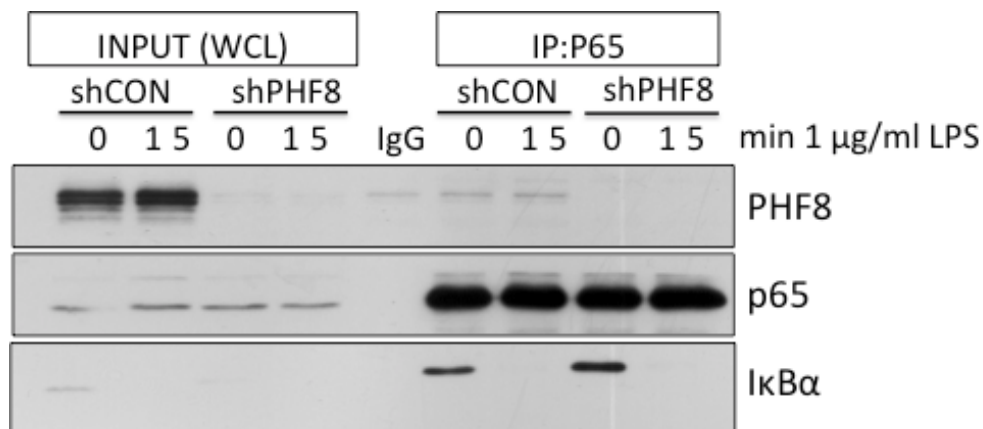


Figure 46 PHF8 is co-immunoprecipitated with p53. Co-immunoprecipitation of p53-bound complexes from total cell lysates from WT and PHF8-KD cells that were stimulated with 1 μg/ml LPS for 0 and 15 min shows PHF8 forming a complex with p53 only in WT cells (Erdoğan et al, 2016).

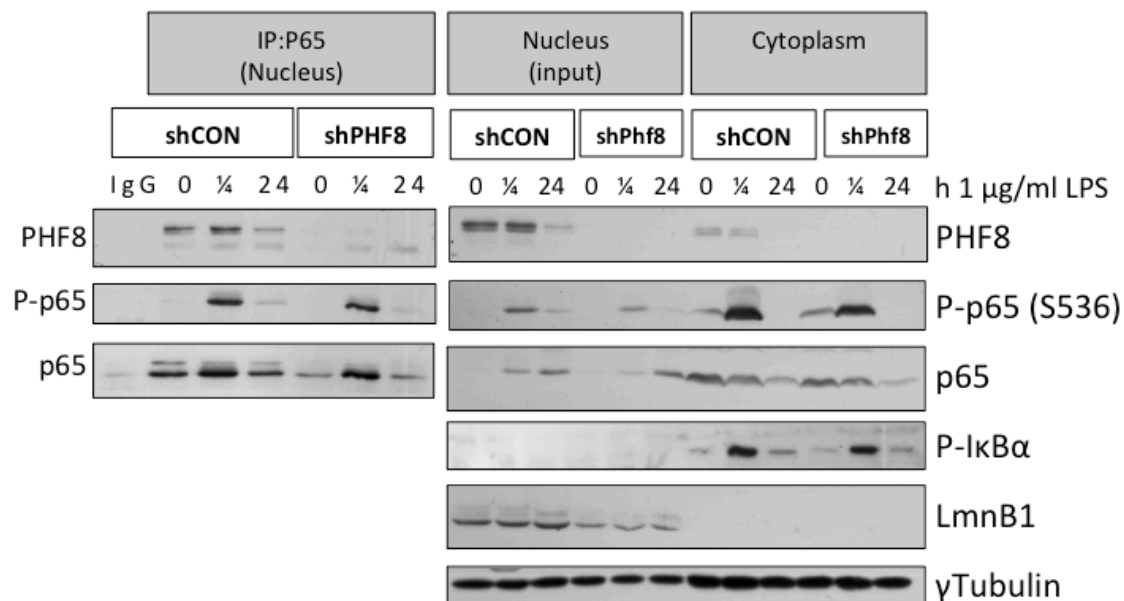


Figure 47 PHF8 forms an LPS-inducible complex with p65

WT and PHF8-KD stable RAW cells were treated with 1 µg/ml LPS for 0, ¼, and 24h. Following subcellular fractionation, nuclear fractions were co-immunoprecipitated with p65 antibody and immunoblotted with PHF8 antibody to detect complex formation in the nucleus (Erdoğan et al, 2016).

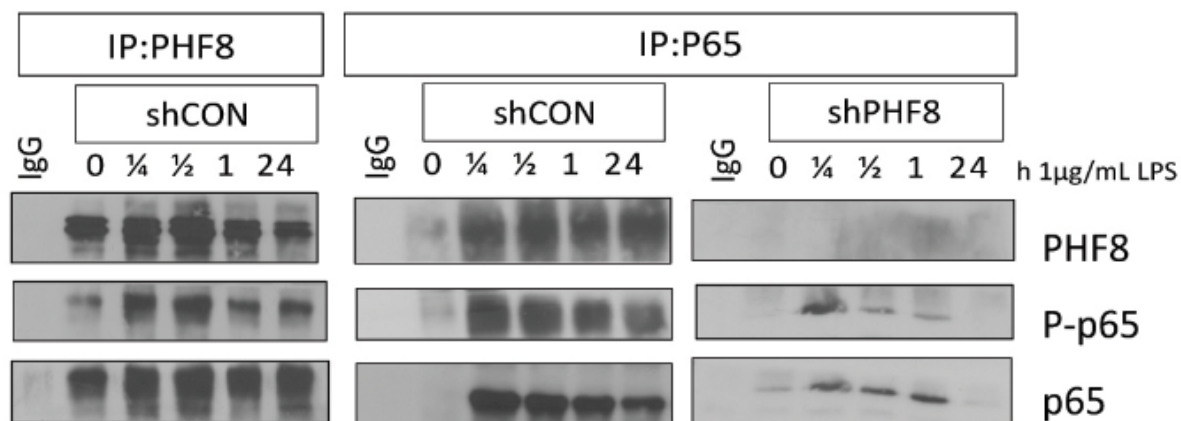


Figure 48 Nucleus-specific CoIP of PHF8 and p65

WT and PHF8-KD stable RAW cells were treated with 1 µg/ml LPS for 0, ¼, ½, 1, and 24h. Following subcellular fractionation, nuclear fractions of WT cells were co-immunoprecipitated with p65 or PHF8 antibody while nuclear fractions of PHF8-KD cells were co-immunoprecipitated with p65 antibody only. The complexes were immunoblotted with PHF8, P-p65, and p65 to detect

complex formation in the nucleus. 1/3 of the CoIP mixture was used for each immunoblot (Erdoğan et al, 2016).

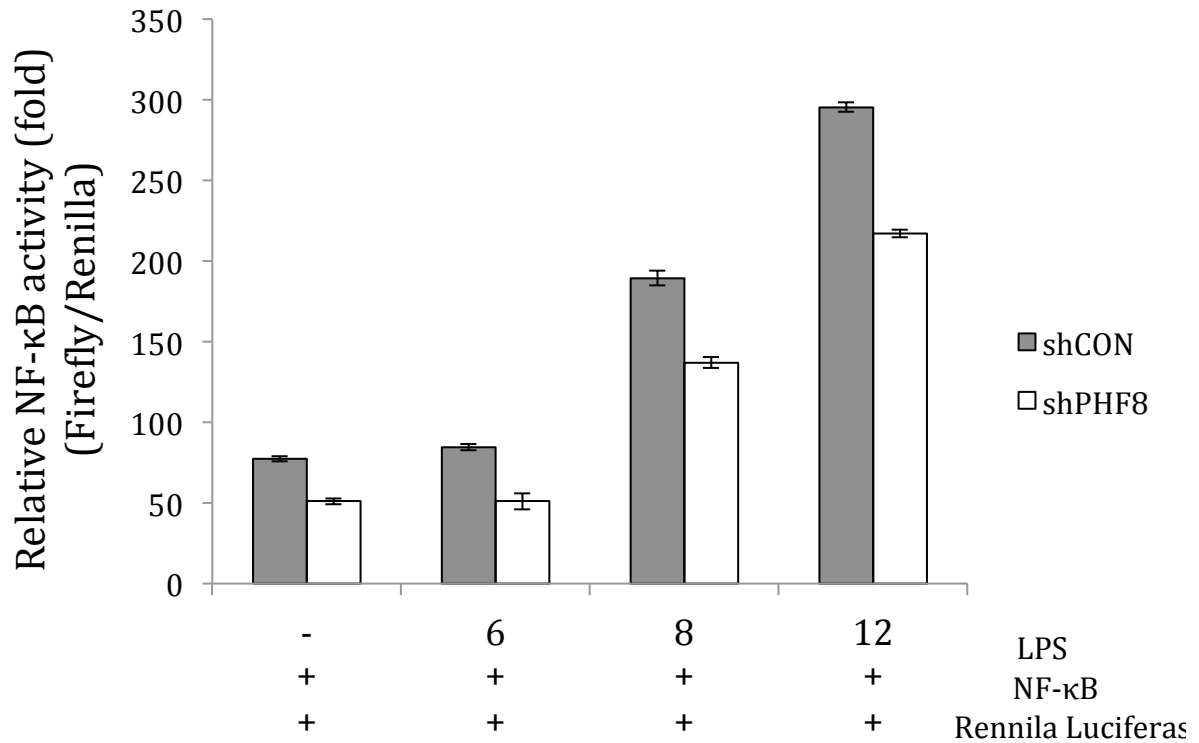


Figure 49 PHF8 positively regulates the transcriptional activity of p65. PHF8-KD leads to reduced NFκB activity. 293-TLR4-MD2-CD14 cells stably expressing WT (shCON) or PHF8-KD (shPHF8) were transfected with Firefly luciferase. 24 hours after the transfection, the cells were stimulated with 1μg/ml LPS and were collected at 0, 6, 8, or 12 h with three biological replicates. The activity of each sample was normalized to Renilla luciferase. Each column shows mean ±s.e. of at least three independent experiments. *P<0.05 compared with mock-transfected cells (Student's t-test) (Erdoğan et al, 2016).

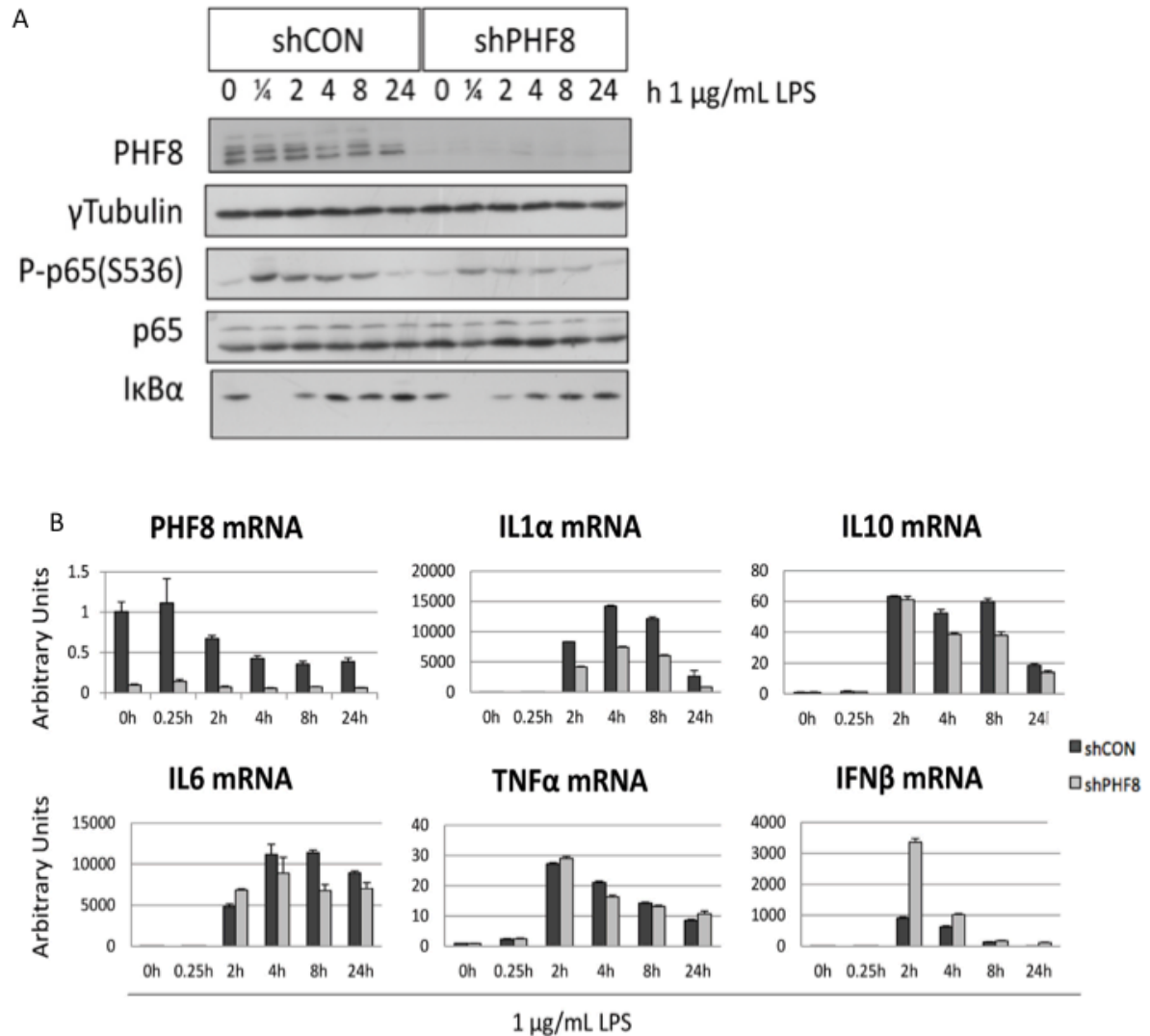


Figure 50 PHF8 regulates the expression of select pro-inflammatory cytokines.
(A) Immunoblot analysis was conducted to monitor indicated inflammatory markers (top) **(B)** qPCR analysis (bottom) shows the mRNA expression of select proinflammatory cytokines in paired WT (shCON, dark grey bars) and PHF8-KD (shPHF8, light grey bars) with LPS stimulation while error bars show the mean \pm s.e. of three independent experiments. Time points are indicated for the non-stimulated (0 h) and stimulated RAW cells (0.25, 2, 4, 8, and 24 h) (Erdoğan et al, 2016).

**CHAPTER 4: PHF8 REGULATES THE SECRETION OF SPECIFIC ‘TOLERIZABLE’
GENES INCLUDING CYTOKINES AND CHEMOKINES IN LPS-INDUCED
MACROPHAGES FOR SUCCESSFUL ACTIVATION OF ADAPTIVE IMMUNITY**

OVERVIEW

As the initial pathogenic detection modulators, macrophages are responsible for identification of the pathogen, cytokine/chemokine production and secretion, induction of apoptosis, and construction of a signaling platform to promote migration, activation, or proliferation of cells of adaptive immunity. Here, we studied the secreted protein products of WT and PHF8-KD macrophages to understand specific products that are involved in PHF8-dependent activation of inflammation response in bacterial infection. Moreover, in our analysis we identified various molecules of innate immunity that were regulated by PHF8 upon LPS stimulation. Some of those molecules were also involved in the activation of adaptive immunity. Common LPS-induced PHF8-dependent secretion products and activators of adaptive immunity indicate that PHF8 is involved in the missing link between innate and adaptive immunity. Further, we show evidence on the regulation of activation and proliferation of CD8⁺ T cells by the PHF8-dependent macrophage secretome via T cell activation and proliferation assays. Overall our data indicates that PHF8 is a major regulator of the macrophage secretome upon LPS stimulation that clarifies the missing link between innate and adaptive immunity. Our analysis also shows that proteomic screening of secreted proteins is a powerful

technique in identification of signaling molecules/pathways at the crossroad of signaling pathways in interplay.

INTRODUCTION

The Role of Macrophage Secretome in Inflammation Response

The induction of proper immune response depends on the successful cross-talk between macrophages and adaptive immunity cells upon bacterial infection (Chapes et al, 1992). Macrophages are highly abundant, widely distributed in the body, motile, responsive, and versatile; thus, they widely influence immune and inflammatory responses (Nathan, 1987). Moreover, macrophages are the sources of expression and secretion of various proteins that are responsible for activation of adaptive immunity. These proteins include polypeptide hormones, cytokines, complement components, coagulation factors, various enzymes, extracellular proteins, and proteins of cell adhesion (**Table 6**).

The macrophage secretome is complex and various products affect each other. These products may affect each other's release and actions as well as protein release from surrounding cells. These proteins lead to various biological outcomes such as inhibition or promotion of cell proliferation, chemotactic attraction, induction of fever, etc. (**Table 7**). More importantly, various enzymes (**Table 8**) secreted by macrophages participate in a wide range of inflammatory functions including killing tumors or bacteria, accelerating inflammation, inflammation site clearing, and lipoprotein metabolism (Takemura & Werb, 1984).

Table 6 Secretory products of mononuclear phagocytes (Manes et al, 2011).

<p>Polypeptide hormones</p> <p>Interleukin 1-α and 1-β (collectively, IL-1)</p> <p>Tumor necrosis factor- α (TNFα)</p> <p>Interferon-α</p> <p>Interferon-γ</p> <p>Platelet-derived growth factor(s)</p> <p>Fibroblast growth factors</p> <p>Fibroblast activating factors</p> <p>Transforming growth factor-β (TGFβ)</p> <p>Insulin like activity</p> <p>Thymosin B4</p> <p>Erythropoietin</p> <p>Colony-stimulating factor for granulocytes and macrophages (CSF-G/M)</p> <p>Colony-stimulating factor for granulocytes (CSF-G)</p> <p>Erythroidcolony-potentiating factor</p> <p>Factor-inducing monocytopoiesis</p> <p>β-Endorphin</p> <p>Adrenocorticotrophic hormone</p> <p>Plasmacytoma growth factor</p> <p>Neutrophil-activating factor</p> <p>Complement (C) components</p> <p>Classicalpath: C1, C4, C2, C3, C5</p> <p>Alternativepath: factor B, factor D, properdin</p> <p>Inhibitors: C3b inactivator, β-1H</p> <p>Active fragments generated by macrophage proteases: C3a, C3b, C5a, Bb</p> <p>Coagulation factors</p> <p>Intrinsicpath: IX, X, V, prothrombin</p> <p>Extrinsicpath: VII</p> <p>Surface activities: tisuefactor, prothrombinase</p> <p>Prothrombolytic activity: plasminogen activator</p> <p>Antithrombolytic activities:plasminogen activator inhibitors, Plasmin inhibitors</p> <p>Other enzymes</p> <p>Neutralproteases: plasminogen activator, elastase, collagenases, angiotensin convertase, others</p> <p>Lipases: lipoprotein lipase, phospholipaseA2</p> <p>Glucosaminidase: lysozyme</p> <p>Lysosomal acid hydrolases: proteases, lipases, (deoxy)ribonucleases, phosphatases, glycosidases, sulfatases</p> <p>Deaminase: arginase</p> <p>Inhibitors of enzymes and cytokines</p> <p>Protease inhibitors: α-2-macroglobulin, α-1-antiprotease, plasminogen activator inhibitors, plasmin inhibitors, collagenase inhibitor</p> <p>Phospholipase inhibitor: lipomodulin (macro cortin)</p> <p>IL-1 inhibitors</p> <p>Proteins of extracellular matrix or cell adhesion</p> <p>Fibronectin</p> <p>Gelatin-binding protein of 95 kD</p> <p>Thrombospondin</p>
--

Chondroitin sulfate proteoglycans

Other binding proteins

For metals: transferrin, acidic isoferitins, transcobalamin I

For lipids apolipoprotein E, lipid transfer protein

For biotin: avidin

Purine and pyrimidine products

Thymidine, uracil, uric acid, deoxycytidine

Neopterin (2-amino-4-oxo-6-trihydroxypropylpteridine)

Bioactive lipids

Cyclooxygenase products: prostaglandin E₂ (PGE₂), prostaglandin

F_{2a}, prostacyclin, thromboxane

Lipoxygenase products: monohydroxyeicosatetraenoic acids, dihydroxyeicosatetraenoic acids, leukotrienes B₄, C, D, E

Platelet-activating factors (1-O-alkyl-2-acetyl-sn-glycerol-3-Phosphorylcholine)

Sterol hormones: 1 α ,25-Dihydroxyvitamin D₃

Bioactive oligopeptides: Glutathione

Reactive oxygen intermediates: Superoxide, hydrogen peroxide, hydroxyl radical, hypohalous acids

Reactive nitrogen intermediates: Nitrites, nitrates

To understand the factors that regulate the secretion of regulators of adaptive immunity, quantitative analysis of secreted proteins from the antigen presenting cells through various screening methods can be applied. In this chapter, I will describe various methods that are used for screening of secretomes, and their disadvantages, and advantages. Finally, I will describe the global quantitative analysis of macrophage secretome via proteomics and demonstrate its strength in unbiased secretome screening as well as identification of novel secretome components.

Table 7 Macrophage products with similar activities (Manes et al, 2011)

Bioactivity	Products
Inhibition of cell proliferation	Reactive oxygen intermediates, TNF- α , IL-1- α , IL-1- β , transforming growth factor- β , interferons- α , interferon- γ , oxidized soluble immune response suppressor, CSF-G/M (action on leukemic cells), arginase, PGE ₂ , thymidine, reactive nitrogen intermediates? (speculative)
Promotion of cell proliferation	TNF- α , IL-1- α , IL-1- β , fibroblast growth factors, platelet-derived growth factor, CSF-G/M, erythropoietin, erythroid colony-stimulating factor, plasmacytoma growth factor, leukotriene B ₄ (for keratinocytes)
Chemotactic attraction	Leukotrienes B ₄ and C, IL-1- α , IL-1- β , platelet-derived growth factor, platelet-activating factor, β -endorphin, γ -induced protein 10? (speculative) (194), fragments of fibronectin and elastin
Induction of fever	IL-1- α , IL-1- β , TNF- α , interferons- α , interferon- γ

Table 8 Enzymes secreted by macrophages (Takemura & Werb, 1984)

Product	Synonyms	Regulation*	Function
Plasminogen activators	Tissue activator, urokinase, factor B	B ¹ , G	Inflammatory, tissue repair
Collagenase I, II, III		B ¹	Inflammatory
Collagenase V		B ¹	Inflammatory
Collagenase IV		B ¹	Inflammatory
Elastase	Proteoglycan-degrading enzyme, myelin basic protein-degrading enzyme	B ² , G	Inflammatory
Cytolytic proteinase		B ³	Tumoricidal
Complement components		E	Antimicrobial, inflammatory, opsonic
C1, C2			
Factor B			
Factor D			
Factor I			
Coagulation factors		D	Coagulation, tissue repair
Factor VII			
Factor IX			
Factor X			
Angiotensin-converting enzyme		F ¹	Activation of angiotensin
Acid hydrolases	Lysosomal enzymes, acid glycosidases, cathepsin	B ¹	Inflammatory
Arginase		B ¹	Antimicrobial, tumoricidal, immunoregulatory
Lysozyme		A	Antimicrobial
Lipoprotein lipase		A	Metabolism of lipoprotein breached into blood vessel wall

* Regulation types are A, constitutive; B¹, increased in inflammatory or activated macrophages; B², increased in inflammatory but not activated macrophages; B³, increased in activated but not in inflammatory macrophages; D, not determined; E, various; F¹, increased by glucocorticoids; and G, varies during differentiation of mononuclear phagocytes.

Secretome Analysis Methods

To understand how innate immunity regulates the adaptive immunity upon LPS stimulation, various methods have been developed to analyze the secreted cytokines/proteins. The very early traditional methods that were used extensively for this purpose are (1) qPCR, which measures the cytokine mRNA transcript abundance (Amsen et al, 2009), and (2) cDNA microarray analysis (Welsh et al, 2003). qPCR technique is simple, quantitative, and has high detection efficiency with small amount of sample; but its major drawback is that the intracellular RNA abundance doesn't necessarily reflect the level of expression or secretion of a protein. In addition, it measures relative abundance with respect to a selected control protein, leading to detection issues such as inefficiency in reverse transcription, RNA degradation, or PCR cross-contamination. Moreover it is a technique to screen for proteins whose sequence has already been identified; thus, it lacks the ability to identify novel proteins that get secreted. cDNA microarray analysis, similarly, screens for various RNAs in the serum or tissues; thus, has the same drawback of need for prior knowledge of the sequence, and low correlation between RNA abundance and protein secretion. Although this technique enables the discovery of novel proteins through computational methods, its specificity and sensitivity are very low.

To detect cytokine abundance at the protein level Enzyme-linked immunosorbent assay (ELISA) has been extensively used (Sullivan et al, 2000). ELISA detects and quantifies the abundance of cytokines/proteins using specific antibodies in a given sample (**Figure 51**). Although this technique is simple, quantitative, and sensitive, it has some drawbacks. First of all, it requires prior knowledge on the

proteins to be screened because it is an antibody-based technique; thus, novel target discovery is not achievable with ELISA. Moreover, the antibody-based techniques rely on the sensitivity and specificity of the antibody; non-specific binding can always contaminate the results leading to false positives. Another major flaw of ELISA is that cytokines have very short half-life making it hard to detect in complex samples such as serum. An alternative to this technique is microarray-based immunoassay, which is very similar to ELISA in terms of sensitivity and methodology; but is more advantageous due to higher detection capability with smaller sample volume (Jones et al, 2008). Antibody microarrays have been extensively used for analysis of secreted proteins **(Figure 52)** (Mustafa et al, 2011). But it cannot overcome the dependence on specific antibodies or the short cytokine half-life.

Many of the challenges that arise during those traditional methods can be overcome with the use of proteomics for secreted cytokine/protein analysis as proteomics enables unbiased global analysis of proteins in biological samples (Hathout, 2007). Currently, with the development of technology and bioinformatics approaches, hundreds to thousands of proteins can be identified from a small amount of sample. Various studies have demonstrated the detection sensitivity of proteomics in secreted protein identification. Moreover the proteomic analysis can reveal disease biomarkers (Grønborg et al, 2006), secretion of proteins involved in cancer aggressiveness (Makridakis et al, 2010), human plasma proteome (Anderson & Anderson, 2002), or inflammation-response related protein secretion (Eichelbaum et al, 2012). Proteomic secretome analysis overcomes the problems associated with RNA based approaches

due to quantification of secreted protein abundance and with antibody-based approaches such as specificity, quantification, and false-positives (Hathout, 2007).

Here, we used a global secretome profiling method to identify the proteins that are secreted by macrophages upon LPS stimulation and we used qPCR to validate the identified novel and known secreted proteins to show the high accuracy of this method. Moreover, bioinformatics analysis of secretome data demonstrated the strength of this method in data-dependent discovery.

MATERIALS AND METHODS

Reagents

LPS was purchased from Invitrogen. All protease inhibitor cocktails were purchased from Sigma-Aldrich (St. Louis, MO). All culture media and FBS were obtained from GIBCO. Trypsin was purchased from Promega. All chemicals were sequence- or HPLC-grade unless specifically indicated. Antibodies for p-I κ Ba (S32), I κ Ba, p-p65 NF κ B (S536), and p65 were purchased from Cell Signaling. Antibodies for Lmn1 and p65 were from Santa Cruz Biotechnology while antibodies to γ -tubulin, histone H3, H3K9me2, H3K9me1, H3K27me2 were from Abcam. Antibody for PHF8 was from Bethyl Labs. Bacterial clones for shRNA against PHF8 or against PLKO.1 were purchased from Sigma-Aldrich.

Cell Culture

RAW 264.7 cells were maintained in 4.5 g/L glucose DMEM with 10% FBS. For all LPS treatment 1 μ g/mL LPS is used.

Transfection and Stable PHF8-KD RAW Cell Line

The lentiviral plasmids pLKO.1 expressing shRNA-PHF8 (targeting sequences CGACCCTGATAATAAGACCAA and GCAAGATGAAACTCGGTGATT in human and mouse, respectively) were purchased from Sigma. A pLKO.1 empty vector without a specific shRNA sequence was used as the wild-type control. To produce virus, pLKO.1-shRNA plasmids were co-transfected into 293T cells with ViraPowerMix (Invitrogen) by jetPRIME™ in vitro DNA and siRNA transfection reagent (Polyplus). Pseudo-virus in supernatants was collected 48 h after transfection and used to transduce RAW 264.7 cells by spinoculation. 48 h after transfection, 8 µg/ml puromycin was added to select puromycin-resistant clones. Stable clones were maintained in medium containing 4 µg/mL puromycin. The expression level of PHF8 in PHF8-KD cell line was monitored with immunoblotting and qPCR.

PHF8-dependent Secretome Profiling

The Secretome profiling workflow is shown in **Figure 53**.

Sample Preparation

Paired WT and PHF8-KD RAW 264.7 cells were cultured in regular DMEM medium with 10% FBS. 24 hours prior to the LPS challenge, cells were washed with and cultured in serum-free DMEM containing 1 mM sodium pyruvate and 10 mM L-glutamine with no phenol red. Cells were cultured in the same medium and were either left unstimulated (0) or subjected to a single LPS challenge at 1 µg/mL for indicated hours (2, 4, 8, 24). The secretome containing culture medium was centrifuged at 400 x g for 5 min for removal of dead cell debris. The supernatant was collected with an 18-

gauge needle, syringe-filtered with 0.2 μ m 13 mm diameter PTFE filters (VWR International), and transferred into fresh tubes to be kept at -80°C until further processed. After the removal of extracellular media, the remaining attached cells were lysed with 1 X SDS-loading buffer to perform Western blots for confirmation of the inflammation phenotype.

Immunoblotting

To confirm the inflammation phenotype, we used immunoblotting (**Figure 54**) on the lysates denatured in SDS-loading buffer were sonicated twice at level 3 for 5 sec for successful release of the chromatin then were separated on an SDS-PAGE gel under reducing conditions and then transferred to a PVDF membrane. The membranes were blocked with milk for 1 h at RT on an orbital shaker. Following primary antibody incubation for 1 h at RT, we probed the membranes with a horseradish peroxidase conjugated secondary antibody and bands were detected using an ECL Western Blotting Detection Kit (GE Life Sciences).

Protein Digestion

To prepare the medium for MS analysis, we thawed the secretome-containing medium and diluted in 4 X lysis buffer (8 M urea, 40 mM HEPES pH 7.9) to bring the final urea concentration to 2 M. The mixture was then sonicated at level 3 for 5 seconds. The proteins were reduced with DTT (10 mM final) for 40 min at RT and alkylated with IAA (50 mM final) for 40 min in the dark at RT. Alkylation was quenched with freshly prepared thiourea (100 mM final). CaCl₂ was added to 1 mM final concentration for

optimum trypsin digestion overnight at RT. The digestion was quenched with TFA (0.5% final). Peptides were dried and resuspended at 0.1% FA for MS/MS.

LC-MS/MS

We used reversed phase LC-MS/MS using a Proxeon 1000 nano LC system coupled to an LTQ Orbitrap Velos mass spectrometer (Thermo Scientific, San Jose, CA). The peptides were trapped using a 3 cm long 100 μ m i.d. C18 column at 5 μ L/min liquid flow that was diverted from the analytical column via a vent valve while elution was performed by switching the valve to make the trap column in-line with a 15 cm long, 75 μ m i.d., 3.5 μ m, 300 Å particle C18 analytical column. The digested peptides were separated with a linear gradient of 2-35% buffer B over 240 min at a 300 nL/min flow rate using 0.1% formic acid (buffer A) and ACN with 0.1% formic acid (buffer B). Each secretome sample with two biological replicates were subjected to 3 single-shot independent LC-MS runs for global peptide analysis. Database search of the mass spectra, peptide identification, and Label-free Quantification (LFQ) were performed as previously described (Liu et al, 2014).

Bioinformatic Analysis

Mass spectra were analyzed using MaxQuant software **version 1.5.0.30** using the Andromeda search engine against the mouse Uniprot sequence database including 248 common contaminants and reversed versions of all sequences (Cox & Mann, 2008; Cox et al, 2011). Maximum allowed mass error was set to 4.5 ppm for monoisotopic precursor ions and 0.5 Da for MS/MS peaks. Enzyme specificity was set to trypsin and a maximum of two missed cleavages were allowed. We set carbamidomethyl-cysteine as

a fixed modification, and N-terminal acetylation and methionine oxidation as variable modifications. For identification of proteins, we kept requirements of at least one unique or razor peptide per protein group. LFQ was performed in MaxQuant using the built in Extracted ion chromatograms (XIC)-based fast LFQ algorithm (Luber et al, 2010). We set the required false positive rate as 1% at the peptide and 5% at the protein level, and the minimum required peptide length as 7 amino acids. Contaminants, reverse identification and proteins only identified by site were excluded from further data analysis.

For each LPS treated sample of a given phenotype and time point, ratios were calculated from the individual protein LFQ intensities, and the corresponding median LFQ intensities of the untreated sample. Missing values were imputed only for untreated samples by random sampling from a generated narrow normal distribution around the detection limit for proteins. The calculated ratios were log2 normalized. In order to retrieve the proteins with a statistically different quantitative ratios among different LPS stimulation durations, we used multiple samples statistic analysis via ANOVA with a permutation-based FDR controlled filter. The p-value cut-off was calculated at 5% FDR. This multiple samples test technique does not capture proteins with no dynamic (i.e. stable over time) since they are of no interest. The correlation between different replicates was confirmed with a Pearson correlation analysis. Finally, we benchmarked our LFQ secretome profiling for validation by comparing our data with that of the two separate studies of LPS-inducible secretome from primary bone marrow-derived macrophages (BMDM) (Liu et al, 2014; Meissner et al, 2013). Further, to understand the role of PHF8 in regulation of LPS-induced inflammation and

interacting signaling pathways, we comprehensively analyzed the functional categories of the LPS-inducible PHF8-dependent T-class secretome using David bioinformatics database in the context of Gene Ontology (GO) Biological Processes (GOBP), GO Cellular Components (GOCC), GO Molecular Functions (GOMF), and Kyoto Encyclopedia of Genes and Genomes (KEGG) pathways (Huang et al, 2009).

RNA Isolation and qPCR

Stable cell lines were seeded into 12 well cell culture dishes and treated with LPS for indicated times. Total RNA was isolated using illustra RNAspin Mini Kit (GE Healthcare Life Sciences). First-strand cDNA was synthesized by M-MLV reverse transcriptase (Promega) and diluted 5-fold for qPCR. qPCR was performed using Maxima SYBR Green/ROX (Thermo Scientific). All measurements were normalized against GAPDH as the internal control using $2^{-\Delta\Delta C_t}$ method. The sequences of primers are included in **Table 9**.

Table 9 Primer Sequences used in the qPCR of T-cell regulatory genes

Gene (mouse)	Primer Sequence	
	Left (5' to 3')	Right (5' to 3')
IL1a	GCAACGGGAAGATTCTGAAG	TGACAACTTCTGCCTGACG
IL1b	GCCCATCCTCTGTGACTCAT	AGGCCACAGGTATTTTGTCTG
IFNb	CCATCCAAGAGATGCTCCAG	GTGGAGAGCAGTTGAGGACA
IL6	CCGGAGAGGAGACTTCACAG	CAGAATTGCCATTGCACAAC
IL10	GGTTGCCAAGCCTTATCGGA	ACCTGCTCCACTGCCTTGCT
GAPDH	AACTTTGGCATTGTGGAAGG	ACACATTGGGGGTAGGAACA
TNFa	CCCCAAAGGGATGAGAAGTT	GTGGGTGAGGAGCACGTAGT
PHF8	AACACAACAAATGCTAATCT	AGAAGTTCCCTCCGAATGCT
ADAM17	AAGTGCAAGGCTGGGAAATG	CACACGGGCCAGAAAGGTT
B2M	CCGAACATACTGAACTGC	AGAAAGACCAGTCCTTGC
CCL2	AGGTCCTGTCTGCTTCTG	TCTGGACCCATTCTTCTTG
CCL7	AATGCATCCACATGCTGCTA	CTTTGGAGTTGGGGTTTTCA
CCL9	GGTCTGTCTGCCTTTTTGC	GGGCTACACAGAGAAACCCT
CCL22	GCTCTCGTCCTTCTTGCTGT	GCAGGATTTTGAGGTCCAGA
CD74	ACGGCAAATGAAGTCAGAACA	AAGACTACTAATGGGTCAGAAAT
CFB	CTCGAACCTGCAGATCCAC	TCAAAGTCCTGCGGTCGT
CTSB	GCCCCGACCATTGGACAGAT	GCCCCAAATGCCCAACA
CTSL1	GACCGGGACAACCACTGTG	CCCATCAATTCACGACAGGAT
CTSS	AAGCGGTGTCTATGACGACCC	GAGTCCCATAGCCAACCACAA
CTSZ	CCTGTCCGGGAGGGAGAA	TGTTGATAACGGCCTGGTC
CXCL16	TCCTTTTCTTGTTGGCGCTG	CAGCGACACTGCCCTGGT
IFI30	GTCAGCTGTACCAGGGAACG	GTCTGGGCTTTGTGGGACAT
ITGA4	TGCACCTCTTGCTGTCTTGTT	GTGGCCTTAGCTCCTCTCT
LIF	AATGCCACCTGTGCCATACG	CAACTTGGTCTTCTGTGCCG
TNFSF9	GCAAGCAAAGCCTCAGGTAG	TCCAGGAACGGTCCACTAAC
TREM2	AGAGTGTGGTGACGGGTTCC	TATGACGCCTTGAAGCACTG

P14 CD8+ T cell activation assay

For T cell activation assay, CD8+ T cells from P14 transgenic mouse were first isolated with CD8a microbeads according to manufacturer's instruction. Isolated CD8+ T cells were re-suspended in 1 mL 1640 medium. Meanwhile WT (shCON) and PHF8-KD (shPHF8) RAW 264.7 cells were seeded in 6 well plates, treated with 1 µg/mL LPS for 0, 8, and 24 h; then were treated with 50 µg/mL mitomycin C for 30 min at 37°C. Mitomycin C-treated cells were washed with 1 mL PBS twice. 0.1x10⁶ P14 T cells are co-cultured with 2x10⁵ WT or PHF8-KD RAW cells in 96-well plates in RPMI medium

containing 50 U/mL mIL-2. The activation of CD8⁺ T cells was assessed by flow cytometry at day 6 with analysis of T cell activation markers of CD25, CD44, and CD69.

P14 CD8⁺ T cell proliferation assay

For T cell proliferation assay, CD8⁺ T cells from P14 transgenic mouse were first isolated with CD8a microbeads according to manufacturer's instruction. Isolated CD8⁺ T cells were re-suspended in 1 mL 1640 medium and labeled with 1 mL of the 10 μ M Carboxyfluorescein diacetate succinimidyl ester (CFSE) for 8 min at RT. Cells were washed with 10 mL 1640 medium containing 10% FBS. Meanwhile WT (shCON) and PHF8-KD (shPHF8) RAW 264.7 cells were seeded in 6 well plates, treated with 1 μ g/mL LPS for 0, 8, and 24 h; then were treated with 50 μ g/mL mitomycin C for 30 min at 37°C. Mitomycin C-treated cells were washed with 1 mL PBS twice and then labeled with 0.4 mL of the 30 μ g/mL GP33-41 peptide in PBS for 30 min at 37°C. The unattached peptides were washed with PBS. 0.1x10⁶ P14 T cells are co-cultured with 2x10⁵ WT or PHF8-KD RAW cells in 96-well plates in RPMI medium containing 50 U/mL mIL-2. The proliferation of CD8⁺ T cells was assessed by flow cytometry at day 6.

RESULTS

PHF8 selectively promotes the secretion of a specific group of 'tolerizable' proteins including cytokines and chemokines

To understand how PHF8 regulates the LPS-induced inflammation and overall inflammation response we employed an unbiased LFQ proteomic method to profile the LPS-induced, time resolved proteins that are differentially secreted from paired WT versus PHF8-KD RAW cells as shown in **Figure 53**. The non-biased, discovery-driven

secretome screening is a powerful method that can identify not only PHF8-regulated secretory proteins but also unknown extracellular functions of PHF8 that control inflammation. To this end, we stimulated WT and PHF8-KD RAW cells with LPS for 0, 2, 4, 8, and 24 h; representing non-stimulated (N), acutely stimulated (NL), and prolonged stimulated (T) inflammatory states. The inflammation phenotype were confirmed via immunoblotting for the levels of phospho-p65, I κ B α , and phospho-I κ B α (**Figure 54**). Our immunoblots revealed that PHF8-KD was stable. Moreover, the immunoblots of P-p65 (S536) and P-I κ B α showed LPS-dependent increase that was diminished over 24 h LPS stimulation confirming the accurate inflammation response. γ Tubulin was used as a cellular loading control.

We performed the LFQ analysis on two biological replicates, in which each biological set was further measured with three technical replicates. The time-resolved or inflammatory-phenotypic changes in the amounts of secreted proteins were filtered to proteins with a 5% permutation-based FDR that show statistically distinct patterns in each time-point of LPS stimulation and normalized for all inflammatory states according to the Z-score. The correlation between different replicates was confirmed with a Pearson correlation analysis (score >0.7) (**Figure 55**).

From this analysis **1002** proteins were selected, which grouped by unsupervised hierarchical clustering into **368** LPS-induced in WT cells (**Figure 56**), **318** of which (86% of LPS-induced) showed PHF8-dependency in secretion as their LPS-induced secretion diminished in PHF8-KD. Moreover, approximately **254** proteins (80% of LPS-inducible PHF8-dependent secretome) showed a secretion pattern similar to the inflammatory phenotype-specific mRNA expression of *T-class genes* (Foster et al, 2007);

prolonged LPS stimulation caused a reduction in secretion of proteins that has been increased by an acute LPS stimulation (**Figure 56, left**). Therefore, we defined this cluster of LPS-inducible, secretory proteins as the ‘tolerizable’- or ‘T-class secretome’ (highlighted in green in the cluster column). The T-class secretome is given in **Appendix 1**. The remaining 64 LPS-inducible proteins (**Figure 56, right**) were secreted in a trend similar to the mRNA expression of the *non-tolerizable (NT)-class genes* (highlighted in yellow in the cluster column), which are clustered as the ‘NT-class secretome’. This set of proteins is given in **Appendix 2**.

To benchmark the LFQ secretome profiling for validation, we compared our data of the RAW cell secretome with that of the LPS-inducible secretome from BMDM (Meissner et al, 2013). This comparison revealed 175 secretome components in common (**Figure 57, Appendix 3**), 40% of which are cytokines and chemokines (**Table 10**). Further, a comparison with a more recent BMDM secretome (Liu et al, 2014) revealed 632 common components (**Figure 57, Appendix 4**), 192 of which (30%) were found in the LPS-inducible portion including most of the cytokines and chemokines (**Appendix 5**). Some defense or wounding response-related proteins were found secreted upon LPS stimulation, including multiple cytokines/chemokines, complement factors, Integrin beta 2 (Itgb2), Interleukin 27 (IL27), and lymphocyte antigen 86 (Ly86), in line with a recent report indicating the regulatory role of PHF8 in wound healing by bone-marrow stromal cells (Han et al, 2015).

These overlapping results not only validated the accuracy of our LFQ secretome screening, but also, and more importantly, indicated that the acute LPS-induced secretion of select cytokines/chemokines, and many other immune response-related

proteins, is PHF8-dependent, supporting the conclusion that PHF8 is the primary *re-programmer* of chromatin modifications associated with various inflammatory genes specifically in acutely inflamed macrophages.

Table 10 List of cytokines and chemokines identified in the LPS-inducible secretome
The table also shows the comparison with previous BMDM secretome studies.

Cytokine/Chemokine	PHF8-dependent secretion	Identified in (Meissner et al, 2013)	Identified in (Liu et al, 2014)
Aimp1	✓		✓
Ccl2	✓	✓	✓
Ccl22		✓	
Ccl3		✓	✓
Ccl4		✓	✓
Ccl5		✓	✓
Ccl7	✓	✓	
Ccl9	✓	✓	✓
Csf3		✓	
Cxcl10	✓	✓	✓
Cxcl16	✓	✓	
Cxcl2	✓	✓	✓
Ebi3	✓	✓	
Ifnb1		✓	
Il27	✓	✓	
Il6		✓	✓
Lif	✓		
Mif			
Osm			
Spp1		✓	

PHF8-dependent T-class secretome is involved in regulation of diverse extracellular processes and pathways upon LPS stimulation

Since our previous qPCR and immunoblotting results revealed PHF8 as a pro-inflammatory active demethylase, we primarily focused on the T-class PHF8-dependent secretome for further analysis. To explore novel functions of PHF8 in regulation of LPS-

induced inflammation and interacting signaling pathways, we comprehensively analyzed the functional categories of the LPS-inducible PHF8-dependent T-class secretome using David bioinformatics database in the context of GOBP, GOCC, GOMF, and KEGG pathways (Huang et al, 2009).

PHF8 regulates the antigen processing and presentation BP upon LPS stimulation

GOBP analysis revealed that the LPS-inducible PHF8-dependent T-class secretome is involved in various extracellular BPs such as defense response, response to wounding, immune/inflammatory response, antigen processing and presentation, regulation of complement factors, cell metabolism, glycolysis-related cell adhesion, cell migration, cell-to-cell communication, and T cell activation (**Figure 58**). More importantly, the PHF8-dependent T-class proteins of inflammation response are also involved in other related BPs, including defense response, immune response, response to wounding, antigen presentation, DNA replication, chromosome organization, and mRNA processing (**Table 11**).

Table 11 T-class GOBP enrichment

Defense Response
CD74 antigen (invariant polypeptide of major histocompatibility complex, class II antigen-associated)
aminoacyl tRNA synthetase complex-interacting multifunctional protein 1
beta-2 microglobulin
chemokine (C-C motif) ligand 2
chemokine (C-C motif) ligand 7
chemokine (C-X-C motif) ligand 2
complement component factor h; similar to complement component factor H
complement factor B
histocompatibility 2, D region; histocompatibility 2, D region locus 1
histocompatibility 2, K1, K region; similar to H-2K(d) antigen
insulin-like growth factor binding protein 4
integrin beta 2
interleukin 27
lymphocyte antigen 86
lysozyme 2

phospholipase A2, activating protein protein tyrosine phosphatase, non-receptor type 6
Immune Response
CD74 antigen (invariant polypeptide of major histocompatibility complex, class II antigen-associated) MHC class I like protein GS10 beta-2 microglobulin chemokine (C-C motif) ligand 2 chemokine (C-C motif) ligand 7 chemokine (C-C motif) ligand 9 chemokine (C-X-C motif) ligand 2 collectin sub-family member 12 complement component factor h; similar to complement component factor H complement factor B histocompatibility 2, D region; histocompatibility 2, D region locus 1 histocompatibility 2, K1, K region; similar to H-2K(d) antigen interleukin 27 lymphocyte antigen 86 protein tyrosine phosphatase, non-receptor type 6 tumor necrosis factor (ligand) superfamily, member 9
Response to wounding
aminoacyl tRNA synthetase complex-interacting multifunctional protein 1 cathepsin B chemokine (C-C motif) ligand 2 chemokine (C-C motif) ligand 7 chemokine (C-X-C motif) ligand 2 complement component factor h; similar to complement component factor H complement factor B insulin-like growth factor binding protein 4 integrin beta 2 interleukin 27 lymphocyte antigen 86 phospholipase A2, activating protein plasminogen activator, urokinase receptor protein tyrosine phosphatase, non-receptor type 6
Antigen presentation
CD74 antigen (invariant polypeptide of major histocompatibility complex, class II antigen-associated) MHC class I like protein GS10 beta-2 microglobulin histocompatibility 2, D region; histocompatibility 2, D region locus 1 histocompatibility 2, K1, K region; similar to H-2K(d) antigen interferon gamma inducible protein 30
DNA Replication
minichromosome maintenance deficient 2 mitotin (<i>S. cerevisiae</i>) minichromosome maintenance deficient 4 homolog (<i>S. cerevisiae</i>) minichromosome maintenance deficient 6 (MIS5 homolog, <i>S. pombe</i>) (<i>S. cerevisiae</i>) minichromosome maintenance deficient 7 (<i>S. cerevisiae</i>)
Chromosome organization

<p> H2A histone family, member V RuvB-like protein 1 RuvB-like protein 2 histone cluster 1, H1b histone cluster 1, H1c histone cluster 1, H1d histone cluster 1, H1e histone cluster 1, H2ad; histone cluster 1, H2ae; histone cluster 1, H2ag; histone cluster 1, H2ah; histone cluster 1, H2ai; similar to histone 2a; histone cluster 1, H2an; histone cluster 1, H2ao; histone cluster 1, H2ac; histone cluster 1, H2ab histone cluster 1, H2bg; histone cluster 1, H2be; histone cluster 2, H2bb; histone cluster 1, H2bc histone cluster 1, H4k; histone cluster 1, H4m; histone cluster 4, H4; similar to germinal histone H4 gene; histone cluster 1, H4h; histone cluster 1, H4j; histone cluster 1, H4i; histone cluster 1, H4d; histone cluster 1, H4c; histone cluster 1, H4f; histone cluster 1, H4b; histone cluster 1, H4a; histone cluster 2, H4; similar to histone H4 histone cluster 2, H3b; histone cluster 1, H3f; histone cluster 1, H3e; histone cluster 2, H3c1; histone cluster 1, H3d; histone cluster 1, H3c; histone cluster 1, H3b; histone cluster 2, H3c2; histone cluster 2, H2aa1; histone cluster 2, H2aa2 histone deacetylase 2 minichromosome maintenance deficient 2 mitotin (<i>S. cerevisiae</i>) nucleosome assembly protein 1-like 4 poly (ADP-ribose) polymerase family, member 1 replication protein A1 </p>
<p>mRNA Processing</p> <p> DEAD (Asp-Glu-Ala-Asp) box polypeptide 5; DEAH (Asp-Glu-Ala-His) box polypeptide 15 HLA-B-associated transcript 1A PRP19/PSO4 pre-mRNA processing factor 19 homolog (<i>S. cerevisiae</i>) RNA binding motif protein, X chromosome retrogene U2 small nuclear ribonucleoprotein auxiliary factor (U2AF) 2 amyloid beta (A4) precursor protein heterogeneous nuclear ribonucleoprotein H1 heterogeneous nuclear ribonucleoprotein L non-POU-domain-containing, octamer binding protein; predicted gene 8806 similar to heterogeneous nuclear ribonucleoprotein A2/B1; heterogeneous nuclear ribonucleoprotein A2/B1 small nuclear ribonucleoprotein polypeptide A; NHP2 non-histone chromosome protein 2-like 1 (<i>S. cerevisiae</i>); eukaryotic translation initiation factor 4A, isoform 3; similar to peptidylprolyl isomerase-like 1; peptidylprolyl isomerase (cyclophilin)-like 1 splicing factor 3a, subunit 1 splicing factor 3a, subunit 3 splicing factor 3b, subunit 2 splicing factor 3b, subunit 3 splicing factor 3b, subunit 5 splicing factor proline/glutamine rich (polypyrimidine tract binding protein associated); splicing factor, arginine/serine-rich 1 (ASF/SF2); </p>

Similarly, antigen processing and presentation was found in the KEGG pathway enrichment of T-class PHF8-dependent secretome (**Figure 59**). This indicates that PHF8 modulates the inflammation-induced secretion of various proteins involved in antigen processing and presentation, an essential and significant part of the inflammation response. In line with this observation, multiple members of a major antigen processing/presentation complex called the minichromosome maintenance (MCM) protein complex were found as a highly enriched GOBP in the T-class PHF8-dependent secretome (**Figure 58**). MCMs were expressed on the surface of different types of malignant/proliferative cells (Das et al, 2013) but there is little knowledge of how they are regulated during a pro-inflammatory response. Here, the MCM complex constituted the pathways associated with DNA replication in enriched KEGG pathways (**Figure 59**). Because DNA replication is an inflammatory process (Ishii & Akira, 2006), PHF8 may regulate DNA metabolism of pathogens in the extracellular matrix via regulating the secretion of MCM complexes.

We compared our PHF8-dependent T-class secretome to a previous PHF8 Chromatin immunoprecipitation (ChIP)-sequencing (ChIP-seq) study for both validation and analysis. PHF8 ChIP-seq study revealed that active PHF8 was bound to the promoters of genes involved in RNA processing, mRNA splicing, DNA repair, and cell cycle (**Figure 60, Table 12**). In agreement with the ChIP-seq study, our T-class secretome analysis involved these processes in the GOBP enrichment (**Figure 58**); given these processes are involved in the inflammatory response regulation, we concluded that our secretome analysis revealed inflammatory-specific regulation of PHF8-dependent secretome upon LPS stimulation.

Table 12 DAVID analysis of functionally active PHF8 targets (Wang et al, 2014a).

Gene group	Term	Count	p-value	FDR
PHF8-activated targets	Macromolecule metabolic process	427	6.56E-24	1.17E-20
	Gene expression	281	1.12E-21	1.99E-18
	Cellular process	682	2.70E-16	4.00E-13
	Transcription	195	1.34E-13	2.38E-10
	Chromatin organization	57	1.84E-07	3.27E-04
	RNA splicing	38	1.38E-06	2.45E-03
	Cell cycle process	57	2.12E-05	3.78E-03

PHF8 regulates lysosome activation

KEGG pathway enrichment of the T-class PHF8-dependent secretome revealed metabolic pathways, antigen processing and presentation, and lysosomal pathways as exclusively T-class-specific (**Figure 57**). Lysosome-related secreted proteins were mostly peptidase family members, which were previously identified in LPS-induced macrophage secretome (Eichelbaum et al, 2012; Liu et al, 2014; Meissner et al, 2013), are part of the antigen processing and presentation pathways and are involved in multiple immunity-related processes (Conus & Simon, 2010). The T-class PHF8-dependent secretion of these lysosome-related proteins indicates that *PHF8 regulates lysosome formation and activity upon LPS stimulation*.

PHF8 regulates the MHC expression and shedding upon LPS stimulation

GOCC enrichment revealed various LPS-induced extracellular compartments including vesicle, lysosome, vacuole, and, more importantly in agreement with GOBP and KEGG enrichment, Major histocompatibility complex (MHC) complexes (**Figure 61**). In line with the role of PHF8 as a regulator of antigen presentation GOBP, according to GOCC enrichment, PHF8 regulates LPS-inducible MHC expression and shedding from the cell membrane to the extracellular space in macrophages. MHC complex is a major regulator of adaptive immunity as it is responsible for the pathogenic antigen

presentation on the antigen presenting cells upon activation of inflammatory response, to facilitate recognition of these peptides by T cells (**Figure 62**) (Janeway et al, 2001); thus, as a regulator of MHC components, PHF8 may be an important mediator of activation of adaptive immunity.

PHF8 regulates the LPS-induced secretion of proteins with cytokine/chemokine activity

The GOMF enrichment of T-class PHF8-dependent secretome also revealed various inflammation response-related proteins showing more than 2-fold enrichment (**Figure 63**). More importantly, cytokine activity and chemokine activity were among the PHF8-dependent T-class GOMF and these were in common with previous LPS-inducible secretome of BMDMs (**Appendix 5**), indicating that PHF8 is a major regulator of secretion of proteins with cytokine or chemokine activity in LPS response.

PHF8 promotes adhesion, communication, and activation of the cells of adaptive immunity

In our manual analysis, we observed that PHF8 affected the LPS-induced secretion of select adaptive immunity regulators, including Complement factors B (Cfb) and H (Cfh), Interleukin Enhancer Binding Factor 3 (ILF3) (Marcoulatos et al, 1998), Ly86 (Nagai et al, 2002), amyloid precursor protein (APP) (Gitter et al, 2000), integral membrane protein 2B (Itmb2), and metalloproteinase domain-containing proteins 8 (ADAM8), and 17 (ADAM17). Specifically, LPS-induced secretion of complement factors from macrophages is important for both recognition of pathogens and activation of adaptive immunity (Carroll, 2004), indicating the regulatory role of PHF8 in these BPs. In agreement with previous LPS-induced BMDM secretome (Meissner et al, 2013), we

identified ADAM17 as an LPS-induced macrophage secretome component; ADAM17 is an adaptive immunity regulator responsible for shedding of membrane-bound proteins, one such shed protein being APP (Gitter et al, 2000). The presence of ADAM17 with APP in the LPS-induced secretome confirms APP shedding from the membrane.

GOBP analysis (**Figure 58**) also revealed some components of the PHF8-dependent T-class secretome are involved in cell adhesion and cell communication, including MHC complexes, serglycin (SRGN), Lectin-Galactoside-Binding Soluble 3-Binding Protein (Lgals3BP), intercellular adhesion molecule 1 (Icam1), Integrin alpha 4 (Itga4), Itgb2, cathepsin B (Ctsb), urokinase plasminogen-activator surface receptor (PLAUR), syndecan 4 (Sdc4), and poliovirus receptor-related 1 (Pvr11). SRGN and Lgals3BP are cell-cell communication regulators activated by TLR4 (Kolset & Pejler, 2011; Schnoor et al, 2008). Icam1 is a cell-surface glycoprotein expressed on immune cells that binds to integrins (Frank & Lisanti, 2008); integrins Itga4 and Itgb2 in turn regulate cell migration and adaptive immunity (Harburger & Calderwood, 2009), and are in common with LPS-induced BMDM secretome (Meissner et al, 2013). Similarly, the released adhesion molecules Ctsb (Conus & Simon, 2010), PLAUR (Malla et al, 2011), SDC4 (Götte, 2003), and Pvr11 (Kim et al, 2010) are involved in regulating cell migration in inflammation.

From a system perspective, we next used Search Tool for the Retrieval of Interacting Genes/Proteins (STRING) (Jensen et al, 2009) to explore the pathway links in the PHF8-dependent, T-class secretome. A protein-protein interaction (PPI) network was mapped among the secreted proteins categorized in different GOBP, GOCC, and GOMF (**Figure 64**); this network was dominated by response to signaling BP as

highlighted with red nodes. Based on these protein ‘nodes’ in the PPI network, we used IPA to identify the canonical pathways that share common nodes, which revealed the interplay between pathways involving antigen processing and presentation, complement regulation, cell adhesion, and endocytosis as the coordinator of inflammation response (**Figure 65**).

PHF8 positively regulates the activation and proliferation of T cells via secretion of specific proteins involved in antigen presentation and activation of adaptive immunity

Our findings of the IPA analysis on secreted proteins associated with the activation of adaptive immunity in the PHF8-dependent secretome (**Figure 65**) implicated that PHF8 positively links innate immunity and adaptive immunity. To elucidate the role of PHF8 in this link, we examined the LPS-induced mRNA expression of select genes from the secreted proteins in T-class PHF8-dependent secreted cluster based on their relevance to antigen processing/presentation and the activation of adaptive immunity. Among them, Leukemia inhibitory factor (Lif) is a known regulator of T-cell maturation (Shen et al, 1994). Similarly, the cytokine TNF Superfamily Member 9 (Tnfsf9) regulates innate and adaptive immunity through activation of CD4+ T cells (Fernández Do Porto et al, 2012). The chemokines Ccl2, Ccl7, Ccl9, Ccl22, and Cxcl16 activate adaptive immunity by promoting the activation and migration of T cells (Luther & Cyster, 2001). Cfb is a complement factor that regulates adaptive immunity response (Carroll, 2004). ADAM17 and beta-2-microglobulin (B2m) regulate T cell proliferation and differentiation (Agrawal & Kishore, 2000; Li et al, 2007) while CD74 regulates cell survival in adaptive immunity (Leng et al, 2003). Triggering receptor expressed on

myeloid cells 2 (TREM2) is a T-cell regulator (Sharif & Knapp, 2008) while Itga4 helps traffic leukocytes to the site of inflammation (Grégoire et al, 2007; Harburger & Calderwood, 2009). Moreover, IFN γ -Inducible Protein 30 (Ifi30) is involved in CD8+ T cell proliferation in mice (Singh et al, 2011). As the antigen processing/presentation massagers, cathepsins regulates the formation of CD4+ T lymphocytes (Conus & Simon, 2010). As shown in **Figure 66**, the mRNA expression of these T cell regulating secretion products increased significantly 4 hours following LPS stimulation in WT cells while the increase was disrupted in PHF8-KD cells. Moreover, with the exception of Ccl2 and Ccl7, mRNA expressions of these genes decreased 8 hours after the LPS stimulation, consistent with the pattern of PHF8-dependent, T-class protein secretion. Since previous studies found that Ccl2 and Ccl7 mRNA expression persisted even with the prolonged LPS stimulation (Eichelbaum et al, 2012; Kang et al, 2009) and the secretion pattern did not agree with the secretome analysis, we concluded that there might be other intermediate events affecting their phenotypic regulation. Moreover, this demonstrates that the quantitative proteomic studies are very powerful in understanding the regulation of signaling events in the extracellular space.

After validation of the LPS-induced mRNA expression of T cell activating extracellular proteins, we wanted to determine the immediate outcome of PHF8-dependent secretion of these molecules on the activation and proliferation of T cells. Using flow-cytometry we performed T cell activity and proliferation assays on T cells that were incubated with either WT or PHF8-KD RAW cells that were previously stimulated with LPS for 0, 8, or 24 h.

To assess the T cell activation, we monitored the T cell activation markers CD25, CD44, and CD69 via flow-cytometry (**Figure 67**). CD8+ T cells that were treated with LPS-stimulated WT RAW cells showed efficient activation while those treated with LPS-stimulated PHF8-KD cells showed impaired activation. To determine whether this effect was translated into the proliferation process, we assayed the T cell proliferation using flow cytometry. In line with the activation markers, proliferated CD8+ T cells were found after 6 days of co-incubation with WT cells while PHF8-KD cells lost the ability to promote the proliferation of T cells with or without LPS stimulation (**Figure 68**), all indicating the regulatory function of PHF8 in the activation of adaptive immunity.

DISCUSSION

The mechanism of the gene-specific control of inflammation by TLR4-induced chromatin modification was previously discovered by microarray analysis of LPS-induced differential gene expression. Unknown was exactly how different classes of genes are regulated at the epigenetic level by specific chromatin modifiers. We have now identified the LPS-induced, PHF8-dependent, T-class secretome at the more physiologically relevant protein level, directly and systematically extending the function of PHF8 in a broad range of biological processes and pathways.

Here, we identified PHF8 as a major regulator acute inflammation that modulates the secretion of specific proteins from macrophages upon LPS stimulation. Our proteomic screening demonstrates that PHF8 is a major macrophage regulator in phenotypic response that modulates, not only the transcription, but also the secretion of various components of adaptive immunity activators. Moreover, this report is the first to show evidence on connecting the missing link between innate and adaptive

immunity. Moreover, our analysis revealed various signaling pathways that are in interplay with LPS-induced inflammation via extracellular matrix. Further, deciphering the important regulators of T cell activation and proliferation (Takeda & Akira, 2015), we provided evidence for PHF8-dependent regulation of extracellular pathways involved in activation of adaptive immunity through secretion of specific signaling or messenger molecules: selectins recruit leukocytes, chemokines activate leukocytes activating integrins, and the integrins regulate adhesion to the vascular endothelium (Harburger & Calderwood, 2009). By profiling the LPS-induced PHF8-dependent secretome, we have characterized novel extracellular functions controlled by PHF8 as a broad regulator of the innate immunity-dependent activation of adaptive immunity. This discovery agrees with a previous report suggesting a possible adaptive immunity function of PHF8 as a transcriptional activator of hairy and enhancer of split-1 (HES1), Deltex 1 (DTX1), IL7 Receptor (IL7R), Neurogenic locus notch homolog protein 3 (NOTCH3) for regulating T cell differentiation (Radtke et al, 2013). Specifically, our secretome data indicate that PHF8 is responsible for activation of adaptive immunity by regulating the secretion of multiple chemoattractants as well as multiple products of MHC genes that play crucial roles in antigen presentation to T cell (Agrawal & Kishore, 2000). Our combined results indicate that PHF8 is an epigenetic regulator of a broad range of secreted proteins that are crucial for leukocyte/T cell activation and proliferation.

In this study, we used an unbiased LFQ based proteomic strategy to screen extracellular components, the most significant products of the innate immunity promoting adaptive immunity, of LPS-induced macrophages. First, our proteomic

technique demonstrated that unbiased screening of extracellular proteins can help us identify major regulators of signaling events that are involved in cell-cell communication. This technique is powerful in showing evidence for extracellular functions of well-known signaling molecules as well as uncovering candidates for novel functional characterization. Moreover, this technique can overcome many issues, like the need for previous knowledge or highly specific antibodies, associated with the previously used techniques such as ELISA. In addition, this technique is very efficient as the number of identified proteins in a single proteomic experiment surpasses all the previously known techniques of extracellular screening. Further, we demonstrate that accurate bioinformatic analysis of LFQ screening helps us decipher the functional outcome of the signaling events in extracellular screening while it also provides information on the interplay of various signaling pathways.

Our proteomic analysis of extracellular molecules of LPS-induced macrophages revealed various mechanisms involved in the regulation of macrophage inflammation. This method can also be used in identification of regulators of various other signaling pathways such as immunity, tumor formation or growth, stress prevention, coagulation, adhesion, cell-cell communication, and vascular function as these are main signaling events that are mainly regulated through extracellular components (Teti, 1992; van der Pol et al, 2012; Yáñez-Mó et al, 2015). Moreover, similar extracellular screening of cancer cells or tissues would help us discover deregulated signaling mechanisms that are significant in cancer formation or progression. This method can also be used to identify biomarkers related to cancer. In summary, proteomic analysis of extracellular

proteins can reveal unknown mechanisms; provide information on disease-specific biomarkers, and deregulated signaling pathways.

FUTURE WORK

Here, we performed an extracellular proteomic screening to identify secretion products of LPS-induced macrophages to reveal the role of PHF8 in activation of adaptive immunity. The accurate and fast validation of the secretome data can be achieved through analysis of intracellular expression patterns using various biochemical methods such as ELISA, proteomics, and immunoblotting. However, the most extensive analysis of expression screening can be achieved with proteomics, in which the need for large amounts of samples and previous knowledge of proteins or antibodies is avoided. Thus, the increase in not only the secretion but also expression of the regulators of adaptive immunity will be possible via the intracellular global profiling of paired WT and PHF8-KD that were either left unstimulated or stimulated with LPS. Such unbiased screening will help us understand other signaling events that are in interplay with inflammation response and explain the relationship between the expression and secretion of them. Moreover, that will also enable us monitor other known molecules that are involved in immunosuppression, providing link to regulation of inflammatory phenotype by PP2Ac.

Another advantage of proteomic screening is that it enables us to detect PTMs in an unbiased and quantitative manner. By performing detailed sequence and structural analysis of peptide contents of the extracellular secretome, information on the abundance of PTMs, proteolytic shedding, and alternative splicing can be gathered. This

will enable us identify signaling events in inflammation response as well as discover mechanisms for post-translational regulation of important inflammatory molecules.

FIGURES

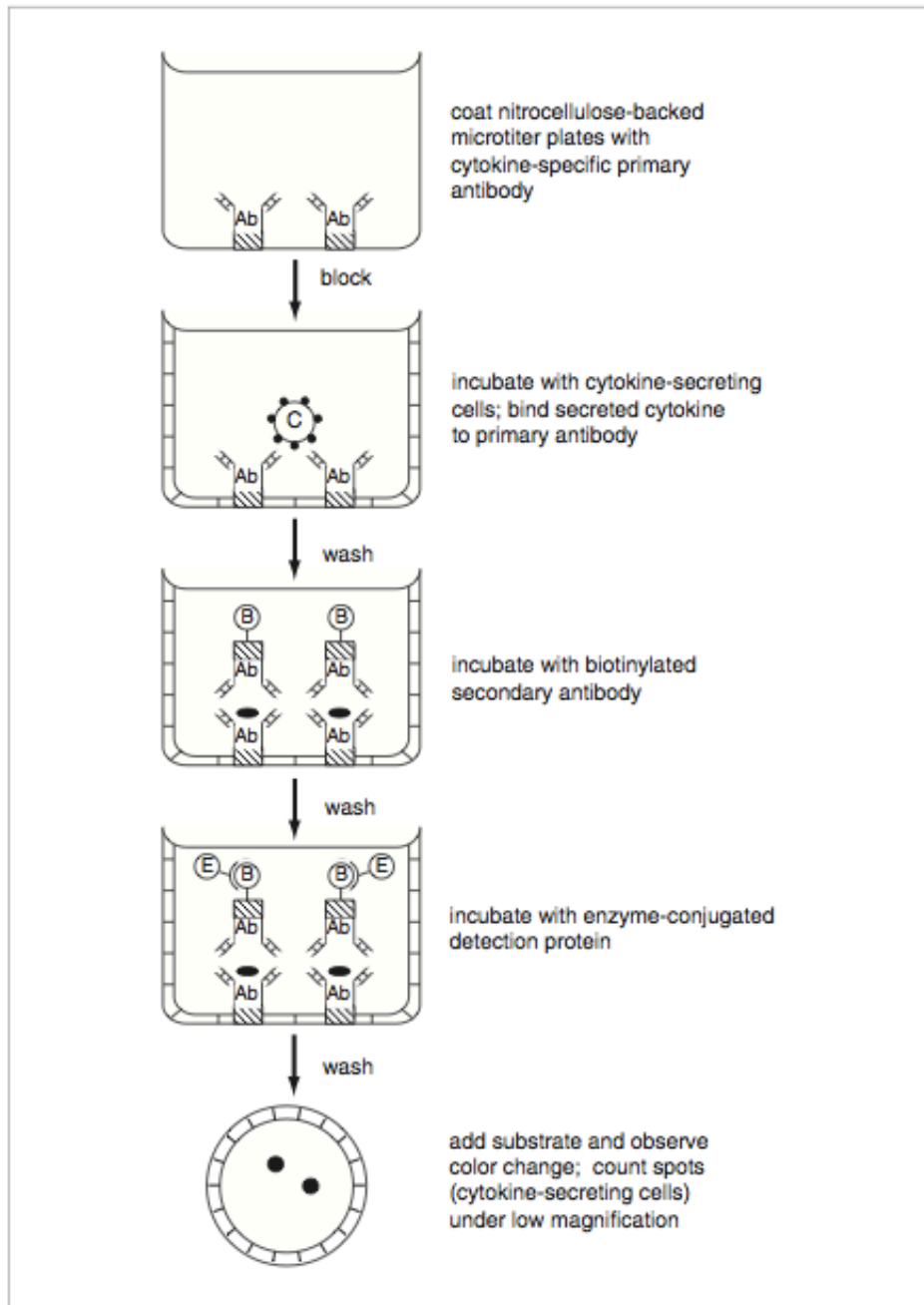


Figure 51 Schematic of ELISA procedure.

Abbreviations: Ab, antibody; B, biotin label; C, cytokine-secreting cells; E, enzyme-conjugated detection protein. Adopted from (Klinman & Nutman, 2001).

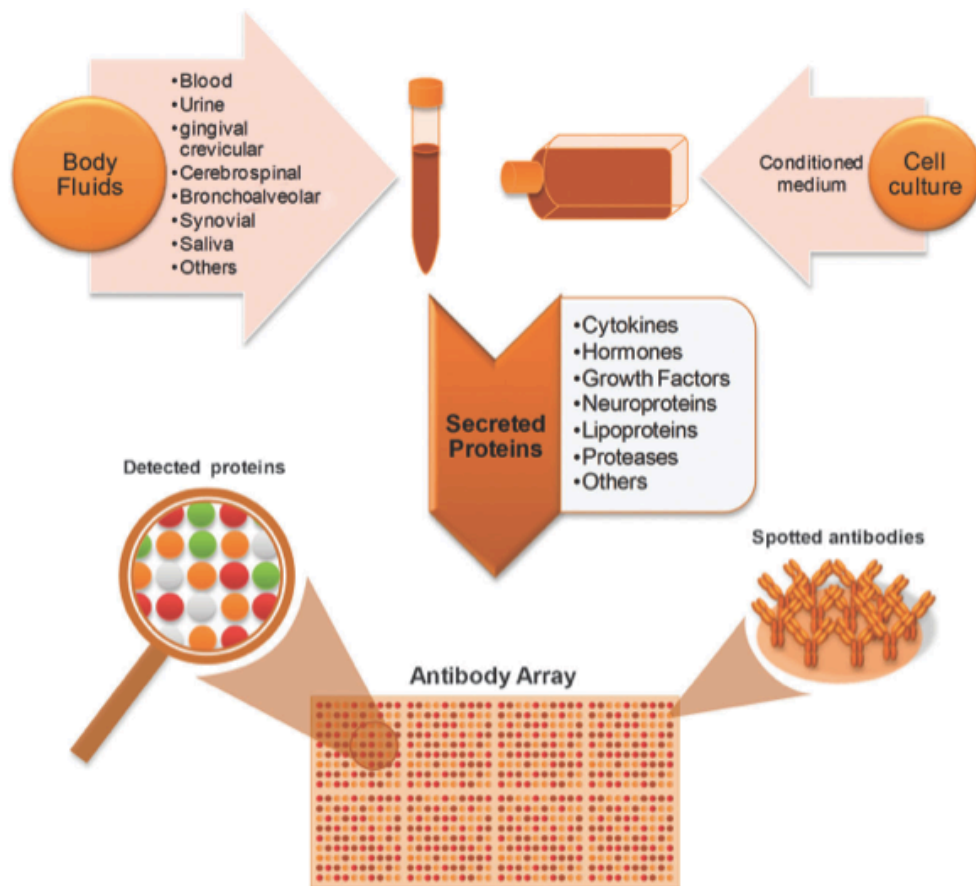


Figure 52 Scheme of the protein profiling process with antibody microarrays. Proteins are isolated from the respective samples, labeled and applied to the array. Adopted from (Mustafa et al, 2011).

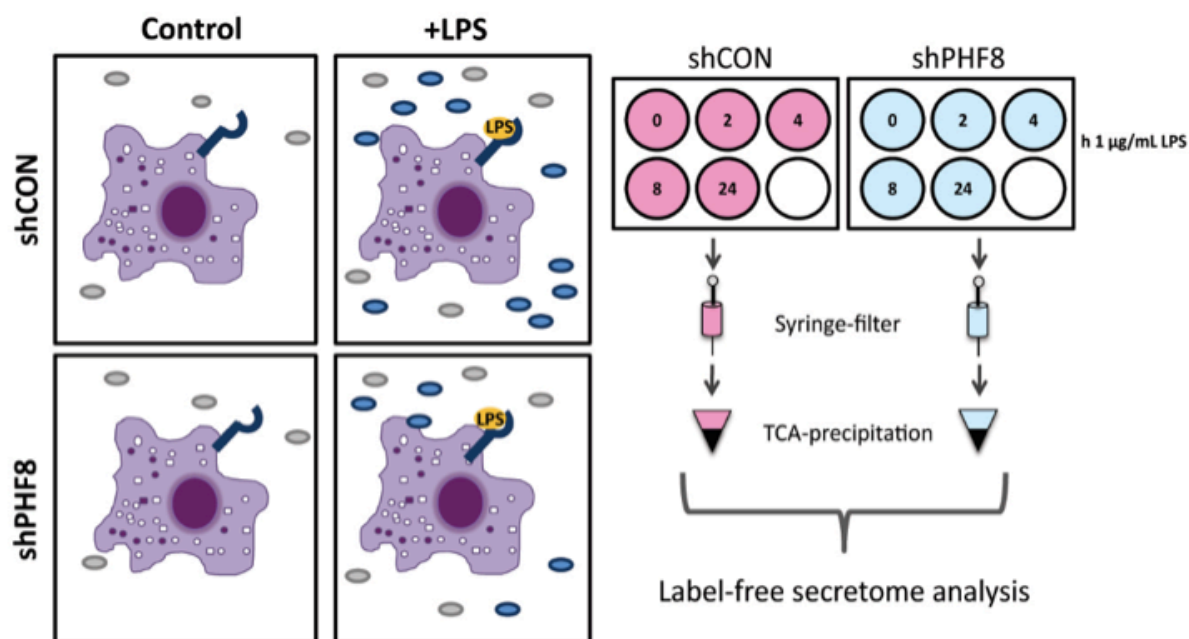


Figure 53 Workflow of the LFQ secretome analysis

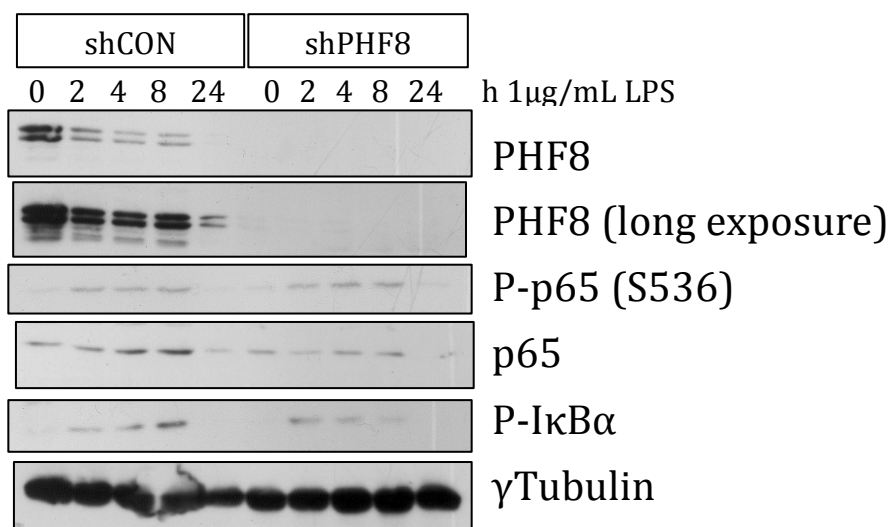


Figure 54 Immunoblot of cell lysates for phenotype detection
Immunoblots show accurate inflammation phenotype and successful PHF8-KD (Erdoğan et al, 2016).

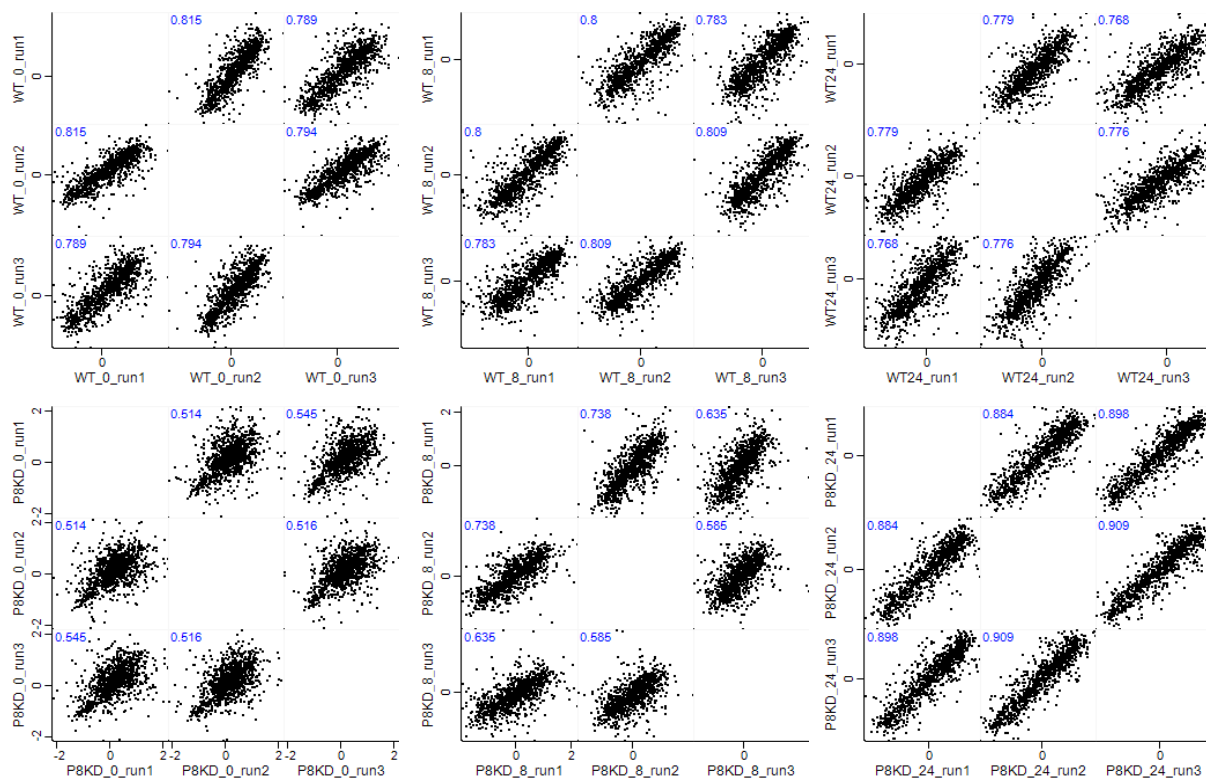


Figure 55 Scatter plots showing Pearson correlation of samples. The replicates of WT (top) and PHF8KD (bottom) secretome with time points indicated 0 (left), 8 (middle) and 24 h (right) (Erdoğan et al, 2016).

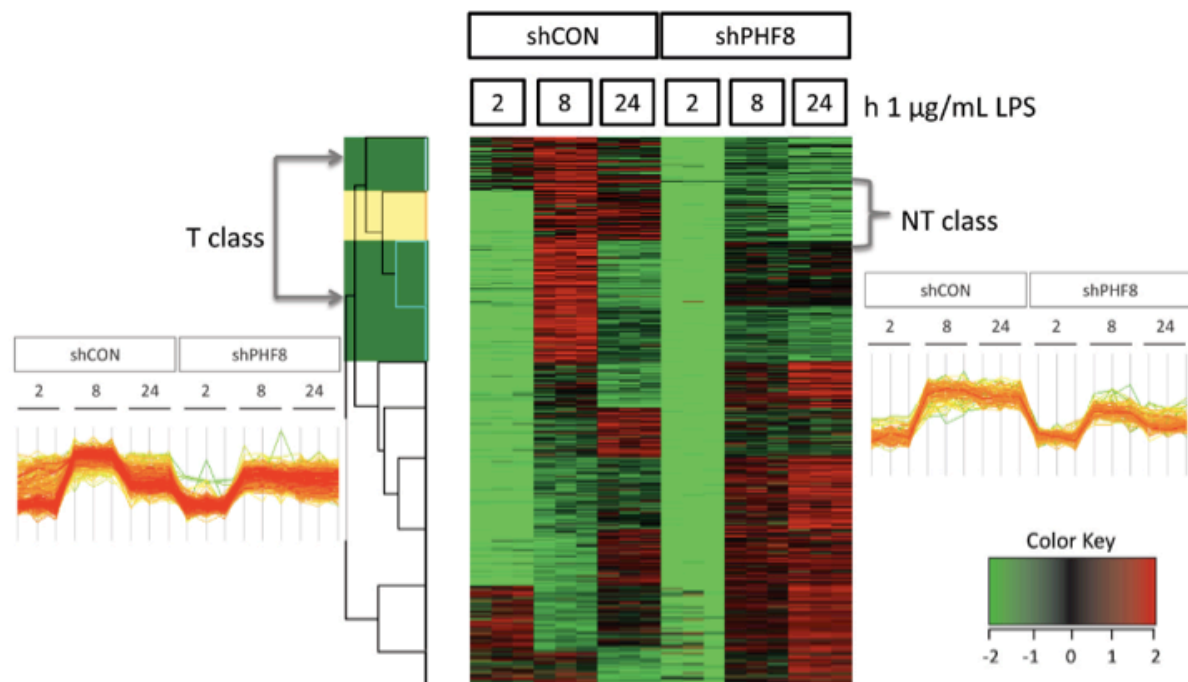


Figure 56 The LFQ secretome heatmap

The LFQ secretome heatmap of the differentially secreted proteins from paired WT (shCON) and PHF8-KD (shPHF8) RAW 264.7 macrophages under different inflammatory conditions. The color key (right bottom) indicates LPS-induced changes (increase in red, decrease in green) in secretion of proteins in logarithmic scale. Time points are indicated for the non-stimulated (0 h) and stimulated cells (8 and 24 h). Two PHF8-dependent classes of proteins are highlighted with green and yellow demonstrating T class (Left), and NT class (Right) PHF8-dependent secretome, respectively, on the cluster column (Erdoğan et al, 2016).

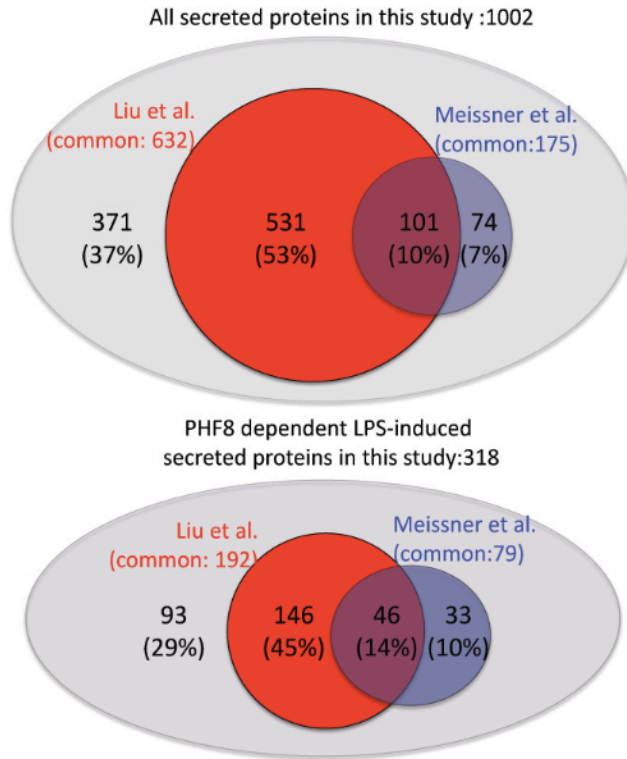


Figure 57 Comparison of the secretome to previous studies

Top panel shows the comparison of all secreted proteins while the bottom panel shows the comparison of LPS-induced secreted proteins. The present study of the secretome is represented by a light grey circle while the Liu et al.(Liu et al, 2014) and Meissner et al.(Meissner et al, 2013) secretome are represented by red and blue circles, respectively (Erdoğan et al, 2016).

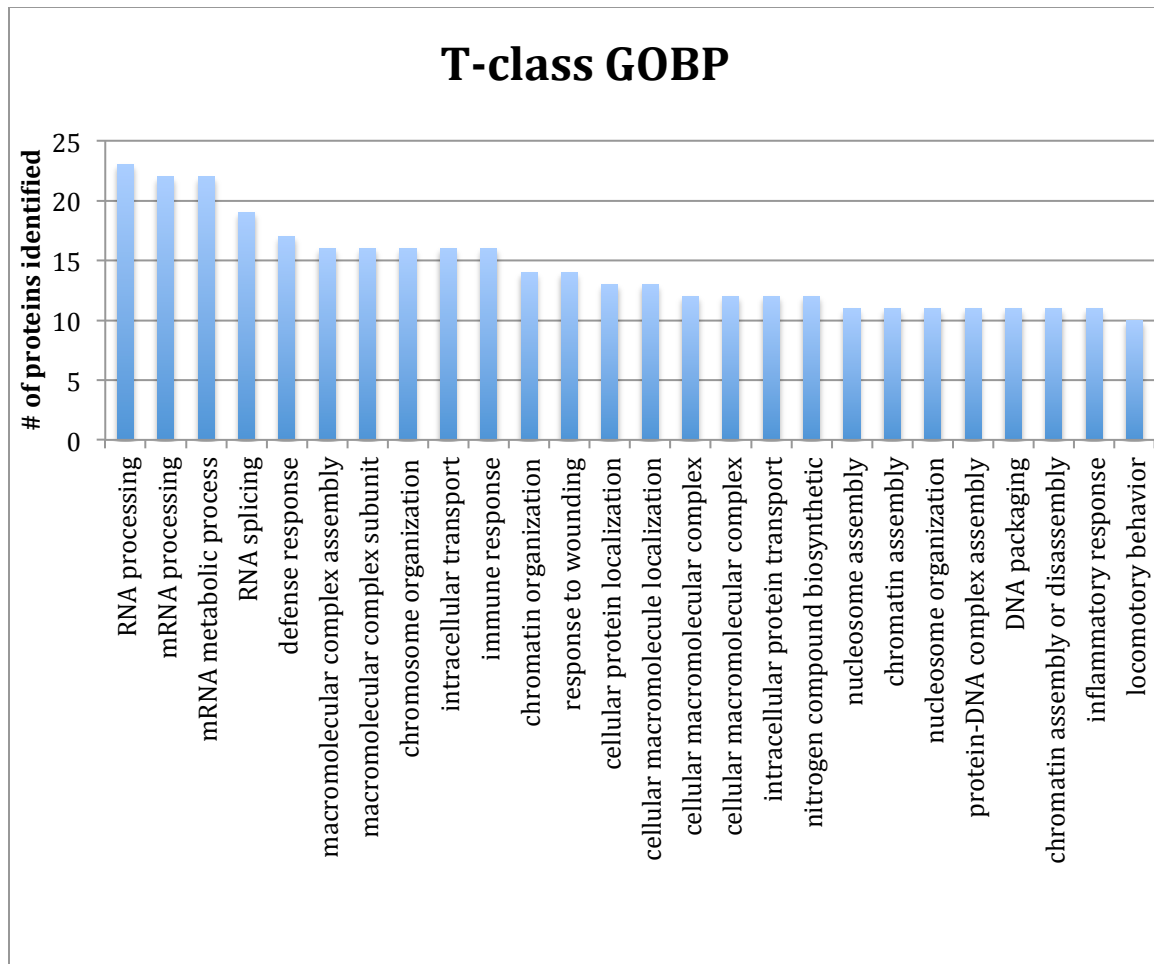


Figure 58 T-class GOBP (Erdoğan et al, 2016).

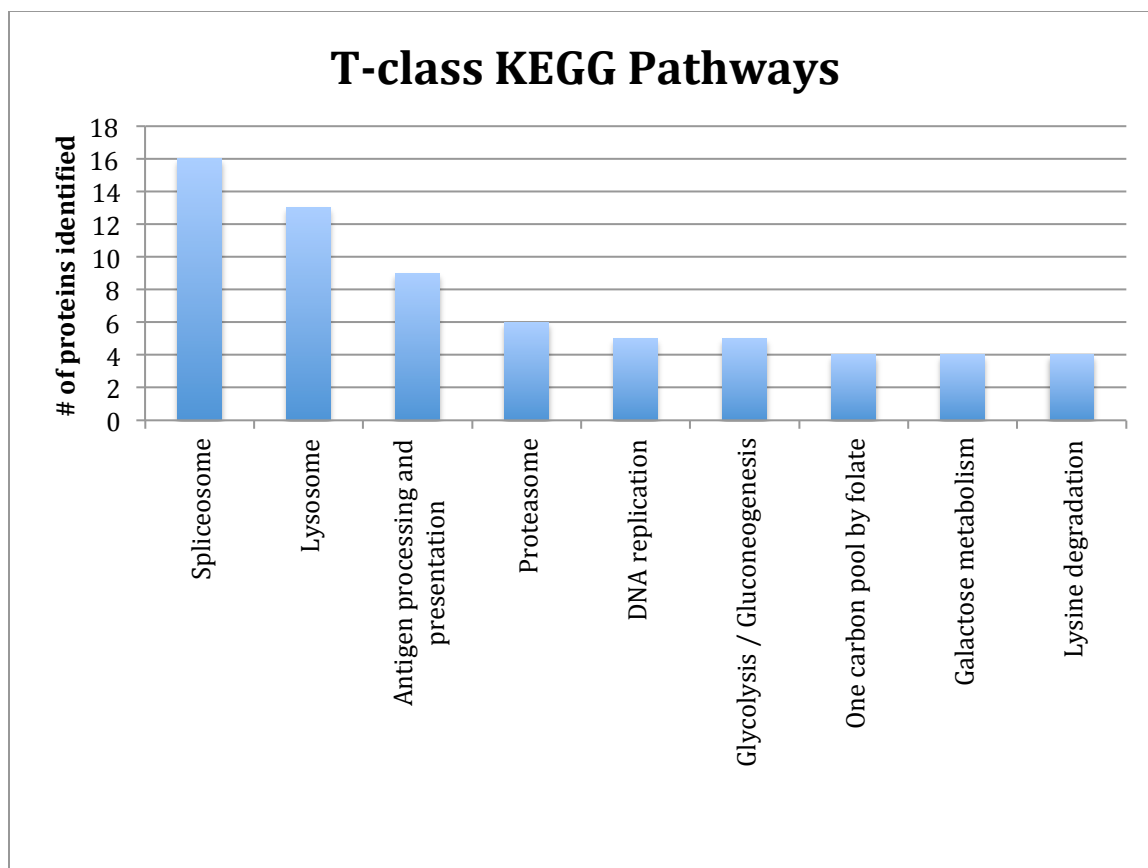


Figure 59 T-class PHF8-dependent KEGG pathways (Erdoğan et al, 2016).

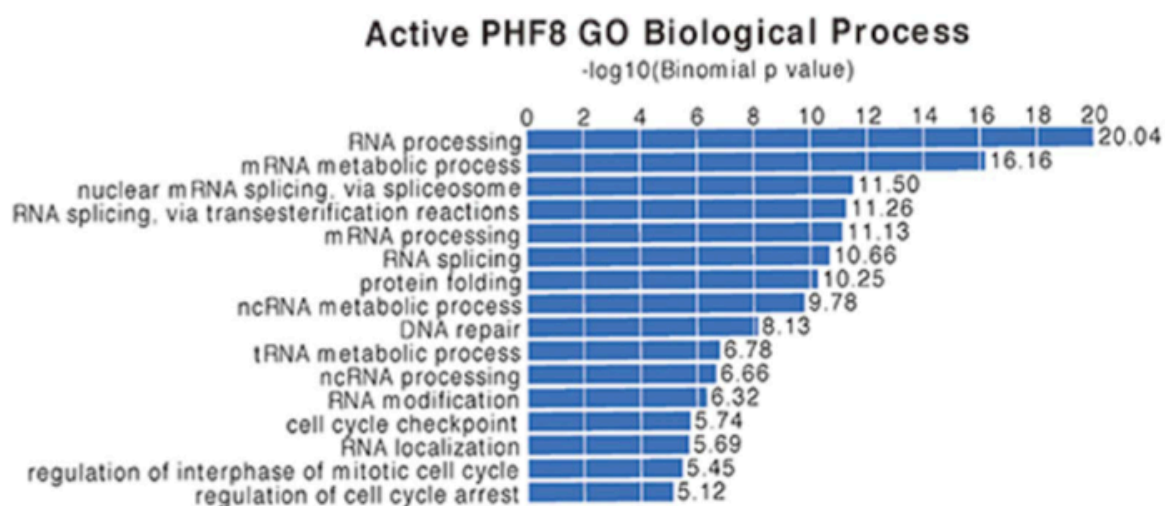


Figure 60 Processes associated with activated PHF8.
DAVID analysis identified biological processes associated with activated PHF8 peaks (Wang et al, 2014a).

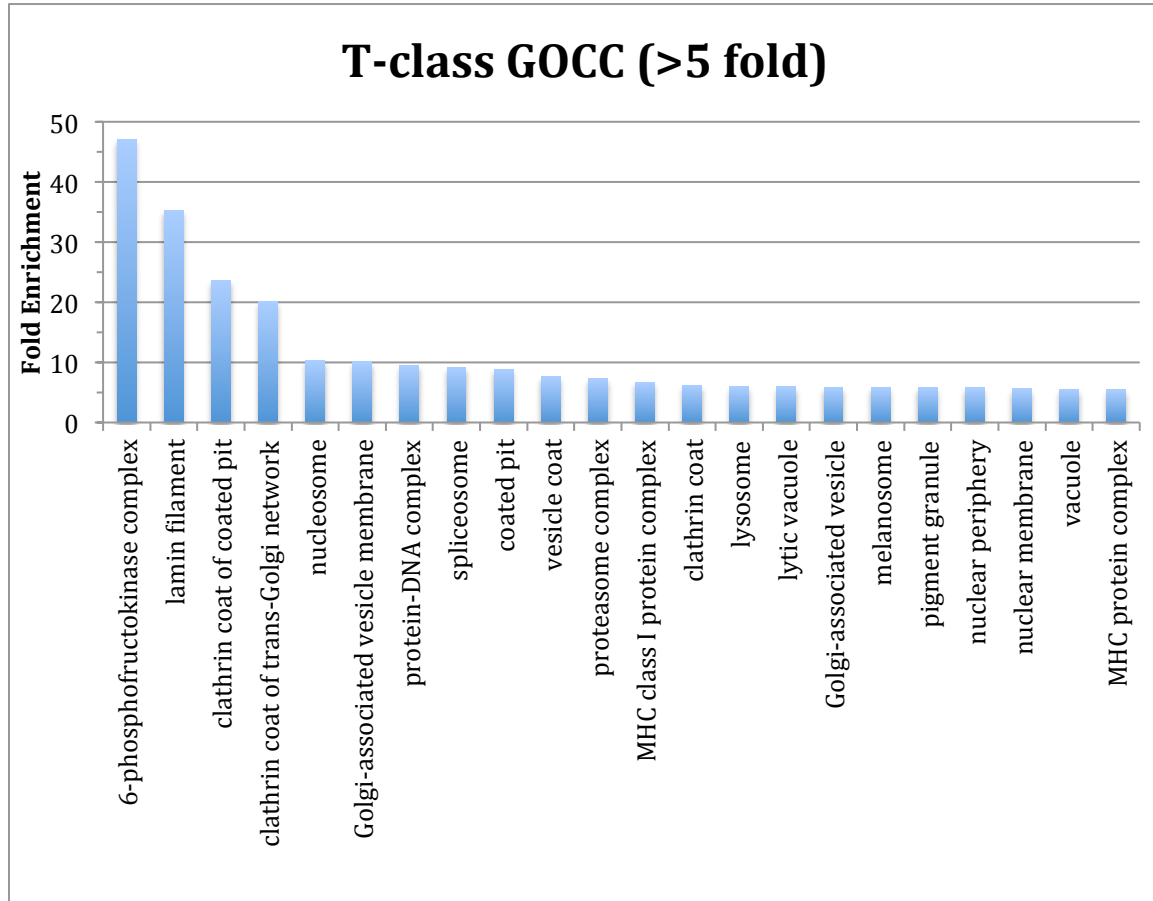


Figure 61 T-class GOCC (Erdoğan et al, 2016).

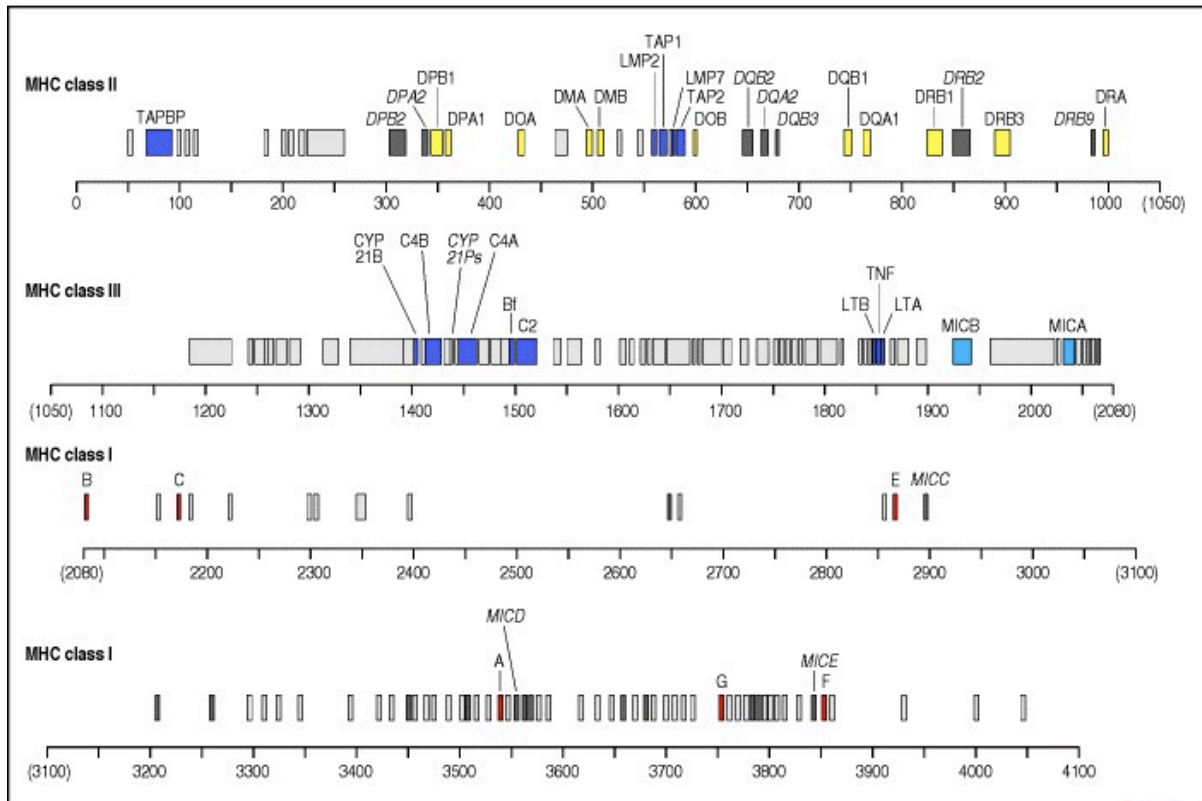


Figure 62 Detailed map of the human MHC

The organization of the class I, class II, and class III regions of the human MHC are shown, with approximate genetic distances given in thousands of base pairs (kb). The genes shown in the class III region encode the complement proteins C4 (two genes, shown as C4A and C4B), C2 and factor B (shown as Bf) as well as genes that encode the cytokines tumor necrosis factor- α (TNF) and lymphotoxin (LTA, LTB). The genes are colour coded, with the MHC class I genes being shown in red, except for the MIC genes, which are shown in blue; these are distinct from the other class I-like genes and are under different transcriptional control. The MHC class II genes are shown in yellow. Genes in the MHC region which have immune functions but are not related to the MHC class I and class II genes are shown in purple.

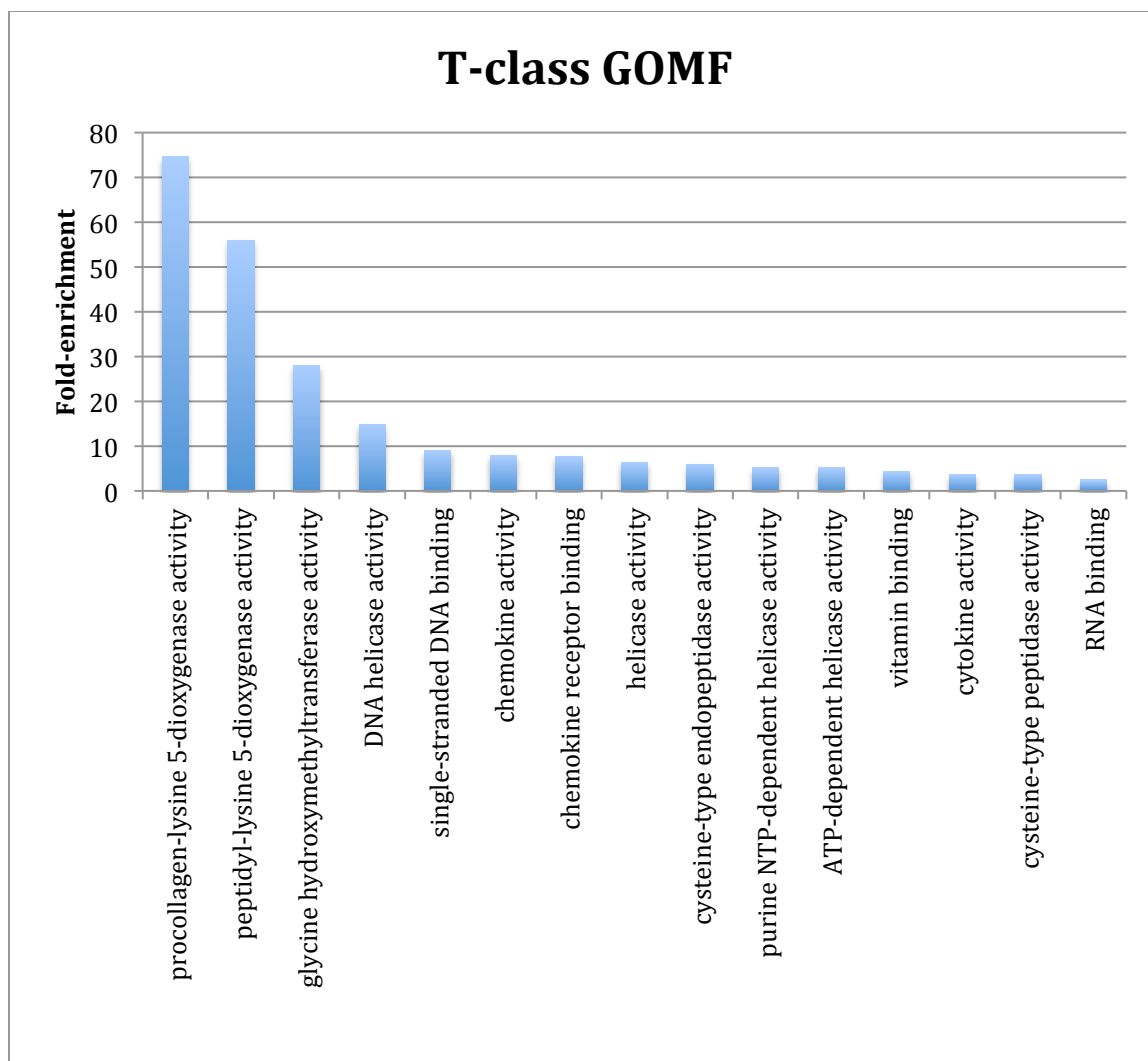


Figure 63 T-class GOMF (Erdoğan et al, 2016).

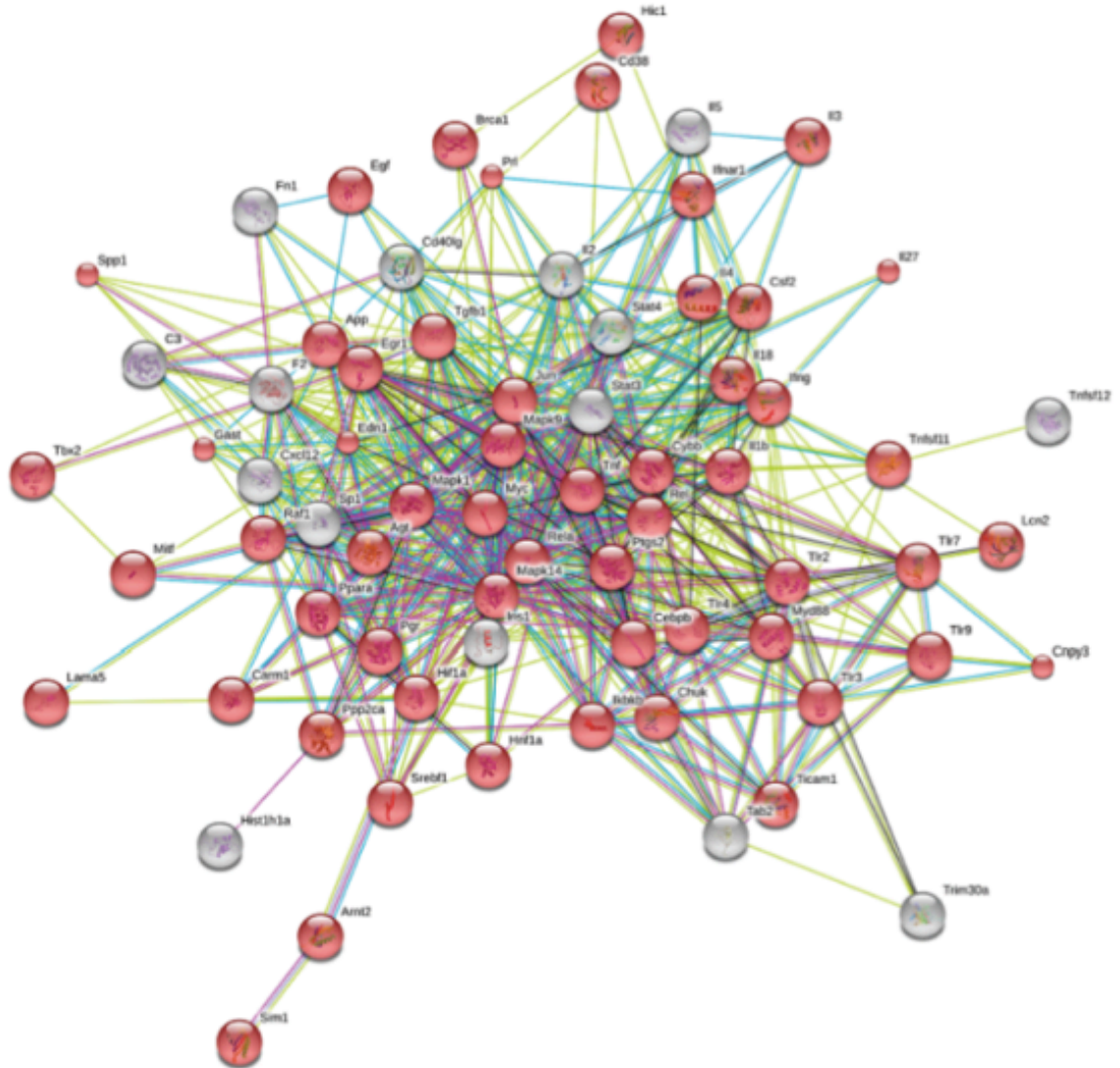


Figure 64 The overall protein-protein interaction network of the T-class secretome PPI covers proteins that belong to the highly enriched GOBP/GOCC/GOMF is composed mostly of response signaling BP (red nodes) (Erdoğan et al, 2016).

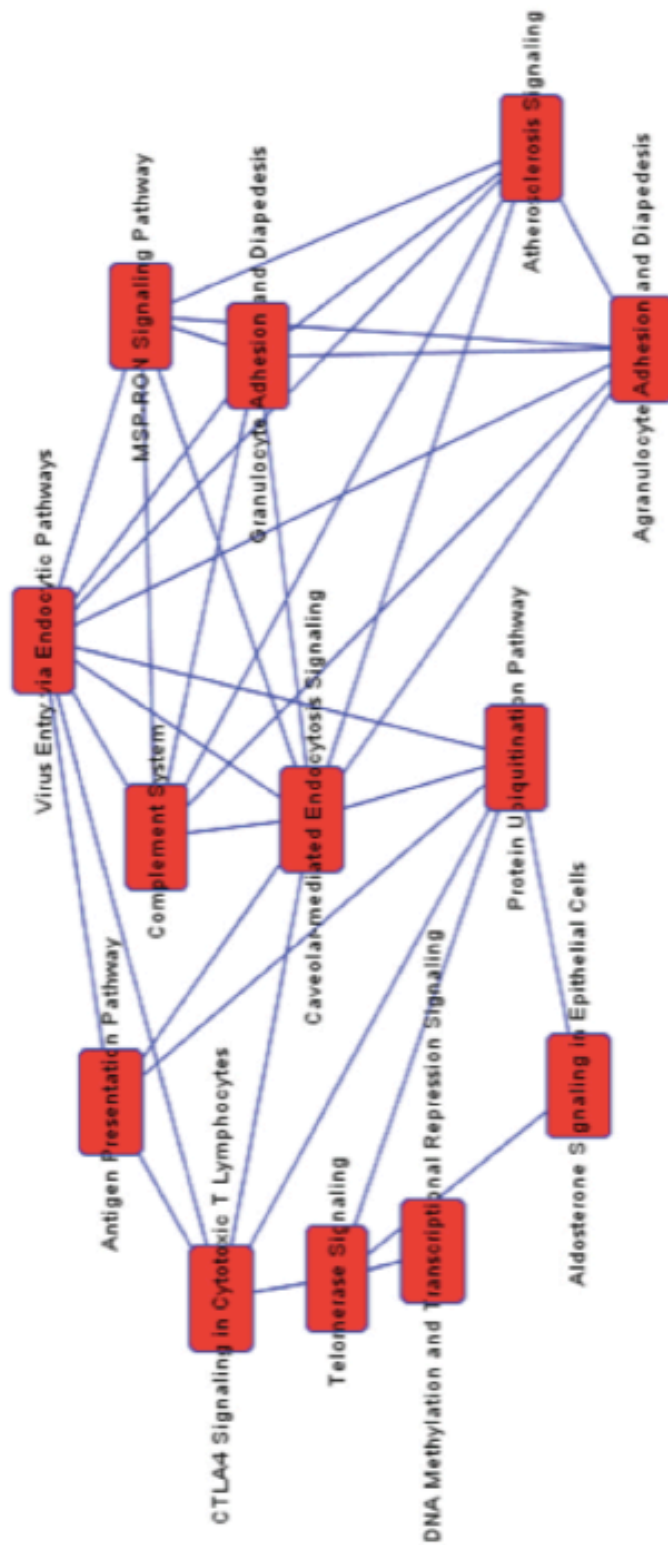


Figure 65 IPA network analysis of T-class secretome
 IPA reveals the interplaying pathways regulated by T-class PHF8-dependent secretome in cross-talk with high confidence ($p < 0.05$) (Erdoğan et al, 2016).

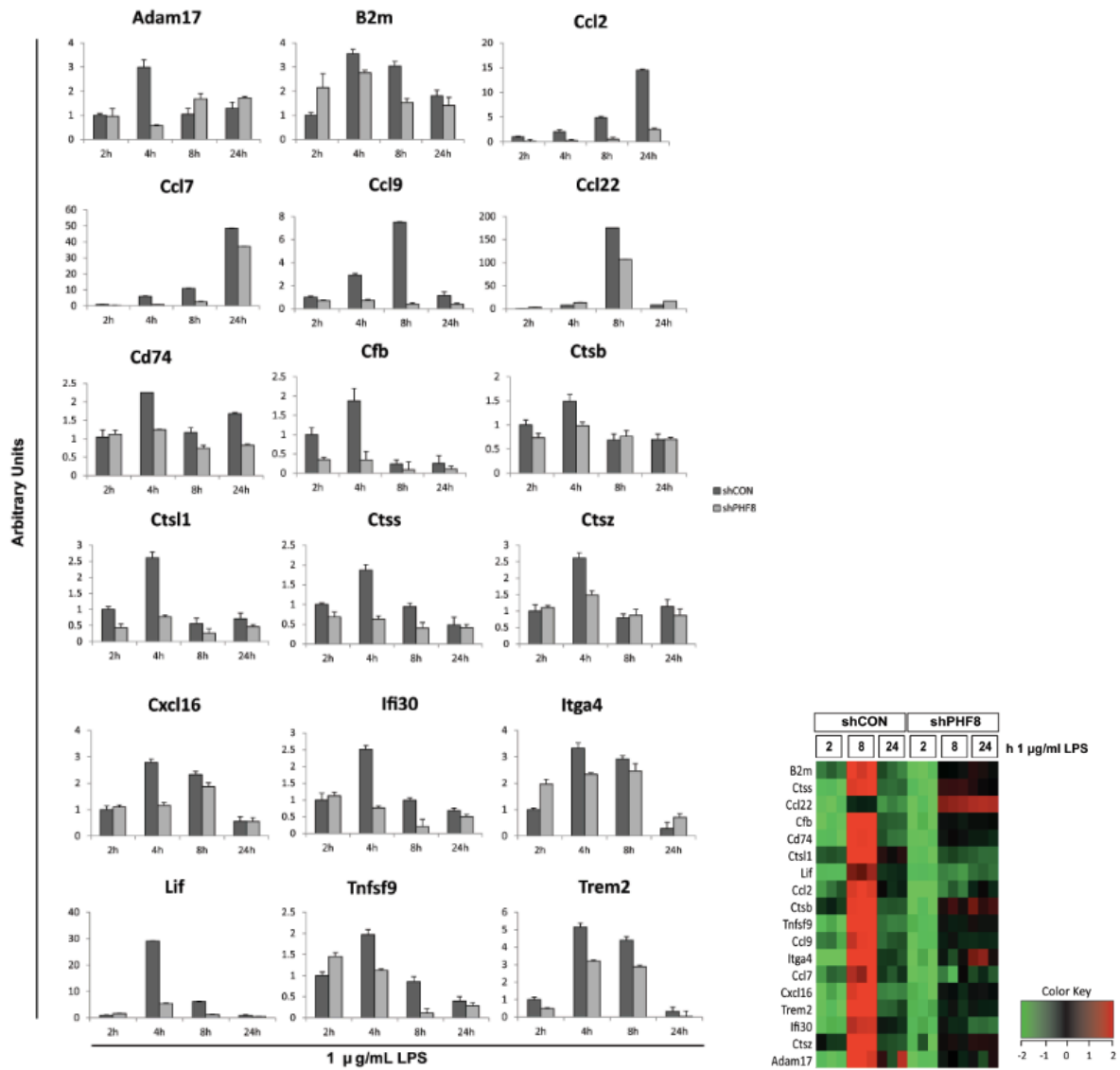


Figure 66 PHF8 regulates the mRNA expression of T cell activating proteins
mRNA expression of the selected genes that are related to antigen processing and presentation, and T cell activation in paired WT (shCON) and PHF8-KD (shPHF8) RAW cells. The heatmap showing the quantitative secretion pattern of these proteins found in the LFQ secretome analysis is given on the right (Erdoğan et al, 2016).

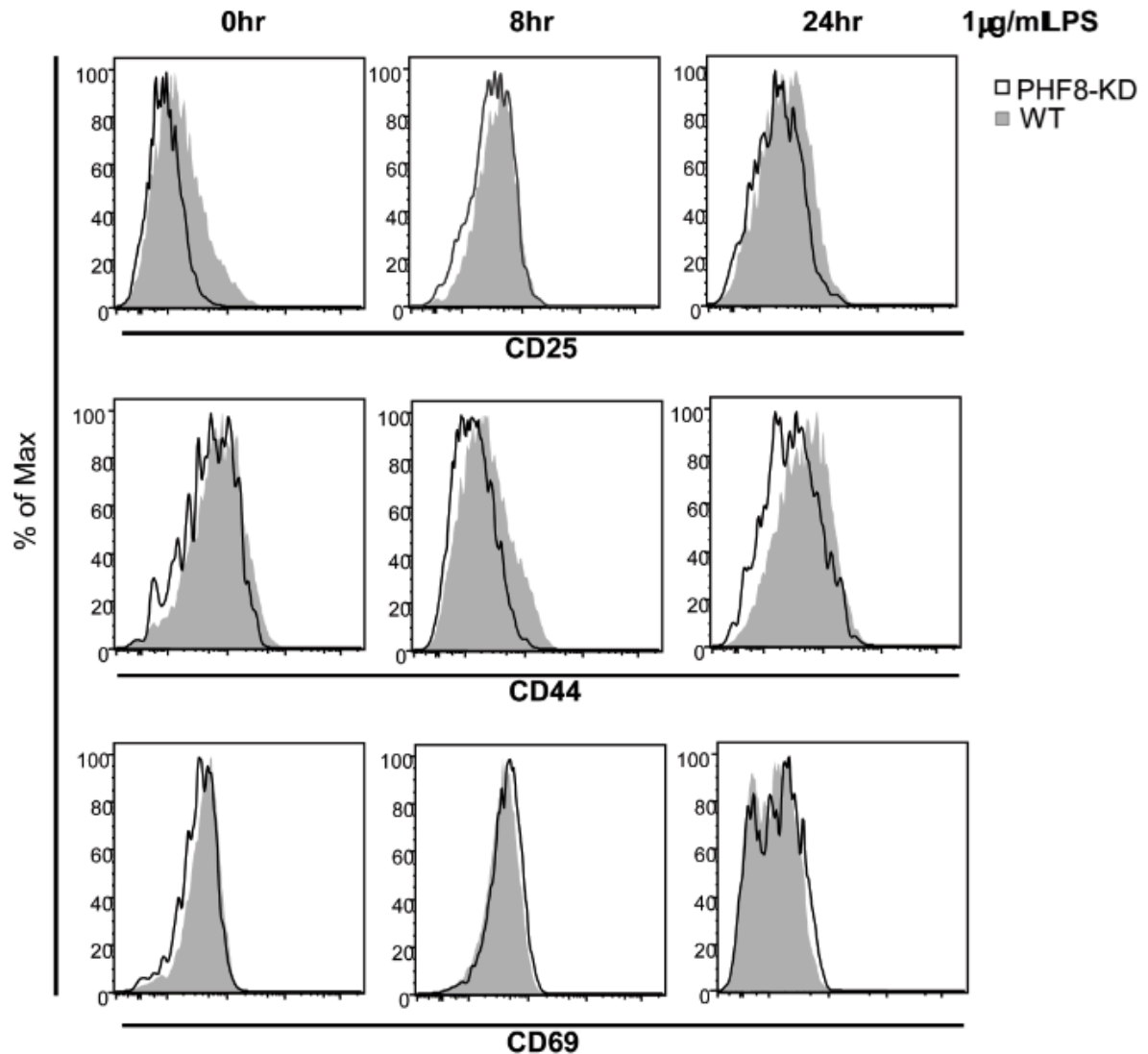


Figure 67 T cell activation markers

The histograms obtained from the T-cell activation assays demonstrates the PHF8 dependence of T-cell activation. CD8⁺ T cells isolated from P14 transgenic mouse were co-cultured with either WT (grey histograms) or PHF8-KD (histograms in black line) RAW cells that were LPS stimulated with 1 µg/ml LPS for 0, 8, and 24 h respectively. The population distributions of multiple surface markers of T cell activation CD25, CD44, and CD69 were analyzed by flow cytometry (Erdoğan et al, 2016).

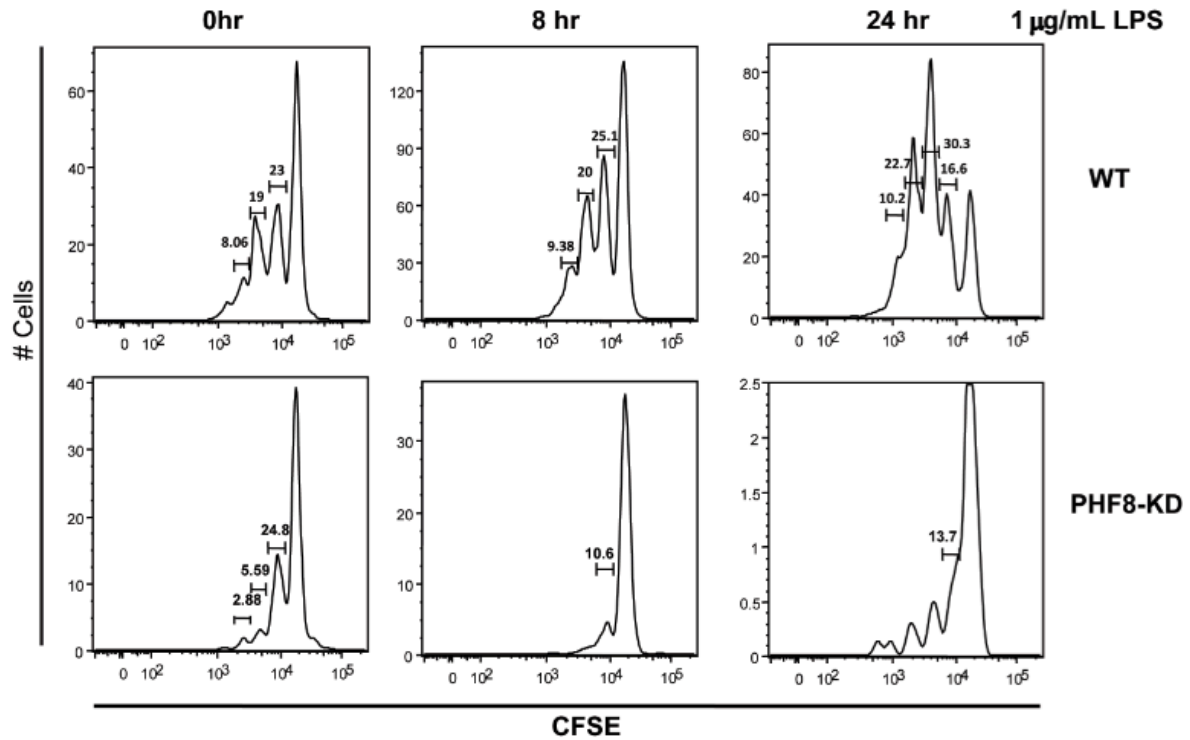


Figure 68 T cell proliferation assay

The flow cytometric assay demonstrates the PHF8 dependence of T-cell proliferation. CD8⁺ T cells isolated from P14 transgenic mouse were labeled with CFSE, then co-cultured with either WT (top) or PHF8-KD (bottom) RAW cells that were LPS stimulated with 1 μ g/ml LPS for 0, 8, and 24 h respectively. The numbers on the proliferation tables show the percentage of every division of proliferated cells among total CD8⁺ T cells (Erdoğan et al, 2016).

CHAPTER 5: PHF8 AND G9A WORK ANTAGONISTICALLY TO REGULATE THE SECRETION OF 'TOLERIZABLE' PROTEINS IN A PHENOTYPE-DEPENDENT MANNER

OVERVIEW

The inflammation response is a tightly regulated process, whose phenotype is determined by the gene-specific transcriptional regulation. G9a is known as one of the essential epigenetic modulators of transcriptional suppression in ET through methylation of H3K9 (Liu et al, 2014). Here, as oppose to G9a, we identified PHF8 as the positive regulator of acute inflammation removing the methyl mark on the H3K9me1/2, the same site that G9a methylates. Our comparison analysis of two separate secretome studies revealed that PHF8 and G9a antagonistically regulate the transcription and translation of the same set of inflammatory genes. Our results shed light on the phenotypic regulation of bacterial inflammation response downstream NFκB pathway. Mechanistically, we found that inflammatory phenotype is determined by the chromatin plasticity (active PHF8 versus active G9a) through a transient switch turned off by PP2Ac inhibiting PHF8 and activating G9a for successful immunosuppression in ET. In summary, PHF8, the eraser of H3K9me1/2, is *the primary driver* for establishing the transcriptionally active state of the gene-specific chromatin in acutely inflamed cells as oppose to enrichment of silent chromatin with H3K9me1/2 by G9a, the writer of H3K9me1/2.

INTRODUCTION

Regulation of K9me-mediated Macrophage Inflammation Response

As the first histone PTM site regulating the phenotypic inflammation response, H3K9 plays a central role in the epigenetic regulation through methylation or acetylation. H3K9 methylation achieves successive repression of pro-inflammatory genes by (1) influencing DNA methylation, (2) formation of heterochromatin, (3) prohibiting the activating H3K9 acetylation, (4) actively recruiting transcriptional repressors of the HP1 family, and (5) preventing the recruitment of RNA-Pol II (Mehta & Jeffrey, 2015). Hypermethylation of H3K9 has been observed in the regulation of inflammatory processes, such as TNF α silencing in ET in THP1 monocytes (El Gazzar et al, 2008), transcriptional state of some of the LPS-induced promoters in human dendritic cells (Saccani & Natoli, 2002), IL-1 β promoter in the severe systemic inflammation (Chen et al, 2009), and IFN β -inducible antiviral genes (Fang et al, 2012). The methylation state of H3K9 is dynamically regulated by specific KMTs, including G9a, and KDMs, including PHF8 (**Figure 69**). On the other hand, H3K9 acetylation has been reported in the regulation of inflammation response. H3K9 acetylation by HATs causes inhibition of HDAC activity as well as activation of transcription of pro-inflammatory genes IL1, IL2, IL8, and IL12 (Villagra et al, 2010; Yang et al, 2009). In addition, acetylation of H3K9 along with phosphorylation of H3S10 is involved in the positive regulation of pro-inflammatory signaling (Saccani & Natoli, 2002) and contributes to the recruitment of RNA-Pol II through decreased H3K9 methylation (Sánchez-Pernaute et al, 2008). Moreover, this phosphoacetylation induces acetylation of H3K14, which in

turn enhances NFκB binding to promoters of pro-inflammatory cytokines (Barnes, 2009; Yamamoto et al, 2003). In ET, this pro-inflammatory effect is reversed for successful suppression of NFκB target genes via increased HDAC activity (Ashburner et al, 2001; Aung et al, 2006; Hamon & Cossart, 2008; Zhong et al, 2002). During immunosuppression, HDACs are recruited by corepressor complexes or transcription factors such as NFκB, STATs, and Forkhead box P3 (FOXP3) (Villagra et al, 2010). These observations suggest that dynamic changes of the H3K9 PTMs constitute the core of the epigenetic regulator of inflammation phenotype.

G9a Histone Methyltransferase

G9a is a major me1 and me2 KMT of euchromatin (Tachibana et al, 2002). G9a methylates H1, H3K9 and H3K27 *in vitro* and *in vivo* (Tachibana et al, 2001; Tachibana et al, 2005; Trojer et al, 2009; Weiss et al, 2010; Wu et al, 2011). G9a is a member of the Suv39h1 subgroup of SET domain containing proteins (Shinkai & Tachibana, 2011) as it contains an evolutionary conserved SET domain involved in methyltransferase activity and an ankyrin repeat domain for protein-protein interactions (**Figure 70**) (Shankar et al, 2013). The SET domain is involved in the transfer of methyl groups from SAM to ε amino group of target lysine. The commercially available inhibitors such of G9a act by binding to the substrate-binding pocket to make it inaccessible (Chang et al, 2010; Vedadi et al, 2011).

G9a recognizes a 7-aminoacid peptide with RK/ARK consensus sequence, such as the amino acid residues 6-TARKSTG-12 of H3 (Chin et al, 2007; Chin et al, 2005; Rathert et al, 2008). Within the consensus sequence, arginine residue adjacent to the target lysine is the requirement for G9a activity. Moreover, G9a prefers a hydrophilic

residue at positions 1 and 5, a small amino acid like Alanine at position 2, and a hydrophobic residue at position 6 of the target peptide (Rathert et al, 2008). In addition, phosphorylation of S10 and T11 on H3 impairs the methylation activity of G9a. The substrate specificity of G9a makes it a demethylase for not only histones but also various non-histone proteins such as p53, CEBP, and Myoblast determination protein (MyoD) (Shinkai & Tachibana, 2011). Methylation by G9a negatively affects the transcription activity of these transcription factors. On the other hand, G9a may act as a transcriptional activator, independently of its methyltransferase activity, based on its interacting partners (**Figure 71**) Moreover, G9a acts as both activator and suppressor of transcriptional activity of Hypoxia-inducible factor 1-alpha (HIF1- α) through alternative methylation of either histone targets or non-histone targets (**Figure 72**) (Casciello et al, 2015).

In addition to having the role to regulate transcription through H3K9 methylation, G9a is specifically involved in gene-specific regulation of various other biological processes such as mouse development (Tachibana et al, 2002; Tachibana et al, 2005), neuronal function (Kramer et al, 2011; Schaefer et al, 2009), ATRA response (Son et al, 2012), rRNA transcription, autophagy (Artal-Martinez de Narvajás et al, 2013), cell migration (Chen et al, 2010; Dong et al, 2012), and cell growth in cancer invasion (Chen et al, 2010; Kondo et al, 2008); thus, it may be a potential target for associated diseases (Casciello et al, 2015; Kelly et al, 2010; Shankar et al, 2013; Suzuki et al, 2014). More importantly, G9a regulates immune responses (Thomas et al, 2008), (Yuan et al, 2007), T-cell development (Lehnertz et al, 2003), and proviral silencing

(Dong et al, 2008; Leung et al, 2011), indicating its significance in the gene-specific regulation of immunity.

G9a in regulation of immunity

G9a activity is a major contributor of the ET due to silencing of the promoters of “T-class” genes (El Gazzar et al, 2008). During ET, G9a is involved in the recruitment of HP1 to RelB for suppression of NFκB target genes (Chan et al, 2005; Chen et al, 2009; El Gazzar et al, 2007). In addition, G9a-HP1 complex subsequently recruits DNMT3 to those target promoters for CpG methylation of the “T-class” genes in ET (El Gazzar et al, 2008). Recently G9a was also discovered as a regulator of major co-repressor complexes in ET of macrophages, indicating its importance in the gene-specific epigenetic control of the ET response (Liu et al, 2014). In addition to TNF target genes, the transcription of interleukin and interferon-inducible genes are regulated by G9a activity (Chen et al, 2009; Fang et al, 2012; Gyory et al, 2004). The role of G9a in regulation of inflammation response is not restricted to innate immunity, adaptive immunity is also regulated by G9a through regulation of lymphocyte development and activation (Thomas et al, 2008), gene expression during CD4⁺ T helper (Th) cell differentiation and function (Lehnertz et al, 2010), and lymphocyte migration (Zhang et al, 2015).

As they share a common methylation/demethylation target, PHF8 and G9a may regulate the same set of genes in an opposite manner. In this system, PHF8 acts as an activator of transcription through demethylation of repressive H3K9me1/2 while G9a acts as a suppressor through methylation of H3K9. As PHF8 is a positive regulator of the LPS-induced gene expression, here we explored whether the H3K9 KMT G9a works

antagonistically to PHF8 to negatively regulate innate immune response. To assess functional relevant targets, we compared G9a-dependent and PHF8-dependent macrophage secretome products in ET and in acute inflammation, respectively. Our comparison analysis revealed that a big portion of inflammatory genes with phenotype-specific secretion pattern was epigenetically regulated by the differential activities of PHF8 and G9a in LPS-induced macrophages.

MATERIALS AND METHODS

Bioinformatic Analysis

Mass spectra were analyzed using MaxQuant software **version 1.5.0.30** using the Andromeda search engine against the mouse Uniprot sequence database including 248 common contaminants and reversed versions of all sequences (Cox & Mann, 2008; Cox et al, 2011). Maximum allowed mass error was set to 4.5 ppm for monoisotopic precursor ions and 0.5 Da for MS/MS peaks. Enzyme specificity was set to trypsin and a maximum of two missed cleavages were allowed. We set carbamidomethylcysteine as a fixed modification, and N-terminal acetylation and methionine oxidation as variable modifications. For identification of proteins, we kept requirements of at least one unique or razor peptide per protein group. LFQ was performed in MaxQuant using the built in XIC-based fast LFQ algorithm (Luber et al, 2010). We set the required false positive rate as 5% at the peptide and 1% at the protein level, and the minimum required peptide length as 7 amino acids. Contaminants, reverse identification and proteins only identified by site were excluded from further data analysis.

For each LPS treated sample of a given phenotype and time point, ratios were calculated from the individual protein LFQ intensities and the corresponding median LFQ intensities of the untreated sample. Missing values were imputed only for untreated samples by random sampling from a generated narrow normal distribution around the detection limit for proteins. The calculated ratios were log2 normalized. In order to retrieve those proteins with a statistically different quantitative ratio among different LPS stimulation length we used multiple samples statistic analysis via ANOVA with a permutation-based FDR controlled filter. The p-value cut-off was calculated at 5% FDR. This multiple samples test technique does not capture proteins with no dynamic (i.e. stable over time) since they are of no interest. Further, to understand the role of antagonistic PHF8-G9a-dependent gene regulation of LPS-induced inflammation and interacting signaling pathways, we comprehensively analyzed the functional categories of the components that show both increased secretion in G9a-inhibitor treated BMDM cells after prolonged LPS stimulation and decreased secretion in PHF8-KD cells after acute LPS stimulation using David bioinformatics database in the context of GOBP, GOCC, and GOMF (Huang et al, 2009). In addition, using STRING database, we analyzed the constituents of the common secretome to visualize the antagonistically regulated pathways of inflammatory response (Snel et al, 2000). Further, we validated these results with the Upstream Regulator Analysis (URA) in IPA.

RESULTS

PHF8 and G9a regulate a subset of inflammatory protein secretion in LPS-induced macrophages in a phenotype-dependent manner

PHF8 is a G9a antagonist that regulates gene-specific chromatin states in acute inflammation as G9a is the writer of H3K9me1/2 in chronically inflamed macrophages while PHF8 is the H3K9me1/2 eraser in acutely inflamed cells. To understand differential regulation of inflammatory response by G9a in ET versus PHF8 in acute inflammation, we compared the ET-specific G9a-dependent secretome (Liu et al, 2014) with that of PHF8 during acute inflammation^[1]. For this comparison we performed the MaxQuant database search with both sets of RAW data for accurate and precise normalization of the LFQ. Moreover, to understand LPS-induced phenotype-specific secretome that are antagonistically regulated by the activities of PHF8 and G9a, in acute inflammation and ET, respectively, we trimmed the dataset to proteins showing increased secretion pattern in G9a-inhibitor UNC0638 treated BMDM cells compared to that of WT after prolonged LPS stimulation and decreased secretion pattern in PHF8-KD cells compared to that of WT after acute LPS stimulation, i.e. identical proteins, which were secreted in an opposite manner. This filtering gave us 373 proteins whose secretion was antagonistically regulated by PHF8 or G9a in a phenotype-dependent manner and we refer to this set of proteins as '*PHF8-G9a common secretome*' throughout this report (**Appendix 6**).

PHF8 is a G9a-antagonist that regulates the inflammatory phenotype in acute inflammation

To understand the role of antagonistic PHF8-G9a-dependent gene regulation of LPS-induced inflammation and interacting signaling pathways, we comprehensively analyzed the functional categories of the PHF8-G9a common secretome using David Bioinformatics database for GOBP, GOMF, and GOCC enrichment. With this analysis, we identified 41, 33, 25, 21, 17, 14, and 11 secreted proteins, respectively, belonging to translation, immune response, defense response, response to wounding, inflammatory response, cell proliferation, and chemotaxis GOBPs (**Figure 73**). Moreover, the wound response proteins were in common with inflammatory response GOBP. Some of these proteins function in cell proliferation and macrophage cell fate decision. Further, secretion of many proteins associated with cell adhesion, cell migration, and movement-associated cytoskeleton was regulated antagonistically by the inflammatory-phenotypic PHF8 versus G9a activity.

In agreement with the GOBP analysis, GOMF enrichment revealed 31, 17, 16, and 7 proteins involved in RNA binding, structural constituents of ribosome, cytokine activity, and chemokine activity, respectively (**Figure 74**). More importantly, the identification of secretion of many cytokines, chemokines, complement factors, CD14, and CD74 antigens in PHF8-G9a common secretome indicates PHF8 and G9a are major regulators of inflammatory-state specific proteins/markers in macrophages. Specifically, immune signaling molecules, select cytokines/chemokines, and antigen processing/presentation factors that were identified as major components of the T-class PHF8-dependent

secretome were identified in the PHF8-G9a common secretome, indicating that PHF8 is a G9a-antagonist in acute inflammation.

GOCC enrichment revealed proteins involved in translational initiation, and ribosome (**Figure 74**); this observation coincided with the fact that the H3K9me1/2 eraser PHF8 acts as a transcriptional/translational activator to regulate ribosomal RNA transcription (Feng et al, 2010). In addition inflammatory-phenotypic compartments such as the lysosome, Golgi-associated vesicles, and MHC complexes were identified in the GOCC enrichment (**Figure 75**); more importantly, all the PHF8-dependent MHC complex components were commonly identified in the G9a-suppressed secretome.

PHF8 and G9a are antagonistic regulators of translation, immune response, and cell adhesion/communication

To uncover the pathways antagonistically regulated by acutely active PHF8 versus chronically active G9a, we performed STRING PPI analysis on the dataset of the PHF8-G9a common secretome. This analysis revealed multiple, interconnected sub-networks linking the signaling of immune response, translational regulation, cell adhesion/communication, nucleotide binding, and lysosome/proteasome (**Figure 76**). Further, IPA canonical pathway analysis revealed cell growth, cell movement, cell death, and cell-cell interaction as macrophage response-dependent pathways regulated by G9a and PHF8 antagonistically (**Figure 77**). Moreover, we identified interconnected pathways of the PHF8-G9a common secretome, including antigen presentation, the communication between innate and adaptive immune cells, IL-8 signaling, differential regulation of cytokine production, adhesion, mTOR, and Eukaryotic initiation factor 2

(EIF2) signaling indicating that PHF8 and G9a regulate immune response antagonistically through affecting the interplay between these pathways (**Figure 78**).

Finally, URA in IPA validated the regulation of inflammatory pathways functioning in inflammatory response, cell movement, chemotaxis, homing of leukocytes, migration of leukocytes, migration of phagocytes, and recruitment of neutrophils through analysis of the secretion pattern of common PHF8-G9a secretome and their previously characterized upstream regulators (**Figure 79**). Moreover, the URA demonstrated that these outcomes are explained by the TLR-dependent signaling, supporting the specificity of the secretome analysis.

These results indicated that, in an opposing manner, G9a and PHF8 regulate the secretion of the same set of LPS-inducible proteins through modulating the methylation level of H3K9 in their associated chromatin.

DISCUSSION

This study is the first to provide the evidence for a novel function of PHF8 in chromatin-associated inflammation control and the subsequent activation of adaptive immunity. In agreement with the previous discovery of ET-specific G9a-dependent modulation of silent chromatin enriched with the transcriptionally repressive histone H3K9me2 code (Liu et al, 2014), we now further reveal that PHF8, the eraser of H3K9me1/2, is *the primary driver* for establishing the transcriptionally active state of the gene-specific chromatin in acutely inflamed cells. For the first time, our *post-translational level* data indicated that acutely active PHF8 promotes the LPS-induced secretion of proteins in common with the ones suppressed by G9a under the chronic

inflammatory condition, we conclude that PHF8 is the antagonist of G9a in regulating the gene-specific chromatin state under the acute inflammatory condition.

The chromatin plasticity that determines the phenotypic outcome by differential activities of PHF8 and G9a is shown in **Figure 80**. This plasticity mechanism regulating inflammatory phenotype-specific chromatin modifications in transcriptional regulation of select classes of genes involved the acute inflammation-specific activity of PHF8 and ET-specific activity of G9a. Our model shows that KDM activity of PHF8 is modulated through reversible phosphorylation by differentially activated kinases or protein phosphatase(s) under different inflammatory conditions. LPS-induced acute inflammation of macrophages leads to H3K9me1/2 demethylation by PHF8, which subsequently increases the secretion of T-class proteins. With prolonged LPS exposure, as in ET, PHF8 KDM activity is suppressed, likely by PP2Ac-mediated dephosphorylation. This leads to decrease in secretion of those T-class proteins. In addition, G9a activity is induced in the ET macrophages, contributing to the suppressed/silent state of the chromatin (Liu et al, 2014). Thus, through targeting similar sets of proteins involved in phenotype-specific inflammatory response, both PHF8 and G9a are the regulators of the LPS-induced chromatin modifications but function *in an opposing manner* under either an acute- or chronic-inflammatory condition. Our studies of the interchangeable chromatin regulators under different inflammatory conditions may mechanistically derive biomarkers of immunopathology associated with the extremes of deregulated inflammation.

FUTURE WORK

Understanding the biochemical dynamics of chromatin regulation in macrophage LPS response is essential in prevention and treatment of diseases of deregulated inflammation. To this end, even though some chromatin regulators of inflammation have been studied individually, a comprehensive study that screens the pool of multiple complexes of chromatin regulators is needed. To analyze chromatin on a broad proteomic scale Chromatin enrichment for proteomics (ChEP) technique has been developed recently (Kustatscher et al, 2014b). This technique is very advantageous to other previous methods, such as Tandem affinity purification (TAP)-MS, in screening the transient chromatin-bound components in the cell and changes in global chromatin composition. Moreover, it is quick, enables comparison of drug treatments, and quantitative analysis. ChEP was previously used to monitor chromatin plasticity in interphase (Kustatscher et al, 2014a); thus, it will be a great method to compare the chromatin components of (a) LPS-stimulated WT and PHF8-KD RAW cells or (b) WT cells treated with/without the G9a inhibitor UNC0638 in ET state, covering the transient changes in chromatin and chromatin plasticity. This will help us discover other complexes involved in PHF8-dependent inflammation response.

In addition to the global chromatin components, understanding specific gene promoters that are PHF8-bound in acute and G9a-bound in chronic inflammation will be essential in understanding the outcome of the chromatin plasticity in inflammation response. To analyze the genes that are differentially regulated by PHF8 and G9a in different inflammation states, we will perform ChIP-Seq analysis of PHF8-bound and G9a-bound DNA in different inflammation states. This analysis will help us discover

specific genes that contribute to inflammation response. In addition, it will also enable us validate and enhance the secretome analysis.

FIGURES

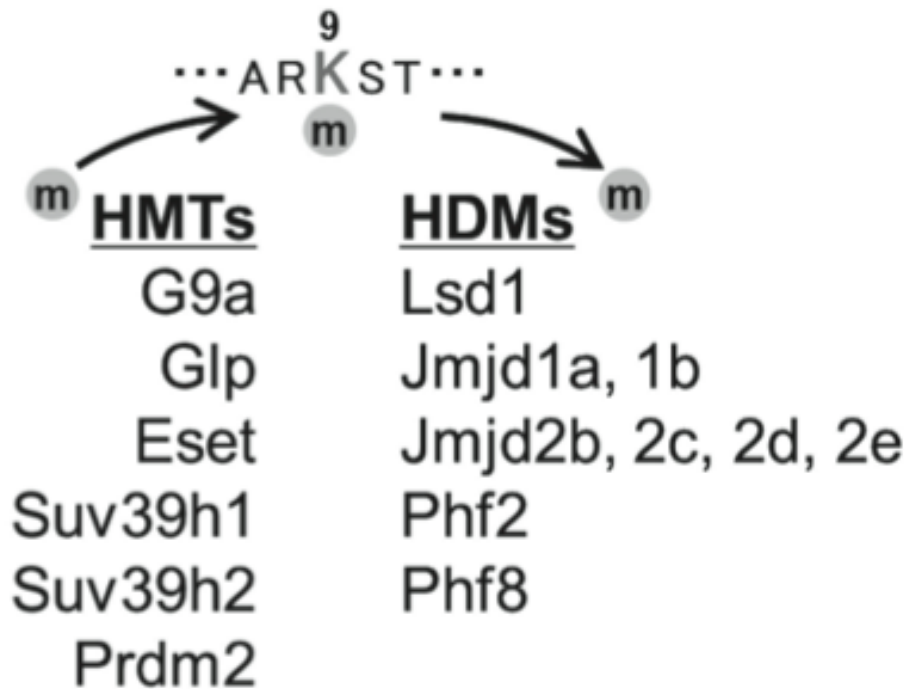


Figure 69 Histone H3K9 methyltransferases (HMTs) and demethylases (HDMs).
Adopted from ideno 2015

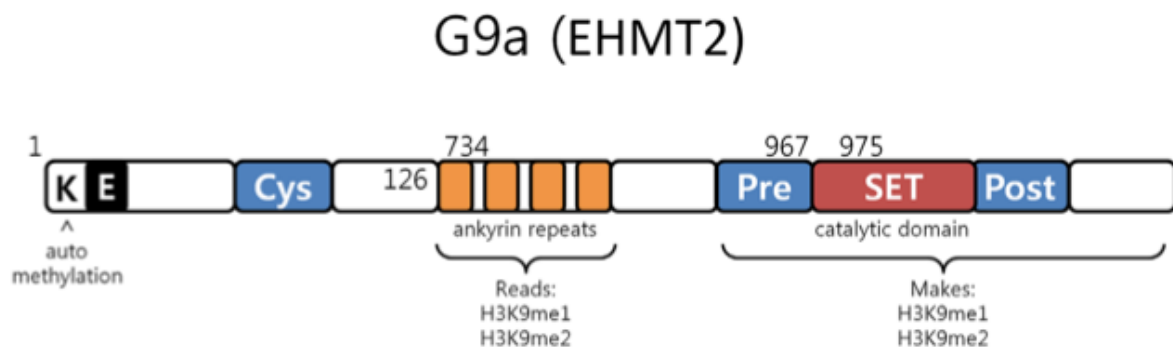


Figure 70 G9a structure.

G9a structural organization characterized by automethylation site at its N-terminal end, ankyrin repeats that recognize mono- and di-methylated H3K9, and a catalytic SET domain responsible for catalytic activity adopted from cascino et al 2015.

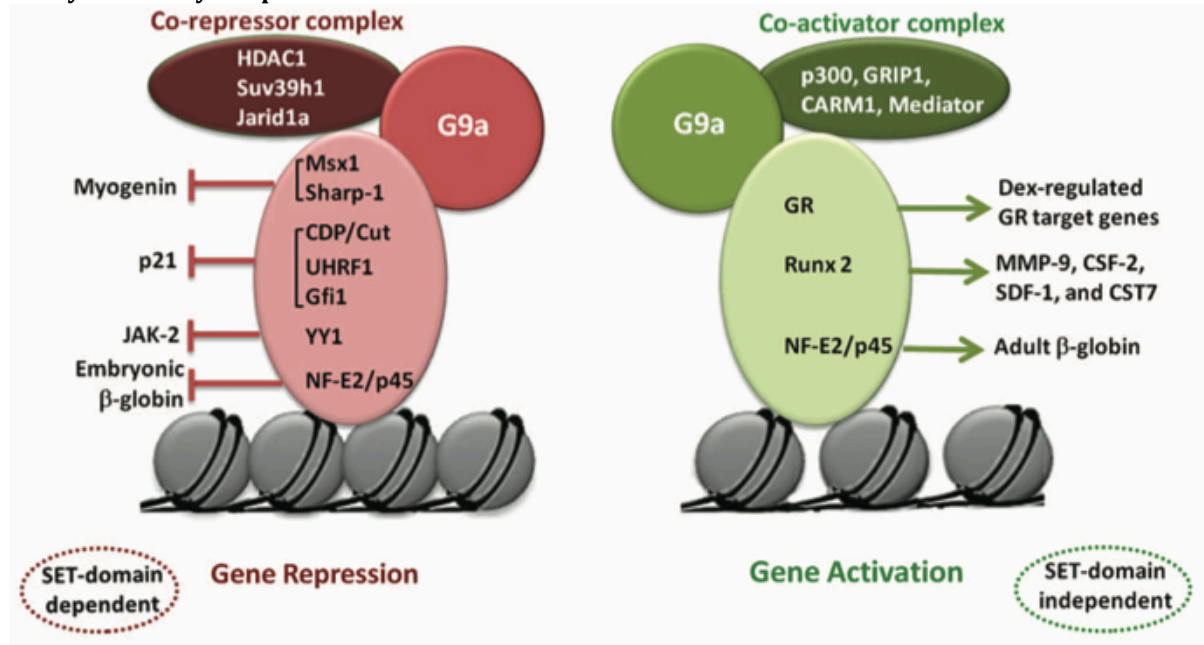


Figure 71 Transcriptional repression and activation by G9a. G9a recruitment by transcription factors and association with distinct co-factor complexes leads to opposing outcomes on gene expression. Transcriptional repression of genes such as myogenin, p21, JAK2 and embryonic β -globin is dependent on G9a methyltransferase activity (SeT domain). On the other hand, G9a recruitment by Gr, runx2 and NF-e2/p45 leads to activation of target genes in a SeT-domain independent manner. This occurs through association of G9a with co-activators such as p300 and CArM1, as well as the Mediator complex. Adopted from Shankar et al

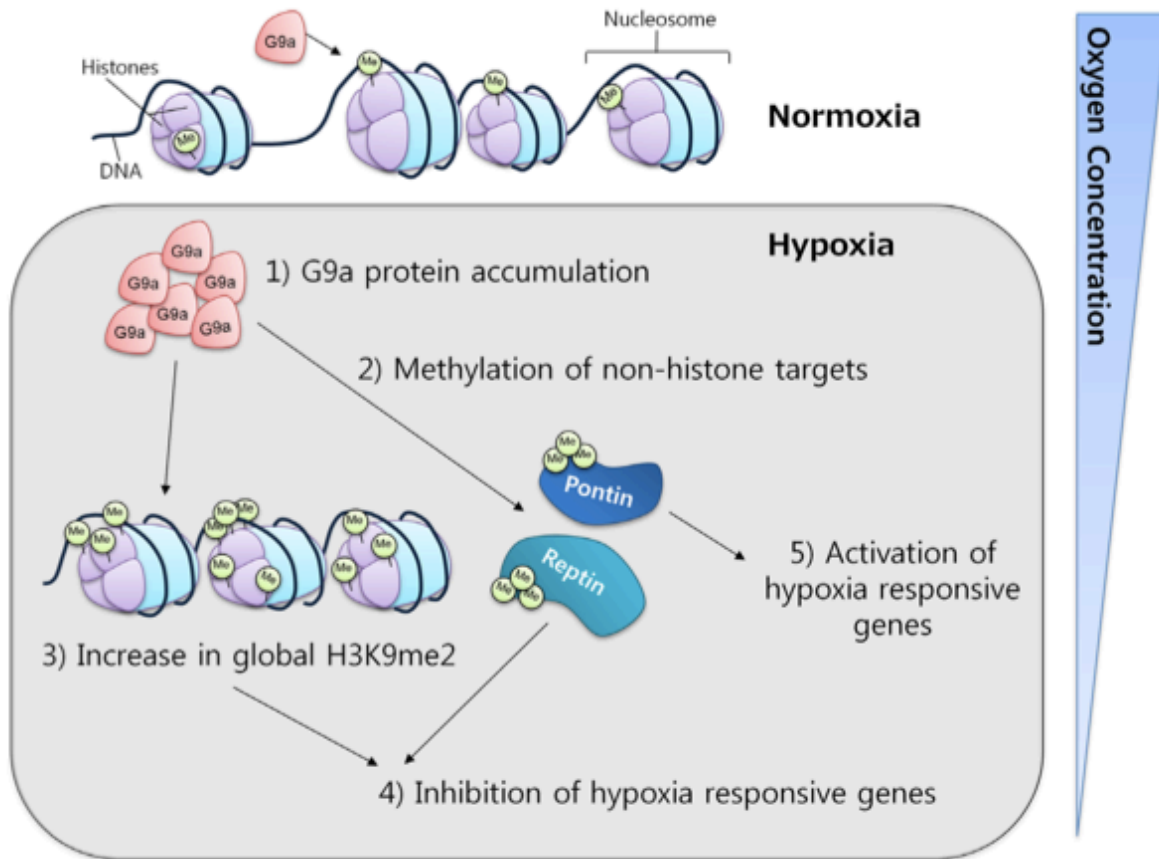


Figure 72 G9a regulates hypoxia response.

Hypoxia leads to increased G9a activity, leading to the repression of a specific subset of hypoxia genes while it is involved in the activation of various target genes. Adopted from Casciello et al.

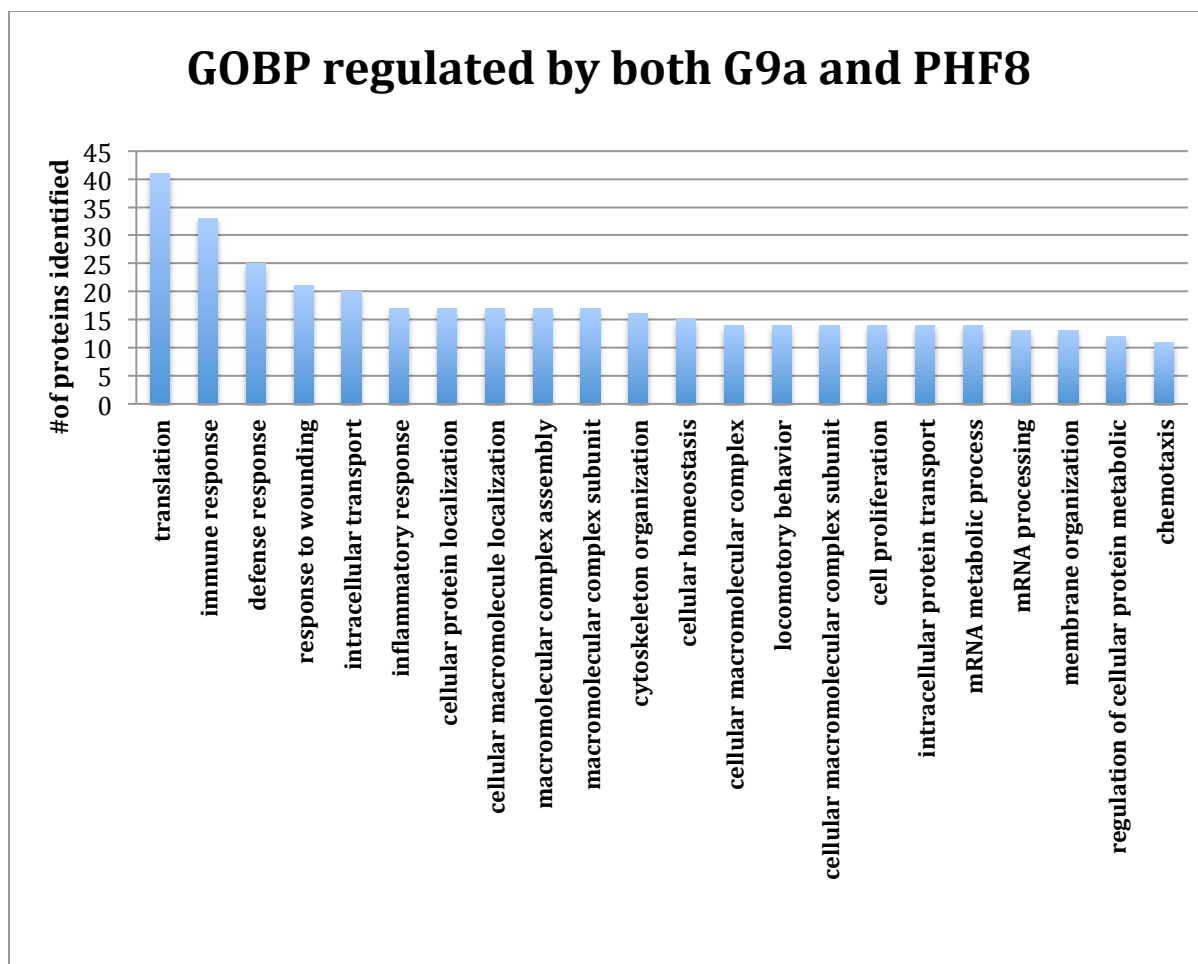


Figure 73 GOBP enrichment of the common secretome
GOBP regulated by both G9a and PHF8 antagonistically (Erdoğan et al, 2016).

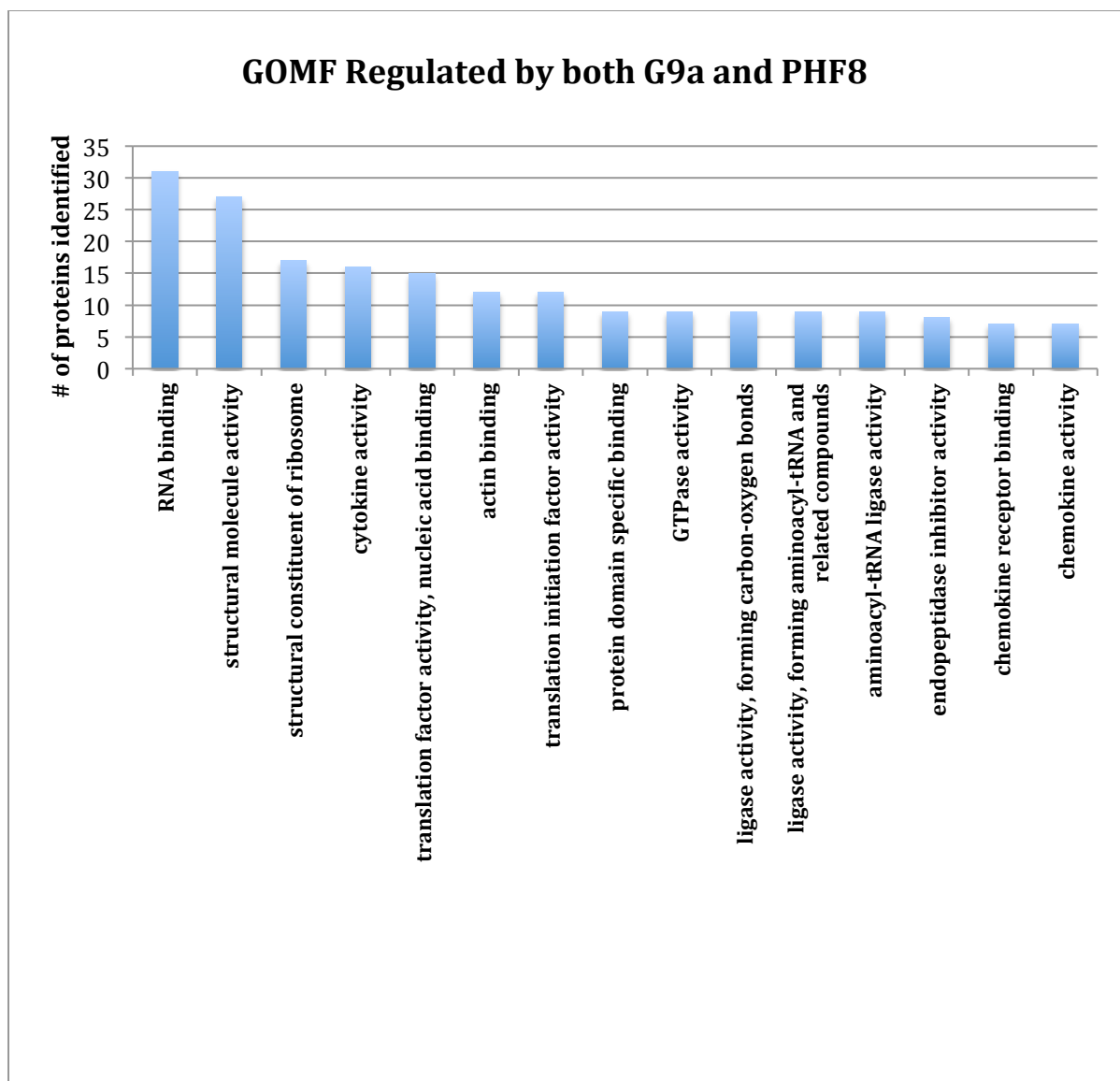


Figure 74 GOMF enrichment of the common sceretome
GOMF regulated by G9a and PHF8 antagonistically (Erdoğan et al, 2016).

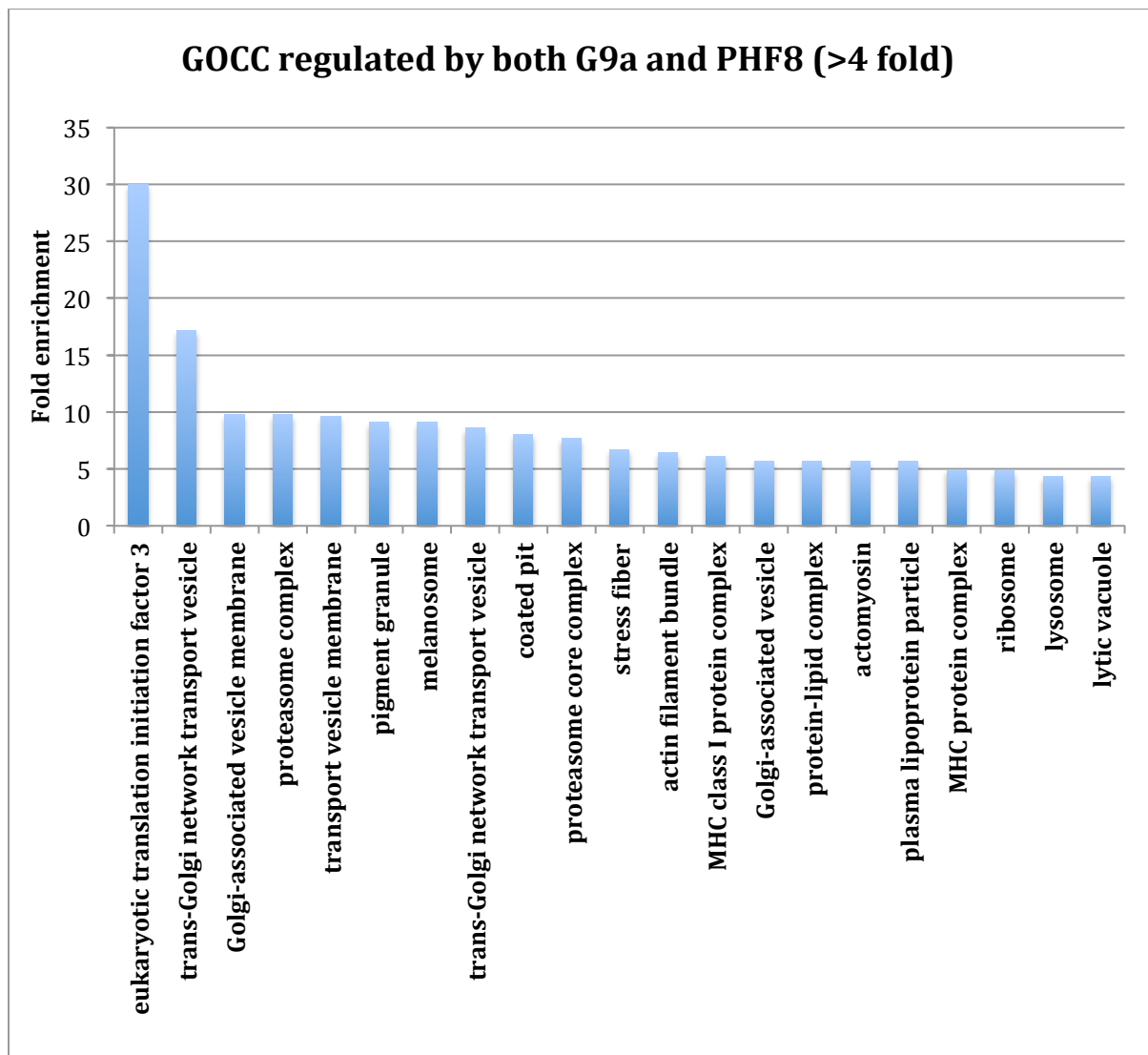


Figure 75 GOCC enrichment of the common secretome
GOCC regulated by both G9a and PHF8 antagonistically (Erdoğan et al, 2016).

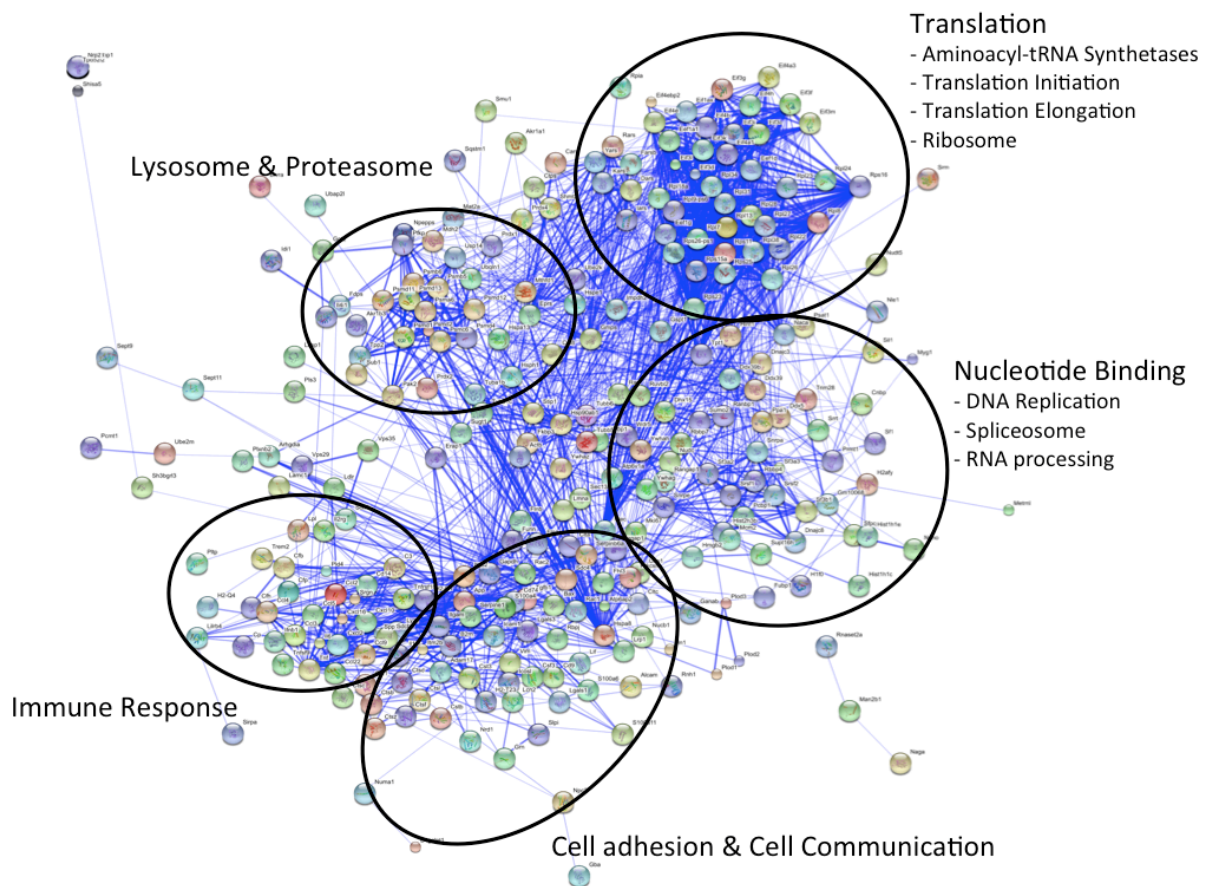


Figure 76 Protein-protein interaction network of the common secretome
PPI of the secretome differentially regulated by G9a and PHF8 was determined by STRING in high confidence (confidence score 0.7) (Erdoğan et al, 2016).

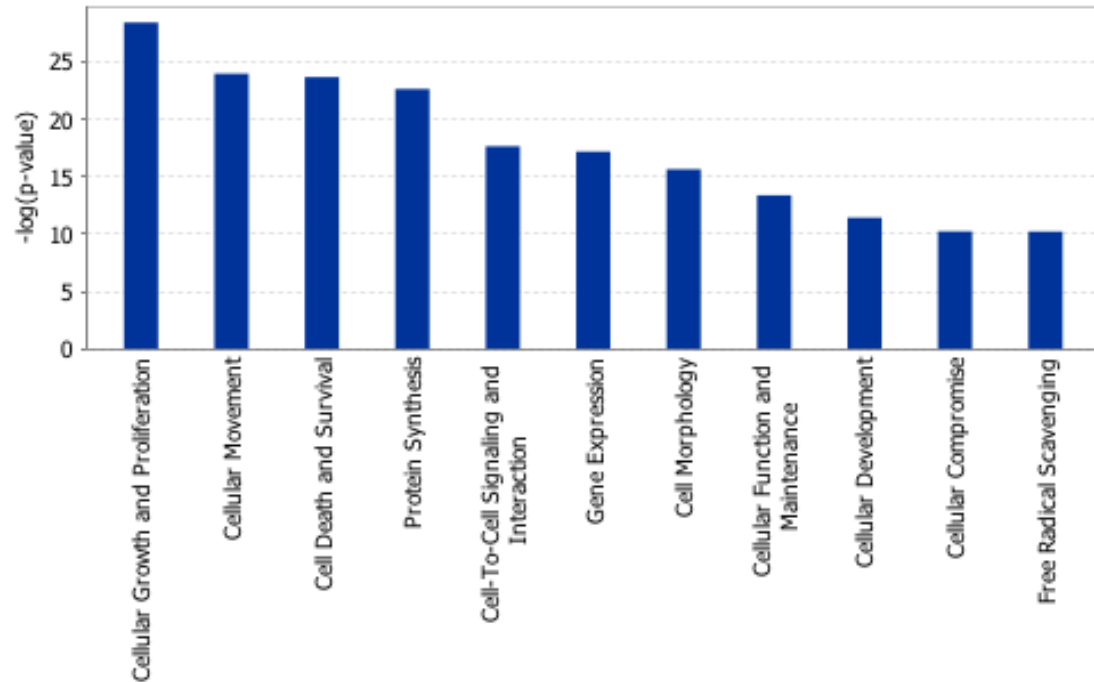


Figure 77 Top 10 canonical pathways regulated antagonistically by G9a and PHF8
 IPA network analysis revealed differentially regulated canonical pathways by PHF8 and G9a depending on the inflammatory phenotype (Erdoğan et al, 2016).

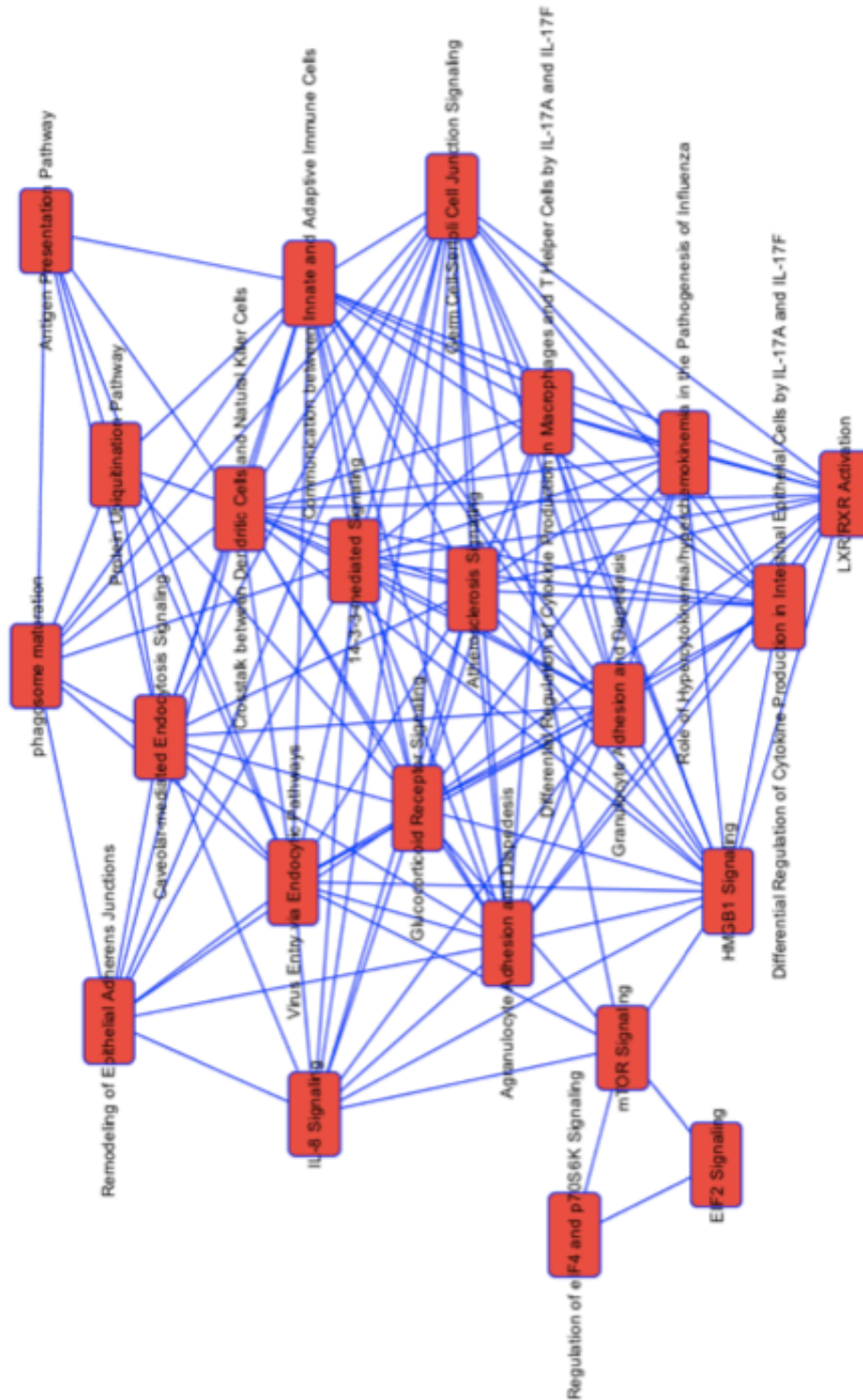


Figure 78 Canonical pathways in cross talk regulated by both G9a and PHF8
The cross talk shows regulation of different innate immune responses (Erdoğan et al, 2016).

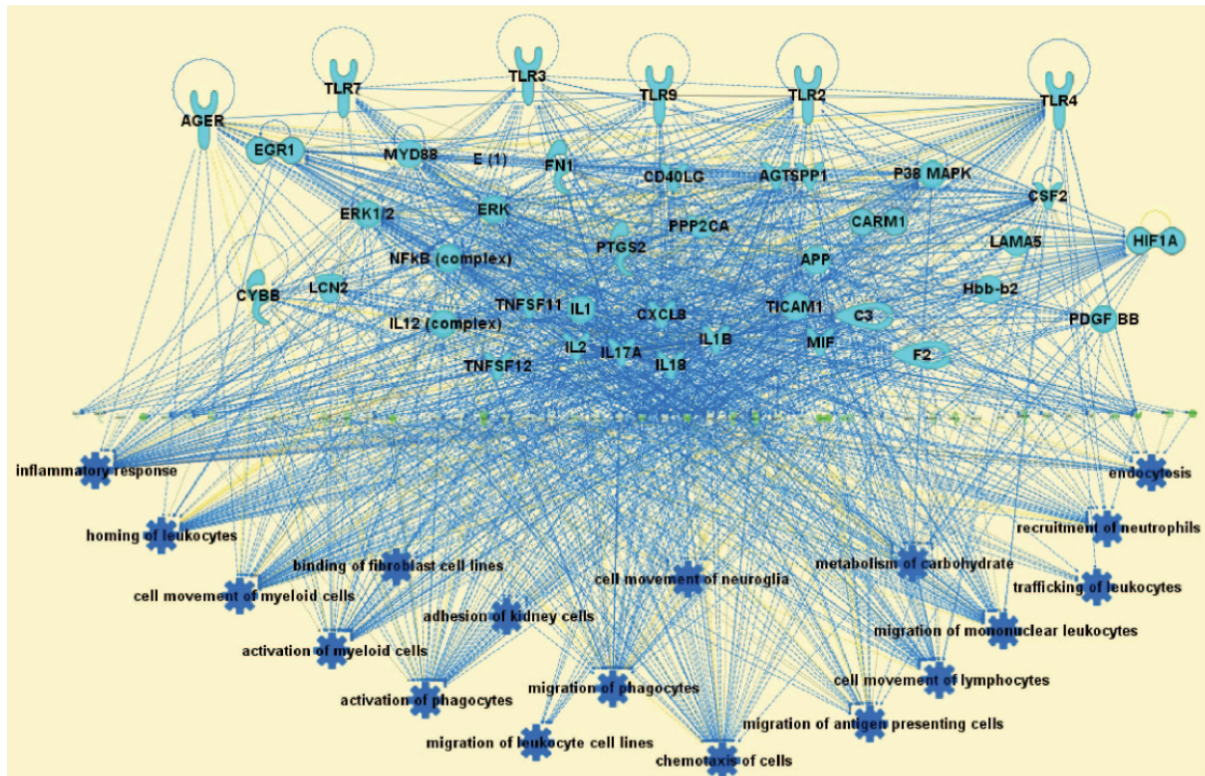


Figure 79 Upstream regulators and targeted canonical pathways

These regulators and pathways are predicted by IPA analysis as due to LPS-inducible, PHF8-dependent secreted proteins. Using the secretome data (proteins in the middle), IPA predicts the possible upstream intracellular proteins (top, cyan) and the canonical pathways that become regulated through signaling (bottom, blue). Green shade shows proteins with decreased secretion, and red shade shows proteins with increased secretion in LPS-stimulated PHF8-KD RAW cells compared with LPS-stimulated WT RAW cells.

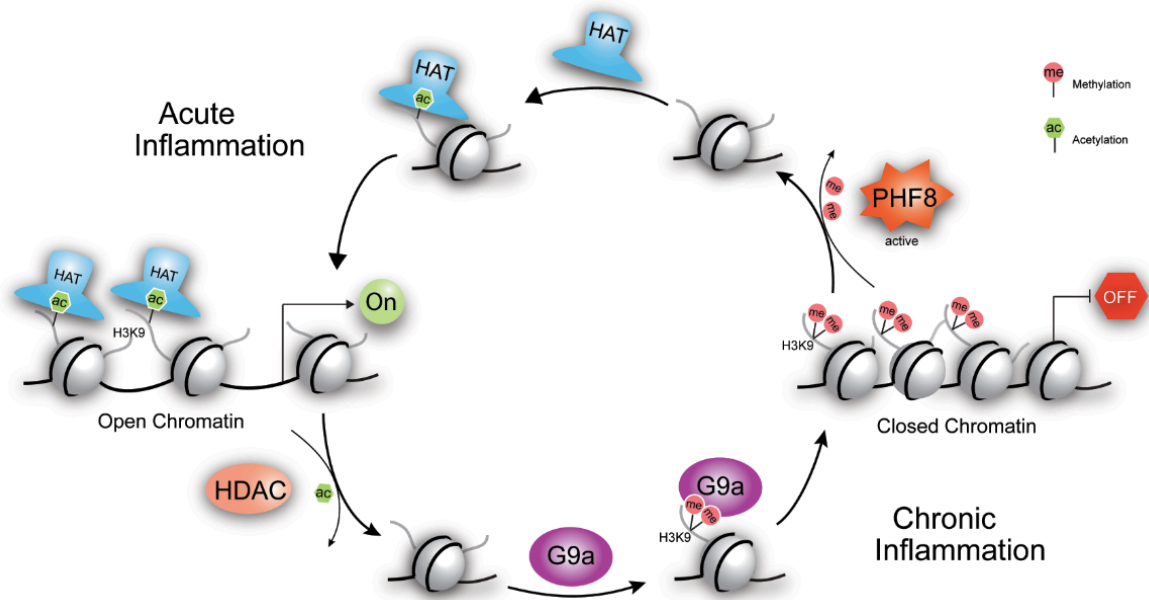


Figure 80 The mechanism of the G9a- vs PHF8- dependent chromatin plasticity
The mechanism underlies gene-specific chromatin plasticity corresponding to the changes of immune cellular responses to LPS stimulation(s). Under the acute inflammatory conditions the gene-specific-repressive function of the Kme writer G9a is antagonized by the Kme eraser PHF8. 'HAT' refers to histone acetylase, and 'HDAC' refers to histone deacetylase (Erdoğan et al, 2016).

APPENDIX 1: T-CLASS SECRETOME

Uniprot ID	Gene name	Uniprot ID	Gene name	Uniprot ID	Gene name
Q921H8	Acaa1a	F8VQG4	H2-T24	Q8CIH9	Ppat
Q8CAY6	Acat2	Q3THW5	H2afv	Q9CR16	Ppid
Q91V92	Acly	P70288	Hdac2	Q9D0W5	Ppil1
Q99KI0	Aco2	P20060	Hexb	Q61074	Ppm1g
Q9Z0F8-2	Adam17	P43276	Hist1h1b	O88531	Ppt1
E9Q359	Adam8	P15864	Hist1h1c	F6SPQ1	Ppt2
P28474	Adh5	P43277	Hist1h1d	Q7TMR0	Prcp
P28650	Adssl1	P43274	Hist1h1e	Q9JIF0-2	Prmt1
E9Q616	Ahnak	Q8CGP6	Hist1h2ah	Q99KP6	Prpf19
P31230	Aimp1	F8WIX8	Hist1h2al	G3UXL2	Prps1l3
Q9JII6	Akr1a1	Q6ZWY9	Hist1h2bc	E9PZ00	Psap
P45376	Akr1b1	P84228	Hist1h3b	O55234	Psemb5
Q9EST5	Anp32b	P62806	Hist1h4a	O88685	Psmc3
E9Q5H2	Anp32e	Q9CX86	Hnrnpa0	Q3TXS7	Psmd1
Q60709	Aplp2	O88569	Hnrnpa2b1	Q9D8W5	Psmd12
P12023	App	Q9Z204-2	Hnrnpc	O35226	Psmd4
Q5XJY5	Arcn1	O35737	Hnrnph1	P26516	Psmd7
Q9CWJ9	Atic	Q8R081	Hnrnpl	P29351	Ptpn6
Q3TKX1	Atp6ap1	G3XA10	Hnrnpu	Q9JKF6	Pvrl1
Q9CYN9	Atp6ap2	P07901	Hsp90aa1	Q8BND5-2	Qsox1
P62814	Atp6v1b2	Q8BM72	Hspa13	Q5SW88	Rab1
P01887	B2m	P38647	Hspa9	P46061	Rangap1
E9QAI5	Cad	P63038	Hspd1	O89086	Rbm3
P10148	Ccl2	Q64433	Hspe1	Q91VM5	Rbmxl1
Q03366	Ccl7	Q8BU30	Iars	Q8BK67	Rcc2
P51670	Ccl9	P13597-2	Icam1	Q9JJH1	Rnase4
P15379-2	Cd44	Q9ESY9	Ifi30	Q8VEE4	Rpa1
P04441	Cd74	O35664-3	Ifnar2	P62983	Rps27a
P04186	Cfb	P47879	Igfbp4	P60122	Ruvbl1
P06909	Cfh	Q8K3I6	Il27	Q9WTM5	Ruvbl2
B1AWE0	Clta	Q45VK5	Ilf3	P14069	S100a6
Q68FD5	Cltc	P24547	Impdh2	D3YXK2	Safb
Q8K4Q8	Colec12	Q792F9	Itga4	P32020-2	Scp2
P61924	Copz1	Q542I8	Itgb2	O35988	Sdc4
Q9WUM4	Coro1c	O89051	Itm2b	Q61112	Sdf4
Q61147	Cp	P52293	Kpna2	P17563	Selenbp1
O88668	Creg1	P70168	Kpnb1	Q62178	Sema4a
P09581	Csf1r	Q61792	Lasp1	Q62179	Sema4b
P21460	Cst3	P35951	Ldlr	O09126	Sema4d
Q8R242-2	Ctbs	Q07797	Lgals3bp	E9Q4Q2	Sf1

Q9CWL8	Ctnnbl1	P48678	Lmna	Q8K4Z5	Sf3a1
P10605	Ctsb	P14733	Lmnb1	G3UVU2	Sf3a2
Q9R013	Ctsf	P11152	Lpl	Q9D554	Sf3a3
P06797	Ctsl1	O88188	Ly86	G5E866	Sf3b1
O70370	Ctss	P08905	Lyz2	Q3UJB0	Sf3b2
Q9WUU7	Ctsz	O09159	Man2b1	Q921M3	Sf3b3
D3YW23	Cxcl10	Q3THS6	Mat2a	Q923D4	Sf3b5
I7HIQ2	Cxcl16	Q8K310	Matr3	Q8VIJ6	Sfpq
P10889	Cxcl2	P97310	Mcm2	Q8BJU0-2	Sgta
Q91UZ6	D17H6S56E-5	P49717	Mcm4	Q9D7I0	Shisa5
Q62165	Dag1	P97311	Mcm6	Q9CZN7	Shmt2
Q922B2	Dars	Q61881	Mcm7	Q6P6I8	Sirpa
Q62418-3	Dbnl	P08249	Mdh2	Q6P5F6	Slc39a10
A2ADY9	Ddi2	Q8VE43	Metrn1	E9Q748	Slpi
Q9JIK5	Ddx21	Q7TPV4	Mybbp1a	Q62189	Snrpa
Q9Z1N5	Ddx39b	Q3V4D5	Naa10	Q78ZM0	Snx3
Q61656	Ddx5	Q6PGB6-2	Naa50	P13609	Srgn
P00375	Dhfr	Q9QWR8	Naga	Q99MR6-3	Srrt
O35286	Dhx15	Q78ZA7	Nap1l4	Q6PDM2	Srsf1
O70133	Dhx9	P09405	Ncl	P84104-2	Srsf3
P63037	Dnaja1	Q62433	Ndrp1	Q8BL97-3	Srsf7
Q91YW3	Dnajc3	Q9D0T1	Nhp2l1	Q8BH40	Stx7
Q6NZB0	Dnajc8	E9Q5C9	Nolc1	G3X956	Supt16
Q8C255	Dpep2	Q99K48	Nono	O08784	Tcof1
Q91WV0	Dr1	Q9Z0J0	Npc2	P40142	Tkt
Q9CQ43	Dut	Q61937	Npm1	Q61029	Tmpo
O35228	Ebi3	Q02819	Nucb1	P41274	Tnfsf9
Q61508	Ecm1	P29758	Oat	Q8BFY9-2	Tnpo1
Q9QZD9	Eif3i	Q9CZ30	Ola1	Q9ER38	Tor3a
Q91VC3	Eif4a3	Q8R357	Olfm1	O89023	Tpp1
P19096	Fasn	Q62422	Ostf1	Q7M739	Tpr
Q920E5	Fdps	Q921K2	Parp1	Q99NH8	Trem2
Q9R059	Fhl3	P31240	Pdgfb	Q9Z0P5	Twf2
Q04646-2	Fxyd2	P12382	Pfkl	Q8CDN6	Txn1l
Q9R0N0	Galk1	Q8C605	Pfklp	P26369	U2af2
P16858	Gapdh	Q8CHP8	Pgp	Q9Z1F9	Uba2
Q64737	Gart	Q61753	Phgdh	Q80X50-2	Ubp1
E9Q7H5	Gm8991	P27612	Plaa	Q9JKB1	Uchl3
P05202	Got2	P35456	Plaur	Q9JMA1	Usp14
P28798	Grn	E9QPE8	Plec	D3YYD5	Vps29
O09131	Gsto1	Q9R0E2	Plod1	Q9EQH3	Vps35
P01900	H2-D1	Q9R0B9	Plod2	P61965	Wdr5

P01902	H2-K1	Q9R0E1	Plod3	Q9CQV8	Ywhab
P01897	H2-L	P55065	Pltp	P10404	
Q8HWB2	H2-Q4	Q923G2	Polr2h		

APPENDIX 2 : NT-CLASS SECRETOME

Uniprot ID	Gene name
Q8BGQ7	Aars
P63260	Actg1
Q8BK64	Ahsa1
Q61024	Asns
P50516	Atp6v1a
P62204	Calm1
Q04447	Ckb
Q9Z1Q5	Clic1
Q8CIE6	Copa
Q9JIF7	Copb1
O55029	Copb2
O89079	Cope
Q9QZE5	Copg1
O89053	Coro1a
Q9ERK4	Cse1l
P97821	Ctsc
Q9JHU4	Dync1h1
Q8CGC7	Eprs
P97855	G3bp1
Q9CQM9	Glr3
P70349	Hint1
Q8JZK9	Hmgcs1
Q9Z2X1	Hnrnpf
P11499	Hsp90ab1
G5E8F1	Itgam
P09056	Lif
P17897	Lyz1
P31938	Map2k1
Q9CQT1	Mri1
Q922D8	Mthfd1
Q99J77	Nans
Q7TQI3	Otub1

Uniprot ID	Gene name
Q9QUR7	Pin1
P58389	Ppp2r4
P62192	Psmc1
P46471	Psmc2
P54775	Psmc4
P62196	Psmc5
P62334	Psmc6
Q8BG32	Psmd11
Q9WVJ2	Psmd13
Q8VDM4	Psmd2
P14685	Psmd3
Q99JI4	Psmd6
Q8BGJ5	Ptbp1
D3Z7C6	Ptges3
Q60972	Rbbp4
Q60973	Rbbp7
Q91VI7	Rnh1
P07091	S100a4
Q920A5	Scpep1
Q3TMX0	Sdcbp
Q9EPK6	Sil1
Q78PY7	Snd1
Q08943	Ssrp1
Q80YX1-2	Tnc
P06804	Tnf
Q62318	Trim28
E9PXX7	Txndc5
Q02053	Uba1
Q9WUP7-2	Uchl5
Q9Z1Z0	Uso1
Q3U4W8	Usp5
P20152	Vim

APPENDIX 3: COMMON PROTEINS WITH SECRETOME FROM MEISSNER ET AL.

Uniprot ID	Gene name
Q99KI0	Aco2
O35598	Adam10
Q9Z0F8	Adam17
P54923	Adprh
P10518	Alad
E9Q4G8	Alcam
P05064	Aldoa
Q60709	Aplp2
P12023	App
Q9WV54	Asah1
Q9CYN9	Atp6ap2
P01887	B2m
Q09200	B4galnt1
Q9JMK0	B4galt5
Q91XV3	Basp1
P01027	C3
E9QAI5	Cad
P14211	Calr
P10148	Ccl2
O88430	Ccl22
P10855	Ccl3
P14097	Ccl4
P30882	Ccl5
Q03366	Ccl7
P51670	Ccl9
P10810	Cd14
P15379	Cd44
P04441	Cd74
P06909	Cfh
P11680	Cfp
Q9D8B3	Chmp4b
Q8WTY4	Ciapi1
Q68FD5	Cltc
O89001	Cpd
O88668	Creg1
P07141	Csf1
P09920	Csf3
P21460	Cst3
Q8R242	Ctbs
P16675	Ctsa
P10605	Ctsb

Uniprot ID	Gene name
P01575	Ifnb1
Q3TBV5	Il1rn
Q8K3I6	Il27
P34902	Il2rg
O09046	Il4i1
P08505	Il6
Q64339	Isg15
Q792F9	Itga4
G5E8F1	Itgam
Q542I8	Itgb2
O89051	Itm2b
P11672	Lcn2
P35951	Ldlr
Q07797	Lgals3bp
O89017	Lgm1
Q64281	Lilrb4
Q9WVG5	Lipg
Q9DBH5	Lman2
P11152	Lpl
Q91ZX7	Lrp1
P19973	Lsp1
O88188	Ly86
O09159	Man2b1
O54782	Man2b2
Q8K2I4	Manba
P08249	Mdh2
Q8VE43	Metrl
Q9Z2L6	Minpp1
P26041	Msn
Q3V4D5	Naa10
Q9QWR8	Naga
O88325	Naglu
O09043	Napsa
Q8VEJ4	Nle1
Q11011	Npepps
O35375	Nrp2
Q02819	Nucb1
P29758	Oat
P09103	P4hb
P29341	Pabpc1
Q9WU78	Pdcd6ip

P97821	Ctsc
P18242	Ctsd
O70370	Ctss
Q9WUU7	Ctsz
D3YW23	Cxcl10
I7HIQ2	Cxcl16
P10889	Cxcl2
Q91UZ6	D17H6S56E-5
Q9CPT4	D17Wsu104e
Q91YW3	Dnajc3
O35228	Ebi3
Q61508	Ecm1
E9QN08	Eef1d
P63242	Eif5a
Q8K482	Emilin2
Q9EQH2	Erap1
P57759	Erp29
Q9D1Q6	Erp44
P09528	Fth1
Q9CPX4	Ftl1
P23188	Furin
P70699	Gaa
Q8BHN3	Ganab
P17439	Gba
Q60648	Gm2a
Q8BFR4	Gns
Q99P91	Gpnmb
P28798	Grn
P01900	H2-D1
P01902	H2-K1
Q8HWB2	H2-Q4
P06339	H2-T23
F8VQG4	H2-T24
P29416	Hexa
P20060	Hexb
P97825	Hn1
Q6PGH2	Hn1l
P08113	Hsp90b1
Q8BM72	Hspa13
P20029	Hspa5
P63038	Hspd1
Q64433	Hspe1
Q9JKR6	Hyou1
P13597	Icam1

P31240	Pdgfb
P08003	Pdia4
Q922R8	Pdia6
P35456	Plaur
Q3TCN2	Plbd2
Q8BG07	Pld4
Q9R0B9	Plod2
Q9R0E1	Plod3
B2RXS4	Plxnb2
P24369	Ppib
O88531	Ppt1
F6SPQ1	Ppt2
Q7TMR0	Prcp
O08795	Prkcsh
Q64695	Procr
Q08761	Pros1
E9PZ00	Psap
B0V2N1	Ptprs
Q9JKF6	Pvrl1
O89086	Rbm3
Q9CQ01	Rnaset2
Q5XJF6	Rpl10a
P07091	S100a4
P04918	Saa3
Q920A5	Scpep1
O35988	Sdc4
Q3TMX0	Sdcbp
Q62179	Sema4b
P22777	Serpine1
P10923	Spp1
P13609	Srgn
P54227	Stmn1
Q8R0B4	Tardbp
O88968	Tcn2
Q62351	Tfrc
Q8C1A5	Thop1
P12032	Timp1
P06804	Tnf
P41274	Tnfsf9
Q62393	Tpd52
O89023	Tpp1
Q99NH8	Trem2
E9PXX7	Txndc5
Q6P5E4	Uggt1

Q9JHJ8	Icoslg
Q9ESY9	Ifi30
O35664	Ifnar2

P20152	Vim
P10404	

APPENDIX 4: COMMON PROTEINS WITH SECRETOME FROM LIU ET AL.

Uniprot ID	Gene name
P42208	1-Sep
O55131	6-Sep
Q80UG5	8-Sep
Q8C1B7	10-Sep
Q8BGQ7	Aars
Q921H8	Acaa1a
Q8CAY6	Acat2
Q91V92	Acly
P28271	Aco1
Q99KI0	Aco2
Q91V12	Acot7
P63260	Actg1
P57780	Actn4
P61164	Actr1a
P61161	Actr2
Q99JY9	Actr3
P28474	Adh5
P54923	Adprh
P46664	Adss
P28650	Adssl1
P50247	Ahcy
E9Q616	Ahnak
Q8BK64	Ahsa1
P31230	Aimp1
Q9WTP6	Ak2
Q9JII6	Akr1a1
P45376	Akr1b1
P47738	Aldh2
Q9JLJ2	Aldh9a1
P05064	Aldoa
P05063	Aldoc
O08583	Alyref
O35381	Anp32a
Q9EST5	Anp32b
E9Q5H2	Anp32e
P07356	Anxa2
Q5SVG5	Ap1b1
P17426	Ap2a1

Uniprot ID	Gene name
Q9CPX4	Ftl1
P97855	G3bp1
Q00612	G6pdx
P70699	Gaa
Q9R0N0	Galk1
Q8BHN3	Ganab
P16858	Gapdh
Q9CZD3	Gars
P17439	Gba
Q61598	Gdi2
Q9CPV4	Glod4
Q9QUH0	GlrX
Q9CQM9	GlrX3
E9PZF0	Gm20390
Q60648	Gm2a
J3QP68	Gm4204
Q9CQI3	Gmfb
P62880	Gnb2
P68040	Gnb2l1
O88958	Gnpda1
Q8BFR4	Gns
P06745	Gpi
Q99P91	Gpnmb
Q60631	Grb2
P28798	Grn
P13020	Gsn
Q8R050	Gspt1
O09131	Gsto1
Q8HWP2	H2-Q4
Q3THW5	H2afv
Q61035	Hars
P49710	Hcls1
P51859	Hdgf
P29416	Hexa
P20060	Hexb
P70349	Hint1
P43276	Hist1h1b
P43277	Hist1h1d

Uniprot ID	Gene name
P46471	Psmc2
P54775	Psmc4
P62196	Psmc5
P62334	Psmc6
Q3TXS7	Psmd1
Q8BG32	Psmd11
Q9D8W5	Psmd12
Q9WVJ2	Psmd13
O35593	Psmd14
Q8VDM4	Psmd2
P14685	Psmd3
O35226	Psmd4
Q99JI4	Psmd6
P26516	Psmd7
G3UXZ5	Psme1
G3X9V0	Psme2
Q8BGJ5	Ptbp1
P29351	Ptpn6
Q3UEB3	Puf60
D3YWR7	Qdpr
P35278	Rab5c
P51150	Rab7a
P63001	Rac1
Q05144	Rac2
P54728	Rad23b
P62827	Ran
P34022	Ranbp1
Q9D0I9	Rars
Q60972	Rbbp4
O89086	Rbm3
Q9CWZ3	Rbm8a
Q91VM5	RbmXl1
Q8BK67	Rcc2
P26043	Rdx
P82343	Renbp
Q9QUI0	Rhoa
Q9CQ01	Rnaset2
Q91VI7	Rnh1

Q9DBG3	Ap2b1
Q8R5A3	Apbb1ip
O35841	Api5
P12023	App
P08030	Aprt
Q5XJY5	Arcn1
P84078	Arf1
Q99PT1	Arhgdia
Q61599	Arhgdib
Q9WV32	Arpc1b
Q9CVB6	Arpc2
Q9JM76	Arpc3
P59999	Arpc4
Q9CPW4	Arpc5
P50429	Arsb
Q9WV54	Asah1
Q9CWJ9	Atic
O08997	Atox1
Q3TKX1	Atp6ap1
Q9CYN9	Atp6ap2
P50516	Atp6v1a
P62814	Atp6v1b2
P01887	B2m
Q91XV3	Basp1
Q07813	Bax
Q8R016	Blmh
Q9CY64	Blvra
Q923D2	Blvrb
Q64152	Btf3
P01027	C3
Q9CXW3	Cacybp
P62204	Calm1
P14211	Calr
Q6ZQ38	Cand1
P40124	Cap1
Q99LB4	Capg
Q60865	Caprin1
Q5RKN9	Capza1
P47754	Capza2
P47757	Capzb
Q9DCC5	Cbx3

P43274	Hist1h1e
Q8CGP6	Hist1h2ah
P84228	Hist1h3b
P62806	Hist1h4a
G3UVV4	Hk1
P63158	Hmgb1
P30681	Hmgb2
P14901	Hmox1
P97825	Hn1
Q6PGH2	Hn1l
Q9CX86	Hnrnpa0
P49312	Hnrnpa1
O88569	Hnrnpa2b1
Q99020	Hnrnpab
Q9Z204	Hnrnpc
Q9Z2X1	Hnrnpf
G3XA10	Hnrnpu
P00493	Hprt1
P07901	Hsp90aa1
P11499	Hsp90ab1
P08113	Hsp90b1
Q3U2G2	Hspa4
P20029	Hspa5
P63017	Hspa8
P38647	Hspa9
P63038	Hspd1
Q64433	Hspe1
Q9JKR6	Hyou1
Q8BU30	Iars
O88844	Idh1
Q9ESY9	Ifi30
P08505	Il6
Q924B0	Impa1
Q8BKC5	Ipo5
E9QKZ2	Ipo9
Q9JKF1	Iqgap1
Q64339	Isg15
Q91V64	Isoc1
Q9JHU9	Isyna1
G5E8F1	Itgam
Q542I8	Itgb2

Q8VCT3	Rnpep
I7HLV2	Rpl10
Q5XJF6	Rpl10a
P35979	Rpl12
P47963	Rpl13
P19253	Rpl13a
Q9CR57	Rpl14
P62717	Rpl18a
A2A547	Rpl19
Q9CQM8	Rpl21
P67984	Rpl22
P62830	Rpl23
E9Q132	Rpl24
P61358	Rpl27
P14115	Rpl27a
P27659	Rpl3
P62889	Rpl30
P62900	Rpl31
P62911	Rpl32
Q9D1R9	Rpl34
Q6ZWV7	Rpl35
Q9JJI8	Rpl38
Q9D8E6	Rpl4
P47962	Rpl5
P47911	Rpl6
P14148	Rpl7
P47955	Rplp1
P99027	Rplp2
P63325	Rps10
P62281	Rps11
Q6ZWZ6	Rps12
P62301	Rps13
P62264	Rps14
P62843	Rps15
P62245	Rps15a
P14131	Rps16
P63276	Rps17
Q9CZX8	Rps19
P25444	Rps2
P60867	Rps20
Q9CQR2	Rps21

P10148	Ccl2
P10855	Ccl3
P14097	Ccl4
P30882	Ccl5
P51670	Ccl9
P80314	Cct2
P80318	Cct3
P80315	Cct4
P80316	Cct5
P80317	Cct6a
P80313	Cct7
P42932	Cct8
P10810	Cd14
P04441	Cd74
Q61081	Cdc37
P60766	Cdc42
P04186	Cfb
P18760	Cfl1
P11680	Cfp
Q9D8B3	Chmp4b
Q9D1P4	Chordc1
Q04447	Ckb
Q9Z1Q5	Clic1
Q9QYB1	Clic4
B1AWE0	Clta
Q68FD5	Cltc
Q9DBP5	Cmpk1
Q3U5Q7	Cmpk2
Q9D1A2	Cndp2
Q8CIE6	Copa
Q9JIF7	Copb1
O55029	Copb2
O89079	Cope
Q9QZE5	Copg1
P61202	Cops2
O88543	Cops3
O88544	Cops4
P61924	Copz1
O89053	Coro1a
Q9WUM3	Coro1b
Q9WUM4	Coro1c

O89051	Itm2b
Q99MN1	Kars
Q3U0V1	Khsrp
P70168	Kpnb1
Q9CPY7	Lap3
Q61792	Lasp1
P11672	Lcn2
Q61233	Lcp1
P06151	Ldha
P16045	Lgals1
Q8C253	Lgals3
Q07797	Lgals3bp
O89017	Lgmh
P48678	Lmna
P14733	Lmnb1
P11152	Lpl
Q91ZX7	Lrp1
Q505F5	Lrrc47
P19973	Lsp1
P24527	Lta4h
O88188	Ly86
Q9WTL7	Lypla2
P08905	Lyz2
O09159	Man2b1
O54782	Man2b2
Q80ZP8	Manf
P31938	Map2k1
P63085	Mapk1
Q61166	Mapre1
Q3THS6	Mat2a
Q8K310	Matr3
P14152	Mdh1
P08249	Mdh2
P34884	Mif
P26041	Msn
Q9CQ65	Mtap
Q922D8	Mthfd1
P62774	Mtpn
Q9JK81	Myg1
Q8VDD5	Myh9
Q60605	Myl6

P62267	Rps23
P62849	Rps24
P62852	Rps25
P62855	Rps26
P62983	Rps27a
P62908	Rps3
P62702	Rps4x
P62754	Rps6
P62242	Rps8
Q6ZWN5	Rps9
P14206	Rpsa
A2AVJ7	Rrbp1
P60122	Ruvbl1
P50543	S100a11
P07091	S100a4
P14069	S100a6
P04918	Saa3
Q9R1T2	Sae1
Q60710	Samhd1
Q9D1J3	Sarnp
P26638	Sars
P32020	Scp2
Q920A5	Scpep1
O35988	Sdc4
Q3TMX0	Sdcbp
Q61112	Sdf4
Q9D662	Sec23b
G3X972	Sec24c
P17563	Selenbp1
Q8BH69	Sephs1
Q60854	Serpinb6
A2BE93	Set
Q8K4Z5	Sf3a1
G5E866	Sf3b1
Q921M3	Sf3b3
Q8VIJ6	Sfpq
Q8BJU0	Sgta
Q9JJU8	Sh3bgrl
Q91VW3	Sh3bgrl3
Q78PY7	Snd1
P62305	Snrpe

Q9CQI6	Cotl1
Q6NVF9	Cpsf6
O88668	Creg1
P63254	Crip1
P09581	Csf1r
P21460	Cst3
Q62426	Cstb
P16675	Ctsa
P10605	Ctsb
P97821	Ctsc
P18242	Ctsd
P06797	Ctsl1
O70370	Ctss
Q9WUU7	Ctsz
D3YW23	Cxcl10
P10889	Cxcl2
Q99LF4	D10Wsu52e
Q922B2	Dars
P31786	Dbi
Q62418	Dbnl
D3YX34	Dctn1
A2ADY9	Ddi2
Q501J6	Ddx17
Q9Z1N5	Ddx39b
Q61656	Ddx5
Q6Q899	Ddx58
P54823	Ddx6
P00375	Dhfr
O35286	Dhx15
O70133	Dhx9
Q8K1M6	Dnm1l
Q9Z2W0	Dnpep
Q8C255	Dpep2
Q99KK7	Dpp3
O08553	Dpysl2
Q9R0P5	Dstn
Q9JHU4	Dync1h1
Q61508	Ecm1
P10126	Eef1a1
O70251	Eef1b
Q9D8N0	Eef1g

Q60817	Naca
Q9QWR8	Naga
O88325	Naglu
Q99KQ4	Nampt
Q99J77	Nans
Q78ZA7	Nap1l4
Q8BP47	Nars
B1AU76	Nasp
P09405	Ncl
P29595	Nedd8
Q9D0T1	Nhp2l1
Q9JHW2	Nit2
P15532	Nme1
Q99K48	Nono
Q9Z0J0	Npc2
Q11011	Npepps
A6PWC3	Nrd1
Q9CZ44	Nsfl1c
Q02819	Nucb1
Q3UKN6	Nucb2
O35685	Nudc
P61971	Nutf2
Q9CZ30	Ola1
Q62422	Ostf1
Q7TQI3	Otub1
P09103	P4hb
P50580	Pa2g4
P29341	Pabpc1
P63005	Pafah1b1
Q61206	Pafah1b2
Q9DCL9	Paics
Q8CIN4	Pak2
Q99LX0	Park7
Q921K2	Parp1
P60335	Pcbp1
Q61990	Pcbp2
P23506	Pcmt1
P17918	Pcna
P56812	Pdcd5
Q9WU78	Pdcd6ip
P27773	Pdia3

Q6NZD2	Snx1
Q9CWK8	Snx2
Q78ZM0	Snx3
Q9D8U8	Snx5
Q6P8X1	Snx6
Q91VH2	Snx9
P08228	Sod1
P10923	Spp1
P13609	Srgn
Q6PDM2	Srsf1
Q62093	Srsf2
P84104	Srsf3
P32067	Ssb
F8WJK8	Stt13
Q60864	Stip1
Q9Z1Z2	Strap
Q8BH40	Stx7
Q64324	Stxbp2
P11031	Sub1
Q9CX34	Sugt1
Q6A028	Swap70
Q7TMK9	Syncrip
Q9WVA4	Tagln2
Q93092	Taldo1
P48428	Tbca
P10711	Tcea1
P83940	Tceb1
P62869	Tceb2
P11983	Tcp1
Q9Z1A1	Tfg
Q9WVA2	Timm8a1
P40142	Tkt
P26039	Tln1
P06804	Tnf
P25119	Tnfrsf1b
Q62393	Tpd52
Q3TUJ9	Tpd52l2
P17751	Tpi1
P21107	Tpm3
Q6IRU2	Tpm4
O89023	Tpp1

P58252	Eef2
Q8C845	Efhd2
Q9WVK4	Ehd1
Q9EQP2	Ehd4
P48024	Eif1
Q8BJW6	Eif2a
Q6ZWX6	Eif2s1
Q99L45	Eif2s2
Q9Z0N1	Eif2s3x
P23116	Eif3a
Q8JZQ9	Eif3b
Q8R1B4	Eif3c
O70194	Eif3d
P60229	Eif3e
Q9DCH4	Eif3f
Q9Z1D1	Eif3g
Q91WK2	Eif3h
Q9QZD9	Eif3i
Q3UGC7	Eif3j1
Q8QZY1	Eif3l
P60843	Eif4a1
Q8BGD9	Eif4b
P63073	Eif4e
Q9WUK2	Eif4h
P59325	Eif5
P63242	Eif5a
O55135	Eif6
P70372	Elavl1
P17182	Eno1
Q8CGC7	Eprs
P84089	Erh
P57759	Erp29
Q9D1Q6	Erp44
Q9R0P3	Esd
Q8BWY3	Etf1
Q5SUT0	Ewsr1
P26040	Ezr
Q05816	Fabp5
Q8R1F1	Fam129b
Q921M7	Fam49b
E9PWY9	Farsa

P08003	Pdia4
Q8K183	Pdxk
P70296	Pebp1
O70591	Pfdn2
Q9WU28	Pfdn5
P12382	Pfkl
Q9DBJ1	Pgam1
Q9DCD0	Pgd
P09411	Pgk1
Q9CQ60	Pgls
Q9D0F9	Pgm1
Q61753	Phgdh
Q9DAK9	Phpt1
Q7M6Y3	Picalm
P53810	Pitpna
P52480	Pkm
P52480	Pkm
Q3TCN2	Plbd2
Q8CIH5	Plcg2
Q8BG07	Pld4
E9QPE8	Plec
Q9R0E2	Plod1
P55065	Pltp
Q543K9	Pnp
Q9D819	Ppa1
P17742	Ppia
P24369	Ppib
Q9CR16	Ppid
Q61074	Ppm1g
P62137	Ppp1ca
Q3UM45	Ppp1r7
P63330	Ppp2ca
Q76MZ3	Ppp2r1a
Q6P1F6	Ppp2r2a
P58389	Ppp2r4
O88531	Ppt1
P35700	Prdx1
Q61171	Prdx2
P99029	Prdx5
Q9QUR6	Prep
Q9DBC7	Prkar1a

Q64514	Tpp2
P63028	Tpt1
Q99NH8	Trem2
Q62318	Trim28
Q9DCG9	Trmt112
P68373	Tuba1c
P68372	Tubb4b
P99024	Tubb5
Q922F4	Tubb6
Q9Z0P5	Twf2
P10639	Txn
Q9CQM5	Txndc17
E9PXX7	Txndc5
Q8CDN6	Txn11
Q9JMH6	Txnrd1
Q3TW96	Uap1l1
Q02053	Uba1
Q9Z1F9	Uba2
P68037	Ube2l3
P61089	Ube2n
Q9CZY3	Ube2v1
Q9D2M8	Ube2v2
Q9JKB1	Uchl3
P61961	Ufm1
Q6P5E4	Uggt1
Q91ZJ5	Ugp2
Q9Z1Z0	Uso1
Q9JMA1	Usp14
Q3U4W8	Usp5
Q9Z1Q9	Vars
P70460	Vasp
Q62465	Vat1
P61759	Vbp1
Q64727	Vcl
Q01853	Vcp
P20152	Vim
Q9EQH3	Vps35
Q99KC8	Vwa5a
P32921	Wars
P70315	Was
O88342	Wdr1

Q9WUA2	Farsb
P19096	Fasn
Q920E5	Fdps
Q91Z50	Fen1
Q8K1B8	Fermt3
P97807	Fh
P26883	Fkbp1a
Q62446	Fkbp3
B7FAU9	Flna

O08795	Prkcsh
Q9Z2Y8	Prosc
Q99KP6	Prpf19
E9PZ00	Psap
Q99K85	Psat1
Q9Z2U1	Psma5
Q9QUM9	Psma6
Q9Z2U0	Psma7
P62192	Psmc1

Q6P1B1	Xpnpep1
Q6P5F9	Xpo1
P62960	Ybx1
P62259	Ywhae
P61982	Ywhag
P68510	Ywhah
P68254	Ywhaq
P63101	Ywhaz

**APPENDIX 5: COMMON PROTEINS WITH LPS-INDUCIBLE SECRETOME FROM LIU
ET AL.**

Uniprot ID	Gene name
Q8BGQ7	Aars
Q921H8	Acaa1a
Q8CAY6	Acat2
Q91V92	Acly
Q99KI0	Aco2
P63260	Actg1
P28474	Adh5
P28650	Adssl1
E9Q616	Ahnak
Q8BK64	Ahsa1
P31230	Aimp1
Q9JII6	Akr1a1
P45376	Akr1b1
Q9EST5	Anp32b
E9Q5H2	Anp32e
P12023	App
Q5XJY5	Arcn1
Q9CWI9	Atic
Q3TKX1	Atp6ap1
Q9CYN9	Atp6ap2
P50516	Atp6v1a
P62814	Atp6v1b2
P01887	B2m
P62204	Calm1
P10148	Ccl2
P51670	Ccl9
P04441	Cd74
P04186	Cfb
Q04447	Ckb
Q9Z1Q5	Clic1
B1AWE0	Clta
Q68FD5	Cltc
Q8CIE6	Copa
Q9JIF7	Copb1
O55029	Copb2
O89079	Cope
Q9QZE5	Copg1
P61924	Copz1
O89053	Coro1a

Uniprot ID	Gene name
Q920E5	Fdps
P97855	G3bp1
Q9R0N0	Galk1
P16858	Gapdh
Q9CQM9	Glr3
P28798	Grn
O09131	Gsto1
Q8HWB2	H2-Q4
Q3THW5	H2afv
P20060	Hexb
P70349	Hint1
P43276	Hist1h1b
P43277	Hist1h1d
P43274	Hist1h1e
Q8CGP6	Hist1h2ah
P84228	Hist1h3b
P62806	Hist1h4a
Q9CX86	Hnrnpa0
O88569	Hnrnpa2b1
Q9Z204	Hnrnpc
Q9Z2X1	Hnrnpf
G3XA10	Hnrnpu
P07901	Hsp90aa1
P11499	Hsp90ab1
P38647	Hspa9
P63038	Hspd1
Q64433	Hspe1
Q8BU30	Iars
Q9ESY9	Ifi30
G5E8F1	Itgam
Q542I8	Itgb2
O89051	Itm2b
P70168	Kpn1b1
Q61792	Lasp1
Q07797	Lgals3bp
P48678	Lmna
P14733	Lmn1b1
P11152	Lpl
O88188	Ly86

Uniprot ID	Gene name
Q61074	Ppm1g
P58389	Ppp2r4
O88531	Ppt1
Q99KP6	Prpf19
E9P200	Psap
P62192	Psmc1
P46471	Psmc2
P54775	Psmc4
P62196	Psmc5
P62334	Psmc6
Q3TXS7	Psm1d1
Q8BG32	Psm1d11
Q9D8W5	Psm1d12
Q9WVJ2	Psm1d13
Q8VDM4	Psm2d2
P14685	Psm3d3
O35226	Psm4d4
Q99JI4	Psm6d6
P26516	Psm7d7
Q8BGJ5	Ptbp1
P29351	Ptpn6
Q60972	Rbbp4
O89086	Rbm3
Q91VM5	Rbm1x11
Q8BK67	Rcc2
Q91VI7	Rnh1
P62983	Rps27a
P60122	Ruvbl1
P07091	S100a4
P14069	S100a6
P32020	Scp2
Q920A5	Scpep1
O35988	Sdc4
Q3TMX0	Sdcbp
Q61112	Sdf4
P17563	Selenbp1
Q8K4Z5	Sf3a1
G5E866	Sf3b1
Q921M3	Sf3b3

Q9WUM4	Coro1c	P08905	Lyz2	Q8VIJ6	Sfpq
O88668	Creg1	O09159	Man2b1	Q8BJU0	Sgta
P09581	Csf1r	P31938	Map2k1	Q78PY7	Snd1
P21460	Cst3	Q3THS6	Mat2a	Q78ZM0	Snx3
P10605	Ctsb	Q8K310	Matr3	P13609	Srgn
P97821	Ctsc	P08249	Mdh2	Q6PDM2	Srsf1
P06797	Ctsl1	Q922D8	Mthfd1	P84104	Srsf3
O70370	Ctss	Q9QWR8	Naga	Q8BH40	Stx7
Q9WUU7	Ctsz	Q99J77	Nans	P40142	Tkt
D3YW23	Cxcl10	Q78ZA7	Nap1l4	P06804	Tnf
P10889	Cxcl2	P09405	Ncl	O89023	Tpp1
Q922B2	Dars	Q9D0T1	Nhp2l1	Q99NH8	Trem2
Q62418	Dbnl	Q99K48	Nono	Q62318	Trim28
A2ADY9	Ddi2	Q9Z0J0	Npc2	Q9Z0P5	Twf2
Q9Z1N5	Ddx39b	Q02819	Nucb1	E9PXX7	Txndc5
Q61656	Ddx5	Q9CZ30	Ola1	Q8CDN6	Txnl1
P00375	Dhfr	Q62422	Ostf1	Q02053	Uba1
O35286	Dhx15	Q7TQI3	Otub1	Q9Z1F9	Uba2
O70133	Dhx9	Q921K2	Parp1	Q9JKB1	Uchl3
Q8C255	Dpep2	P12382	Pfkl	Q9Z1Z0	Uso1
Q9JHU4	Dync1h1	Q61753	Phgdh	Q9JMA1	Usp14
Q61508	Ecm1	E9QPE8	Plec	Q3U4W8	Usp5
Q9QZD9	Eif3i	Q9R0E2	Plod1	P20152	Vim
Q8CGC7	Eprs	P55065	Pltp	Q9EQH3	Vps35
P19096	Fasn	Q9CR16	Ppid		

APPENDIX 6: PHF8-G9a COMMON SECRETOME

Uniprot ID	Protein Name	Gene Name	Uniprot ID	Protein Name	Gene Name
P10404	ENV1	2	Q9DBH5	LMAN2	Lman2
Q80UG5-2	SEPT9	42256	P48678	LMNA	Lmna
Q8C1B7-3	SEP11	42258	P11152	LIPL	Lpl
Q91V92	ACLY	Acly	Q91ZX7	LRP1	Lrp1
P28271	ACOC	Aco1	E9PX73	E9PX73	Ly9
Q99KI0	ACON	Aco2	P17897	LYZ1	Lyz1
Q91V12-2	BACH	Acot7	O09159	MA2B1	Man2b1
P60710	ACTB	Actb	Q3THS6	METK2	Mat2a
J3QNB3	J3QNB3	Adam17	P97310	MCM2	Mcm2
Q64191	ASPG	Aga	P08249	MDHM	Mdh2
P50247	SAHH	Ahcy	Q8VE43	METRL	Metrnl
E9Q616	E9Q616	Ahnak	E9PVX6	E9PVX6	Mki67
Q8BK64	AHSA1	Ahsa1	Q922D8	C1TC	Mthfd1

Q9JII6	AK1A1	Akr1a1
P45376	ALDR	Akr1b1
E9Q4G8	E9Q4G8	Alcam
Q9JLJ2	AL9A1	Aldh9a1
P97822-2	AN32E	Anp32e
P07356	ANXA2	Anxa2
Q60709	Q60709	Aplp2
P12023	A4	App
Q99PT1	GDIR1	Arhgdia
P59999	ARPC4	Arpc4
Q61024	ASNS	Asns
O08997	ATOX1	Atox1
Q9CYN9	RENr	Atp6ap2
P50516	VATA	Atp6v1a
P01887	B2MG	B2m
Q09200	B4GN1	B4galnt1
Q9JMK0	B4GT5	B4galt5
O54962	BAF	Banf1
Q07813	BAX	Bax
Q9CY64	BIEA	Blvra
Q8BGS2-2	BOLA2	Bola2
Q9Z0S1	BPNT1	Bpnt1
P01027	CO3	C3
Q9CXW3	CYBP	Cacybp
Q6ZQ38	CAND1	Cand1
Q60865	CAPR1	Caprin1
P47757-2	CAPZB	Capzb
Q9ER72	SYCC	Cars
Q9DCC5	Q9DCC5	Cbx3
P10148	CCL2	Ccl2
O88430	CCL22	Ccl22
P10855	CCL3	Ccl3
P14097	CCL4	Ccl4
P30882	CCL5	Ccl5
P51670	CCL9	Ccl9
P42932	TCPQ	Cct8
P10810	CD14	Cd14
P15379-2	CD44	Cd44
P04441	HG2A	Cd74
P40240	CD9	Cd9
Q4VAA2	CDV3	Cdv3
P04186	CFAB	Cfb
P06909	CFAH	Cfh
P11680	PROP	Cfp

Q9JK81	MYG1	Myg1
Q60817	NACA	Naca
Q9QWR8	NAGAB	Naga
Q8VEJ4	NLE1	Nle1
Q99K48	NONO	Nono
Q9Z0J0	NPC2	Npc2
E9Q039	E9Q039	Npepps
A6PWC3	A6PWC3	Nrd1
O35375-5	NRP2	Nrp2
Q02819	NUCB1	Nucb1
O35685	NUDC	Nudc
Q9JKX6	NUDT5	Nudt5
E9Q7G0	E9Q7G0	Numa1
Q7TQI3	OTUB1	Otub1
Q8CIN4	PAK2	Pak2
P60335	PCBP1	Pcbp1
P23506	PIMT	Pcmt1
Q9WU78	PDC6I	Pdcd6ip
Q8C605	Q8C605	Pfkip
Q8BG07-2	PLD4	Pld4
E9QPE8	E9QPE8	Plec
Q9R0E2	PLOD1	Plod1
Q9R0B9	PLOD2	Plod2
Q9R0E1	PLOD3	Plod3
Q99K51	PLST	Pls3
P55065	PLTP	Pltp
B2RXS4	PLXB2	Plxbn2
Q9D819	IPYR	Ppa1
P30412	PPIC	Ppic
Q9CR16	PPID	Ppid
Q61074	PPM1G	Ppm1g
P97470	PP4C	Ppp4c
P35700	PRDX1	Prdx1
Q61171	PRDX2	Prdx2
O08807	PRDX4	Prdx4
O08795	GLU2B	Prkcsh
Q9JIF0-2	ANM1	Prmt1
Q64695	EPCR	Procr
Q08761	PROS	Pros1
G3UXL2	G3UXL2	Prps1l3
Q99K85	SERC	Psat1
Q9QUM9	PSA6	Psma6
O55234	PSB5	Psmb5
Q60692	PSB6	Psmb6

Q9Z1Q5	CLIC1	Clic1
Q3UMW8	CLN5	Cln5
B1AWE0	B1AWE0	Clta
Q68FD5	CLH1	Cltc
P53996-2	CNBP	Cnbp
Q8CIE6	COPA	Copa
O35864	CSN5	Cops5
O89053	COR1A	Coro1a
Q9WUM4	COR1C	Coro1c
G3X9T8	G3X9T8	Cp
Q9ERK4	XPO2	Cse1l
P07141	CSF1	Csf1
P09920	CSF3	Csf3
P21460	CYTC	Cst3
Q62426	CYTB	Cstb
Q8R242-2	DIAC	Ctbs
Q9CWL8	CTBL1	Ctnnbl1
P70698	PYRG1	Ctps1
P10605	CATB	Ctsb
P97821	CATC	Ctsc
P18242	CATD	Ctsd
Q9R013	CATF	Ctsf
P06797	CATL1	Ctsl
Q9WUU7	CATZ	Ctsz
D3YW23	D3YW23	Cxcl10
I7HIQ2	I7HIQ2	Cxcl16
P10889	CXCL2	Cxcl2
Q7TMB8	CYFP1	Cyfip1
Q922B2	SYDC	Dars
D3YX34	D3YX34	Dctn1
Q8VDW0	DX39A	Ddx39a
Q9Z1N5	DX39B	Ddx39b
Q61656	DDX5	Ddx5
O35286	DHX15	Dhx15
Q91YW3	DNJC3	Dnajc3
Q6NZB0	DNJC8	Dnajc8
Q8C255	DPEP2	Dpep2
Q91WV0	NC2B	Dr1
P62627	DLRB1	Dynlrb1
Q61508	ECM1	Ecm1
P10126	EF1A1	Eef1a1
E9QN08	E9QN08	Eef1d
Q9D8N0	EF1G	Eef1g
Q8C845	Q8C845	Efh1d2

P62334	PRS10	Psmc6
Q3TXS7	PSMD1	Psm1d1
Q8BG32	PSD11	Psm1d11
Q9D8W5	PSD12	Psm1d12
Q9WVJ2	PSD13	Psm1d13
Q8VDM4	PSMD2	Psm2d1
O35226	PSMD4	Psm4d1
Q99LS3	SERB	Psph
Q9R0Q7	TEBP	Ptges3
B0V2N1-6	PTPRS	Ptprs
Q9JKF6	PVRL1	Pvrl1
P63001	RAC1	Rac1
Q05144	RAC2	Rac2
P62827	RAN	Ran
P34022	RANG	Ranbp1
P46061	RAGP1	Rangap1
Q9D0I9	SYRC	Rars
Q60972	RBBP4	Rbbp4
A2AFJ1	A2AFJ1	Rbbp7
O89086	RBM3	Rbm3
E9Q7W0	E9Q7W0	Rbpj
Q8VE37	RCC1	Rcc1
Q8BK67	RCC2	Rcc2
Q9CQ01	RNT2	Rnaset2
Q91VI7	RINI	Rnh1
P47968	RPIA	Rpia
P47963	RL13	Rpl13
P62717	RL18A	Rpl18a
P67984	RL22	Rpl22
P62830	RL23	Rpl23
E9Q132	E9Q132	Rpl24
P61255	RL26	Rpl26
P61358	RL27	Rpl27
P41105	RL28	Rpl28
P62900	RL31	Rpl31
Q9D1R9	RL34	Rpl34
Q9JJI8	RL38	Rpl38
P14148	RL7	Rpl7
P62918	RL8	Rpl8
G3UW34	G3UW34	Rpl9-ps6
P62281	RS11	Rps11
P62245	RS15A	Rps15a
P14131	RS16	Rps16
P62267	RS23	Rps23

Q9EQP2	EHD4	Ehd4
Q8BMJ3	IF1AX	Eif1ax
Q8R1B4	EIF3C	Eif3c
O70194	EIF3D	Eif3d
Q9DCH4	EIF3F	Eif3f
Q9Z1D1	EIF3G	Eif3g
Q9QZD9	EIF3I	Eif3i
Q9DBZ5	EIF3K	Eif3k
Q8QZY1	EIF3L	Eif3l
Q99JX4	EIF3M	Eif3m
P60843	IF4A1	Eif4a1
A2AFK7	A2AFK7	Eif4a3
Q8BGD9	IF4B	Eif4b
P63073	IF4E	Eif4e
P70445	4EBP2	Eif4ebp2
Q9WUK2-2	IF4H	Eif4h
P70372	ELAV1	Elavl1
P17182	ENOA	Eno1
Q8CGC7	SYEP	Eprs
Q9EQH2	ERAP1	Erap1
H3BLJ9	H3BLJ9	Esd
Q8R1F1	NIBL1	Fam129b
Q9WUA2	SYFB	Farsb
Q920E5	FPPS	Fdps
Q9R059	FHL3	Fhl3
Q62446	FKBP3	Fkbp3
B7FAU9	B7FAU9	Flna
Q80X90	FLNB	Flnb
Q3TUE1	Q3TUE1	Fubp1
P23188	FURIN	Furin
Q8BHN3	GANAB	Ganab
P16858	G3P	Gapdh
B1ATI9	B1ATI9	Gas7
P17439	GLCM	Gba
Q9CPV4	GLOD4	Glod4
D3Z1D6	D3Z1D6	Gm10335
L7N202	L7N202	Gm16477
Q3THK7	GUAA	Gmps
P05202	AATM	Got2
P28798	GRN	Grn
Q8R050-2	ERF3A	Gspt1
P10922	H10	H1f0
P01899	HA11	H2-D1
P01900	HA12	H2-D1

P62852	RS25	Rps25
P62855	RS26	Rps26
Q9WTM5	RUVB2	Ruvbl2
P50543	S10AB	S100a11
P07091	S10A4	S100a4
P14069	S10A6	S100a6
O35988	SDC4	Sdc4
Q9D1M0	SEC13	Sec13
P17563	SBP1	Selenbp1
Q62178	SEM4A	Sema4a
O09126	SEM4D	Sema4d
Q9CY58	PAIRB	Serbp1
Q60854	SPB6	Serpinb6
P22777	PAI1	Serpine1
E9Q4Q2	E9Q4Q2	Sf1
D3YW09	D3YW09	Sf3a2
Q9D554	SF3A3	Sf3a3
G5E866	G5E866	Sf3b1
Q8VIJ6	SFPQ	Sfpq
Q91VW3	SH3L3	Sh3bgrl3
Q9D7I0	SHSA5	Shisa5
Q9CZN7	Q9CZN7	Shmt2
Q9EPK6	SIL1	Sil1
Q6P6I8	Q6P6I8	Sirpa
E9Q748	E9Q748	Slpi
Q3UKJ7	SMU1	Smu1
Q62189	SNRPA	Snrpa
P62305	RUXE	Snrpe
O88307	SORL	Sorl1
Q148R4	Q148R4	Spink5
P10923	OSTP	Spp1
Q64337	SQSTM	Sqstm1
P13609	SRGN	Srgn
Q64674	SPEE	Srm
Q99MR6-3	SRRT	Srrt
Q6PDM2	SRSF1	Srsf1
Q62093	SRSF2	Srsf2
Q60864	STIP1	Stip1
P11031	TCP4	Sub1
Q9CX34	SUGT1	Sugt1
H7BWX9	H7BWX9	Sumo2
G3X956	G3X956	Supt16
Q93092	TALDO	Taldo1
P48428	TBCA	Tbca

P01902	HA1D	H2-K1
P01897	HA1L	H2-L
Q8HWP2	Q8HWP2	H2-Q4
P06339	HA15	H2-T23
Q9QZQ8-2	H2AY	H2afy
P70349	HINT1	Hint1
P15864	H12	Hist1h1c
P43274	H14	Hist1h1e
P84228	H32	Hist1h3b
P30681	HMGB2	Hmgb2
P97825	HN1	Hn1
P11499	HS90B	Hsp90ab1
Q8BM72	HSP13	Hspa13
P63017	HSP7C	Hspa8
Q64433	CH10	Hspe1
Q61699-2	HS105	Hsph1
Q8BU30	SYIC	Iars
P13597-2	ICAM1	Icam1
Q9JHJ8	ICOSL	Icoslg
F6RPJ9	F6RPJ9	Ide
P58044	IDI1	Idi1
P01575	IFNB	Ifnb1
Q3TBV5	Q3TBV5	Il1rn
B0QZX1	B0QZX1	Il2rg
O09046	OXLA	Il4i1
P08505	IL6	Il6
P24547	IMDH2	Impdh2
Q9JKF1	IQGA1	Iqgap1
Q54218	Q54218	Itgb2
O89051	ITM2B	Itm2b
Q99MN1	SYK	Kars
Q6WVG3	KCD12	Kctd12
G3UZG5	G3UZG5	Klhdc4
F8VQJ3	F8VQJ3	Lamc1
Q61792	LASP1	Lasp1
P11672	NGAL	Lcn2
P35951	LDLR	Ldlr
P16045	LEG1	Lgals1
Q8C253	Q8C253	Lgals3
P09056	LIF	Lif
Q64281-2	LIRB4	Lilrb4

P10711	TCEA1	Tcea1
Q62351	TFR1	Tfrc
P04202	TGFB1	Tgfb1
P62075	TIM13	Timm13
P26039	TLN1	Tln1
Q80YX1-2	TENA	Tnc
P06804	TNFA	Tnf
P25119	TNR1B	Tnfrsf1b
P41274	TNFL9	Tnfsf9
Q8BFY9-2	TNPO1	Tnp01
Q9ER38	TOR3A	Tor3a
Q64514-2	TPP2	Tpp2
Q7M739	Q7M739	Tpr
P63028	TCTP	Tpt1
Q99NH8	TREM2	Trem2
Q62318	TIF1B	Trim28
Q9DCG9	TR112	Trmt112
Q62348	TSN	Tsn
P05213	TBA1B	Tuba1b
P68373	TBA1C	Tuba1c
P99024	TBB5	Tubb5
Q922F4	TBB6	Tubb6
Q80X50-2	UBP2L	Ubap2l
P61087	UBE2K	Ube2k
F7CDT0	F7CDT0	Ube2m
Q8R317	UBQL1	Ubqln1
Q9Z1Z0-4	USO1	Uso1
Q9JMA1	UBP14	Usp14
P20152	VIME	Vim
D3YYD5	D3YYD5	Vps29
Q9EQH3	VPS35	Vps35
P61965	WDR5	Wdr5
Q91WQ3	SYYC	Yars
Q9JKB3-2	YBOX3	Ybx3
P61982	1433G	Ywhag
P68510	1433F	Ywhah
P63101	1433Z	Ywhaz
G5E8F1	G5E8F1	
Q3TMX0	Q3TMX0	
Q3TUJ9	Q3TUJ9	

REFERENCES

- Adcock IM, Tsaprouni L, Bhavsar P, Ito K (2007) Epigenetic regulation of airway inflammation. *Curr Opin Immunol* **19**: 694-700
- Adenuga D, Rahman I (2010) Protein kinase CK2-mediated phosphorylation of HDAC2 regulates co-repressor formation, deacetylase activity and acetylation of HDAC2 by cigarette smoke and aldehydes. *Arch Biochem Biophys* **498**: 62-73
- Adib-Conquy M, Adrie C, Moine P, Asehnoune K, Fitting C, Pinsky MR, Dhainaut JF, Cavaillon JM (2000) NF-kappaB expression in mononuclear cells of patients with sepsis resembles that observed in lipopolysaccharide tolerance. *Am J Respir Crit Care Med* **162**: 1877-1883
- Agrawal S, Kishore MC (2000) MHC class I gene expression and regulation. *J Hematother Stem Cell Res* **9**: 795-812
- Akashi S, Shimazu R, Ogata H, Nagai Y, Takeda K, Kimoto M, Miyake K (2000) Cutting edge: cell surface expression and lipopolysaccharide signaling via the toll-like receptor 4-MD-2 complex on mouse peritoneal macrophages. *J Immunol* **164**: 3471-3475
- Akira S, Takeda K (2004) Toll-like receptor signalling. *Nature Reviews Immunology* **4**: 499-511
- Akira S, Uematsu S, Takeuchi O (2006) Pathogen recognition and innate immunity. *Cell* **124**: 783-801
- Amsen D, de Visser KE, Town T (2009) Approaches to determine expression of inflammatory cytokines. *Methods Mol Biol* **511**: 107-142
- Anderson NL, Anderson NG (2002) The human plasma proteome: history, character, and diagnostic prospects. *Mol Cell Proteomics* **1**: 845-867
- Arnaudo AM, Garcia BA (2013) Proteomic characterization of novel histone post-translational modifications. *Epigenetics Chromatin* **6**: 24
- Artal-Martinez de Narvajas A, Gomez TS, Zhang JS, Mann AO, Taoda Y, Gorman JA, Herreros-Villanueva M, Gress TM, Ellenrieder V, Bujanda L, Kim DH, Kozikowski AP, Koenig A, Billadeau DD (2013) Epigenetic regulation of autophagy by the methyltransferase G9a. *Mol Cell Biol* **33**: 3983-3993
- Arteaga MF, Mikesch JH, Qiu J, Christensen J, Helin K, Kogan SC, Dong S, So CW (2013) The histone demethylase PHF8 governs retinoic acid response in acute promyelocytic leukemia. *Cancer Cell* **23**: 376-389

Asensio-Juan E, Gallego C, Martinez-Balbas MA (2012) The histone demethylase PHF8 is essential for cytoskeleton dynamics. *Nucleic Acids Res* **40**: 9429-9440

Ashburner BP, Westerheide SD, Baldwin AS (2001) The p65 (RelA) subunit of NF-kappaB interacts with the histone deacetylase (HDAC) corepressors HDAC1 and HDAC2 to negatively regulate gene expression. *Mol Cell Biol* **21**: 7065-7077

Aung HT, Schroder K, Himes SR, Brion K, van Zuylen W, Trieu A, Suzuki H, Hayashizaki Y, Hume DA, Sweet MJ, Ravasi T (2006) LPS regulates proinflammatory gene expression in macrophages by altering histone deacetylase expression. *FASEB J* **20**: 1315-1327

Bannister AJ, Kouzarides T (2011) Regulation of chromatin by histone modifications. *Cell Res* **21**: 381-395

Barber SA, Perera PY, McNally R, Vogel SN (1995) The serine/threonine phosphatase inhibitor, calyculin A, inhibits and dissociates macrophage responses to lipopolysaccharide. *J Immunol* **155**: 1404-1410

Barisic S, Strozyk E, Peters N, Walczak H, Kulms D (2008) Identification of PP2A as a crucial regulator of the NF-kappaB feedback loop: its inhibition by UVB turns NF-kappaB into a pro-apoptotic factor. *Cell Death Differ* **15**: 1681-1690

Barnes PJ (2009) Targeting the epigenome in the treatment of asthma and chronic obstructive pulmonary disease. *Proc Am Thorac Soc* **6**: 693-696

Barski A, Cuddapah S, Cui K, Roh TY, Schones DE, Wang Z, Wei G, Chepelev I, Zhao K (2007) High-resolution profiling of histone methylations in the human genome. *Cell* **129**: 823-837

Bauerfeld CP, Rastogi R, Pirockinaite G, Lee I, Hüttemann M, Monks B, Birnbaum MJ, Franchi L, Nuñez G, Samavati L (2012) TLR4-mediated AKT activation is MyD88/TRIF dependent and critical for induction of oxidative phosphorylation and mitochondrial transcription factor A in murine macrophages. *J Immunol* **188**: 2847-2857

Bayarsaihan D (2011) Epigenetic mechanisms in inflammation. *J Dent Res* **90**: 9-17

Bell JK, Botos I, Hall PR, Askins J, Shiloach J, Segal DM, Davies DR (2005) The molecular structure of the Toll-like receptor 3 ligand-binding domain. *Proc Natl Acad Sci U S A* **102**: 10976-10980

Berlato C, Cassatella MA, Kinjyo I, Gatto L, Yoshimura A, Bazzoni F (2002) Involvement of suppressor of cytokine signaling-3 as a mediator of the inhibitory effects of IL-10 on lipopolysaccharide-induced macrophage activation. *J Immunol* **168**: 6404-6411

Beutler B, Milsark IW, Cerami AC (1985) Passive immunization against cachectin/tumor necrosis factor protects mice from lethal effect of endotoxin. *Science* **229**: 869-871

Biel M, Wascholowski V, Giannis A (2005) Epigenetics--an epicenter of gene regulation: histones and histone-modifying enzymes. *Angew Chem Int Ed Engl* **44**: 3186-3216

Bierne H, Hamon M, Cossart P (2012) Epigenetics and bacterial infections. *Cold Spring Harb Perspect Med* **2**: a010272

Billiau A (1995) Interferon beta in the cytokine network: an anti-inflammatory pathway. *Mult Scler* **1 Suppl 1**: S2-4

Biswas SK, Tergaonkar V (2007) Myeloid differentiation factor 88-independent Toll-like receptor pathway: Sustaining inflammation or promoting tolerance? *Int J Biochem Cell Biol* **39**: 1582-1592

Björkman M, Östling P, Härmä V, Virtanen J, Mpindi JP, Rantala J, Mirtti T, Vesterinen T, Lundin M, Sankila A, Rannikko A, Kaivanto E, Kohonen P, Kallioniemi O, Nees M (2012) Systematic knockdown of epigenetic enzymes identifies a novel histone demethylase PHF8 overexpressed in prostate cancer with an impact on cell proliferation, migration and invasion. *Oncogene* **31**: 3444-3456

Bohuslav J, Chen LF, Kwon H, Mu Y, Greene WC (2004) p53 induces NF-kappaB activation by an IkappaB kinase-independent mechanism involving phosphorylation of p65 by ribosomal S6 kinase 1. *J Biol Chem* **279**: 26115-26125

Botos I, Segal DM, Davies DR (2011) The structural biology of Toll-like receptors. *Structure* **19**: 447-459

Bracaglia G, Conca B, Bergo A, Rusconi L, Zhou Z, Greenberg ME, Landsberger N, Soddu S, Kilstrup-Nielsen C (2009) Methyl-CpG-binding protein 2 is phosphorylated by homeodomain-interacting protein kinase 2 and contributes to apoptosis. *EMBO Rep* **10**: 1327-1333

Burns K, Janssens S, Brissoni B, Olivos N, Beyaert R, Tschopp J (2003) Inhibition of interleukin 1 receptor/Toll-like receptor signaling through the alternatively spliced, short form of MyD88 is due to its failure to recruit IRAK-4. *J Exp Med* **197**: 263-268

Buss H, Dörrie A, Schmitz ML, Frank R, Livingstone M, Resch K, Kracht M (2004) Phosphorylation of serine 468 by GSK-3beta negatively regulates basal p65 NF-kappaB activity. *J Biol Chem* **279**: 49571-49574

Carroll MC (2004) The complement system in regulation of adaptive immunity. *Nat Immunol* **5**: 981-986

Casciello F, Windloch K, Gannon F, Lee JS (2015) Functional Role of G9a Histone Methyltransferase in Cancer. *Front Immunol* **6**: 487

Chan C, Li L, McCall CE, Yoza BK (2005) Endotoxin tolerance disrupts chromatin remodeling and NF-kappaB transactivation at the IL-1beta promoter. *J Immunol* **175**: 461-468

Chang Y, Ganesh T, Horton JR, Spannhoff A, Liu J, Sun A, Zhang X, Bedford MT, Shinkai Y, Snyder JP, Cheng X (2010) Adding a lysine mimic in the design of potent inhibitors of histone lysine methyltransferases. *J Mol Biol* **400**: 1-7

Chen MW, Hua KT, Kao HJ, Chi CC, Wei LH, Johansson G, Shiah SG, Chen PS, Jeng YM, Cheng TY, Lai TC, Chang JS, Jan YH, Chien MH, Yang CJ, Huang MS, Hsiao M, Kuo ML (2010) H3K9 histone methyltransferase G9a promotes lung cancer invasion and metastasis by silencing the cell adhesion molecule Ep-CAM. *Cancer Res* **70**: 7830-7840

Chen X, El Gazzar M, Yoza BK, McCall CE (2009) The NF-kappaB factor RelB and histone H3 lysine methyltransferase G9a directly interact to generate epigenetic silencing in endotoxin tolerance. *J Biol Chem* **284**: 27857-27865

Chin HG, Estève PO, Pradhan M, Benner J, Patnaik D, Carey MF, Pradhan S (2007) Automethylation of G9a and its implication in wider substrate specificity and HP1 binding. *Nucleic Acids Res* **35**: 7313-7323

Chin HG, Pradhan M, Estève PO, Patnaik D, Evans TC, Pradhan S (2005) Sequence specificity and role of proximal amino acids of the histone H3 tail on catalysis of murine G9A lysine 9 histone H3 methyltransferase. *Biochemistry* **44**: 12998-13006

Christensen J, Agger K, Cloos PA, Pasini D, Rose S, Sennels L, Rappsilber J, Hansen KH, Salcini AE, Helin K (2007) RBP2 belongs to a family of demethylases, specific for tri- and dimethylated lysine 4 on histone 3. *Cell* **128**: 1063-1076

Clifton IJ, McDonough MA, Ehrismann D, Kershaw NJ, Granatino N, Schofield CJ (2006) Structural studies on 2-oxoglutarate oxygenases and related double-stranded beta-helix fold proteins. *J Inorg Biochem* **100**: 644-669

Conus S, Simon HU (2010) Cathepsins and their involvement in immune responses. *Swiss Med Wkly* **140**: w13042

Cox J, Mann M (2008) MaxQuant enables high peptide identification rates, individualized p.p.b.-range mass accuracies and proteome-wide protein quantification. *Nat Biotechnol* **26**: 1367-1372

Cox J, Neuhauser N, Michalski A, Scheltema RA, Olsen JV, Mann M (2011) Andromeda: a peptide search engine integrated into the MaxQuant environment. *J Proteome Res* **10**: 1794-1805

Das M, Prasad SB, Yadav SS, Govardhan HB, Pandey LK, Singh S, Pradhan S, Narayan G (2013) Over expression of minichromosome maintenance genes is clinically correlated to cervical carcinogenesis. *PLoS One* **8**: e69607

De Santa F, Narang V, Yap ZH, Tusi BK, Burgold T, Austenaa L, Bucci G, Caganova M, Notarbartolo S, Casola S, Testa G, Sung WK, Wei CL, Natoli G (2009) Jmjd3 contributes to the control of gene expression in LPS-activated macrophages. *EMBO J* **28**: 3341-3352

De Santa F, Totaro MG, Prosperini E, Notarbartolo S, Testa G, Natoli G (2007) The histone H3 lysine-27 demethylase Jmjd3 links inflammation to inhibition of polycomb-mediated gene silencing. *Cell* **130**: 1083-1094

Delom F, Chevet E (2006) Phosphoprotein analysis: from proteins to proteomes. *Proteome Sci* **4**: 15

DiDonato JA, Hayakawa M, Rothwarf DM, Zandi E, Karin M (1997) A cytokine-responsive IkappaB kinase that activates the transcription factor NF-kappaB. *Nature* **388**: 548-554

Dobrovolskaia MA, Vogel SN (2002) Toll receptors, CD14, and macrophage activation and deactivation by LPS. *Microbes Infect* **4**: 903-914

Dong C, Wu Y, Yao J, Wang Y, Yu Y, Rychahou PG, Evers BM, Zhou BP (2012) G9a interacts with Snail and is critical for Snail-mediated E-cadherin repression in human breast cancer. *J Clin Invest* **122**: 1469-1486

Dong KB, Maksakova IA, Mohn F, Leung D, Appanah R, Lee S, Yang HW, Lam LL, Mager DL, Schübeler D, Tachibana M, Shinkai Y, Lorincz MC (2008) DNA methylation in ES cells requires the lysine methyltransferase G9a but not its catalytic activity. *EMBO J* **27**: 2691-2701

Duran A, Diaz-Meco MT, Moscat J (2003) Essential role of RelA Ser311 phosphorylation by zetaPKC in NF-kappaB transcriptional activation. *EMBO J* **22**: 3910-3918

Eichelbaum K, Winter M, Berriel Diaz M, Herzig S, Krijgsveld J (2012) Selective enrichment of newly synthesized proteins for quantitative secretome analysis. *Nat Biotechnol* **30**: 984-990

El Gazzar M, Yoza BK, Chen X, Hu J, Hawkins GA, McCall CE (2008) G9a and HP1 couple histone and DNA methylation to TNFalpha transcription silencing during endotoxin tolerance. *J Biol Chem* **283**: 32198-32208

El Gazzar M, Yoza BK, Hu JY, Cousart SL, McCall CE (2007) Epigenetic silencing of tumor necrosis factor alpha during endotoxin tolerance. *J Biol Chem* **282**: 26857-26864

Erdoğan Ö, Xie L, Wang L, Wu B, Kong Q, Wan Y, Chen X (2016) Proteomic dissection of LPS-inducible, PHF8-dependent secretome reveals novel roles of PHF8 in TLR4-induced acute inflammation and T cell proliferation. *Sci Rep* **6**: 24833

Falkenberg KJ, Johnstone RW (2014) Histone deacetylases and their inhibitors in cancer, neurological diseases and immune disorders. *Nat Rev Drug Discov* **13**: 673-691

Fang TC, Schaefer U, Mecklenbrauker I, Stienen A, Dewell S, Chen MS, Rioja I, Parravicini V, Prinjha RK, Chandwani R, MacDonald MR, Lee K, Rice CM, Tarakhovsky A (2012) Histone H3 lysine 9 di-methylation as an epigenetic signature of the interferon response. *J Exp Med* **209**: 661-669

Feng W, Yonezawa M, Ye J, Jenuwein T, Grummt I (2010) PHF8 activates transcription of rRNA genes through H3K4me3 binding and H3K9me1/2 demethylation. *Nat Struct Mol Biol* **17**: 445-450

Fernández Do Porto DA, Jurado JO, Pasquinelli V, Alvarez IB, Aspera RH, Musella RM, García VE (2012) CD137 differentially regulates innate and adaptive immunity against *Mycobacterium tuberculosis*. *Immunol Cell Biol* **90**: 449-456

Fortschegger K, de Graaf P, Outchkourov NS, van Schaik FM, Timmers HT, Shiekhataar R (2010) PHF8 targets histone methylation and RNA polymerase II to activate transcription. *Mol Cell Biol* **30**: 3286-3298

Foster SL, Hargreaves DC, Medzhitov R (2007) Gene-specific control of inflammation by TLR-induced chromatin modifications. *Nature* **447**: 972-978

Fradet-Turcotte A, Canny MD, Escribano-Díaz C, Orthwein A, Leung CC, Huang H, Landry MC, Kitevski-LeBlanc J, Noordermeer SM, Sicheri F, Durocher D (2013) 53BP1 is a reader of the DNA-damage-induced H2A Lys 15 ubiquitin mark. *Nature* **499**: 50-54

Frank PG, Lisanti MP (2008) ICAM-1: role in inflammation and in the regulation of vascular permeability. *Am J Physiol Heart Circ Physiol* **295**: H926-H927

Fujihara M, Muroi M, Tanamoto K, Suzuki T, Azuma H, Ikeda H (2003) Molecular mechanisms of macrophage activation and deactivation by lipopolysaccharide: roles of the receptor complex. *Pharmacol Ther* **100**: 171-194

Fujihara M, Wakamoto S, Ito T, Muroi M, Suzuki T, Ikeda H, Ikebuchi K (2000) Lipopolysaccharide-triggered desensitization of TNF- α mRNA expression involves lack of phosphorylation of I κ B α in a murine macrophage-like cell line, P388D1. *J Leukoc Biol* **68**: 267-276

Fujimaki K, Ogihara T, Morris DL, Oda H, Iida H, Fujitani Y, Mirmira RG, Evans-Molina C, Watada H (2015) Set7/9 Regulates Cytokine-Induced Expression of Inducible Nitric

Oxide Synthase Through Methylation of Lysine 4 at Histone 3 in the Islet β cell. *J Biol Chem*

Gibbons RJ (2005) Histone modifying and chromatin remodelling enzymes in cancer and dysplastic syndromes. *Hum Mol Genet* **14 Spec No 1**: R85-92

Gilmore TD (2006) Introduction to NF-kappaB: players, pathways, perspectives. *Oncogene* **25**: 6680-6684

Gitter BD, Boggs LN, May PC, Czilli DL, Carlson CD (2000) Regulation of cytokine secretion and amyloid precursor protein processing by proinflammatory amyloid beta (A beta). *Ann N Y Acad Sci* **917**: 154-164

Goodarzi AA, Jonnalagadda JC, Douglas P, Young D, Ye R, Moorhead GB, Lees-Miller SP, Khanna KK (2004) Autophosphorylation of ataxia-telangiectasia mutated is regulated by protein phosphatase 2A. *EMBO J* **23**: 4451-4461

Goshe MB (2006) Characterizing phosphoproteins and phosphoproteomes using mass spectrometry. *Brief Funct Genomic Proteomic* **4**: 363-376

Grégoire C, Chasson L, Luci C, Tomasello E, Geissmann F, Vivier E, Walzer T (2007) The trafficking of natural killer cells. *Immunol Rev* **220**: 169-182

Grønborg M, Kristiansen TZ, Iwahori A, Chang R, Reddy R, Sato N, Molina H, Jensen ON, Hruban RH, Goggins MG, Maitra A, Pandey A (2006) Biomarker discovery from pancreatic cancer secretome using a differential proteomic approach. *Mol Cell Proteomics* **5**: 157-171

Gyory I, Wu J, Fejér G, Seto E, Wright KL (2004) PRDI-BF1 recruits the histone H3 methyltransferase G9a in transcriptional silencing. *Nat Immunol* **5**: 299-308

Götte M (2003) Syndecans in inflammation. *FASEB J* **17**: 575-591

Hamon MA, Cossart P (2008) Histone modifications and chromatin remodeling during bacterial infections. *Cell Host Microbe* **4**: 100-109

Han Q, Yang P, Wu Y, Meng S, Sui L, Zhang L, Yu L, Tang Y, Jiang H, Xuan D, Kaplan DL, Kim SH, Tu Q, Chen J (2015) Epigenetically Modified Bone Marrow Stromal Cells (BMSCs) in Silk Scaffolds Promote Craniofacial Bone Repair and Wound Healing. *Tissue Eng Part A*

Hanzu FA, Musri MM, Sánchez-Herrero A, Claret M, Esteban Y, Kaliman P, Gomis R, Párrizas M (2013) Histone demethylase KDM1A represses inflammatory gene expression in preadipocytes. *Obesity (Silver Spring)* **21**: E616-625

- Harberts E, Gaspari AA (2013) TLR signaling and DNA repair: are they associated? *J Invest Dermatol* **133**: 296-302
- Harburger DS, Calderwood DA (2009) Integrin signalling at a glance. *J Cell Sci* **122**: 159-163
- Hathout Y (2007) Approaches to the study of the cell secretome. *Expert Rev Proteomics* **4**: 239-248
- Hayden MS, Ghosh S (2004) Signaling to NF-kappaB. *Genes Dev* **18**: 2195-2224
- Hayden MS, Ghosh S (2012) NF-κB, the first quarter-century: remarkable progress and outstanding questions. *Genes Dev* **26**: 203-234
- Hoffmann A, Baltimore D (2006) Circuitry of nuclear factor kappaB signaling. *Immunol Rev* **210**: 171-186
- Hornbeck PV, Chabra I, Kornhauser JM, Skrzypek E, Zhang B (2004) PhosphoSite: A bioinformatics resource dedicated to physiological protein phosphorylation. *Proteomics* **4**: 1551-1561
- Hsieh CY, Hsu MJ, Hsiao G, Wang YH, Huang CW, Chen SW, Jayakumar T, Chiu PT, Chiu YH, Sheu JR (2011) Andrographolide enhances nuclear factor-kappaB subunit p65 Ser536 dephosphorylation through activation of protein phosphatase 2A in vascular smooth muscle cells. *J Biol Chem* **286**: 5942-5955
- Hsu PP, Kang SA, Rameseder J, Zhang Y, Ottina KA, Lim D, Peterson TR, Choi Y, Gray NS, Yaffe MB, Marto JA, Sabatini DM (2011) The mTOR-regulated phosphoproteome reveals a mechanism of mTORC1-mediated inhibition of growth factor signaling. *Science* **332**: 1317-1322
- Huang dW, Sherman BT, Lempicki RA (2009) Bioinformatics enrichment tools: paths toward the comprehensive functional analysis of large gene lists. *Nucleic Acids Res* **37**: 1-13
- Humphrey SJ, Yang G, Yang P, Fazakerley DJ, Stöckli J, Yang JY, James DE (2013) Dynamic adipocyte phosphoproteome reveals that Akt directly regulates mTORC2. *Cell Metab* **17**: 1009-1020
- Ishii KJ, Akira S (2006) Innate immune recognition of, and regulation by, DNA. *Trends Immunol* **27**: 525-532
- Ishii M, Wen H, Corsa CA, Liu T, Coelho AL, Allen RM, Carson WF, Cavassani KA, Li X, Lukacs NW, Hogaboam CM, Dou Y, Kunkel SL (2009) Epigenetic regulation of the alternatively activated macrophage phenotype. *Blood* **114**: 3244-3254

- Jacinto R, Hartung T, McCall C, Li L (2002) Lipopolysaccharide- and lipoteichoic acid-induced tolerance and cross-tolerance: distinct alterations in IL-1 receptor-associated kinase. *J Immunol* **168**: 6136-6141
- Janeway CA, Medzhitov R (2002) Innate immune recognition. *Annu Rev Immunol* **20**: 197-216
- Janeway CJ, Travers P, Walport M (2001) The major histocompatibility complex and its functions. In *Immunobiology: The Immune System in Health and Disease*. New York, USA: Garland Science
- Janzer A, Lim S, Fronhoffs F, Niazy N, Buettner R, Kirfel J (2012) Lysine-specific demethylase 1 (LSD1) and histone deacetylase 1 (HDAC1) synergistically repress proinflammatory cytokines and classical complement pathway components. *Biochem Biophys Res Commun* **421**: 665-670
- Jensen LJ, Kuhn M, Stark M, Chaffron S, Creevey C, Muller J, Doerks T, Julien P, Roth A, Simonovic M, Bork P, von Mering C (2009) STRING 8--a global view on proteins and their functional interactions in 630 organisms. *Nucleic Acids Res* **37**: D412-416
- Johnson LN (2009) The regulation of protein phosphorylation. *Biochem Soc Trans* **37**: 627-641
- Jones CN, Lee JY, Zhu J, Stybayeva G, Ramanculov E, Zern MA, Revzin A (2008) Multifunctional protein microarrays for cultivation of cells and immunodetection of secreted cellular products. *Anal Chem* **80**: 6351-6357
- Kang S, Lee SP, Kim KE, Kim HZ, Mémet S, Koh GY (2009) Toll-like receptor 4 in lymphatic endothelial cells contributes to LPS-induced lymphangiogenesis by chemotactic recruitment of macrophages. *Blood* **113**: 2605-2613
- Kanterman J, Sade-Feldman M, Baniyash M (2012) New insights into chronic inflammation-induced immunosuppression. *Seminars in cancer biology* **22**: 307-318
- Kawai T, Akira S (2011) Toll-like receptors and their crosstalk with other innate receptors in infection and immunity. *Immunity* **34**: 637-650
- Kelly TK, De Carvalho DD, Jones PA (2010) Epigenetic modifications as therapeutic targets. *Nat Biotechnol* **28**: 1069-1078
- Kim J, Lilliehook C, Dudak A, Prox J, Saftig P, Federoff HJ, Lim ST (2010) Activity-dependent alpha-cleavage of nectin-1 is mediated by a disintegrin and metalloprotease 10 (ADAM10). *J Biol Chem* **285**: 22919-22926

Kinjo I, Hanada T, Inagaki-Ohara K, Mori H, Aki D, Ohishi M, Yoshida H, Kubo M, Yoshimura A (2002) SOCS1/JAB is a negative regulator of LPS-induced macrophage activation. *Immunity* **17**: 583-591

Kleine-Kohlbrecher D, Christensen J, Vandamme J, Abarrategui I, Bak M, Tommerup N, Shi X, Gozani O, Rappsilber J, Salcini AE, Helin K (2010) A functional link between the histone demethylase PHF8 and the transcription factor ZNF711 in X-linked mental retardation. *Mol Cell* **38**: 165-178

Klinman DM, Nutman TB (2001) ELISPOT assay to detect cytokine-secreting murine and human cells. *Curr Protoc Immunol* **Chapter 6**: Unit 6.19

Klose RJ, Bird AP (2006) Genomic DNA methylation: the mark and its mediators. *Trends Biochem Sci* **31**: 89-97

Klose RJ, Kallin EM, Zhang Y (2006) JmjC-domain-containing proteins and histone demethylation. *Nat Rev Genet* **7**: 715-727

Klose RJ, Yan Q, Tothova Z, Yamane K, Erdjument-Bromage H, Tempst P, Gilliland DG, Zhang Y, Kaelin WG (2007) The retinoblastoma binding protein RBP2 is an H3K4 demethylase. *Cell* **128**: 889-900

Kobayashi K, Hernandez LD, Galán JE, Janeway CA, Medzhitov R, Flavell RA (2002) IRAK-M is a negative regulator of Toll-like receptor signaling. *Cell* **110**: 191-202

Kohler NG, Joly A (1997) The involvement of an LPS inducible I kappa B kinase in endotoxin tolerance. *Biochem Biophys Res Commun* **232**: 602-607

Kolset SO, Pejler G (2011) Serglycin: a structural and functional chameleon with wide impact on immune cells. *J Immunol* **187**: 4927-4933

Kondo Y, Shen L, Ahmed S, Bumber Y, Sekido Y, Haddad BR, Issa JP (2008) Downregulation of histone H3 lysine 9 methyltransferase G9a induces centrosome disruption and chromosome instability in cancer cells. *PLoS One* **3**: e2037

Kouzarides T (2007) Chromatin modifications and their function. *Cell* **128**: 693-705

Kramer JM, Kochinke K, Oortveld MA, Marks H, Kramer D, de Jong EK, Asztalos Z, Westwood JT, Stunnenberg HG, Sokolowski MB, Keleman K, Zhou H, van Bokhoven H, Schenck A (2011) Epigenetic regulation of learning and memory by Drosophila EHMT/G9a. *PLoS Biol* **9**: e1000569

Kumar H, Kawai T, Akira S (2011) Pathogen recognition by the innate immune system. *Int Rev Immunol* **30**: 16-34

Kuo YC, Huang KY, Yang CH, Yang YS, Lee WY, Chiang CW (2008) Regulation of phosphorylation of Thr-308 of Akt, cell proliferation, and survival by the B55alpha regulatory subunit targeting of the protein phosphatase 2A holoenzyme to Akt. *J Biol Chem* **283**: 1882-1892

Kustatscher G, Hégarat N, Wills KL, Furlan C, Bukowski-Wills JC, Hochegger H, Rappsilber J (2014a) Proteomics of a fuzzy organelle: interphase chromatin. *EMBO J* **33**: 648-664

Kustatscher G, Wills KL, Furlan C, Rappsilber J (2014b) Chromatin enrichment for proteomics. *Nat Protoc* **9**: 2090-2099

Kutikhin AG, Yuzhalin AE, Tsitko EA, Brusina EB (2014) Pattern recognition receptors and DNA repair: starting to put a jigsaw puzzle together. *Front Immunol* **5**: 343

Köhler C, Villar CB (2008) Programming of gene expression by Polycomb group proteins. *Trends Cell Biol* **18**: 236-243

Laumonnier F, Holbert S, Ronce N, Faravelli F, Lenzner S, Schwartz CE, Lespinasse J, Van Esch H, Lacombe D, Goizet C, Phan-Dinh Tuy F, van Bokhoven H, Fryns JP, Chelly J, Ropers HH, Moraine C, Hamel BC, Briault S (2005) Mutations in PHF8 are associated with X linked mental retardation and cleft lip/cleft palate. *J Med Genet* **42**: 780-786

Lehnertz B, Northrop JP, Antignano F, Burrows K, Hadidi S, Mullaly SC, Rossi FM, Zaph C (2010) Activating and inhibitory functions for the histone lysine methyltransferase G9a in T helper cell differentiation and function. *J Exp Med* **207**: 915-922

Lehnertz B, Ueda Y, Derijck AA, Braunschweig U, Perez-Burgos L, Kubicek S, Chen T, Li E, Jenuwein T, Peters AH (2003) Suv39h-mediated histone H3 lysine 9 methylation directs DNA methylation to major satellite repeats at pericentric heterochromatin. *Curr Biol* **13**: 1192-1200

Leng L, Metz CN, Fang Y, Xu J, Donnelly S, Baugh J, Delohery T, Chen Y, Mitchell RA, Bucala R (2003) MIF signal transduction initiated by binding to CD74. *J Exp Med* **197**: 1467-1476

Leung DC, Dong KB, Maksakova IA, Goyal P, Appanah R, Lee S, Tachibana M, Shinkai Y, Lehnertz B, Mager DL, Rossi F, Lorincz MC (2011) Lysine methyltransferase G9a is required for de novo DNA methylation and the establishment, but not the maintenance, of proviral silencing. *Proc Natl Acad Sci U S A* **108**: 5718-5723

Li L, Cousart S, Hu J, McCall CE (2000) Characterization of interleukin-1 receptor-associated kinase in normal and endotoxin-tolerant cells. *J Biol Chem* **275**: 23340-23345

Li N, Wang Y, Forbes K, Vignali KM, Heale BS, Saftig P, Hartmann D, Black RA, Rossi JJ, Blobel CP, Dempsey PJ, Workman CJ, Vignali DA (2007) Metalloproteases regulate T-cell proliferation and effector function via LAG-3. *EMBO J* **26**: 494-504

Li Q, Verma IM (2002) NF-kappaB regulation in the immune system. *Nat Rev Immunol* **2**: 725-734

Li X, Tupper JC, Bannerman DD, Winn RK, Rhodes CJ, Harlan JM (2003) Phosphoinositide 3 kinase mediates Toll-like receptor 4-induced activation of NF-kappa B in endothelial cells. *Infect Immun* **71**: 4414-4420

Li Y, Reddy MA, Miao F, Shanmugam N, Yee JK, Hawkins D, Ren B, Natarajan R (2008) Role of the histone H3 lysine 4 methyltransferase, SET7/9, in the regulation of NF-kappaB-dependent inflammatory genes. Relevance to diabetes and inflammation. *J Biol Chem* **283**: 26771-26781

Lim HJ, Dimova NV, Tan MK, Sigoillot FD, King RW, Shi Y (2013) The G2/M regulator histone demethylase PHF8 is targeted for degradation by the anaphase-promoting complex containing CDC20. *Mol Cell Biol* **33**: 4166-4180

Lin SC, Lo YC, Wu H (2010) Helical assembly in the MyD88-IRAK4-IRAK2 complex in TLR/IL-1R signalling. *Nature* **465**: 885-890

Liu C, Yu Y, Liu F, Wei X, Wrobel JA, Gunawardena HP, Zhou L, Jin J, Chen X (2014) A chromatin activity-based chemoproteomic approach reveals a transcriptional repressome for gene-specific silencing. *Nat Commun* **5**: 5733

Liu W, Tanasa B, Tyurina OV, Zhou TY, Gassmann R, Liu WT, Ohgi KA, Benner C, Garcia-Bassets I, Aggarwal AK, Desai A, Dorrestein PC, Glass CK, Rosenfeld MG (2010) PHF8 mediates histone H4 lysine 20 demethylation events involved in cell cycle progression. *Nature* **466**: 508-512

Liu X, Wang X, Bi Y, Bu P, Zhang M (2015) The histone demethylase PHF8 represses cardiac hypertrophy upon pressure overload. *Exp Cell Res* **335**: 123-134

Luber CA, Cox J, Lauterbach H, Fancke B, Selbach M, Tschopp J, Akira S, Wiegand M, Hochrein H, O'Keeffe M, Mann M (2010) Quantitative proteomics reveals subset-specific viral recognition in dendritic cells. *Immunity* **32**: 279-289

Luther SA, Cyster JG (2001) Chemokines as regulators of T cell differentiation. *Nat Immunol* **2**: 102-107

Makridakis M, Roubelakis MG, Bitsika V, Dimuccio V, Samiotaki M, Kossida S, Panayotou G, Coleman J, Candiano G, Anagnou NP, Vlahou A (2010) Analysis of secreted proteins for the study of bladder cancer cell aggressiveness. *J Proteome Res* **9**: 3243-3259

Malla RR, Gopinath S, Gondi CS, Alapati K, Dinh DH, Gujrati M, Rao JS (2011) Cathepsin B and uPAR knockdown inhibits tumor-induced angiogenesis by modulating VEGF expression in glioma. *Cancer Gene Ther* **18**: 419-434

Manes NP, Dong L, Zhou W, Du X, Reghu N, Kool AC, Choi D, Bailey CL, Petricoin EF, 3rd, Liotta LA, Popov SG (2011) Discovery of mouse spleen signaling responses to anthrax using label-free quantitative phosphoproteomics via mass spectrometry. *Mol Cell Proteomics* **10**: M110 000927

Marcoulatos P, Avgerinos E, Tsantzas DV, Vamvakopoulos NC (1998) Mapping interleukin enhancer binding factor 3 gene (ILF3) to human chromosome 19 (19q11-qter and 19p11-p13.1) by polymerase chain reaction amplification of human-rodent somatic cell hybrid DNA templates. *J Interferon Cytokine Res* **18**: 351-355

Martin C, Zhang Y (2005) The diverse functions of histone lysine methylation. *Nat Rev Mol Cell Biol* **6**: 838-849

Maslash-Hubbard AE-w, N. Shanley, T.P.Cornell, T.T. (2011) Negative Regulators of the Host Response in Sepsis. *The Open Inflammation Journal* **4**: 61-66

Mattioli I, Dittrich-Breiholz O, Livingstone M, Kracht M, Schmitz ML (2004) Comparative analysis of T-cell costimulation and CD43 activation reveals novel signaling pathways and target genes. *Blood* **104**: 3302-3304

Mayer AM, Brenic S, Stocker R, Glaser KB (1995) Modulation of superoxide generation in in vivo lipopolysaccharide-primed rat alveolar macrophages by arachidonic acid and inhibitors of protein kinase C, phospholipase A2, protein serine-threonine phosphatase(s), protein tyrosine kinase(s) and phosphatase(s). *J Pharmacol Exp Ther* **274**: 427-436

Medvedev AE, Kopydlowski KM, Vogel SN (2000) Inhibition of lipopolysaccharide-induced signal transduction in endotoxin-tolerized mouse macrophages: dysregulation of cytokine, chemokine, and toll-like receptor 2 and 4 gene expression. *J Immunol* **164**: 5564-5574

Mehta S, Jeffrey KL (2015) Beyond receptors and signaling: epigenetic factors in the regulation of innate immunity. *Immunol Cell Biol* **93**: 233-244

Meissner F, Scheltema RA, Mollenkopf HJ, Mann M (2013) Direct proteomic quantification of the secretome of activated immune cells. *Science* **340**: 475-478

Metzger E, Wissmann M, Yin N, Muller JM, Schneider R, Peters AH, Gunther T, Buettner R, Schule R (2005) LSD1 demethylates repressive histone marks to promote androgen-receptor-dependent transcription. *Nature* **437**: 436-439

- Mosammaparast N, Shi Y (2010) Reversal of histone methylation: biochemical and molecular mechanisms of histone demethylases. *Annu Rev Biochem* **79**: 155-179
- Muranko K (2014) Characterization of the anti-apoptotic function of the lysine demethylase plant homeodomain finger protein 8 (PHF8). Master of Science Thesis, Biochemistry The University of Western Ontario, London, Ontario, Canada
- Mustafa SA, Hoheisel JD, Alhamdani MS (2011) Secretome profiling with antibody microarrays. *Mol Biosyst* **7**: 1795-1801
- Nagai Y, Shimazu R, Ogata H, Akashi S, Sudo K, Yamasaki H, Hayashi S, Iwakura Y, Kimoto M, Miyake K (2002) Requirement for MD-1 in cell surface expression of RP105/CD180 and B-cell responsiveness to lipopolysaccharide. *Blood* **99**: 1699-1705
- Nathan CF (1987) Secretory products of macrophages. *J Clin Invest* **79**: 319-326
- Nomura F, Akashi S, Sakao Y, Sato S, Kawai T, Matsumoto M, Nakanishi K, Kimoto M, Miyake K, Takeda K, Akira S (2000) Cutting edge: endotoxin tolerance in mouse peritoneal macrophages correlates with down-regulation of surface toll-like receptor 4 expression. *J Immunol* **164**: 3476-3479
- Nowak SJ, Pai CY, Corces VG (2003) Protein phosphatase 2A activity affects histone H3 phosphorylation and transcription in *Drosophila melanogaster*. *Mol Cell Biol* **23**: 6129-6138
- O'Neill LA, Golenbock D, Bowie AG (2013) The history of Toll-like receptors - redefining innate immunity. *Nat Rev Immunol* **13**: 453-460
- Ohnishi H, Tochio H, Kato Z, Orii KE, Li A, Kimura T, Hiroaki H, Kondo N, Shirakawa M (2009) Structural basis for the multiple interactions of the MyD88 TIR domain in TLR4 signaling. *Proc Natl Acad Sci U S A* **106**: 10260-10265
- Peng B, Wang J, Hu Y, Zhao H, Hou W, Wang H, Liao J, Xu X (2015) Modulation of LSD1 phosphorylation by CK2/WIP1 regulates RNF168-dependent 53BP1 recruitment in response to DNA damage. *Nucleic Acids Res* **43**: 5936-5947
- Peters AH, O'Carroll D, Scherthan H, Mechtler K, Sauer S, Schöfer C, Weipoltshammer K, Pagani M, Lachner M, Kohlmaier A, Opravil S, Doyle M, Sibilia M, Jenuwein T (2001) Loss of the Suv39h histone methyltransferases impairs mammalian heterochromatin and genome stability. *Cell* **107**: 323-337
- Pflum MK, Tong JK, Lane WS, Schreiber SL (2001) Histone deacetylase 1 phosphorylation promotes enzymatic activity and complex formation. *J Biol Chem* **276**: 47733-47741

Poltorak A, He X, Smirnova I, Liu MY, Van Huffel C, Du X, Birdwell D, Alejos E, Silva M, Galanos C, Freudenberg M, Ricciardi-Castagnoli P, Layton B, Beutler B (1998) Defective LPS signaling in C3H/HeJ and C57BL/10ScCr mice: mutations in Tlr4 gene. *Science* **282**: 2085-2088

Ptaschinski C, Mukherjee S, Moore ML, Albert M, Helin K, Kunkel SL, Lukacs NW (2015) RSV-Induced H3K4 Demethylase KDM5B Leads to Regulation of Dendritic Cell-Derived Innate Cytokines and Exacerbates Pathogenesis In Vivo. *PLoS Pathog* **11**: e1004978

Qi HH, Sarkissian M, Hu GQ, Wang Z, Bhattacharjee A, Gordon DB, Gonzales M, Lan F, Ongusaha PP, Huarte M, Yaghi NK, Lim H, Garcia BA, Brizuela L, Zhao K, Roberts TM, Shi Y (2010) Histone H4K20/H3K9 demethylase PHF8 regulates zebrafish brain and craniofacial development. *Nature* **466**: 503-507

Radtke F, MacDonald HR, Tacchini-Cottier F (2013) Regulation of innate and adaptive immunity by Notch. *Nat Rev Immunol* **13**: 427-437

Rathert P, Dhayalan A, Murakami M, Zhang X, Tamas R, Jurkowska R, Komatsu Y, Shinkai Y, Cheng X, Jeltsch A (2008) Protein lysine methyltransferase G9a acts on non-histone targets. *Nat Chem Biol* **4**: 344-346

Rothbart SB, Strahl BD (2014) Interpreting the language of histone and DNA modifications. *Biochim Biophys Acta* **1839**: 627-643

Saccani S, Natoli G (2002) Dynamic changes in histone H3 Lys 9 methylation occurring at tightly regulated inducible inflammatory genes. *Genes Dev* **16**: 2219-2224

Saccani S, Pantano S, Natoli G (2002) p38-Dependent marking of inflammatory genes for increased NF-kappa B recruitment. *Nat Immunol* **3**: 69-75

Sakurai H, Chiba H, Miyoshi H, Sugita T, Toriumi W (1999) IkappaB kinases phosphorylate NF-kappaB p65 subunit on serine 536 in the transactivation domain. *J Biol Chem* **274**: 30353-30356

Schaefer A, Sampath SC, Intrator A, Min A, Gertler TS, Surmeier DJ, Tarakhovsky A, Greengard P (2009) Control of cognition and adaptive behavior by the GLP/G9a epigenetic suppressor complex. *Neuron* **64**: 678-691

Schnoor M, Cullen P, Lorkowski J, Stolle K, Robenek H, Troyer D, Rauterberg J, Lorkowski S (2008) Production of type VI collagen by human macrophages: a new dimension in macrophage functional heterogeneity. *J Immunol* **180**: 5707-5719

Seshacharyulu P, Pandey P, Datta K, Batra SK (2013) Phosphatase: PP2A structural importance, regulation and its aberrant expression in cancer. *Cancer Lett* **335**: 9-18

- Shankar SR, Bahirvani AG, Rao VK, Bharathy N, Ow JR, Taneja R (2013) G9a, a multipotent regulator of gene expression. *Epigenetics* **8**: 16-22
- Shanley TP, Vasi N, Denenberg A, Wong HR (2001) The serine/threonine phosphatase, PP2A: endogenous regulator of inflammatory cell signaling. *J Immunol* **166**: 966-972
- Sharif O, Knapp S (2008) From expression to signaling: roles of TREM-1 and TREM-2 in innate immunity and bacterial infection. *Immunobiology* **213**: 701-713
- Shen MM, Skoda RC, Cardiff RD, Campos-Torres J, Leder P, Ornitz DM (1994) Expression of LIF in transgenic mice results in altered thymic epithelium and apparent interconversion of thymic and lymph node morphologies. *EMBO J* **13**: 1375-1385
- Shen Y, Pan X, Zhao H (2014) The histone demethylase PHF8 is an oncogenic protein in human non-small cell lung cancer. *Biochem Biophys Res Commun* **451**: 119-125
- Shi Y, Lan F, Matson C, Mulligan P, Whetstine JR, Cole PA, Casero RA (2004) Histone demethylation mediated by the nuclear amine oxidase homolog LSD1. *Cell* **119**: 941-953
- Shi Y, Whetstine JR (2007) Dynamic regulation of histone lysine methylation by demethylases. *Mol Cell* **25**: 1-14
- Shinkai Y, Tachibana M (2011) H3K9 methyltransferase G9a and the related molecule GLP. *Genes Dev* **25**: 781-788
- Simboeck E, Sawicka A, Zupkovitz G, Senese S, Winter S, Dequiedt F, Ogris E, Di Croce L, Chiocca S, Seiser C (2010) A phosphorylation switch regulates the transcriptional activation of cell cycle regulator p21 by histone deacetylase inhibitors. *J Biol Chem* **285**: 41062-41073
- Singh SK, Baumgart S, Singh G, Konig AO, Reutlinger K, Hofbauer LC, Barth P, Gress TM, Lomberg G, Urrutia R, Fernandez-Zapico ME, Ellenrieder V (2011) Disruption of a nuclear NFATc2 protein stabilization loop confers breast and pancreatic cancer growth suppression by zoledronic acid. *J Biol Chem* **286**: 28761-28771
- Snel B, Lehmann G, Bork P, Huynen MA (2000) STRING: a web-server to retrieve and display the repeatedly occurring neighbourhood of a gene. *Nucleic Acids Res* **28**: 3442-3444
- Son HJ, Kim JY, Hahn Y, Seo SB (2012) Negative regulation of JAK2 by H3K9 methyltransferase G9a in leukemia. *Mol Cell Biol* **32**: 3681-3694
- Strahl BD, Allis CD (2000) The language of covalent histone modifications. *Nature* **403**: 41-45

Sullivan KE, Cutilli J, Piliero LM, Ghavimi-Alagha D, Starr SE, Campbell DE, Douglas SD (2000) Measurement of cytokine secretion, intracellular protein expression, and mRNA in resting and stimulated peripheral blood mononuclear cells. *Clin Diagn Lab Immunol* **7**: 920-924

Sun L, Huang Y, Wei Q, Tong X, Cai R, Nalepa G, Ye X (2015a) Cyclin E-CDK2 Protein Phosphorylates Plant Homeodomain Finger Protein 8 (PHF8) and Regulates Its Function in the Cell Cycle. *J Biol Chem* **290**: 4075-4085

Sun L, Li AL, Pham TT, Shanley TP (2015b) Study of Protein Phosphatase 2A (PP2A) Activity in LPS-Induced Tolerance Using Fluorescence-Based and Immunoprecipitation-Aided Methodology. *Biomolecules* **5**: 1284-1301

Sun SC, Maggirwar SB, Harhaj E (1995) Activation of NF-kappa B by phosphatase inhibitors involves the phosphorylation of I kappa B alpha at phosphatase 2A-sensitive sites. *J Biol Chem* **270**: 18347-18351

Sun X, Qiu JJ, Zhu S, Cao B, Sun L, Li S, Li P, Zhang S, Dong S (2013) Oncogenic features of PHF8 histone demethylase in esophageal squamous cell carcinoma. *PLoS One* **8**: e77353

Sun Z, Andersson R (2002) NF-kappaB activation and inhibition: a review. *Shock* **18**: 99-106

Sung SJ, Walters JA (1993) Stimulation of interleukin-1 alpha and interleukin-1 beta production in human monocytes by protein phosphatase 1 and 2A inhibitors. *J Biol Chem* **268**: 5802-5809

Suzuki K, Yu C, Qu J, Li M, Yao X, Yuan T, Goebel A, Tang S, Ren R, Aizawa E, Zhang F, Xu X, Soligalla RD, Chen F, Kim J, Kim NY, Liao HK, Benner C, Esteban CR, Jin Y et al (2014) Targeted gene correction minimally impacts whole-genome mutational load in human-disease-specific induced pluripotent stem cell clones. *Cell Stem Cell* **15**: 31-36

Sánchez-Pernaute O, Ospelt C, Neidhart M, Gay S (2008) Epigenetic clues to rheumatoid arthritis. *J Autoimmun* **30**: 12-20

Tachibana M, Sugimoto K, Fukushima T, Shinkai Y (2001) Set domain-containing protein, G9a, is a novel lysine-preferring mammalian histone methyltransferase with hyperactivity and specific selectivity to lysines 9 and 27 of histone H3. *J Biol Chem* **276**: 25309-25317

Tachibana M, Sugimoto K, Nozaki M, Ueda J, Ohta T, Ohki M, Fukuda M, Takeda N, Niida H, Kato H, Shinkai Y (2002) G9a histone methyltransferase plays a dominant role in euchromatic histone H3 lysine 9 methylation and is essential for early embryogenesis. *Genes Dev* **16**: 1779-1791

Tachibana M, Ueda J, Fukuda M, Takeda N, Ohta T, Iwanari H, Sakihama T, Kodama T, Hamakubo T, Shinkai Y (2005) Histone methyltransferases G9a and GLP form heteromeric complexes and are both crucial for methylation of euchromatin at H3-K9. *Genes Dev* **19**: 815-826

Takeda K, Akira S (2015) Toll-like receptors. *Curr Protoc Immunol* **109**: 14.12.11-14.12.10

Takemura R, Werb Z (1984) Secretory products of macrophages and their physiological functions. *Am J Physiol* **246**: C1-9

Takeuchi H, Hirano T, Whitmore SE, Morisaki I, Amano A, Lamont RJ (2013) The serine phosphatase SerB of *Porphyromonas gingivalis* suppresses IL-8 production by dephosphorylation of NF- κ B RelA/p65. *PLoS Pathog* **9**: e1003326

Tao J, Hu K, Chang Q, Wu H, Sherman NE, Martinowich K, Klose RJ, Schanen C, Jaenisch R, Wang W, Sun YE (2009) Phosphorylation of MeCP2 at Serine 80 regulates its chromatin association and neurological function. *Proc Natl Acad Sci U S A* **106**: 4882-4887

Tchevkina E, Komelkov A (2012) Protein Phosphorylation as a Key Mechanism of mTORC1/2 Signaling Pathways. In *Protein Phosphorylation in Human Health*, Huang C (ed).

Teti A (1992) Regulation of cellular functions by extracellular matrix. *J Am Soc Nephrol* **2**: S83-87

Thomas LR, Miyashita H, Cobb RM, Pierce S, Tachibana M, Hobeika E, Reth M, Shinkai Y, Oltz EM (2008) Functional analysis of histone methyltransferase g9a in B and T lymphocytes. *J Immunol* **181**: 485-493

Trojer P, Zhang J, Yonezawa M, Schmidt A, Zheng H, Jenuwein T, Reinberg D (2009) Dynamic Histone H1 Isotype 4 Methylation and Demethylation by Histone Lysine Methyltransferase G9a/KMT1C and the Jumonji Domain-containing JMJD2/KDM4 Proteins. *J Biol Chem* **284**: 8395-8405

Turgeon N, Blais M, Delabre JF, Asselin C (2013) The histone H3K27 methylation mark regulates intestinal epithelial cell density-dependent proliferation and the inflammatory response. *J Cell Biochem* **114**: 1203-1215

van der Pol E, Böing AN, Harrison P, Sturk A, Nieuwland R (2012) Classification, functions, and clinical relevance of extracellular vesicles. *Pharmacol Rev* **64**: 676-705

Varier RA, Timmers HT (2011) Histone lysine methylation and demethylation pathways in cancer. *Biochim Biophys Acta* **1815**: 75-89

Varma TK, Toliver-Kinsky TE, Lin CY, Koutrouvelis AP, Nichols JE, Sherwood ER (2001) Cellular mechanisms that cause suppressed gamma interferon secretion in endotoxin-tolerant mice. *Infect Immun* **69**: 5249-5263

Vedadi M, Barsyte-Lovejoy D, Liu F, Rival-Gervier S, Allali-Hassani A, Labrie V, Wigle TJ, Dimaggio PA, Wasney GA, Siarheyeva A, Dong A, Tempel W, Wang SC, Chen X, Chau I, Mangano TJ, Huang XP, Simpson CD, Pattenden SG, Norris JL et al (2011) A chemical probe selectively inhibits G9a and GLP methyltransferase activity in cells. *Nat Chem Biol* **7**: 566-574

Vermeulen L, De Wilde G, Van Damme P, Vanden Berghe W, Haegeman G (2003) Transcriptional activation of the NF-kappaB p65 subunit by mitogen- and stress-activated protein kinase-1 (MSK1). *EMBO J* **22**: 1313-1324

Vermeulen L, Vanden Berghe W, Haegeman G (2006) Regulation of NF-κB Transcriptional Activity. In *The Link Between Inflammation and Cancer*, Dalglish A, Haefner B (eds), pp 89-102. Springer US

Villagra A, Sotomayor EM, Seto E (2010) Histone deacetylases and the immunological network: implications in cancer and inflammation. *Oncogene* **29**: 157-173

Virshup DM (2000) Protein phosphatase 2A: a panoply of enzymes. *Curr Opin Cell Biol* **12**: 180-185

Wallace AM, Hardigan A, Geraghty P, Salim S, Gaffney A, Thankachen J, Arellanos L, D'Armiento JM, Foronjy RF (2012) Protein phosphatase 2A regulates innate immune and proteolytic responses to cigarette smoke exposure in the lung. *Toxicol Sci* **126**: 589-599

Wang D, Baldwin AS (1998) Activation of nuclear factor-kappaB-dependent transcription by tumor necrosis factor-alpha is mediated through phosphorylation of RelA/p65 on serine 529. *J Biol Chem* **273**: 29411-29416

Wang J, Lin X, Wang S, Wang C, Wang Q, Duan X, Lu P, Liu XS, Huang J (2014a) PHF8 and REST/NRSF co-occupy gene promoters to regulate proximal gene expression. *Sci Rep* **4**: 5008

Wang X, Ju L, Fan J, Zhu Y, Liu X, Zhu K, Wu M, Li L (2014b) Histone H3K4 methyltransferase Mll1 regulates protein glycosylation and tunicamycin-induced apoptosis through transcriptional regulation. *Biochim Biophys Acta* **1843**: 2592-2602

Wang X, Zhu WG (2008) Advances in histone methyltransferases and histone demethylases. *Ai Zheng* **27**: 1018-1025

Ward IM, Minn K, van Deursen J, Chen J (2003) p53 Binding protein 53BP1 is required for DNA damage responses and tumor suppression in mice. *Mol Cell Biol* **23**: 2556-2563

Weintz G, Olsen JV, Fruhauf K, Niedzielska M, Amit I, Jantsch J, Mages J, Frech C, Dolken L, Mann M, Lang R (2010) The phosphoproteome of toll-like receptor-activated macrophages. *Mol Syst Biol* **6**: 371

Weiss T, Hergeth S, Zeissler U, Izzo A, Tropberger P, Zee BM, Dundr M, Garcia BA, Daujat S, Schneider R (2010) Histone H1 variant-specific lysine methylation by G9a/KMT1C and Glp1/KMT1D. *Epigenetics Chromatin* **3**: 7

Welsh JB, Sapinoso LM, Kern SG, Brown DA, Liu T, Bauskin AR, Ward RL, Hawkins NJ, Quinn DI, Russell PJ, Sutherland RL, Breit SN, Moskaluk CA, Frierson HF, Hampton GM (2003) Large-scale delineation of secreted protein biomarkers overexpressed in cancer tissue and serum. *Proc Natl Acad Sci U S A* **100**: 3410-3415

Wen H, Dou Y, Hogaboam CM, Kunkel SL (2008) Epigenetic regulation of dendritic cell-derived interleukin-12 facilitates immunosuppression after a severe innate immune response. *Blood* **111**: 1797-1804

Wu H, Chen X, Xiong J, Li Y, Li H, Ding X, Liu S, Chen S, Gao S, Zhu B (2011) Histone methyltransferase G9a contributes to H3K27 methylation in vivo. *Cell Res* **21**: 365-367

Wu X, Tian L, Li J, Zhang Y, Han V, Li Y, Xu X, Li H, Chen X, Chen J, Jin W, Xie Y, Han J, Zhong CQ (2012) Investigation of receptor interacting protein (RIP3)-dependent protein phosphorylation by quantitative phosphoproteomics. *Mol Cell Proteomics* **11**: 1640-1651

Xia M, Liu J, Wu X, Liu S, Li G, Han C, Song L, Li Z, Wang Q, Wang J, Xu T, Cao X (2013) Histone methyltransferase Ash1l suppresses interleukin-6 production and inflammatory autoimmune diseases by inducing the ubiquitin-editing enzyme A20. *Immunity* **39**: 470-481

Xie L, Liu C, Wang L, Gunawardena HP, Yu Y, Du R, Taxman DJ, Dai P, Yan Z, Yu J, Holly SP, Parise LV, Wan YY, Ting JP, Chen X (2013) Protein phosphatase 2A catalytic subunit alpha plays a MyD88-dependent, central role in the gene-specific regulation of endotoxin tolerance. *Cell Rep* **3**: 678-688

Xu G, Liu G, Xiong S, Liu H, Chen X, Zheng B (2015) The histone methyltransferase Smyd2 is a negative regulator of macrophage activation by suppressing interleukin 6 (IL-6) and tumor necrosis factor α (TNF- α) production. *J Biol Chem* **290**: 5414-5423

Yamamoto Y, Verma UN, Prajapati S, Kwak YT, Gaynor RB (2003) Histone H3 phosphorylation by IKK-alpha is critical for cytokine-induced gene expression. *Nature* **423**: 655-659

Yang J, Fan GH, Wadzinski BE, Sakurai H, Richmond A (2001) Protein phosphatase 2A interacts with and directly dephosphorylates RelA. *J Biol Chem* **276**: 47828-47833

Yang J, Park Y, Zhang H, Xu X, Laine GA, Dellsperger KC, Zhang C (2009) Feed-forward signaling of TNF- α and NF- κ B via IKK- β pathway contributes to insulin resistance and coronary arteriolar dysfunction in type 2 diabetic mice. *Am J Physiol Heart Circ Physiol* **296**: H1850-1858

Yeh PY, Yeh KH, Chuang SE, Song YC, Cheng AL (2004) Suppression of MEK/ERK signaling pathway enhances cisplatin-induced NF- κ B activation by protein phosphatase 4-mediated NF- κ B p65 Thr dephosphorylation. *J Biol Chem* **279**: 26143-26148

Yu L, Wang Y, Huang S, Wang J, Deng Z, Zhang Q, Wu W, Zhang X, Liu Z, Gong W, Chen Z (2010) Structural insights into a novel histone demethylase PHF8. *Cell Res* **20**: 166-173

Yu Y, Yoon SO, Poulogiannis G, Yang Q, Ma XM, Villén J, Kubica N, Hoffman GR, Cantley LC, Gygi SP, Blenis J (2011) Phosphoproteomic analysis identifies Grb10 as an mTORC1 substrate that negatively regulates insulin signaling. *Science* **332**: 1322-1326

Yuan X, Feng W, Imhof A, Grummt I, Zhou Y (2007) Activation of RNA polymerase I transcription by cockayne syndrome group B protein and histone methyltransferase G9a. *Mol Cell* **27**: 585-595

Yue WW, Hozjan V, Ge W, Loenarz C, Cooper CD, Schofield CJ, Kavanagh KL, Oppermann U, McDonough MA (2010) Crystal structure of the PHF8 Jumonji domain, an Nepsilon-methyl lysine demethylase. *FEBS Lett* **584**: 825-830

Yun M, Wu J, Workman JL, Li B (2011) Readers of histone modifications. *Cell Res* **21**: 564-578

Yáñez-Mó M, Siljander PR, Andreu Z, Zavec AB, Borràs FE, Buzas EI, Buzas K, Casal E, Cappello F, Carvalho J, Colás E, Cordeiro-da Silva A, Fais S, Falcon-Perez JM, Ghobrial IM, Giebel B, Gimona M, Graner M, Gursel I, Gursel M et al (2015) Biological properties of extracellular vesicles and their physiological functions. *J Extracell Vesicles* **4**: 27066

Zaric SS, Coulter WA, Shelburne CE, Fulton CR, Zaric MS, Scott A, Lappin MJ, Fitzgerald DC, Irwin CR, Taggart CC (2011) Altered Toll-like receptor 2-mediated endotoxin tolerance is related to diminished interferon beta production. *J Biol Chem* **286**: 29492-29500

Zhang P, Nelson S, Summer WR, Spitzer JA (2000) Serine/threonine phosphorylation in cellular signaling for alveolar macrophage phagocytic response to endotoxin. *Shock* **13**: 34-40

Zhang X, Cook PC, Zindy E, Williams CJ, Jowitt TA, Streuli CH, MacDonald AS, Redondo-Muñoz J (2015) Integrin α 4 β 1 controls G9a activity that regulates epigenetic changes and nuclear properties required for lymphocyte migration. *Nucleic Acids Res*

Zhong H, May MJ, Jimi E, Ghosh S (2002) The phosphorylation status of nuclear NF-kappa B determines its association with CBP/p300 or HDAC-1. *Mol Cell* **9**: 625-636

Zhong H, SuYang H, Erdjument-Bromage H, Tempst P, Ghosh S (1997) The transcriptional activity of NF-kappaB is regulated by the IkappaB-associated PKAc subunit through a cyclic AMP-independent mechanism. *Cell* **89**: 413-424

Zhong H, Voll RE, Ghosh S (1998) Phosphorylation of NF-kappa B p65 by PKA stimulates transcriptional activity by promoting a novel bivalent interaction with the coactivator CBP/p300. *Mol Cell* **1**: 661-671

Zhu G, Liu L, She L, Tan H, Wei M, Chen C, Su Z, Huang D, Tian Y, Qiu Y, Liu Y, Zhang X (2015) Elevated expression of histone demethylase PHF8 associates with adverse prognosis in patients of laryngeal and hypopharyngeal squamous cell carcinoma. *Epigenomics* **7**: 143-153

Zhu Z, Wang Y, Li X, Xu L, Wang X, Sun T, Dong X, Chen L, Mao H, Yu Y, Li J, Chen PA, Chen CD (2010) PHF8 is a histone H3K9me2 demethylase regulating rRNA synthesis. *Cell Res* **20**: 794-801